Master's thesis

NTNU
Norwegian University of Science and Technology
Faculty of Engineering
Department of Marine Technology

Sander Nesse-Hansen

Dynamics of arrays of floating structures with shared mooring

Master's thesis in Marin technology
Supervisor: Prof. Erin Bachynski-Polić
Co-supervisor: Even Nærum
June 2023

NTNU
Norwegian University of
Science and Technology

AkerSolutions

Sander Nesse-Hansen

Dynamics of arrays of floating structures with shared mooring

Master's thesis in Marin technology
Supervisor: Prof. Erin Bachynski-Polić
Co-supervisor: Even Nærum
June 2023

Norwegian University of Science and Technology
Faculty of Engineering
Department of Marine Technology

NTNU
Norwegian University of
Science and Technology

NTNU
Kunnskap for en bedre verden

DEPARTMENT OF MARINE TECHNOLOGY

TMR4930
MARINE STRUCTURES, MASTER THESIS

Dynamics of arrays of floating structures with shared mooring

Author:
Sander Nesse-Hansen

June, 2023

NTNU Trondheim
Norwegian University of Science and Technology *Faculty of Engineering*
Department of Marine Technology

THESIS WORK SPRING 2023
for

Stud. Tech. Sander Nesse-Hansen

Dynamics of arrays of floating structures with shared moorings
Dynamikken av flytende konstruksjoner med delt forankring

In an effort to reduce the cost of floating offshore wind farms, innovative shared mooring systems are being proposed. Previous studies indicate potential cost reductions in deep water (depths greater than 400 m) when sharing mooring lines or anchors among several floating structures. The interconnections among floaters introduce new resonant modes and complex responses to environmental loads.

A challenge in assessing these systems is that the numerical models quickly become computationally demanding when dynamic responses are considered. The applicability of simpler models should therefore be investigated for use in design.

1. Literature review into wave and wind loads, FWT dynamics and mooring system design, including fatigue and extreme strength assessment, anchor types and umbilical lines. Literature review into previous studies on floating structures with shared anchors (floating wind turbines, aquaculture, wave energy converters).
2. Further development of the simplified analysis tool from the project work in order to include time integration, hydrodynamic loading, and simplified aerodynamic loading in the form of pre-computed rotor loads and a linear damper.
3. Develop and compare numerical models of differing fidelity for the considered shared mooring layouts:
   a. Full SIMA model with bar elements for the lines
   b. SIMA model with shared lines modelled with bar elements and anchor lines modelled quasi-statically
   c. Simplified analysis tool

   The comparison should focus on floater motions and line tensions in combined irregular wave and turbulent wind conditions.
4. Assess the importance of coherence and correlation in wind field models, including the frozen turbulence hypothesis, by applying rotor loads based on different wind field models:
   a. Synthetic wind fields from engineering tools (i.e. TurbSim or MannSim)
   b. LES wind fields (provided)
5. Report and conclude on the investigation.

The work scope may prove to be larger than initially anticipated. Subject to approval from the supervisors, topics may be deleted from the list above or reduced in extent.

In the project report, the candidate shall present his personal contribution to the resolution of problems within the scope of the project work

Theories and conclusions should be based on mathematical derivations and/or logic reasoning identifying the various steps in the deduction.

The candidate should utilise the existing possibilities for obtaining relevant literature.

Project report format

The project report should be organised in a rational manner to give a clear exposition of results, assessments, and conclusions. The text should be brief and to the point, with a clear language. Telegraphic language should be avoided.

The report shall contain the following elements: A text defining the scope, preface, list of contents, summary, main body of thesis, conclusions with recommendations for further work, list of symbols and acronyms, references and (optional) appendices. All figures, tables and equations shall be numerated.

The supervisors may require that the candidate, in an early stage of the work, presents a written plan for the completion of the work.

The original contribution of the candidate and material taken from other sources shall be clearly defined. Work from other sources shall be properly referenced using an acknowledged referencing system.

The report shall be submitted in electronic format (.pdf):
- Signed by the candidate
- The text defining the scope shall be included (this document)
- Drawings and/or computer models that are not suited to be part of the report in terms of appendices shall be provided on separate (.zip) files.

Ownership

NTNU has according to the present rules the ownership of the project reports. Any use of the report has to be approved by NTNU (or external partner when this applies). The department has the right to use the report as if the work was carried out by a NTNU employee, if nothing else has been agreed in advance.

Thesis supervisors:

Prof. Erin Bachynski-Polić, NTNU, erin.bachynski@ntnu.no
Even Nærum, Aker Solutions, Even.Sandoy.Naerum@akersolutions.com

Deadline: June 11th, 2023, 14:00

Preface

The Master thesis is carried out in the spring of 2023 and is a continuation of the specialization project for Marine Structures at the Department of Marine Technology during the autumn of 2022. Numerical analysis in SIMA has been conducted for shared mooring adapted to VolturnUS-s. Parts of the theory and literature study are from the specialization project [1].

11/06/2023 - Sander Nesse-Hansen

Sander Nesse-Hansen
Trondheim, June 11, 2023

Acknowledgements

Firstly I want to express my sincere gratitude to my supervisor Erin Bachynski-Polić. Throughout the project and master thesis, weekly meetings have been held, which has given stable progress in the thesis. Thank you for your consistency and knowledge.

My supervisor, Even Nærum in Aker Solutions, deserves a thank you for the bi-weekly meetings, which have helped me get an industrial perspective on the thesis.

Erin Bachynski-Polić, Irene Rivera Arreba, and Zhen Gao deserve gratitude for their help modeling floating wind turbines with shared mooring, which gave many unexpected troubles.

Irene Rivera Arreba deserves recognition for postprocessing LES files from Adam Wise, enabling me to compare turbulence models influence on shared mooring.

Thank you to all my friends and colleagues in office B.170, which has created a good learning environment and discussions.

Finally, Thea Berge deserves a special thank you. For active listening to endless hours talking about floating offshore wind and shared mooring.

Abstract

Floating offshore wind turbines could be a necessity to reduce emissions as more of the produced energy has to come from renewable resources. Increased energy production is necessary to meet the requirements of increased living standards and further industrialization. Floating wind turbines are considered a solution to increase energy production. Wind turbines have increased enormously in size in recent years, as increasing the hub height is still economical.
As wind turbines are getting larger and wind turbine parks are getting larger, the conflict level between local society and wind turbines has increased due to aesthetic, noise, ecology etc. Therefore, offshore wind turbines de-escalate conflicts.

As offshore wind moves further into deeper water for licenses, less competition, and ideal wind, the relative cost of mooring systems gets higher. Lowering the mooring cost will significantly impact the total investment cost. In many articles, shared mooring has been proposed to lower the investment cost, and a few studies have been carried out to look deeper into the consequences of shared mooring.

Shared mooring could be of special interest to many nations as the water depth is deep for many coastlines. Shared mooring is a concept in which floating offshore wind turbines are connected by mooring lines. The shared mooring line reduces the length and the number of anchors per floating offshore wind turbine.

Today few analysis tools can analyze shared mooring systems for floating offshore wind, as the programs are incompatible with several control systems. Another issue is that several wind turbines must be analyzed in the same system, increasing analysis time. With long simulation time, few shared mooring designs could be considered. It is, therefore, essential to compare different numerical models of different fidelity to investigate if the analysis time could be reduced. Four topologies were chosen from Hall and Wilson linearized models to investigate how the degrees of fidelity affect different shared mooring topologies. The shared mooring topologies were adapted to VolturnUS-s, a 15 MW semi-submersible floating offshore wind turbine.

These results show that simplifying the wind as a thrust force gives adequate results, and it is possible to further extend the model for a better fit. Since the thrust force where modeled in a global reference frame, it has some problems with large yaw motions, but this could be corrected in an improved model. Nevertheless, a complex shared mooring system is very stable for yaw motions. Also, a one-hour simulation was too short, as the natural periods in the surge motion are long. It is therefore proposed to run three-hour simulations.

Quasi-static mooring gives adequate results for shared mooring line tension and floater motions, but it is important with a good estimation of minimum and maximum tension for each mooring line since SIMA minimum tension is not designed for shared mooring systems. The tension in upwind mooring lines could have been better for some analysis.

Today engineering tools such as Turbsim and Mannsim are used to generate synthetic wind fields to evaluate the dynamics and performance of wind turbines. The synthetic wind fields are validated with experiments but on a limiting scale. It is, therefore, important to compare the synthetic wind fields with experimental data to evaluate if the difference is important for floating offshore wind turbines. The LES standard deviation in sway and pitch was larger than the Mann turbulence generator. The motions were underestimated in Turbsim since the standard deviation in the u-component of wind was calculated to low.

Taylor's frozen turbulence hypothesis is important in aerodynamics, especially for shared mooring systems, as simulations use this hypothesis. The frozen turbulence did correspond well with real turbulence and was conservative in yaw, with little difference in pitch. Also, there was little difference in the mooring tension, but frozen turbulence was not conservatively close to the rated wind speed. It is expected that the difference between frozen and real turbulence could be significant for low wind speeds with high turbulence intensity and larger wind turbines as the necessary distance between the floaters has to increase.

Sammendrag

Flytende vindturbiner til havs kan være en nødvendighet for å redusere utslippene ettersom mer av den produserte energien må komme fra fornybare ressurser. Også med høyere levestandard og industrialisering av samfunnet er det nødvendig med økt energiproduksjon. Vindturbiner sin størrelse har økt de siste årene, da det fortsatt er økonomisk å øke størrelsen. De siste årene har konfliktnivået mellom lokalsamfunnet og vindturbiner økt ettersom vindturbinene har blitt større og mer utbredt. Med å flytte vindturbinene på havet kan konflikt med lokal samfunnet unngås.

Havvind kan også bli en nødvendighet ettersom grunne havområder med høykvalitets vind er allerede utbygd. Derfor kan det bli en nødvendighet for bransjen å bygge flytende havvind ettersom hav dybden blir større, konkurransen minker ettersom det er flere felt å velge mellom og større fleksibilitet til å velge områder med høykvalitets vind. Et problem med å bygge flytende vindturbiner på dypt vann er at kostnaden til fortøyning systemet er betydelig. Derfor har mange forskere foreslått delt forankring, for å senke investeringskostnaden til forankrings systemet ettersom mindre kjetting og færre ankere er nødvendig. Felles forankring kan være av spesiell interesse for mange nasjoner siden vanndybden er dyp for mange kystlinjer.

Delt fortøyning er et konsept der flytende havvindturbiner kobles sammen med fortøyningsliner. Den delte fortøyningslinen reduserer lengden og antall ankere per vindturbin.

Det er gjort få studier på delt fortøyning, ettersom det er få analyseverktøy som kan analysere delt fortøyningssystem til flytende havvind. Det største problemet er at program varer er inkompatibel med flere kontrollsystem i samme modell. Dette er et stort problem ettersom kontroll systemet regulerer vindlastene og derav dynamikken til vindturbinen. Et annet problem er at kjøre tiden øker betraktelig med flere forankringssystemer og vindturbiner i samme modell. Vindlastene er av spesiell interesse ettersom de øker simulering tiden betraktelig. Lengre simulering tid for delt fortøyning enn flytende havvind er et problem ettersom design iterasjon tar lengre tid. Dette øker kostnadene for prosjektering av systemer med delt fortøyning. Det er derfor viktig å sammenligne ulike numeriske modeller med ulik nøyaktighet for å undersøke om analysetiden kan reduseres, uten stor tap av nøyaktighet. Fire forankrings modeller ble valgt fra Hall og Wilson for å undersøke hvordan delt fortøyning påvirker dynamikken til systemene og om modeller med lavere nøyaktighet gir ett godt svar uavhengig av fortøyningsgeometri.De delte fortøyningstopologiene ble tilpasset VolturnUS-s, en 15 MW halvt nedsenkbar flytende havvindturbin som er utviklet av NREL.

Resultatene viste at å forenkle vinden som en kraft gir tilstrekkelige resultater, og det er muligheter til å forbedre metodikken til å gi enda bedre overensstemmelse. Siden kraften ble modellert i et globalt referansesystem, har den noen problemer med store gir bevegelser. Dette kan korrigeres i en forbedret modell hvor kraften er i et lokalt referansesystem. Det kan være at dette problemet er mindre for komplisert delt fordøyingssystem ettersom gir bevegelser er mer stabile. Resultatene er også veldig påvirket av resonans ettersom analysene er bare en time, og den naturlige perioden er lang. Derfor burde det blitt kjørt tre timers simulering istedenfor.

Kvasi-statisk fortøyning gir tilstrekkelige resultater for delt forankringsliner og flytebevegelser, men det er viktig med gode spenningsestimater ettersom modellen er sensitiv på dette. I SIMA blir minimumspenning valgt for systemet, men den er ofte ikke tilstrekkelig. Det er derfor viktig å sette et fornuftig maksimum og minimum spenning i hver av linene. Spenningen i

motvinds fortøyningsliner kunne vært bedre for noen analyser, ettersom de er mest sensitive på modellerings valg.

I dag brukes ingeniørverktøy som Turbsim og Mannsim til å generere syntetiske vindfelt for å evaluere dynamikken og ytelsen til vindturbiner. De syntetiske vindfeltene er validert med eksperimenter, men i begrensende skala. Det er derfor viktig å sammenligne de syntetiske vindfeltene med eksperimentelle data for å vurdere om forskjellen er viktig for flytende vindturbiner til havs. De syntetiske vind filene var sammenlignet med ≪Large eddy simulation≫ som er et høy ordens analyse verktøy. Resultatene viste at standardavviket i svai og trim var større for LES enn de syntetiske vind feltene. Den syntetiske vindfelts modellen Turbsim, underestimerte alle bevegelsene siden standardavviket i u-komponenten til vinden var mindre enn det som var bestilt. Derfor er det vanskelig å sammenligne Turbsim med LES ettersom premissene er galt. I tidligere forskning hadde Turbsim større bevegelser i jag og trim, og mindre gir og svai enn Mannsim.

Taylors frosne turbulenshypotese er viktig innen aerodynamikk, spesielt for vindturbin felt og delte fortøyningssystemer, da simuleringer bruker denne hypotesen. Hypotesen antar at turbulensen forandrer seg ikke, for små avstander når vinden propagerer i rommet. Den frosne turbulensen samsvarte godt med ekte turbulens og var konservativ i giring, med liten forskjell i trim. Dessuten var det lite forskjell i fortøyningsspenningen, men frosne turbulensen var ikke konservativt nær den nominelle vindhastigheten. Det forventes at forskjellen mellom frossen og ekte turbulens kan være betydelig for lave vindhastigheter med høy turbulensintensitet og større vindturbiner ettersom nødvendig avstand mellom flyterne må øke. Ettersom vindfeltene som ble simulert hadde høy hastighet og lav turbulens intensitet, ble forskjellen liten i bevegelse, men observerbar. Det er derfor viktig med flere studier på frossen turbulens, ettersom det kan påvirke dynamikken til flytende vind med delt fortøyning.

Nomenclature

BEM	Blade Element Momentum
CAA	Constant Average Acceleration
CFD	Computational Fluid Dynamics
COG	Centre of Gravity
DLF	Dynamic Load Factor
DNS	Direct Numerical Simulation
DOF	Degree of Freedom
FE	Finite Element
Floater	Semi submersible
FOWT	Floating Offshore Wind Turbine
FWT	Floating Wind Turbine
GDW	Generalized Dynamic Wake
KC	Kaulegan-Carpenter
LES	Large Eddy Simulation
MDOF	Multiple Degrees of Freedom
NREL	National Renewable Energy Laboratory
NS	Navier-Stokes Equation
NTM	Normal Turbulence Model
PSD	Power Spectral Density
QTF	Quadratic Transfer Function

RAO	Response Amplitude Operator
RAO	Rotor Nacelle Assembly
TIMESR	Point Measurement Based Model
TLP	Tension-Leg Platform
ULS	Ultimate Limit State

Contents

List of Figures

List of Tables

Chapter 1

Introduction

The European Climate Law sets an intermediate target for 2030, reducing at least 55% of net greenhouse gas emissions compared to 1990 levels, and in 2050 the European states should be climate neutral. Today Europe's energy mixture is mainly fossil fuels. According to the European Union, 17.4% of the energy mix comes from renewable energy, and 12.7% comes from nuclear power. According to the DNV energy transition report, wind, solar, and hydropower production have to increase drastically to achieve FN and European Union's climate goals and meet the need for increased energy consumption due to decarbonization and increased world population, Figure 1.0.1, [2], and [3]. According to DNV 2022 energy transition report, Norway is not on schedule to meet its climate goals, and few actions have been taken to create an energy shift. Most of Norway's emissions come from heavy industry, heavy transport, oil and gas, and agriculture due to hydropower's low carbon intensity, which dominates the electrical grid. The change from fossil cars to battery electric vehicles (BEVs) has decarbonized the transport sector. Still, few actions have been taken to electrify heavy industry and the oil and gas sector.

According to DNV 2022 energy transition report, Norway's greenhouse gas emissions (GHG) should be reduced by 25% by 2030 and 70% by 2050. This shows a development far behind the political ambitions. Figure 1.0.1 shows that Norway's energy demand is increasing from today's level. Historically, Norway has had sufficient energy resources for normal years, but an increasing energy demand could threaten the energy surplus, even though population growth has decreased. Since 2008 energy efficiency has counteracted population growth until now. Due to the electrification in society, energy consumption is expected to increase, but with improved technology and population decay, the energy need could be stabilized. According to Figure 1.0.1, Norway's increased energy production will mainly come from floating offshore wind, fixed offshore wind, and onshore wind, which ensures sufficient energy production and exportation. According to DNVs predictions, export revenues from power and hydrogen will only be a fraction of today's oil and gas production in 2050. Oil exports will only be around 5% of today's level since many existing fields will end their life. If today's oil and gas revenues are going to be replaced, it is necessary with a massive development of wind and hydrogen. Today's development of wind and hydrogen is far from the emission goals and maintaining Norway's high energy revenue. Therefore research on offshore wind is crucial for the economy, energy safety, and environment.

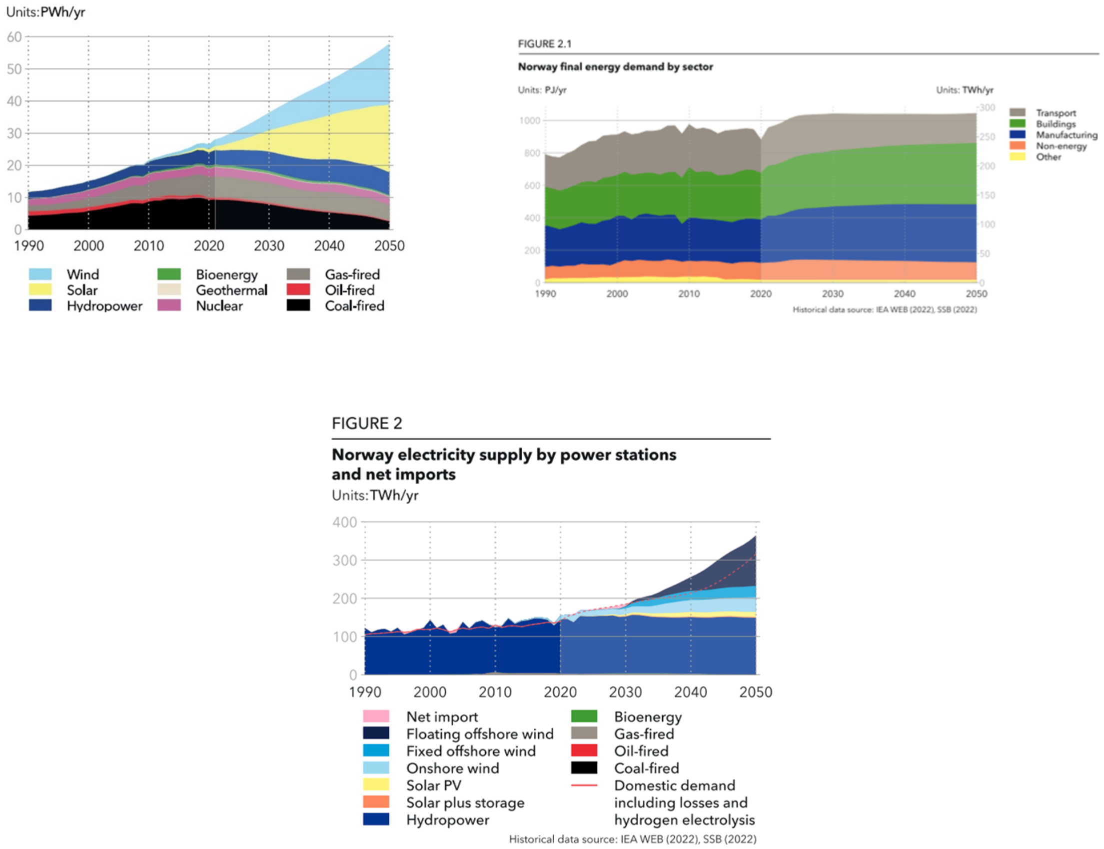

Figure 1.0.1: DNV energy transition report - Norway electricity supply [2],[3]

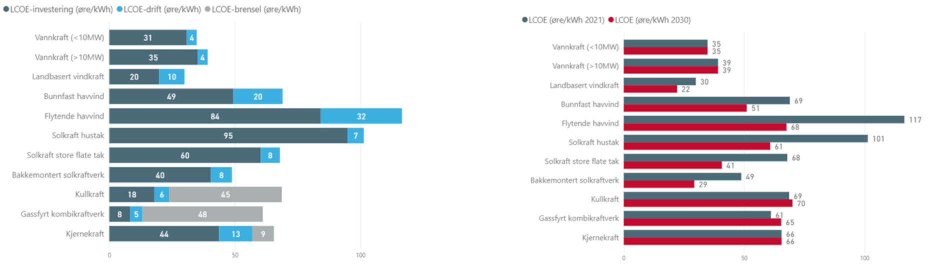

Figure 1.0.2: Levelized cost of energy - LCOE[4]

Figures 1.0.2 are estimates from NVE - Norway's water and energy directory, which uses, NVE long-term power analysis, finance directorate, SSB, and energy reports. The report separates wind energy into three categories: onshore, fixed, floating offshore wind, and investment versus operation cost. Also, an estimate for the development in energy prices for different technologies is given in 2030 in today's currency. Fossil prices are the main contributor to high electricity prices, as the infrastructure and operation costs are low. In estimation, fuel prices remain high since there are fewer suppliers and little technological change. Also, regulative power demand will increase as more renewable energy is connected to the grid. Today onshore wind is the cheapest energy, and in 2030 floating offshore wind will be cheaper than fossil fuels. The main disadvantage of wind power production versus fossil production is the ability to regulate power production to meet the needed energy production. Even though renewable energy will be cheap and cleaner, storage solutions are necessary to phase out regulatory power.

More wind turbines are installed in the ocean space, mainly bottom fixed, but floating offshore wind in shallow waters has grown in popularity due to less ideal areas for fixed wind turbines. Floating offshore wind has its main advantage due to its flexibility; it is not as depth restrained as bottom fixed is. Higher wind velocities and less turbulent wind often occur for larger distances to shore, meaning higher power production. Also, offshore wind is not restrained by infrastructure. Therefore, up-scaling is only restricted to lifting capacity. Figure 1.0.3, and 1.0.4 shows the bathymetry in Europe and the North Sea. This shows that most of Europe's water depth is above 60 m, meaning bottom fixed wind turbines has a limitation in their potential. Also, Figure 1.0.5 and 1.0.6 show the mean annual wind speed for Europe and the North Sea. By combining all four Figures, it can be seen that wind speed does increase for deeper water. According to the equation, 1.0.1 power density in the wind is proportional to the third to mean wind speed. This means that deeper water indirectly increases electrical production in many areas assuming that the turbine can handle the wind loads. Equation 1.0.1 relates the wind speed u to the power output P_0, where A is the area, and ρ the density to air.

$$\frac{P_0}{A} = \rho \frac{u^3}{2} \tag{1.0.1}$$

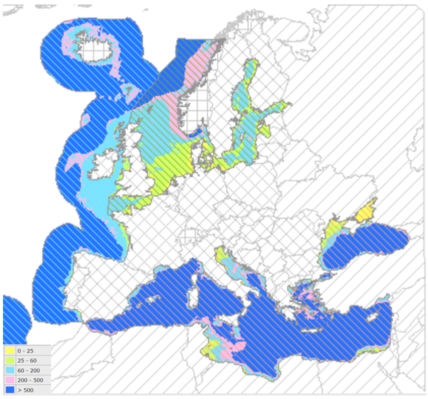

Figure 1.0.3: Europe water depth

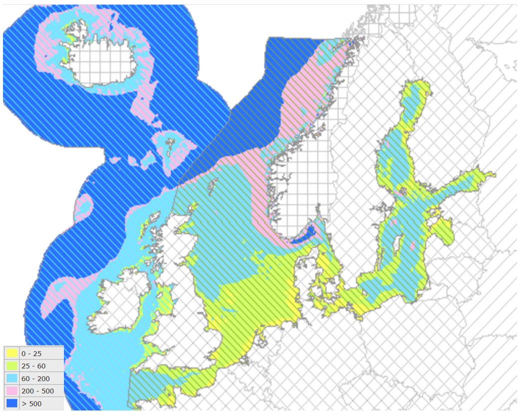

Figure 1.0.4: North sea water depth

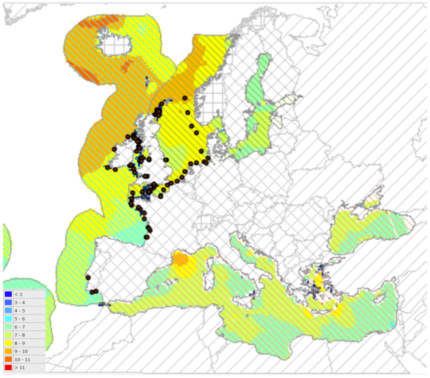

Figure 1.0.5: European mean wind speed

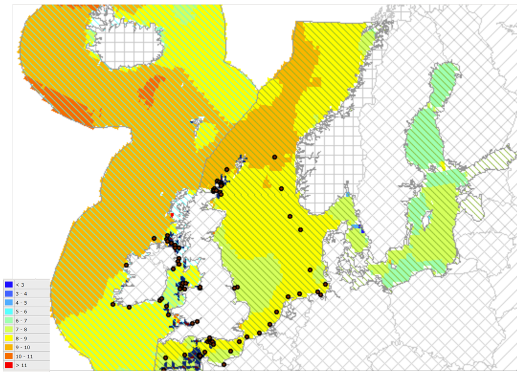

Figure 1.0.6: North sea mean wind speed, [5]

Bottom-fixed wind turbines are only suitable in shallow waters, typically 50-60 m in depth, depending on the structure. Typically bottom fixed structures are monopile, GBS - gravity-based structures, tripod, jacket, and tri-pile. In deeper water, the investment cost is substantially increased for bottom-fixed wind turbines, and floating structures are necessary. There are several solutions to floating offshore wind turbines. Common marine floating structures are TLP, semi-sub, and spar.

Investment costs mainly drive upscaling of wind turbines. Installation, operation, mooring system, engineering, maintenance, turbine, etc are all costs that are very much the same, disregarding the size of the wind turbine. Therefore, upscaling wind turbines is profitable even though the structure gets more expensive compared to the revenues. Upscaling has an additional positive effect. As the size increases, the hub height of the wind turbine gives access to higher mean wind speed due to the wind profile power law. Wind turbines differ from the oil and gas sector, where few floaters are needed, and therefore, not many mooring lines are needed. For floating wind, it is necessary with one floater per wind turbine, as the wake will affect the performance. Therefore mooring systems will have great economic importance when designing floating wind turbines.

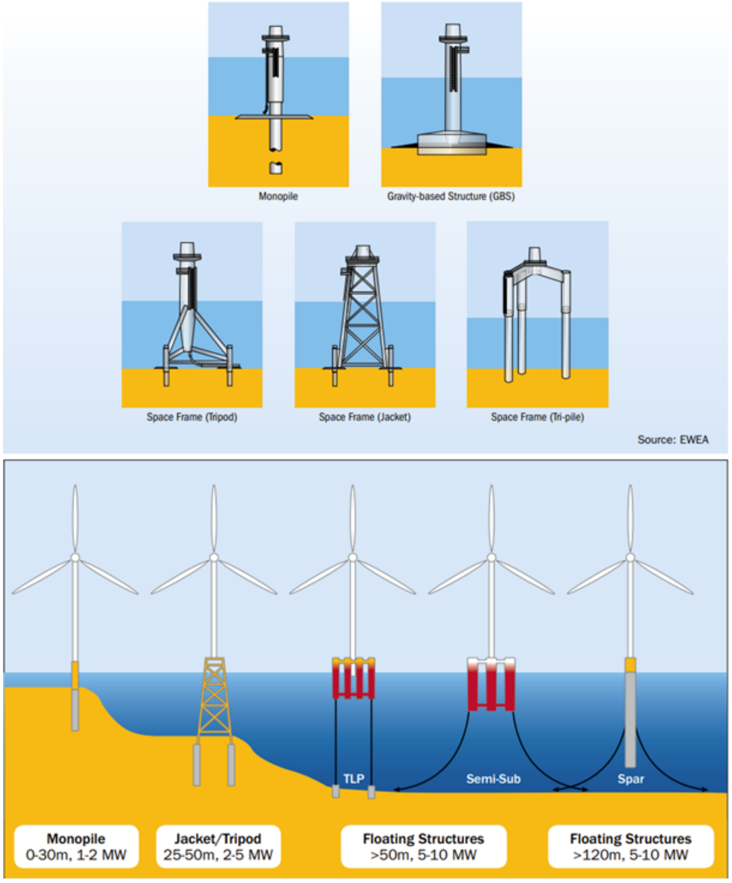

Figure 1.0.7: Illustration of bottom fixed and floating wind turbine structures [6]

1.1 Objective

As offshore wind moves further into deeper water for licenses, less competition, and ideal wind, the relative cost of mooring systems gets higher. Lowering the mooring cost will significantly impact the total investment cost of deep water floating offshore wind. In many articles, shared mooring has been proposed to lower the investment cost, and a few studies have been carried out to look deeper into the consequences of shared mooring. Shared mooring is a concept in which floating offshore wind turbines are connected together by mooring lines. The shared mooring line reduces the length and the number of anchors per floater. Since the mooring lines are connected between FOWT and not only to the seabed, the tension in the shared mooring line is affected by the motions of each other. Therefore the horizontal stiffness of the FOWT is not only dependent on the stiffness relation to displacement but also the relative displacement to each other.

Few studies have been conducted evaluating the dynamics of shared mooring systems. Hall [7] and Goldschmidt [8] looked into the economic potential of the shared mooring by using simplified models. Goldschmidt concluded that there was substantial economic potential, but there is a limit to how many platforms can be connected due to the thrust accumulation. Hall compared different systems with water depth and did figure out that water depth is crucial when looking into the economy of shared mooring. The conclusion was that shared mooring became profitable at around 400 m depth for several shared mooring topologies. Therefore the water depth is 600 m in this thesis, the same as for Wilson and Hall [9]. Wilson and Hall made a simplified method by using linearized mooring stiffness in surge and sway, and found optimized shared mooring topologies [9].

Today few analysis tools can analyze shared mooring systems for floating offshore wind, as the programs are incompatible with several control systems. Another issue is that several wind turbines must be analyzed in the same system, increasing analysis time. With long simulations and few tools to analyze shared mooring, it is difficult to design an optimal system. Therefore, several numerical models of different fidelity must be investigated to evaluate if the analysis time could be reduced. Four fidelity models have been investigated. 1) Turbulent wind with RIFLEX mooring, 2) simplified wind with RIFLEX mooring, 3) simplified wind with quasi-static mooring, and 4) simplified dynamic model in Python. Four topologies were chosen from Hall and Wilson linearized models to investigate how the degrees of fidelity affect different shared mooring topologies.

Today engineering tools such as Turbsim and Mannsim are used to generate synthetic wind fields to evaluate the dynamics and performance of wind turbines. The synthetic wind fields are validated with experiments but on a limiting scale. It is, therefore, important to compare the synthetic wind fields with experimental data to evaluate if the difference is important for floating offshore wind turbines with and without shared mooring. Since there are limited experimental data, Large-eddy simulations are used in comparison with the synthetic wind files in this master thesis. Taylor's frozen turbulence hypothesis is well-used in aerodynamics but simplifies the turbulence structure in the wind. The frozen turbulence hypothesis assumes that the turbulence in the wind does not change spatial. This hypothesis is important for wind parks and shared mooring systems as it could affect the performance of the systems. Therefore, the frozen turbulence hypothesis is investigated using data for large-eddy simulation in two spatial coordinates and evaluating if the system behaves dynamically the same.

1.2 Structure

For a more straightforward overview, the structure of the thesis is addressed in the following section:

- The literature study is presented in Chapter 2, where articles about shared mooring and wind modeling are presented.
- Chapter 3 provides an overview of the theoretical foundations of the master's thesis.
- Chapter 4 explains the approach and decisions made throughout the modeling process.
- The static performance of the shared mooring topologies and natural periods are discussed in Chapter 5.
- Results from verifying the simplified wind and mooring model are presented in Chapter 6.

- Chapter 7 addresses dynamic comparisons between shared mooring topologies and cost estimation.
- A wind turbulence study comparing synthetic wind fields, LES, and frozen turbulence assumption is carried out in Chapter 8.
- Chapter 9 contains the conclusion and recommendations for future research.

Chapter 2

Literature

2.1 Shared mooring

Wilson and Halls's article [9] shows that shared mooring could reduce mooring line length and anchor quantities. Wilson and Hall have designed several shared mooring systems by an optimization algorithm that optimizes the mooring line weight with an offset constraint considering all wind directions. In the optimization algorithm, a linearized mooring system has been used.

Goldschmidt and Muskulus [8] have simulated three systems with shared mooring, using both time domain and frequency domain calculations to look deeper into the dynamic phenomena that occur for the different coupled systems. Previous studies have shown a thrust accumulation in the shared mooring system on the upwind mooring system, which where also identified in this study. The article focuses on row (one, five and ten FOWT), triangular (three FOWT), and rectangular (four FOWT) arrangement, where only row arrangement has been looked into by simplified one-dimensional time domain simulation. Irregular waves have been applied to the system using the Morison equation, wave drift and wind forces. The diffraction effect has been estimated by the use McCamy-Fuchs big volume diffraction model. The model is only precise for cylinders with linear waves. Simulations have been carried out for four operational conditions and one extreme condition. The calculations are carried out for a simplified DeepC semi-submersible model. The mooring system is modeled by the catenary equation and irregular waves by JONSWAP wave spectra. Second-order effects have been taken care of by using Newman‘s approximation.

The conclusion to the article is that 60% of the mooring cost is possible to save, giving a total cost reduction of 8% for the entire system. The cost comparison is based on the mooring chain diameter, length, and anchor cost corresponding to the loading. Cost advantages for shared mooring are reduced for higher numbers of turbines since the static loads are transferred to the upwind floater, causing a thrust accumulation effect. Therefore the system needs more stiffness, which demands more material.The maximum total saving is 8% for the total system, but this is only for depths of 200 m. Therefore, larger savings for deeper depths are possible since the mooring and anchor costs will increase for deeper waters.

Connolly and Hall have also looked into the potential cost saving for reducing mooring weight and the influence of the displacement [7]. Connolly and Hall mention the same cost advantages with shared mooring and the wind farm's footprint that can be lowered by using less sea space and seabed. The analysis uses a quasi-static model considering steady wind thrust forces, nonlinear mooring line, and four different water depths. The article's main focus is how the system's performance and cost are affected by water depths, testing out three different layouts; see Figure 2.1.2.

All systems are equally spaced with a distance of 1260 m, 10 rotor diameters, and displacement is maximum 20 m. Anchor spacing, mooring length and weight correspond to the original mooring system to DeepCwind, which has a maximum of 20 m displacement. For the design algorithm, linear force-displacement calculates the restoring force. For anchor spacing, line length, and weight quasi-static mooring line has been used (adapted catenary equation from FAST). The shared mooring length is 1280 m giving a small catenary shape. Strength requirements are also scaled based on the original mooring system. The cost estimate for the mooring line is linear with length and maximum line tension. Anchor cost is estimated for drag anchors as a linear model, proportional to the maximum force on anchors and constant contribution per anchor. All shared mooring systems are beneficial for depths larger than 400 m. Line tension is always the highest for square 2, see Figure 2.1.2 since the system has only one anchored mooring system per floater, and the tension will therefore be less distributed than for systems with two or three anchored mooring lines. Line tension is generally low for square 3. According to Halls model, line tension increases rapidly with mooring depth, making the shared mooring system less profitable than Goldschmidt and Muskulus. Tension is assumed proportional with linear density to the mooring line. Anchor cost is not dependent on water depth but only anchor tension. Herefore, square 1 only saves a little expense, according to Hall, in saving one anchor per floater. Also, the mooring systems do not fulfill the maximum displacement criterion for lower depth, meaning the actual would be higher. For the 800 m mooring system, the relative savings are from roughly around 17% to 25%. The model is conservative, according to Hall, meaning the potential cost saving could be even higher.

Liang, Jiang and Merz is using another approach by evaluating the dynamics of two FOWTs with one shared mooring and four anchored mooring lines 120 degrees from each other, see Figure 2.1.3.

The model uses the OC3 Hywind, a spar, catenary equation using a multi-segment design where the mooring stiffness, dynamics, and current effects are neglected in the mooring lines. One part of the mooring line is chains that have nonlinear geometric stiffness from the weight of the cable, and another part is rope using its elastic stiffness. Hydrodynamic properties from WADAM are used to calculate the eigenvalue and time domain solution. The mooring system is linearized around a static position. A unit deflection in all DOF finds the change in mooring stiffness. The system has a water depth of 320 m, and uses environmental data from "Norway 5". One operational wind-dominated case and one extreme loading condition for a wave-dominated case are considered. The system is optimized to reduce the mooring cost for chain and wire, using a maximum offset of 20 m. Dynamic analysis is carried out in SIMA using RIFLEX. There is a small difference in the natural period between the linearized model and decay test in SIMA, 1% to 6%, depending on the mode shape.

The article discusses that the error may come from either a simplified Irvines method (catenary equation), mass distribution, nonlinearities, or data extrusion error. The coupling significantly affects natural periods in sway and surge direction since all stiffness in this direction comes from the mooring system. Also, the sway, which is normal to the shared mooring, is affected by the diameters since changes in tension influence the sway tension.By increasing the density/diameter of the shared mooring, the floaters get closer together (since the total mass increases), stiffness contribution from the anchored line increases, and shared mooring decreases. Natural periods in surge and sway are also affected by choice of the wire due to a change of static position. Longer wire with a smaller diameter has less stiffness. Since the shared line is almost perpendicular to the surge, coupling effects are limited. The conclusion of the article is that natural periods for surge and sway are sensitive for mooring properties for shared and anchored mooring. Low natural periods are possible in sway and surge direction due to the shared mooring and should therefore be analyzed with great care.

Gozcu, Kontos, Bailey and Rambøll looked into shared mooring systems for three different locations [10] testing out concepts for one shared mooring 200 m, shared anchor 870 m depth, and four turbine layout with shared mooring 870 m depth. The analysis is carried out with Orcaflex, focusing on anchor loads and natural periods. The model used is the spar WindCrete. The use of shared anchors could be a conservative introduction to the shared mooring, lowering fabrication, transportation, and installation cost for several anchors. Shared anchors lead to several challenges with sizing, monitoring during installation, a higher consequence for failure, less flexibility in anchor positioning, and increased cost for anchor refusal since two mooring lines are affected. Hydrodynamics are calculated by Morison drag and WAMIT. Aerodynamic analysis with aero-servo-hydro-elastic analysis is performed in HAWC2 with Timoshenko beams (calculates the real shear stresses for a beam).

Dynamic mooring line formulation is based on nonlinear beam elements using green strain. The first system is analyzed with two different shared mooring line lengths. The shared mooring length will decide the system's static position. For the longest line, the stiffness gets reduced, leading to the systems going 13.58 m away from each other, versus for a shorter line, they get 23.6 m closer. Buoyancy elements can prevent this. The longest line system has a lower first natural frequency than the original system. (longer line, less stiffness, therefore lower frequency). Shorter mooring line results in a higher first natural frequency due to higher stiffness. For configuration two, shared mooring is added by the use of delta lines with polyester lines connected to the chain. Buoyancy elements are added to see the influence on the dynamics. Five different cases are run for different buoyancy elements and shared mooring lengths. The buoyancy elements affect the stiffness in the system and added mass from hydrodynamics. Buoyancy elements influence little the natural period since the added mass and increased stiffness contributions cancel each other out. A very large buoyancy force is needed to see any effects, which increases the element's volume and decreases the effect. Therefore it is practically difficult to use buoyancy elements to influence the natural periods. Natural frequencies can be controlled without changing the stiffness of the anchored mooring system by disturbing the mode shapes with the shared mooring tension by changing the total length. By the use of a 13 m shorter line, 2MN extra tension are in the shared mooring, giving a 33% higher natural frequency due to the extra stiffness. For this model, there are results in the 1P region for the wind turbine, something that should be avoided. Mooring line tensions are very similar to the single turbine case

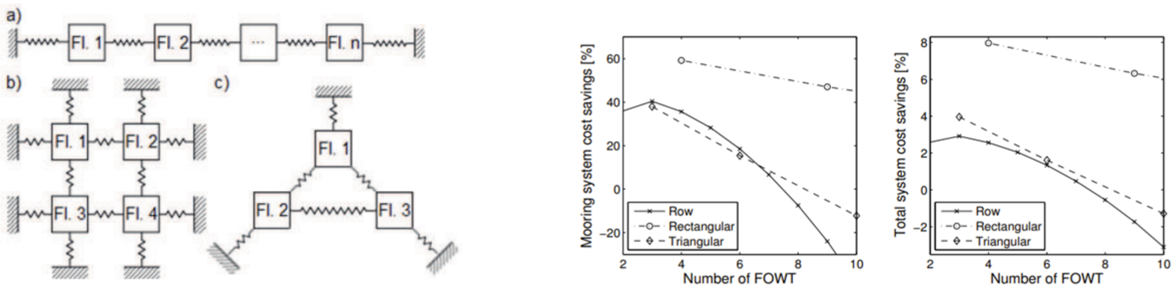

Figure 2.1.1: Wind farm configurations and cost saving potential Goldschmidt [8]

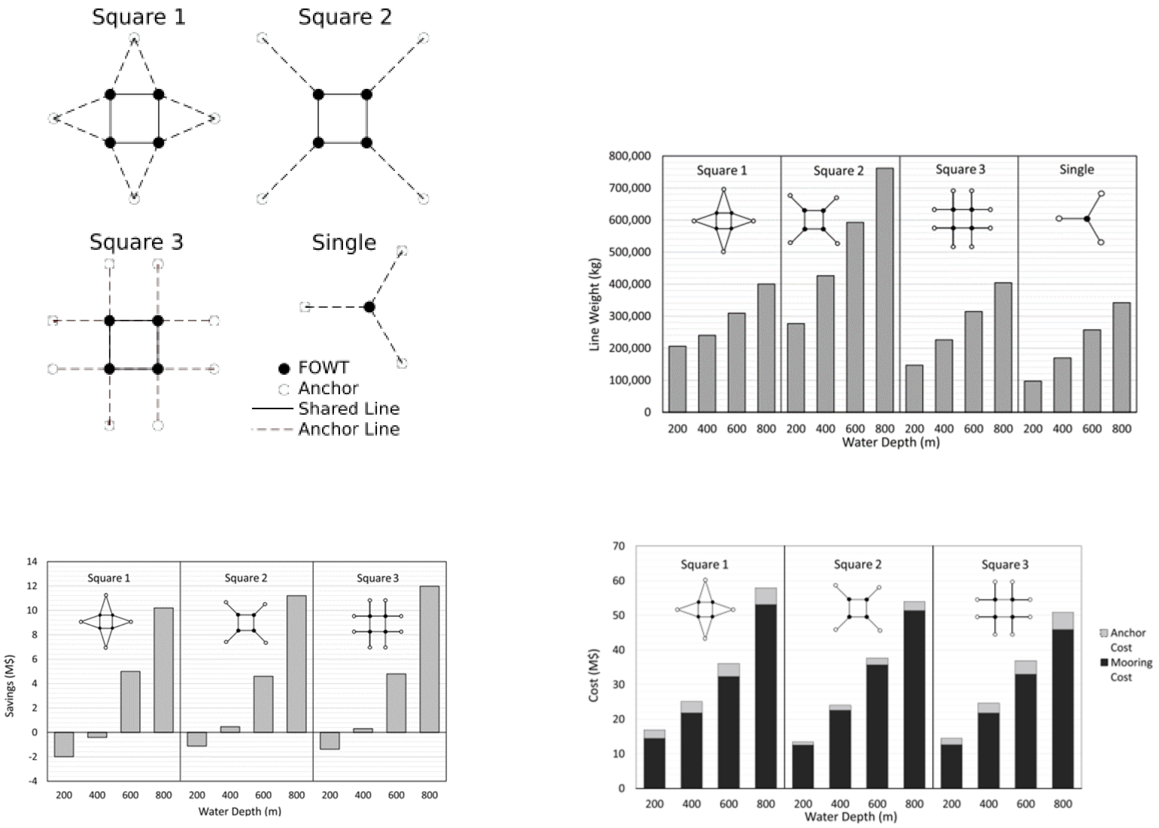

Figure 2.1.2: Wind farm configurations and data for each system Connolly and Hall[7]

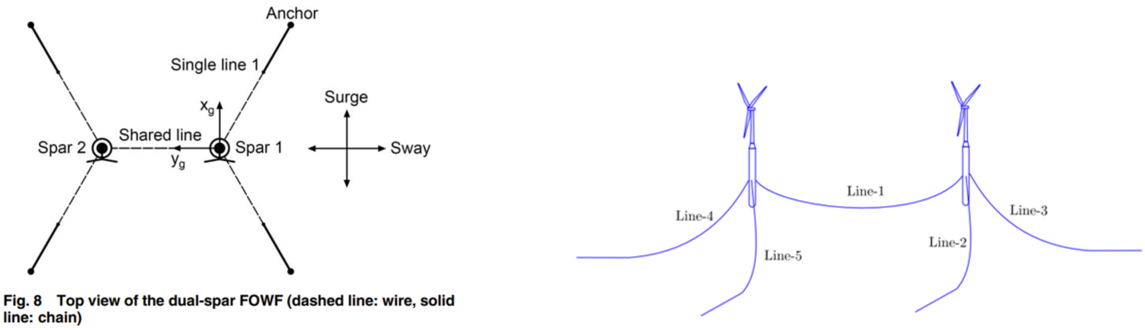

Fig. 8 Top view of the dual-spar FOWF (dashed line: wire, solid line: chain)

Figure 2.1.3: Wind farm configurations Liang, Jiang and Merz [11] and wind farm configuration system 1 Goscu [10]

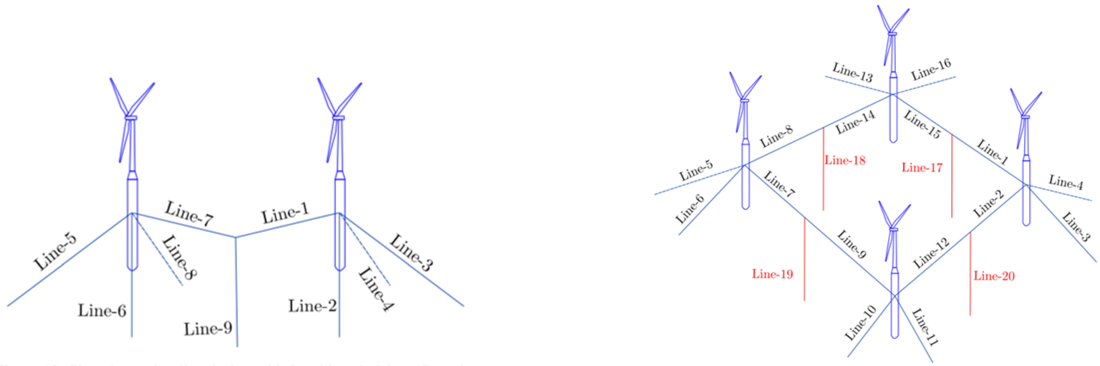

Figure 18: Shared mooring line design with 2 turbines in Morro Bay site

Figure 33: Shared mooring line design with four turbines in Morro Bay site

Figure 2.1.4: Wind farm configurations Gozcu [10]

2.2 Aerodynamics

Irene et al. have been evaluating the effects of atmospheric stability on the structural response by modeling a 12 MW semisubmersible floating wind turbine with a dynamic global response model [12]. When designing floating offshore wind turbines, neutral atmospheric stability is assumed, which is only sometimes representative. It has been observed unstable conditions for low wind speeds. Therefore four atmospheric models are looked into: stable, neutral, under, and unstable. Several wind field models have been used:

- Exponential Coherence model (Kaimal)
- Kaimal spectrum
- Large-eddy simulation (LES).
- Mann spectral Tensor Model (Mann
- Point measured based model (TIMESR)

In the low-frequency range, turbulence and atmospheric stability influence the structural response. In unstable conditions, the response where higher than in neutral and under stable conditions. When the models were fitted to the meteorological mast, surge, and pitch were higher for TIMESR and Kaimal model and lower in yaw. The models were also fitted to LES. The predicaments were better, but yaw was still underpredicted. The opposite results were observed for Mann. Therefore the turbulence intensity and coherence in the models will affect the response. Atmospheric stability affects TI and coherence and should therefore be considered in the modeling of FOWT. Therefore the turbulence intensity and coherence in the models will affect the response. Atmospheric stability affects TI and coherence and should therefore be considered in the modeling of FOWT. Higher fatigue loads are observed in the blade root-out of plane moments for TIMESR and Kaimal than the Mann model for overrated wind speeds. In rated wind speed, the fatigue is almost the same. This agrees with previous studies [12].

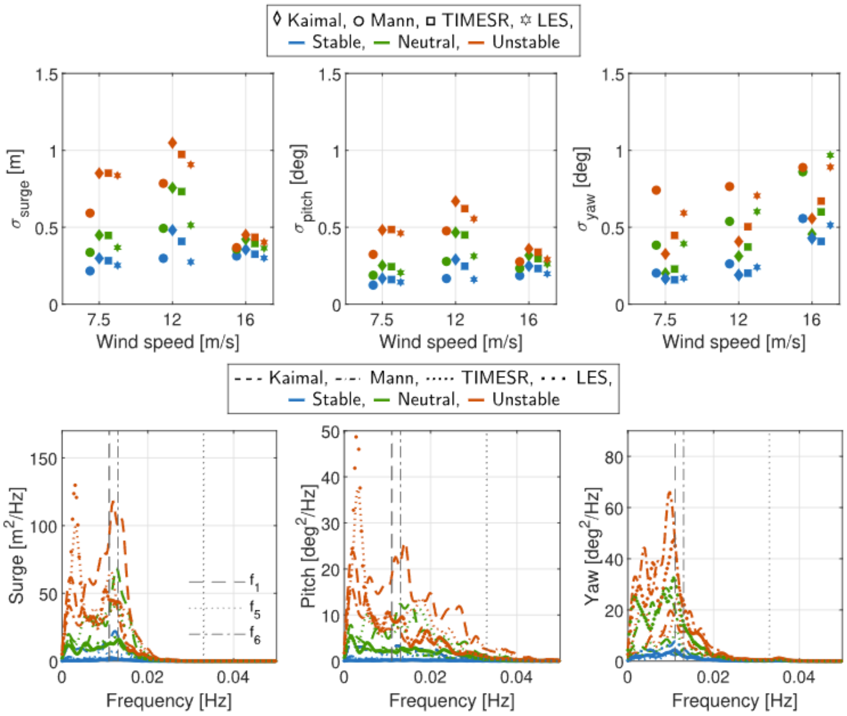

Figure 2.2.1: Average of standard deviation of surge, pitch, and yaw fitted to LES data. [12]

Eliassen and Bachynski have looked into how the response of floating wind turbines is affected by turbulence models by modeling two semi-submersible floating wind turbines, CSC 5 MW and 10 MW [13]. Three wind speeds have been investigated 8 m/s, 14 m/s, and 20 m/s, by both Kaimal and Mann models. Each wind condition is simulated with three different environmental conditions for waves. Second-order wave forces are calculated with Newman's approximation for the 5 MW and full quadratic transfer function for 10 MW wind turbine.

Design standards for wind turbines recommend using Mann or Kaimal model. Previous studies show that there is little difference in fatigue loads for bottom-fixed wind turbines, but some floating wind turbines have shown sensitivity to the chosen turbulence model.

The normal turbulence model is used according to the standard in calculations of the turbulence intensity. The wind mesh is generated with the same width, length, and nodes for all the cases with a time step of 0.1 s.

Kaimal turbulence model has a larger variation in tension than Mann, since the surge motion has a higher variation. For the highest wind speed, the wind frequency is not triggered by the surge natural period, and the Mann turbulence model generates more fatigue in the mooring line. Mann, however, has higher loads in the blade passing frequency, also known as the 3P frequency. Surge and pitch have a larger standard deviation response in surge and pitch. This is most likely caused by the coherence in the wind. Kaimal has an even-distributed coherence in all directions. On the other hand, the Mann model has a higher coherence in the horizontal direction. The Mann turbulence generator has a larger standard deviation in the other global motions, especially yaw.

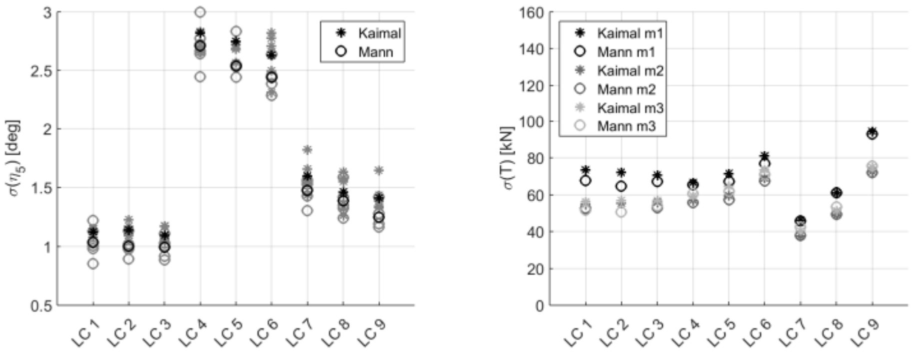

(a) CSC 5 MW (a) CSC 5 MW

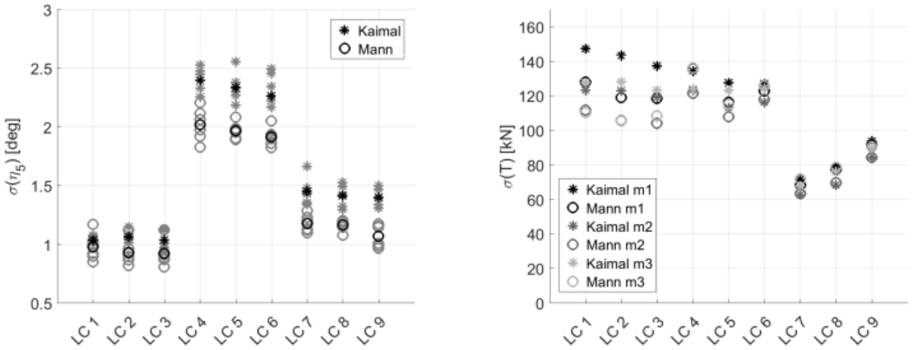

(b) CSC 10 MW (b) CSC 10 MW

Figure 2.2.2: Pitch motion and standard deviation of the mooring line tension for nine load cases. [13]

Nybø et al. have evaluated different wind field's effect on the dynamic response to floating offshore wind turbines [14]. The exponential coherence model, Kaimal spectral and Mann turbulence model has been compared to large eddy simulations constructed from offshore measurements.

The importance of realistic spatiotemporal distribution of wind fields has become more important in the latest year as the size of wind turbines has increased. The problem with today's turbulence generators is that they do not consider atmospheric stability.

Kaimal and Mann turbulence generators have been fitted to wind conditions by changing the turbulence intensity and the wind profile. 1-hour simulations are conducted. The DTU 10 MW wind turbine is used in the simulations.

All the methods had good results in unstable and neutral atmospheric conditions. The probability density functions are very similar for Kaimal and Mann turbulence generators and have a higher kurtosis and minimal skewness in comparison to TIMESR. The yaw motions did increase with less coherence, especially horizontal coherence, which is why the Mann turbulence generator has a higher yaw motion than Kaimal. Pitch is mostly dependent on the thrust force, and the local distribution of wind over the rotor disc is less important. A fully coherent wind field was run in comparison to Kaimal. Standard deviation in surge, pitch, and mooring line tension did increase with 84%, 38% and 27%. It was observed that yaw motions did increase with wind speed. Lower turbulence intensity caused a lower standard deviation.

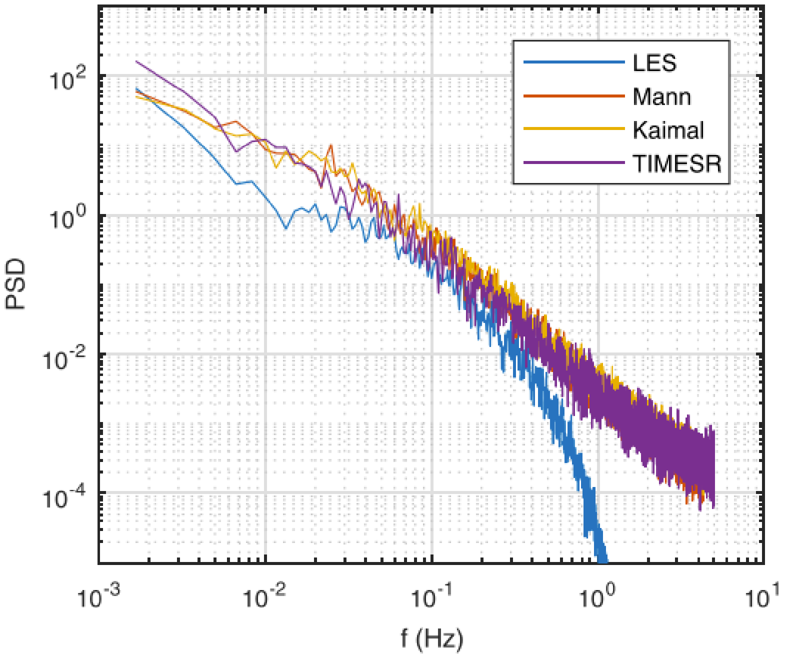

Figure 2.2.3: Energy spectrum at hub location of the neutral 12.5 m/s case [14]

Chapter 3

Theory

3.1 Dynamic analysis

In dynamic analysis, the force dependence is of importance [15]. This is in contrast to static analysis, where all the forces are calculated at the same time. The main differences between dynamic and static analysis are the time dependency of the force, damping in the system, and mass and stiffness could be frequency/ time dependent. A dynamic system is dependent on the DLF - dynamic load factor. The time dependency of the forces could cancel each other out or increase the loads. The DLF factor can therefore be separated into three domains, dependent on the natural period of the system: stiffness, resonance, and mass domain.

The equation of motion can be derived from Newton's second law, stating that the sum of forces equals the mass times the acceleration, where forces and acceleration are a vector, and mass is a scalar.

$$\sum \vec{F} = m\vec{a} \tag{3.1.1}$$

In a linear dynamic system, three effects are considered: mass, stiffness, and damping.

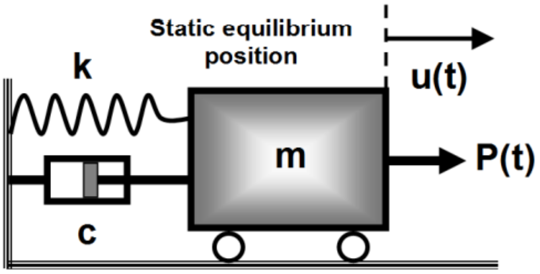

Figure 3.1.1: First degree of freedom - dynamic equilibrium [15]

$$m\ddot{u}(t) + c\dot{u}(t) + ku(t) = P(t) \tag{3.1.2}$$

The dynamic equilibrium is written as a 2-order differential equation of response to the system, from Newton's second law. $P(t)$ is an external load that excites the system. The external load on the body could act as a mass, stiffness, or damping effect, depending on the phase of the force.

$$F_{inertia} + F_{damping} + F_{restoring} + P(t) = 0 \tag{3.1.3}$$

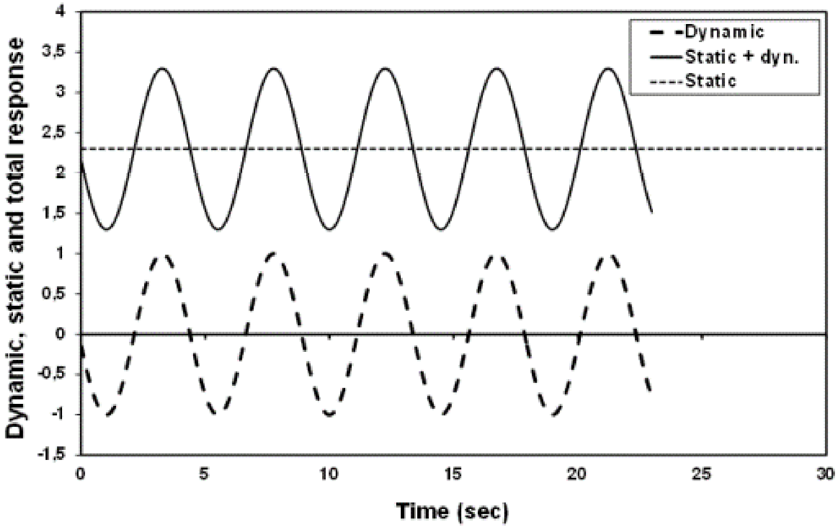

Figure 3.1.2: Static and dynamic decomposition [15]

Static analysis can be done by solving the stiffness matrix, which contains information about the local stiffness for rigid bodies and structural elements in a global system. Structural elements can be analytically derived, such as trusses and beams, but often the numerical method, FEM is used for more advanced elements to calculate the stiffness. Dynamic analysis is often more time-consuming compared to static analysis. Therefore is common to simplify the stiffness matrix to save computational time.

$$\boldsymbol{K}\boldsymbol{r} = \boldsymbol{F}_{external} \tag{3.1.4}$$

The natural frequency is defined as:

$$w_0 = \sqrt{\frac{k}{m}} \tag{3.1.5}$$

The natural periods of a dynamic system are of great importance as the external loads are amplified if the periods are close. When resonance is triggered, the most important parameter is the damping in the system, which limits the resonance.

$$T_0 = \frac{2\pi}{w_0} \tag{3.1.6}$$

The critical damping ratio defines the relative effect of the damping compared to the stiffness and mass of the system. A high critical damping ratio means that the damping in the system is high. Since damping radiates energy out of the system, a system with a high critical damping ratio would return faster to its natural state. There are no oscillations if the critical damping ratio is above one, but this is not common for marine systems.

$$\xi = \frac{C}{C_{critical}} = \frac{C}{2\ m\ w_0} \tag{3.1.7}$$

Figure 3.1.3 shows how damping is taking energy out of the system. Free decay SDOF can be expressed as:

$$u(t) = \exp^{-\xi w_0 t} R \cos\left(w_d t - \theta\right) \tag{3.1.8}$$

Sub-critical damping is a system where damping ratio $\xi < 1$

$$w_d = w_0 \sqrt{1 - \xi^2} \tag{3.1.9}$$

In theory, there is a difference between the damped natural frequency and the natural frequency, but in practice, the difference is negligible as the critical damping ratio is low for marine systems.

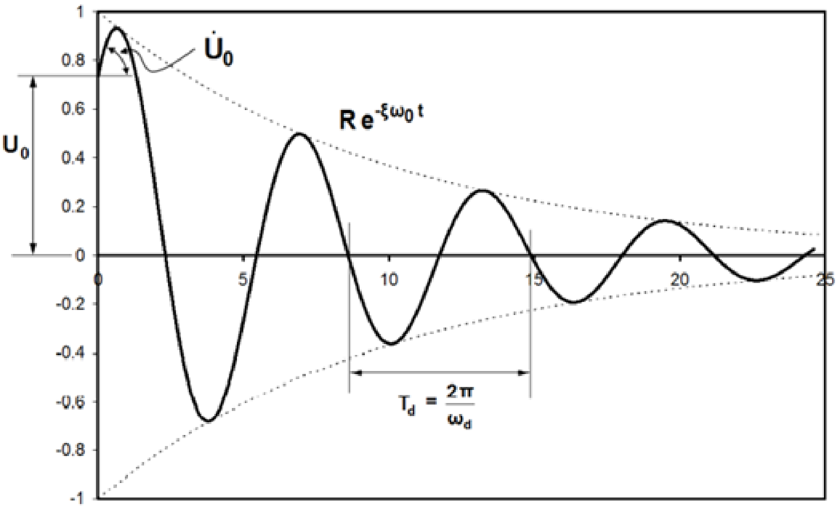

Figure 3.1.3: Free oscillated system with sub-critical damping [15]

3.1.1 Measurement of damping

Damping can be estimated by a decay test in SIMA. Firstly apply a constant force in the system until it reaches equilibrium. Secondly, the force gets shut down, meaning the system will try to reach equilibrium. Then it is possible to look at the oscillation to estimate the damping by assuming constant frequency.

By taking the difference between one peaks amplitude and divide it the next peak, damping can be estimated.

$$\frac{u_i}{u_{i+n}} = \frac{u(t_i)}{u(t_{i+nT_d})} = \mathrm{e}^{\xi w_0 (t_i + n\ T_d)} \tag{3.1.10}$$

logarithmic decrement;

$$\Lambda = \ln{(\frac{u_i}{u_{i+1}})} = \xi w_0 T_d = 2\pi \frac{\xi}{\sqrt{1-\xi^2}} \tag{3.1.11}$$

This equation can be approximated using Taylor expansion.

$$\sqrt{1-\xi^2} = 1 - \frac{\xi^2}{2} - O(\xi^4) \tag{3.1.12}$$

$$\xi \approx \frac{-2\pi + \sqrt{4\pi^2 + 2\Lambda^2}}{\Lambda} \approx \frac{\Lambda}{2\pi} = ln(\frac{u_i}{u_{i+1}})\frac{1}{2\pi} \tag{3.1.13}$$

Also damping ratio can be estimated by looking after n periods the amplitude. This will give greater accuracy for low critical damping.

$$\xi \approx ln(\frac{u_i}{u_{i+n}})\frac{1}{2\pi n} \tag{3.1.14}$$

Dynamic load factor - DLF can be found by evaluating the equation of motion 4.7.3 by complex numbers.

$$(-\omega^2 m + i\omega c + k)\tilde{x} = \tilde{P} \tag{3.1.15}$$

DLF can then be found by evaluating the maximum versus static response.

$$DLF = |\frac{u_{max}}{u_s t}| = \frac{1}{\sqrt{(1-\beta^2)^2 + (2\xi\beta)^2}} \tag{3.1.16}$$

$$\phi = \tan{(\frac{-2\xi\beta}{1-\beta^2})}^{-1} \tag{3.1.17}$$

$$|\tilde{x}| = \frac{P_0}{k} \times DLF \tag{3.1.18}$$

For a harmonic load, the particular solution to the one DOF differential equation can therefore be found as the maximum response from the dynamic load factor with the same frequency as the load applied and phase shift. Also an additional phase shift due to damping is introduced. The homogeneous solution will die out and the stationary solution will dominate as long as the system has damping.

$$u_p = |\tilde{x}| cos(wt + \alpha + \phi) \tag{3.1.19}$$

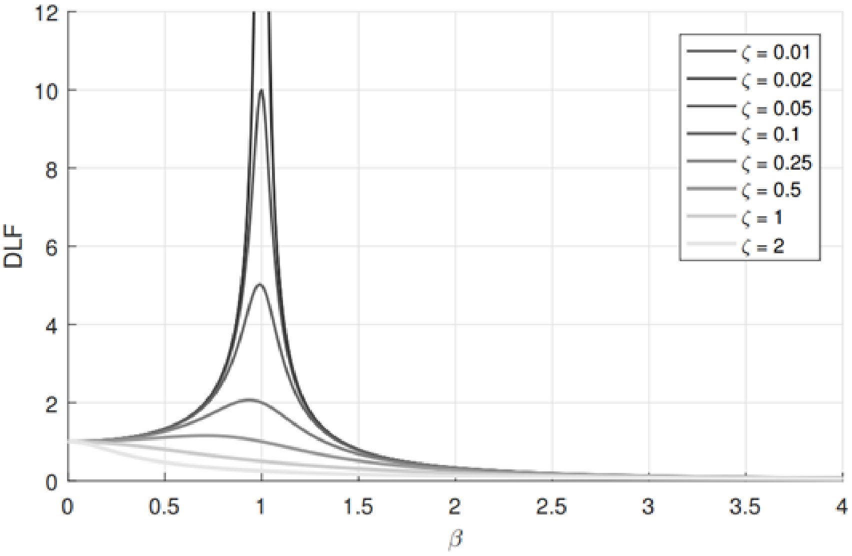

Figure 3.1.4: Frequency ration versus DLF for several critical damping values [15]

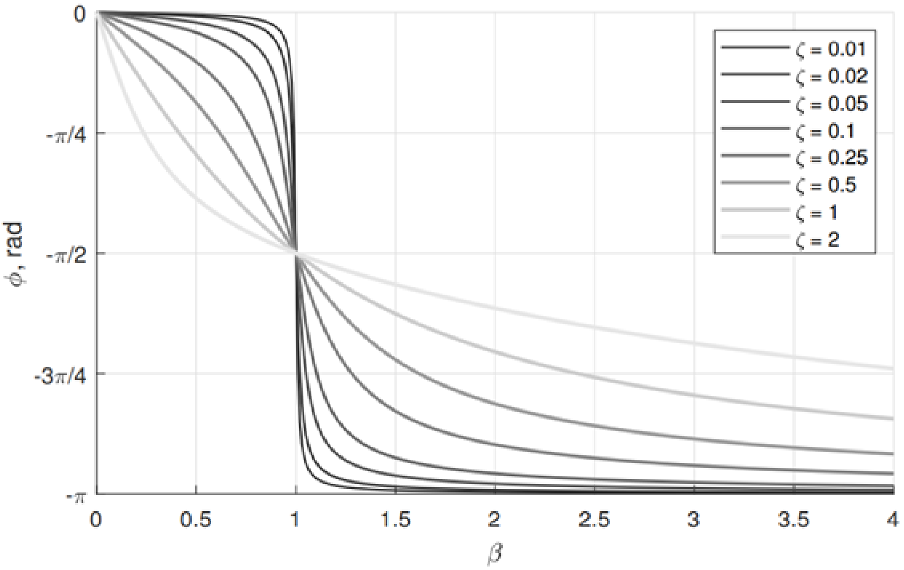

Figure 3.1.5: Frequency ratio versus phase angle shift due to damping between response and load, for different damping ratio. [15]

DLF function in Figure 3.1.4 shows clearly the effect of resonance, and why natural frequencies have great importance in structural engineering.
For small critical damping ratio, the maximum DLF can be estimated by taking $\sqrt{1-\xi^2} \approx 1$

$$DLF_{max} \approx \frac{1}{2\xi} \tag{3.1.20}$$

The consequence of resonance is that a small amplitude in oscillating loads can cause a significant response if the load hits a natural frequency. A dynamic system can therefore be separated into three regions dependent on the forces dominating the problem. Firstly, for a small frequency ratio, stiffness will dominate the problem meaning the problem will behave almost statically, and the DLF is around one. The inertia in the system needs to be higher to contribute. Secondly, the problem will be dominated entirely by damping around the natural frequency. Stiffness and inertia forces will cancel each other out, and damping can only contain the problem. Thirdly for high-frequency ratios, the inertia force will dominate the system, and the dynamic load factor will be less than one. Therefore, the force is less than static. The decrease in the dynamic load factor can be explained by the fact that the frequency is so significant that the system cannot respond in time to the changes in the forces because the mass of the system takes time to accelerate. DLF is also why a dynamic problem can be separated into static, dynamic, and impulse analysis depending on the load's duration compared to the system's natural period. [15]

3.1.2 Multiple degrees of freedom

Rigid body motions can be defined for each object as six degrees of freedom: surge, sway, heave, roll, pitch, and yaw [15] [16]. Three transnational modes and three rotational modes in x, y, and z directions. The 6 degrees of freedom can express every motion for a rigid body. Therefore all motions can be defined from COG - centre of gravity as shown in 3.1.6.

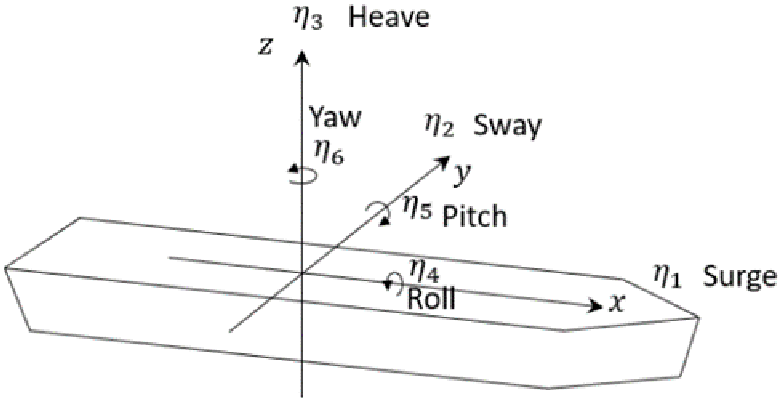

Figure 3.1.6: Rigid body motions for earth-fixed coordinate system [15]

Any motion on the body can be expressed from one equation for small motions. Small motion is defined as small motions compared to the size of the body. For large motions, a body-fixed reference frame cannot be used, and an inertial referenced frame is necessary. y.

$$S = \eta_1 \boldsymbol{i} + \eta_2 \boldsymbol{j} + \eta_3 \boldsymbol{k} + \boldsymbol{w} \times \boldsymbol{r} \tag{3.1.21}$$

$$\boldsymbol{\omega} = \eta_4 \boldsymbol{i} + \eta_5 \boldsymbol{j} + \eta_6 \boldsymbol{k} \tag{3.1.22}$$

$$\boldsymbol{r} = x\boldsymbol{i} + y\boldsymbol{j} + z\boldsymbol{k} \tag{3.1.23}$$

$$S = (\eta_1 + z\eta_5 - y\eta_6)\boldsymbol{i} + (\eta_2 - z\eta_4 + x\eta_6)\boldsymbol{j} + (\eta_3 + y\eta_4 - x\eta_5)\boldsymbol{k} \tag{3.1.24}$$

Another analysis must be performed for elastic bodies such as wind turbine blades. Here aero-elasticity counts. This means aerodynamic loads will affect the motions between each element, influencing the loads. Rigid bodies cannot express curvature and, therefore, not relative motions. This comes from the definition that no points can move relative to each other. In SIMA, rigid body analysis is used for SIMO body, and elasticity is added with RIFLEX elements. Thus, both rigid body modes and elasticity are often used for the same system. [15] [16]

3.1.3 Eigenvalue analysis

Eigenvalue analysis is possible to run in SIMA using both RIFLEX and SIMO [15] [17]. Eigenvalue analysis is calculated in the static position. Therefore it is important to calculate the natural periods in relevant positions. SIMA cannot calculate the natural periods with $A(T = \infty)$, but only $A(T = 0)$ for analysis with both RIFLEX element and SIMO bodies. It is possible to use $A(T = \infty)$ in frequency domain analysis with SIMO, but then the RIFLEX elements inertia has to be added to SIMO body, and only rigid-body natural periods can be calculated. Therefore a decay test is often relevant to get the correct added mass in the analysis.

The eigenvalue analysis can be done directly using matrix notation to find the natural periods, including elastic elements [17]. According to newtons second law sum of forces should be equal to mass times acceleration for all nodal points.

$$\sum_k F_i^k - m_i \ddot{u}_i = 0 \tag{3.1.25}$$

Newton's second law can be seen as a dynamic equilibrium equation when the inertia force is added to the other forces using d'Alembert's principle. This means that inertia and damping forces can be added to the load vector when calculating the dynamics using the established static solution. Either mass is added to nodal points, meaning the discretization should be good enough to represent the mass distribution to the system adequately or continuously calculated from the shape functions of the elements. In SIMA both options are available, but often continuous mass is used. Often the rotational mass is neglected by solvers to avoid numerical instabilities. This approximation is acceptable for sufficient nodal points.
Using d'Alambert's principle, the load vector can be written as equation 3.1.27, where $\overline{\boldsymbol{Q}}$ is the total load in the system expressed as the sum of inertia, viscous damping and time-dependent external forces.

$$\overline{\boldsymbol{Q}} = \boldsymbol{K}\boldsymbol{r} \tag{3.1.26}$$

$$\overline{\boldsymbol{Q}} = -\boldsymbol{M}\ddot{r} - \boldsymbol{C}\dot{r} + \boldsymbol{Q}(\boldsymbol{t}) \tag{3.1.27}$$

Using d'Alambert's principle, the static calculations can be used to calculate the linear dynamic equilibrium equation. [15] [17]

$$\boldsymbol{Q}(\boldsymbol{t}) = \boldsymbol{M}\ddot{r} + \boldsymbol{C}\dot{r} + \boldsymbol{K}r \tag{3.1.28}$$

3.1.4 Eigenvalue problem

Since the previous eigenvalue analysis is only valid for rigid body modes [17]. An approach to calculate the natural periods for an elastic system is necessary.

Mass, damping, stiffness, and external force are discretized in the Finite element formulation/ matrix method. Expressing that the system's internal and external energy should be the system's total energy.

$$U = \frac{1}{2}\boldsymbol{r}^T\boldsymbol{K}\boldsymbol{r} \tag{3.1.29}$$

$$T = \frac{1}{2}\dot{\boldsymbol{r}}^T\boldsymbol{M}\dot{\boldsymbol{r}} \tag{3.1.30}$$

Displacement r is described by the shape function N based on the static FEM formulation or modified to get a quicker answer. A common modification is by Rayleigh mode shapes ϕ, which approximates the eigenvalue based on "guessed" mode shapes.

$$\boldsymbol{r} = \boldsymbol{\phi} sin(wt) \tag{3.1.31}$$

$$\boldsymbol{r} = u = \boldsymbol{N}\boldsymbol{v} \tag{3.1.32}$$

This gives the Rayleigh-quotient equation, which calculates the eigenvalue. The system's natural frequency is then only the square root of the eigenvalue.

$$\lambda = w^2 = \frac{\boldsymbol{\phi}^{\boldsymbol{T}}\boldsymbol{K}\boldsymbol{\phi}}{\boldsymbol{\phi}^{\boldsymbol{T}}\boldsymbol{M}\boldsymbol{\phi}} \tag{3.1.33}$$

If all eigenvalues are of interest, the eigennumbers determinant can be used, but this is very computationally demanding for any real system. Therefore iterative algorithms are used to calculate the problem faster.

$$det(\boldsymbol{K} - w^2\boldsymbol{M}) = 0 \tag{3.1.34}$$

To use iterative algorithms, the special eigenvalue problems have to be formulated. Then the eigenvalues are found for the matrix A.

$$det(\boldsymbol{A} - \lambda\boldsymbol{I}) \tag{3.1.35}$$

Matrix A can be found by Cholensky decomposition using upper and lower triangular matrix.

$$\boldsymbol{M} = \boldsymbol{L}\boldsymbol{L}^T \tag{3.1.36}$$

With some algebra, A matrix can be established. On the right side identity matrix (diagonal with ones), and one the left side, A matrix is established.

$$[\boldsymbol{L}^{-1}\boldsymbol{K}(\boldsymbol{L}^{\boldsymbol{T}})^{-1} - w^2\boldsymbol{L}^{-1}\boldsymbol{L}^T]\boldsymbol{x} = 0 \tag{3.1.37}$$

The smallest eigenvalue can be found using inverse iteration, and by establishing shift μ after each found eigenvalue, the algorithm will converge to the next eigenvalue. K stands for the index in the iteration, where the z vector is calculated. Z is an approximation of the eigenvector.

$$z_k = \boldsymbol{A}^{-1}z_{k-1} \tag{3.1.38}$$

The eigenvector can find the approximated eigenvalue and, thereby, the approximated natural frequency.

$$w_i^2 = \lambda_i = \mu + \frac{\boldsymbol{z_k}^T\boldsymbol{M}z_{k-1}}{\boldsymbol{z_k}^T\boldsymbol{M}z_k} \tag{3.1.39}$$

The choice of method will depend on the matrix size, matrix bandwidth, type of mass matrix, and how many eigenvalues are needed. Static condensation can be used for computational efficiency since the accuracy needed for stress calculations (static problem) are much higher than mass and damping distribution. Therefore nodes or substructures with little effect can be static condensate, where the nodes are statically dependent on the dynamic nodes. Also, it is possible to use subspace if the dynamic modes of interest are local.(Rayleigh or Rayleigh-Ritz can also be used if the eigenmodes are "known"). This was of great importance when the computers were slow, but with faster software and hardware, the importance has been lesser.[17]

3.1.5 Global Rayleigh damping model

Damping is the ability to dissipate kinetic energy from the system and turn the energy into other forms [17]. There are mainly three types of damping in marine engineering, viscous damping, which is velocity dependent, structural damping, which is displacement dependent and coulomb damping, which is constant above a threshold, and is caused by friction. Viscous damping is calculated by WAMIT or other potential theory solvers but is limited to linear viscous damping. Potential solvers cannot calculate quadratic viscous damping. Therefore methods such as CFD or semi-analytical expressions are needed. The damping is imported in SIMA through calculated radiation data/ retardation function. Structural damping comes from the internal friction of the material following a hysteresis curve for cyclic loads. The model is independent of frequency and proportional to the square of strain amplitude. For many cases, determining the structural damping matrix is difficult and is therefore often expressed as a linear combination between mass and stiffness matrix. α_1 is the damping force proportional to the velocity of the mass, and α_2 is proportional to strain velocity. For high frequencies, the system will be approximately only stiffness damped. Structural damping is important when dynamic analysis of structured components is considered. An example that is relevant for offshore wind is tower bending mode. [17]

$$\boldsymbol{C} = \alpha_1 \boldsymbol{M} + \alpha_2 \boldsymbol{K} \tag{3.1.40}$$

3.1.6 Newmark's β-family

Solving equation 3.1.28, a solution technique is needed to find the motions. [15] This can be done by introducing a stepwise method that integrates the equation for each step in time. For each time step, the solver must iterate until demanded precision is good enough if the system is not linear, and the equation of motion has to be expanded to include nonlinear effects such as quadratic viscous damping or nonlinear drag. The solutions error can be checked by using equation 3.1.28, and see if the step has the same solution (good enough solution) for each side of the equation. The time step is chosen dependent on the environmental loads, as a higher time step would filter out higher frequencies. Therefore, choosing a time step where the frequencies of interest are included is essential. The step length is analog to the Nyquist theorem demanding twice the sampling frequency then the highest frequency to be able to represent a sinus wave. To properly represent a sinus wave, 15 times higher sampling frequency is often necessary, meaning the time step has to be 1/15 of the lowest load period.

Newmark's β is a generalized method where β and λ will vary depending on the chosen method. (Methods such as second central difference, constant average acceleration, linear acceleration and Fox-Goodwin are all methods in the Newmark's β-family). All methods will have different numerical stability conditions, meaning that the maximum step length is determined by the minimum natural period of the system. Some of the Newmark's β-family numerical methods are implicit, which are unconditionally stable. Since the minimum natural period determines the numerical stability, filters are introduced to avoid numerical instabilities. The cut-off filter must not take out relevant periods, as this will change the system's physical properties. High-order numerical methods will demand a small maximum step length which can be time-consuming. Therefore the best method will depend on the physics complexity and necessary accuracy. For a linear system, constant accuracy or Wilson θ method is often used. In wind turbine analysis in SIMA, the modified constant average acceleration is often used, introducing some numerical damping to make the system more stable (having problems with false high-frequency components). It is important that the numerical damping is sufficiently small enough, if not, the resonance could be underpredicted. Both constant average acceleration and Wilsons method are unconditionally stable, meaning step length will not cause numerical instabilities. By determining λ and β all Newmark's β-family numerical schemes can be derived by equations 3.1.41, and 3.1.42.

$$\dot{r}_{k+1} = \dot{r} + (1-\lambda)h\ddot{r}_k + \lambda h\ddot{r}_k + 1 \tag{3.1.41}$$

$$r_{k+1} = r_k + h\dot{r}_k + (\frac{1}{2} - \beta)h^2\ddot{r}_{k+1} \tag{3.1.42}$$

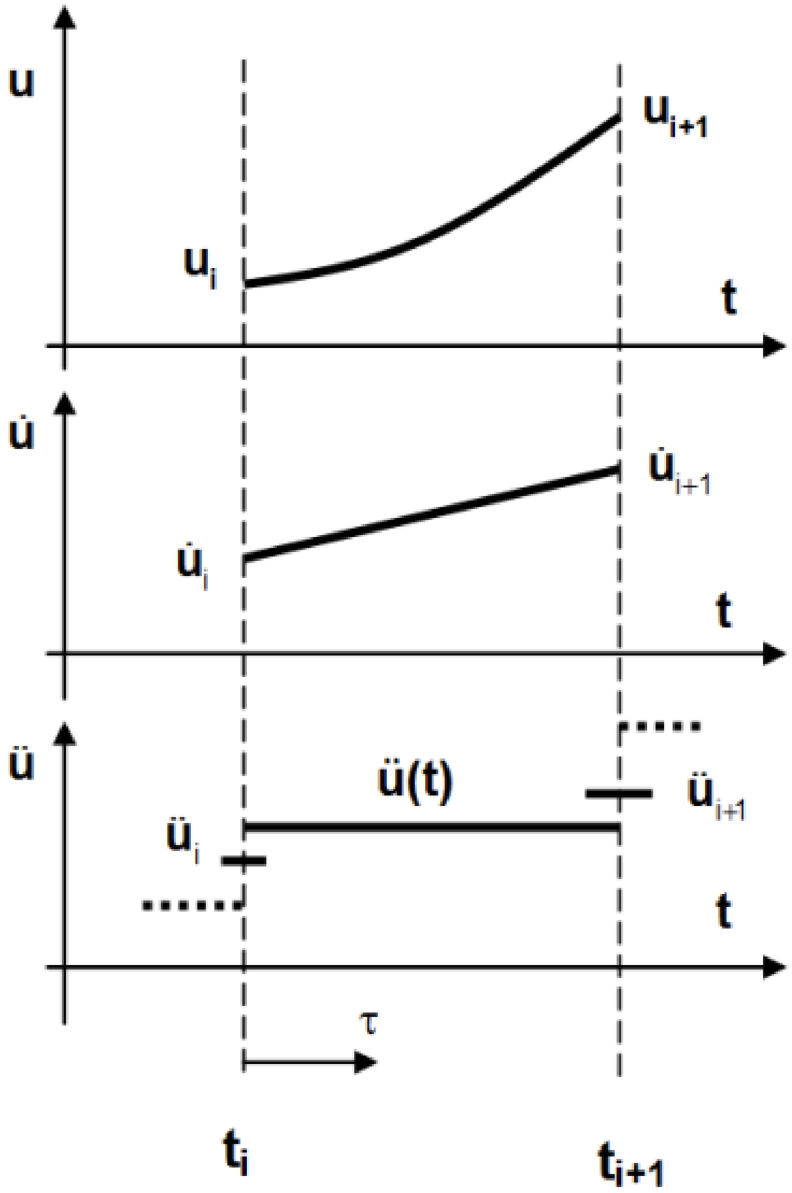

Figure 3.1.7: Constant average acceleration [15]

For constant average acceleration, the acceleration is assumed constant for each time step. The dynamic equation can be written as:

$$m\ddot{u}_{i+1} + c\dot{u}_{i+1} + ku_{i+1} = P_{i+1} \tag{3.1.43}$$

$$\ddot{u}(h) = \frac{1}{2}(\ddot{u}_i + \ddot{u}_{i+1} \tag{3.1.44}$$

By using the assumption for constant acceleration in the equation 3.1.45 for a given time step h, the following equation can be derived 3.1.45. Even though the equations are written with scalar values for mass, damping, and stiffness. The equations could be further expanded using matrix notation, and therefore calculate the displacement for all degrees of freedom in a system. [15]

$$(\frac{4}{h^2}m + \frac{2}{h}c + k)u_{i+1} = P_{i+1} + (\frac{4}{h}m + c)\dot{u}_i + (\frac{4}{h^2}m + \frac{2}{h}c)u_i \tag{3.1.45}$$

3.2 Aerodynamics of wind turbines

3.2.1 One-dimensional momentum theory and Betz limit

Many aerodynamic solvers are based on the one-dimensional momentum theory, which can determine a wind turbine's power production and thrust force.[18] [19] [20] The model is based on the momentum theory assuming a control volume with two boundaries; inlet and outlet. The wind will flow from the inlet to a uniform actuator disk and then to the outlet. The analysis assumes that the fluid is homogeneous and incompressible, there is no frictional drag, and the actuator disk is continuous, meaning there are infinite blades. The thrust is uniform over the disc area, there is no rotating drag, and the static pressure far from the rotor equals the ambient pressure.
Conservation of momentum from inlet to outlet accounting for a change in momentum due to thrust force is:

$$T = v_0(\rho A_0 v_0) - v_1(\rho A_1 v_1) \tag{3.2.1}$$

Though conservation of mass flow. The mass flow is the same through volumes zero and one.

$$\dot{m} = \rho A_0 v_0 = \rho A_1 v_1 \tag{3.2.2}$$

Combining the equations.

$$T = \dot{m}(v_0 - v_1) \tag{3.2.3}$$

Using Bernoulli's equation on both sides of the rotor, assuming no discontinuity across the rotor and that the pressure in the inlet and outlet equals the ambient pressure. Gives equation number 3.2.4

$$p_a - pb = \frac{1}{2}\rho v_0^2 - \frac{1}{2}\rho v_0^2 \tag{3.2.4}$$

The generated thrust is equal to the pressure drop times the area.

$$T = \frac{1}{2}\rho A(v_0^2 - v_1^2) \tag{3.2.5}$$

This gives two equations for thrust. By using algebra, the following equation can be derived.

$$v_a = \frac{1}{2}(v_0 + v_1) \tag{3.2.6}$$

This means that the velocity on the rotor disk equals the average of the upstream and downstream velocities. The axial induction factor is then introduced as a factor for decreasing wind velocity downstream.

$$a = \frac{(v_0 - v_a)}{v_0} \tag{3.2.7}$$

By implementing the axial induction factor, equation 3.2.6 can be rewritten as:

$$v_a = v_0(1 - a) \tag{3.2.8}$$

$$v_1 = v_0(1 - 2a) \tag{3.2.9}$$

The equations show that the induction factor cannot be negative since then the system would have gained energy. Also, if the axial induction factor is above 0.5, downstream velocity would be negative, which is nonphysical. From this, power could be calculated by thrust force times the velocity at the disk, introducing the axial induction factor.

$$P = \frac{1}{2}\dot{m}(v_0^2 - v_1^2) = \frac{1}{2}\rho A v_0^3 4a(1-a)^2 \tag{3.2.10}$$

The power coefficient is then defined as the power extracted from the wind divided by potential power in the wind from the velocity in the inlet, v_0.

$$C_p = \frac{P_A}{P_0} = \frac{P}{\frac{1}{2}\rho v_0^3 A} = 4a(1-a)^2 \tag{3.2.11}$$

To find the maximum theoretical power available in the wind, the derivative of the power coefficient with respect to the induction factor equals zero. This gives the solutions $a = 1\frac{1}{3}$. 1 is a false solution. By using $a = \frac{1}{3}$ the maximum power coefficient is $Cp = \frac{16}{27}$, also know as the Betz limit. In reality, this is only a theoretical maximum, as many idealizations have been assumed. In reality, there will be wake rotations and drag. Also, an infinite number of blades is unrealistic, meaning blade correction is necessary.[18] [19] [20]

3.2.2 Blade element momentum theory

SIMA uses BEM formulation to calculate the aerodynamic loads on the blades. [19] [20] From momentum theory, the expressions for infinitesimal thrust and torque can be derived as::

$$dT = 4a(1-a)\frac{1}{2}\rho v_0^2 2\pi r dr \tag{3.2.12}$$

$$dT = 4a'(1-a)\frac{1}{2}\rho v_0 \Omega r^2 2\pi r dr \tag{3.2.13}$$

The angle ϕ is both the angle of attack for the wind and the blade pitch angle. (This includes blade twist and control system pitch). The thrust and drag can be decomposed into tangential and normal force directions by rotation ϕ.

$$p_N = L * cos\phi + D sin\phi \tag{3.2.14}$$

The thrust force can then be calculated as the normal force over B number of blades.

$$dT = B p_N dr \tag{3.2.15}$$

The normal coefficient can be derived in the same way as the force, but non dimensional.

$$C_n = C_l cos\phi + C_d sin\phi \tag{3.2.16}$$

The solidity ratio can be defined as the length of the blades divided on the circumference.

$$\sigma = \frac{Bc}{2\pi r} \tag{3.2.17}$$

The axial induction ratio can be then derived based on the normal coefficient, angle of attack and the solidity ratio.

$$a = \frac{1}{\frac{4sin^2\phi}{\sigma C_n} - 1} \tag{3.2.18}$$

$$a' = \frac{1}{\frac{4sin\phi cos\phi}{\sigma C_n} + 1} \tag{3.2.19}$$

axial and angular induction factors are dependent on ϕ, C, and σ which is dependent on the axial and angular induction factor. This means an iterative procedure is necessary to calculate the axial and angular induction factors.
1) a and a' should be guessed
2) Calculate ϕ which gives the other variables
3) update a and a' based on the new variables. 4) Iterate until given tolerance.
The BEM momentum method has several correction formulations to account for several effects that are not included in the theory. [19] [20]

3.2.3 Prandtl correction

Prandtl correction corrects for the blade tip effect. [19] [20] The air flow will follow the pressure gradient, from lower to the upper side of the blade, reducing the aerodynamic force. The pressure is lower on the suction side of the blade.

B is the total number of blades, R is the outer radius of the rotor, ϕ is the angle of the relative wind, and r position of the blade. Since F is a correction factor, it's nondimensional, and can only be a number between 0 and 1. The correction factor can then be directly implemented into momentum theory. lim $\frac{r}{R} \to 0$ then F = 1, meaning no correction away from the blade tip.

$$F = \frac{2}{\pi} cos^{-1}[exp(-\frac{B\Big(1-\frac{r}{R}}{\frac{2rsin(\phi)}{R}}\Big)] \tag{3.2.20}$$

$$dT = F\rho U^2 4a(1-a)\pi r dr \tag{3.2.21}$$

$$dQ = Fa^{'}\rho U 4a(1-a)\pi r^3 \Omega dr \tag{3.2.22}$$

3.2.4 Glauert correction

Glauert correction is presented in equation 3.2.23.

$$a = \frac{\frac{C_T}{F} - C_{T1}}{C_{T2} - C_{T1}}(a_2 - a_1) + a_1 \tag{3.2.23}$$

$a_2 = 1.0$, $C_{T2} = 1.82$, $a_1 = 1 - 0.5\sqrt{C_{T2}}$, $C_{T1} = 4a_1(1-a_1)$, where F is the Prandtl factor.[19] [20] This is a empirical correction for BEM momentum theory recomended by Burton for large induction factor $a > 0.4$. It can be seen from figure 3.2.1 that the correction has no effect for low induction factors. Also, as already discussed momentum theory is nonphysical for induction factors greater than 0.5 due to negative velocity. Glauert correction will then correct momentum theory in the nonphysical regime. The iterative procedure to BEM momentum theory remains the same with the exception for $a > 0.4$, the thrust coefficient has to be corrected by a new axial induction factor for the given blade element. The angular induction factor, is not affected. [19] [20]

3.2.5 Dynamic wake

In the given BEM momentum theory the procedure is quasi-static, and not fully dynamic since the previous loads only have an indirect influence on the calculations from the beam elasticity, but the air flow is considered independent, meaning the change in wind velocity would change all the blade properties (pitch angle, rotor speed etc).[19] [20] In reality there is some time lag in induced velocity. The effect is most important for a heavy loaded rotor, meaning high induction factors / low wind speed. SIMA modells this effect by "Stig Øye dynamic inflow model", a filter model for the velocity. W is the new induced velocity vector, W_{qs} is the calculated quasi-induced velocity vector from BEM momentum theory, τ_1 and τ_2 are time constant which is determined experimentally. [19] [20]

$$W + \tau_2 \frac{dW}{dt} = W_{int} \tag{3.2.24}$$

$$W_{int} + \tau_1 \frac{dW_{int}}{dt} = W_{qs} + 0.6\tau_1 \frac{dW_{int}}{dt} \tag{3.2.25}$$

3.2.6 Dynamic Stall

The drag and lift coefficients are constant for a given angle of attack and are therefore static.[19] [20] The effect are causing rapid aerodynamic changes that change the flow properties. The effect comes from rapid changes in wind speed causing flow detachment and reattachment of the airflow. This is an airfoil surface effect with an analogy to wake effect in hydrodynamics. The time scale of the effect is dependent on the relative wind speed at the blade to the blade chord. Which can be approximated as $\frac{c}{\Omega r}$. For large turbines, this effect is around 0.2 s close to the blade root and 0.01 s at the blade tip. Dynamic stalls can cause high transient forces due to higher wind speeds. In SIMA "Stig Øye" model is used with an empirical time constant.

f_s is the effect of stall on the lift coefficient, where $C_{L,inv}$ is the original lift coefficient without separation, and $C_{L,fs}$ is fully separation lift coefficient. C_L is then found from linear interpolation between fully stall and no stall. f_s can be calculated by agreement with static airfoil data.[19] [20]

$$C_L = fsC_{L,inv}(\alpha) + (1 - f_s)C_{L,fs}(\alpha) \tag{3.2.26}$$

$$\frac{df_s}{dt} = \frac{f_s^{st} - f_s}{\tau} \tag{3.2.27}$$

$$f_s(t + \Delta t) = f_s^{st} + (f_s(t) - fs^{st})e^{-\frac{\Delta t}{\tau}} \tag{3.2.28}$$

The lift coefficient can therefore be calculated by α, angle of attack, α_0 zero angle of attack degrees, f_s stall effect and the derivative of the lift coefficient for fully stall.

$$C_L = \frac{1}{4} \frac{dC_L}{d\alpha}(\alpha - \alpha_0)(1 + \sqrt{1 - |f_s|})^2 \tag{3.2.29}$$

For a fully stalled flow, the equation can be simplified as:

$$C_L = C_{L,qs}(1 + \sqrt{1 - |f_s|})^2 \tag{3.2.30}$$

In order to calculate the initialize dynamic stall, the software finds several important points on the lift curve as α_0, the maximum slope (the maximum derivative with respect to the angle of attack) in both the positive and negative regions for both local maximum and minimum.

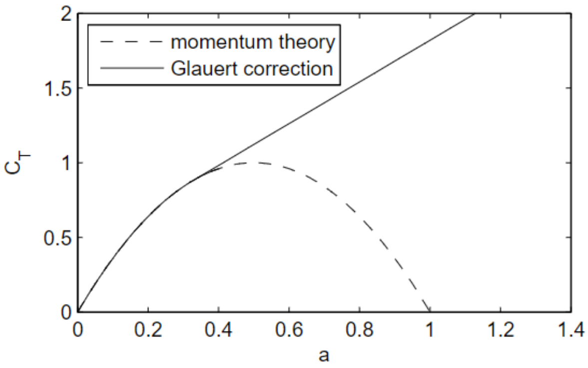

Figure 3.2.1: Glauert correction for Prandtl number $F = 1$ [19]

3.3 Aerodynamic turbulence models

Mainly there are two wind turbulence models that are used today and recommended by IEC, Kaimal Spectrum and Exponential Coherence model - called Kaimal and Mann Spectral Tensor model - called Mann. LES, also called Large-eddy simulation is a computational fluid dynamic method - CFD that can calculate turbulent wind based on Navier Stokes equation for turbulent gas and the physical boundary condition for example the ground. LES simulations are not as tedious as direct numerical simulation that only calculates Navier-Stokes with boundary condition. Since local effects can influence the global fluid system, a very refine mesh is necessary both in time and space. LES reduces the computational time by neglecting the smallest length effects, which are the most demanding. LES is also called low-pass filtering for its ability to filter out high-frequency content, and thereby increase the numerical stability. By the use of LES it is possible to verify the turbulence models Kaimal and Mann, in lack of good experimental data. Both Kaimall and Mann has the same frequency content, but the spatial coherence is different from each other. Coherence is a statistical measurement off how well two waves correlate. $\gamma^2_{xy}(f) = \frac{(S_{xy}(f)^2)}{S_{xx}(f)S_{yy}(f)}$. The turbulence models are validated through experiments on different locations. Mann in Bridge - Denmark, Kaimal onshore in Kansas - USA.

For low windspeeds, Mann turbulence model has a good agreement with LES data and experimental measurements. For higher wind speeds, Kaimal is closer to LES. In the models, atmospheric stability is assumed. This means turbulent wind parameters such as turbulence intensity, coherence, and wake recovery.[18] [21] [22]

3.3.1 Synthetic wind generation models

Several aerodynamic coefficients are used when generating synthetic wind field, and is defined in ”Floating wind turbine structures” by DNV [21] [23].

Longitudinal turbulence scale parameter Λ_1 at hub height z and are used in Mann turbulence generator.

$$\begin{cases} \Lambda_1 = 0.7z & z \leq 60 \\ \Lambda_1 = 42m & z \geq 60 \end{cases} \tag{3.3.1}$$

There is also a minimum turbulence standard deviation that the different turbulence models have to follow, but the actual standard deviation will be dependent on the chosen turbulence model and longitudinal turbulence scale parameter.

$$\sigma_2 \geq 0.7\sigma_1 \tag{3.3.2}$$

$$\sigma_3 \geq 0.5\sigma_1 \tag{3.3.3}$$

For the Kaimal model, the standard deviation v and w follows the lateral turbulence standard deviation.

$$\sigma_2 = 0.8\sigma_1 \tag{3.3.4}$$

$$\sigma_3 = 0.5\sigma_1 \tag{3.3.5}$$

Also the modified Kaimal shall asymptotically approach the given value in the equation for high frequencies.

$$S_1(f) = 0.05\sigma_1^2(\Lambda/v_{hub})^{-\frac{2}{3}}f^{-\frac{5}{3}} \tag{3.3.6}$$

$$S_1(f) = S_3(f) = \frac{4}{3}S_1(f) \tag{3.3.7}$$

The normal turbulence model - NTM is often used in synthetic wind fields. It is defined by equation

$$\sigma_1 = I_{ref}(0.75v_{hub} + b), b = 5.6 \tag{3.3.8}$$

The formula is estimated by taking the 90% quantile for given hub height wind speed. I_{ref} is defined by the turbulence category, which is chosen as B. Which are defined as a medium turbulence area and are therefore general. [21] [23]

Kaimal spectrum and exponential coherence model

The modified Kaimal spectrum is defined by standard IEC 61400 as [24] [21]:

$$\frac{fS_k(f)}{\sigma_k^2} = \frac{4fL_K/v_{hub}}{(1+6fL_k/v_{hub})^{\frac{5}{3}}} \tag{3.3.9}$$

where f is the frequency, k is subnotation for direction, S is the velocity spectrum, σ standard deviation and L as integral scale parameter.
The integral scale parameter is defined in the standard as:

$$\begin{aligned} L_1 &= 8.71\Lambda_1 \\ L_2 &= 2.7\Lambda_1 \\ L_3 &= 0.66\Lambda_1 \end{aligned} \tag{3.3.10}$$

Exponential coherence model used with Kaimal auto spectrum.

$$coh(r,f) = exp[-12((fr/V_{hub})^2 + (0.12r/L_c)^2)^{0.5}] \tag{3.3.11}$$

$$BSCR = \sqrt{\sum_{i,j} Corr_{i,j}SCR_iSCR_j} \tag{3.3.12}$$

3.3.2 Mann uniform shear turbulence generator

The model is based on a three-dimensional velocity spectral tensor $\phi_{i,j}(K)$ by Von Karman energy spectrum, which is distorted by a uniform mean velocity shear. The model uses three parameters that have to be estimated when using the model, Γ, L and $\alpha\epsilon^{\frac{2}{3}}$, where the last parameter is Kologorov's constant *alpha* multiplied with the energy dissipation ϵ [13]. These parameters are fitted against the wanted turbulence intensity factor and mean velocity. Γ is a parameter that determines the eddy lifetime, where L describes the size of the eddies. In the IEC6400 $\Gamma = 3.9$, $L = 0.8\Lambda$, $\sigma_{iso} = 0.55\sigma_1$. *Gamma* can be found by least squares fitting the Kaimal model.$\sigma_2 = 0.7\sigma_1$ and $\sigma_3 = 0.5\sigma_1$ follows definition of the model.[24] [21]

$$\frac{fS_i(f}{\sigma_i^2} = \frac{\sigma_{iso}^2}{\sigma_i^2}(\frac{4\pi lf}{V_{hub}})\Psi_{ii}(\frac{2\pi lf}{v_{hub}}) \tag{3.3.13}$$

where Ψ is the one-dimensional wave number spectrum that has to be calculated by numerical integration and fitted to the Kaimal model. [24]

3.3.3 Wind speed variation with height

Figure 3.3.3 shows how the wind power spectral density function for sampled data and Von Karman synthetic wind. The actual wind would vary in time and space, fluctuating around a mean value due to turbulence effects. The figure illustrates that the wind speed increases with increased wind height. For Von Karman turbulence model the wind speed varies linearly for a logarithmic plot, meaning that the wind speed is logarithmic dependent. This effect is also known as wind shear. Since a wind turbine rotates through the wind field vertically, the distribution of the wind field is crucial for the estimation of thrust and energy production. Two mathematical models are used to model the vertical profile over homogeneous, flat terrain. Something that is the case for offshore wind turbines. Firstly the logarithmic law can be derived from boundary layer flow from fluid mechanics. Due to the boundary layer and the no-slip condition around the terrain, the wind speed at the ground has to be zero. The second law is the power assumption. Figure 3.3.2 plots the experimental data over a profile. The dotted line represents the average wind speed.[20]

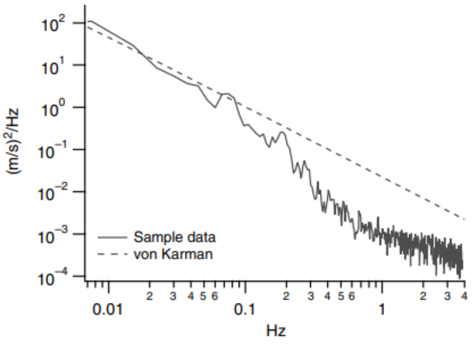

Figure 3.3.1: Wind data power spectral density function [20]

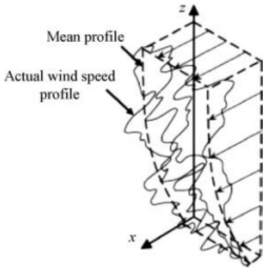

Figure 3.3.2: Experimental speed profile [20]

Logarithmic Profile - log law

Wortman (1982) uses a mixing length derivation of the logarithmic profile [20]. Near the boundary layer the momentum equation is reduced to:

$$\frac{dP}{dx} = \frac{d}{dz}\tau_{xz} \tag{3.3.14}$$

where x is horizontal and z is vertical coordinates, τ_{xz} is the shear stress in xz-direction and P is pressure. Near the surface, the pressure is independent of z.

$$\tau_{xz} = \tau_0 + z\frac{dP}{dx} \tag{3.3.15}$$

τ_0 is an integration constant which is the surface value of the shear stress. The pressure gradient is small near the surface, meaning it can be neglected. Therefore the shear stress is only dependent on the boundary layer. Using Prandtl mixing length theory.

$$\tau_{xz} = \rho l^2 (\frac{dU}{dz})^2 \tag{3.3.16}$$

U is the velocity, l mixing length and rho density of air.

$$U^* = \sqrt{\frac{\tau_0}{\rho}} \tag{3.3.17}$$

Friction velocity definition is defined in equation 3.3.18.

$$\frac{dU}{dz} = \frac{U^*}{l} \tag{3.3.18}$$

By assuming a smooth surface. the mixing length can be expressed as $l = kz$ with k as a constant. z0 is the surface roughness length. [20]

$$U(z) = \frac{U^*}{k} ln(\frac{z}{z_0}) \tag{3.3.19}$$

Power law profile

U(z) is the wind speed for height z, where $U(z_r)$ is the wind speed at the reference height zr. 'α is the power law exponent. Early experimental work showed that the power coefficient was 0.14 in most cases. Therefore, 0.14 is often used in simulations. In reality, the power coefficient is not constant. There are several methods to estimate the power coefficient but often, it is chosen to match experimental measurements from the site. [18] [20]

$$\frac{U(z)}{U(z_r)} = \left(\frac{z}{z_r}\right)^{\alpha} \tag{3.3.20}$$

3.3.4 Wind farm

Shared mooring is equivalent to small land-based wind farms. The electrical system has to be designed based on the overall system, minimizing electrical loss and investment costs [20]. Several technical problems exist for the close spacing of multiple wind turbines. For land-based wind farms, the localization of wind turbines is based on the available wind resources at the location. However, close wind turbines would cause lower energy output from downwind wind turbines since the upwind turbine has extracted energy. If the turbines are too close together versus the rotor diameter, the turbulent wind field cannot return to the ambient condition, and wake effects will influence the wield field. The downwind wind turbines will then experience lower mean wind speeds, and higher turbulence, increasing fatigue due to higher dynamic loading. Since the mean wind speed is lower and the turbulence is higher, the energy output would fluctuate more, causing more costs connected to energy regulation. [20]

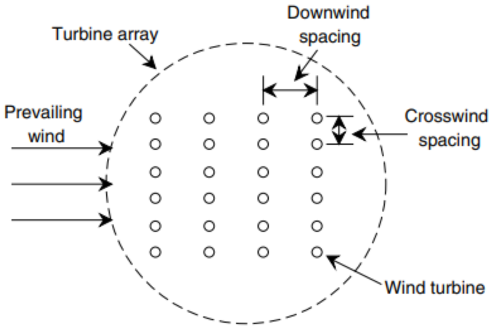

Figure 3.3.3: Wind farm array schematic [20]

Array loss is a function of the following factors:

- Spacing
- Thrust curve
- Total number of turbines and the rotor size
- TI - turbulence intensity factor
- Wind direction and its frequency content

The wake effect will transfer kinetic energy to its surroundings until a certain distance in length and width [20]. Array loss could be by optimization by considering the geometry of the wind farm and the locations wind field. Turbine spacing for all inflow angles will affect the wake effect, which reduces the energy output from the wind. Offshore wind farms would have the advantage of an even distribution of wind energy since terrain elevations are several km from the wind park, leading to more uniform distribution of wind turbines. Floating wind turbines would also be less dependent on the geology since the anchor points could be chosen semi-independently on the floater's position. Customization of the mooring system is then needed so that the stiffness is even distributed for all wind directions. This gives a higher flexibility to design the wind park. For shared mooring, the flexibility is lesser since the anchor position would influence the whole system's performance. Also, increased distance between wind turbines demands more mooring and lowers the , which increases the cost and lowers the normal stiffness of the mooring [9]. The pretension has to be increased to compensate for this effect, meaning a heavier mooring system is necessary.

Areas with higher turbulence in the wind field will cause an acceleration in the momentum and energy exchange in the prevailing wind. Since more energy and momentum are transferred, the velocity will converge faster to the ambient wind field, causing fewer effects for downstream wind turbines, and creating a higher energy production [20]. With a higher turbulence intensity factor, the wake effect would therefore be smaller. For offshore class B, lower speed will have a higher turbulence intensity factor, and, therefore, higher relative turbulence, but rotor design would influence substantial the generated wake effect. The tubulence intensity factor increases substantially by the rotating blades from the wind turbines. Therefore if the wind does not converge to ambient conditions, the wind becomes more turbulent for each downwind wind turbine.

Studies have shown that wind turbines that are placed downwind, eight to ten diameters apart, and a minimum of five in crosswind would generally have an energy loss of less than 10%. Figure 3.3.4 shows how a six times six array of ten diameters in downwind are influenced by crosswind spacing for different turbulence intensity factors. The results are for conditions where the turbines are in the wake of each other, and the wind is evenly distributed from all directions. It is important to mention that energy output is sensitive to the mean wind speed since it is in the second power of velocity.

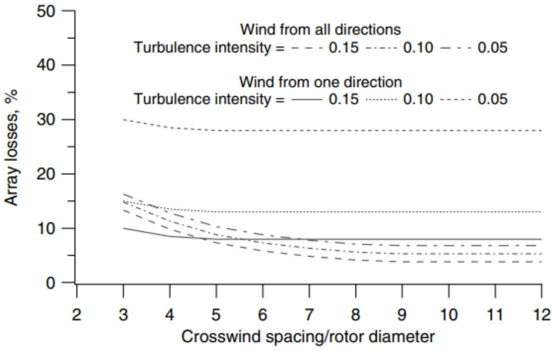

Figure 3.3.4: Wind farm array losses [20]

Wake loss is a large uncertainty in energy production estimates. It is still common to calculate with 50% uncertainty in wake loss [25]. The paper in Wind Energy [25], has calculated that errors in wake assumptions are less than 25% for the maximum error. Therefore the influence of wake effects is often overestimated, meaning that in practice shared mooring concepts would have a higher energy production than anticipated. Wake models in recent years gives a better prediction of wake effects, and therefore wake effects would have a smaller uncertainty in the following years, which is good for the shared mooring concepts.

Array losses have to be calculated through wake models. Several options exist, such as [20]:

- Roughness
- Semi-empirical
- Eddy viscosity
- CFD

3.4 Hydrodynamic

Hydrodynamics is a subgroup of fluid dynamics. The fluid dynamics fundamental equation is the Navier-Stokes equation for a 3D continuum, which is a partial differential equation. The theory could be derived from the three principles of 1) conservation of mass, 2) material derivative 3) Newton's second law by conservation of momentum. The mass continuity equation calculates the conservation of mass. For incompressible fluids and irrotational flow, the equation can be simplified due to constant density and zero curl from equation 3.4.1 to equation 3.4.1. Where ρ is the density of the fluid, ∇ is the divergence operator, $\overrightarrow{V}$ is the velocity vector, P the pressure and ν the kinematic viscosity of the fluid.

$$\frac{\partial \rho}{\partial t} + \nabla \cdot (\rho \overrightarrow{V}) = 0 \tag{3.4.1}$$

$$\nabla \cdot (\overrightarrow{V}) = 0 \tag{3.4.2}$$

In tensor form for $i = 1, 2, 3$ Navier-Stokes, NS can be written as:

$$\frac{\partial u_i}{\partial t} + u_j \cdot \frac{\partial u_i}{\partial x_j} = -\frac{1}{\rho}\frac{\partial P}{\partial x_i} + \nu \frac{\partial u_i^2}{\partial x_j^2} \tag{3.4.3}$$

In total, there are three momentum equations and one continuity equation. In this tensor format, gravity terms are neglected. Navier-Stokes are computationally expensive and are less used in engineering problems, even though it has gained more and more popularity through the years. Navier-Stokes has no analytical solutions and are one of the "millennium" problems. Therefore NS has to be solved numerically, which has many problems irrelevant to this project's scope. Direct Navier-Stokes without approximations are extremely computationally expensive, so approximations are needed to increase the efficiency.

In the wave potential theory, the viscous term in Navier-Stokes is neglected, resulting in the Bernoulli time-dependent equation, often named the Euler equation, and its thereafter derived using boundary conditions. Since the drag forces are neglected, the Morison equation drag term is often used with the potential wave theory to correct the drag semi-empirically. Since irrotational fluid is assumed in the wave potential theory the Kaulegan-Carpenter number, KC is assumed to be zero, meaning wake effects are neglected.

Velocity potential for a wave with deep water approximation can be expressed as:

$$\phi = \frac{\zeta_A g}{\omega} e^{kz} cos(\omega t - kx) \tag{3.4.4}$$

By deduction from velocity potential ϕ the acceleration and velocity can be calculated for the regular waves.

$$u = \frac{\phi}{dx} = \omega \zeta_a e^{kz} sin(\omega t - kx) \tag{3.4.5}$$

$$a_1 = \frac{\phi}{dxdt} = \omega^2 \zeta_a e^{kz} cos(\omega t - kx) \tag{3.4.6}$$

In linear potential theory, each subproblem can be separated into several problems, meaning the total problem is a sum of all the subproblems. The interaction between the body and the fluid can then be separated into incident wave, hydrostatic, radiation, and diffraction.

$$\phi = \phi_I + \phi_r + \phi_d \tag{3.4.7}$$

or written fully as:

$$\phi = \phi_0 + \phi_7 + \sum_{j=1}^{6} \phi_j \tag{3.4.8}$$

There are a total of eight potential problems, incident, diffraction, and six radiation potentials, since a rigid body has six degrees of freedom. In all potentials, boundary conditions have to be fulfilled. Wave diffraction can be explained as how the body disturbs the fluid, since the fluid has to flow around the body, therefore diffracting the fluid. Radiation is how the body's motions disturb the fluid and create radiating waves. Diffraction and incident wave creates excitation loads, and it is an external load to the dynamic system. Radiation provides additional forces called added mass and hydrodynamic damping. These additional forces have to be taken into account for hydrodynamic problems. Waves will, therefore, contribute to extra loads and a different dynamic behavior by additional inertia forces and damping. This will influence the natural frequency greatly.

Instead of using potential theory, it is possible to use the Morison equation and calculate the forces by using the potential velocity of waves. Morison equation is a huge simplification that should be used with precaution, but it is valid for small volume structures where strip theory can be used. When the wavelength becomes large compared to the characteristic length, added mass and damping will converge since the body's influence is negligible on the waves. Therefore is sufficient to calculate the forces by the undisturbed incident wave and diffraction. Morison will also neglect the free-surface diffraction [15].

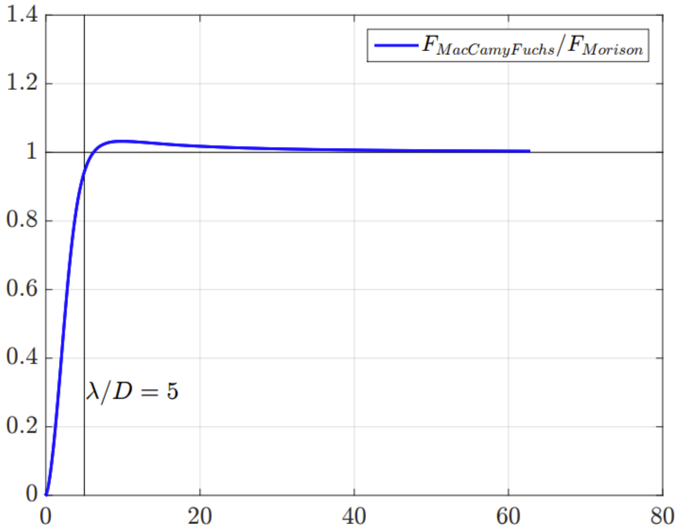

Figure 3.4.1: Comparison between MacChamy-Fuchs and strip theory with the inertia term in Morison equation for a bottom fixed cylinder [15]

Figure 3.4.1 shows how the Morison equation will converge to the correct answer for large waves for a bottom fixed cylinder. Morison equation can calculate the force by dividing the geometry into vertical strips with distance dz. For each strip, the force is calculated by calculating the velocity and acceleration from the wave.

$$dF(t) = \rho\frac{\pi D^2}{4}(C_f a_w(t) + C_a a_r(t))dz + \frac{1}{2}\rho D C_D u_r(t) \mid u_r(t) \mid dz \tag{3.4.9}$$

The Morison equation is then divided into inertia and drag terms, where the force has to be integrated along the z-axis. C_f is the Froude-Kriloff coefficient, C_a is the added mass coefficient and C_d is the drag coefficient. Potential flow solvers or experiments can calculate values for added mass. The drag coefficient is more difficult to estimate since potential theory cannot solve it. Therefore CFD or experiments are necessary. Since potential theory can not estimate the drag force, often Morison drag term is used with potential theory. The drag force will be dependent on the relative velocity $u_r = u_w - u_b$, the difference between wave and body velocity. This term is nonlinear, meaning it has to be linearized to be able to solve in the frequency domain. Since the drag force is dependent on the body velocity and the body velocity is dependent on the force. Drag cannot be estimated directly. Therefore is necessary to iterate the calculated drag force in dynamic simulation and update the velocity until an acceptable answer. [16] [15] [26]

3.4.1 Irregular long-crested waves

Figure 3.4.2: Irregular waves as a sum of regular waves [15]

N regular waves can express the surface elevation by assuming the wave process is stationary and normally distributed and that the stochastic process is ergodic. Velocity and acceleration for an irregular wave can then be calculated for N regular waves.

$$\zeta(x,t) = \sum_{j=1}^{N} A_j sin(\omega t - k_j x + \epsilon) \tag{3.4.10}$$

$$u = \sum_{j=1}^{N} \omega_j A_j e^{k_j z} sin(\omega t - k_j x + \epsilon) \tag{3.4.11}$$

$$a_1 = \sum_{j=1}^{N} \omega_j^2 A_j e^{k_j z} cos(\omega t - k_j x + \epsilon) \tag{3.4.12}$$

where A_j, ω_j, k_j, and ϵ_j are the wave amplitude, frequency, wave number, and random phase angle of wave component j [16]. The phase angle is uniformly distributed between 0 and 2π and is constant with time. Amplitude can be calculated from a wave spectrum.

$$\frac{1}{2}A_j^2 = S(\omega_j)\Delta\omega \tag{3.4.13}$$

Jonswap spectrum is used in SIMA calculations for $\gamma = 3.3$ where $\beta = 1.25$ and $\sigma_a = 0.07, w < w_p$ and $\sigma_b = 0.09, w > w_p$. [26] [16]

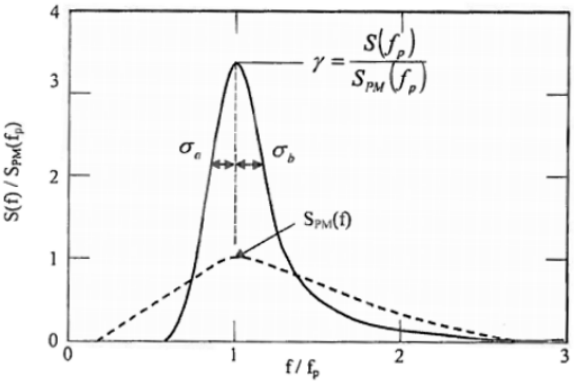

Figure 3.4.3: JONSWAP and PM spectrum for the same sea state [15]

$$S(w) = \frac{\alpha g^2}{w^5} exp(-\beta(\frac{w_p}{w})^4 \gamma^{exp(\frac{(\frac{w}{w_p}-1)^2}{2\sigma^2})}) \tag{3.4.14}$$

$$\alpha = 5.061\frac{Hs^2}{T_p^4}(1 - 0.287ln(\gamma)) \tag{3.4.15}$$

3.5 Mooring system

3.5.1 Mooring

Mooring lines are necessary for all floating structures that would maintain their position [27] [16]. Floating structures has little stiffness in the horizontal plane, η_1, η_2 and η_6. Surge, sway, and yaw. The stiffness in the horizontal plane will help the floater maintain its position and reduce motions. This will also change the floater's total stiffness, affecting the natural frequency. The mooring system also aims to protect the riser or floating wind power cable. The mooring system has, therefore, several interests that are not in line with each other. Higher stiffness can create resonance if the natural period is too small. On the other hand, a sufficiently stiff mooring system decreases the power cable/ riser cost but increases the mooring cost since the tension is higher, and a larger mooring dimension is necessary. The mooring system should also be sufficiently strong enough to handle large dynamic loads and fatigue.

In quasi-static conditions, the total restoring force of a mooring system comes from the geometric and elastic stiffness. Geometric stiffness is a nonlinear phenomenon determined from the mooring weight and pretension. Therefore the shape of the mooring line will determine the stiffness. The consequence is that stiffness for different floater conditions will vary due to the change in weight distribution, which is why geometric stiffness is nonlinear. Nonlinearity can be defined as not proportional against the parameter of interest, in this case, displacement versus stiffness.

Elastic stiffness is calculated from the axial stiffness to the mooring, the line elongation effect. Generally, floating systems' vertical stiffness comes primarily from the floater, not the mooring line. Mooring lines should contribute to horizontal stiffness. Therefore stiffness for mooring lines is referred to as horizontal stiffness. Mooring systems should carry nonlinear wave force and aerodynamic loads. Regular waves will not contribute to mean force, and the mooring system should not carry linear wave forces since they are too large.[27] [16]

3.5.2 Mooring design regulations

According to DNV standard for floating wind turbines [21], the ultimate limit state in mooring loads has to be calculated as for a characteristic mean tension and a characteristic dynamic tension. γ_{mean} and γ_{dyn} are load factors.

$$Td = \gamma_{mean} T_{c,mean} + \gamma_{dyn} T_{c,dyn} \tag{3.5.1}$$

when breaking strength statistics are not available, the minimum breaking strength of a new component of mooring line $Smbs$ has to be used. [21]

$$S_c = 0.95 S_{mbs} \tag{3.5.2}$$

If the strength statistic is known, the underlining uncertainty depends on the total number of samples. A cautious statistical estimate has to be used. According to DNV-st-0119 [21]:

$$S_c^* = S_c(1 - 2\frac{COV_s}{n}) \tag{3.5.3}$$

$$COV_s = \frac{\sigma_s}{\mu_s} \tag{3.5.4}$$

COV is the coefficient of variation, which can be calculated if the standard deviation and mean value of breaking strength are known. n are the total number of tests, which shall not be less than 5.

Load factor requirements for the design of mooring lines:

Limit state	Load factor	Consequence class 1	Consequence class 2
ULS	γ_{mean}	1.3	1.5
ULS	γ_{dyn}	1.75	2.2
ALS	γ_{mean}	1.00	1.00
ALS	γ_{dyn}	1.10	1.25

Table 3.5.1: Load factor requirements for design of mooring lines DNV-ST-0119 [21]

When looking into ULS condition, a 50-year value on the sea state environmental contour has to be used, but for a wind turbine, not the highest sea state creates the largest mooring tension due to different thrusts.

Since a mooring line is assembled by a large number of different components, such as chains connected by the connection of links, steel wire, and synthetic fiber rope, the overall strength of a long line will be lesser than for a component, and therefore this should be taken into consideration in the characteristic capacity. The properties are for a specific component in the mooring line.

$$S_c = \mu_s(1 - COV_s(3 - 6COV_s)), COV < 0.10 \tag{3.5.5}$$

The strength criterion is then [21]:

$$\frac{S_c}{S_c^*} > Td \tag{3.5.6}$$

3.5.3 Taut mooring system

The principle of a taut mooring system is that the weight of the system is negligible, and therefore geometric stiffness is negligible [16] [27]. The stiffness is only dependent on elastic stiffness. Since the mooring line is straight, there will be an angle between the anchor and the floater. This means that the force can be decomposed into vertical and horizontal force, meaning that the anchor has to handle vertical loads. Since taut mooring lines do not use more seafloor than only the anchor, taut mooring systems will have a smaller environmental impact than catenary mooring lines. Due to the use of elastic stiffness, less material and weight is needed. Therefore a cost reduction is possible, but the vertical loads increase the anchor cost, as few anchor types can handle large vertical loads. Using long mooring lines, compared to the distance to the seabed, the angle between the seabed and anchor is small. Therefore, a small vertical restoring force is needed from the anchor, but the mooring cost increases.

$$k_E = \frac{EA}{l} sin(\alpha) \tag{3.5.7}$$

For a taut mooring line with no mass, the stiffness will only come from the elastic stiffness module, which is only the elastic stiffness module for a bar decomposed.α is the angle between the touchdown point and fairlead [27]. Restoring force will then come from the deformation of the rope.

An elastic cable line equation is necessary for extreme conditions if the rope's weight is considered or a combined mooring system between rope and chain. In this case, each section's static stiffness must be calculated.

$$h = \frac{T_H}{w}\Big[\frac{1}{cos(\phi_w) - 1} + \frac{w}{2AE} ls^2\Big] \tag{3.5.8}$$

The touchdown point can be calculated considering the horizontal and vertical tension, weight, unstretched length, and elastic stiffness. [16] [27]

$$x = \frac{T_H}{w} \log\Big(\frac{(T_H^2 + T_z^2)^{\frac{1}{2}} + T_z}{T_H}\Big) + \frac{T_H}{AE} l_s \tag{3.5.9}$$

3.5.4 Catenary mooring system

Currently steel chain is the most used mooring system [27]. Stiffness in the system comes from geometric and elastic properties. Heavy systems with high Youngs e-modulus will be dominated by the geometric stiffness; typical material is heavy chain. The pros with Catenary mooring are that there is limited or no vertical load from the mooring due to mooring on the seabed. The catenary mooring system is often designed to ensure that some mooring will always be at the seabed except for extreme conditions. The weight of the system will create a pretension that gives a horizontal tension that works as a stiffener.

The horizontal geometric stiffness from catenary moorings follows the catenary equation. The equation is based on static assumptions, where the tension is calculated based on the floater and anchor position,the difference in the horizontal position is X. l is the total length of the mooring line. The difference between l and ls is that ls do not include the mooring line that is on the seabed, and it's, therefore the minimum length. This is also the difference between X and x. The minimum length can be estimated using the equation 3.5.10. By using equation 3.5.10 and 3.5.11, the minimum length l_s necessary can be reformulated to equation 3.5.13 .

$$ls = asinh\Big(\frac{x}{a}\Big), a = \frac{T_H}{w} \tag{3.5.10}$$

$$h = a\Big[cosh(\frac{x}{a}) - 1\Big] \tag{3.5.11}$$

$$ls^2 = h^2 + 2ha \tag{3.5.12}$$

Relation between anchor position X and horizontal tension can be calculated by combining equation 3.5.11 and 3.5.13. The geometrical stiffness can be calculated by the water weight w, horizontal tension T_H, and height H between the mooring points in equation 3.5.14. In Figure 3.5.1, the parameters in a mooring system have been drawn.[16] [27]

$$X = l - h(1 + 2\frac{a}{h})^{\frac{1}{2}} + acosh^{-1}(1 + \frac{h}{a}) \tag{3.5.13}$$

$$K_G = \frac{dT_H}{dx} = w\Big[-\frac{2}{\sqrt{1 + 2\frac{T_H}{wh}}} + cosh^{-1}(1 + \frac{wh}{T_H})\Big]^{-1} \tag{3.5.14}$$

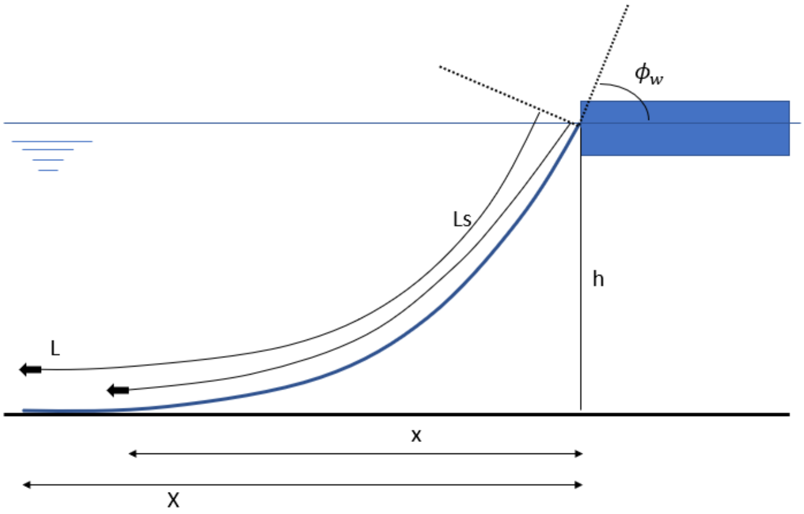

Figure 3.5.1: Definition of mooring parameters, inspired by Faltinsen,[16]

3.5.5 Tension leg mooring system

Tension leg mooring system is a principle where a large portion of the stiffness in the system comes from pretension, which is generated from a high buoyancy force versus gravity. TLP systems are stiff due to the pretension and often have a low natural period. Higher-order hydrodynamic loads such as ringing and springing can be necessary to evaluate. Since the vertical loads are high, suction or pile anchors are possible anchor types. Horizontal stiffness in the system is generated through small angle changes in the tether line. Large horizontal and vertical motions can be critical due to snapping from slack in the tether [27] [28].

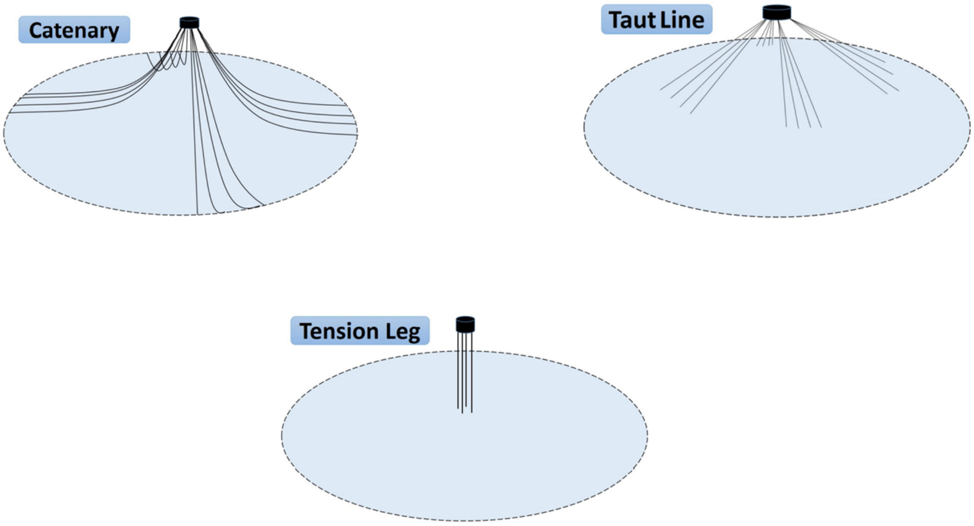

Figure 3.5.2: Different mooring systems for floating structures [27]

3.5.6 Beam theory

Truss equation has to be established to understand how a RIFLEX mooring works. A rod with length L , cross section area A, elasticity module E which are loaded with the force P in axial direction [29]. The truss will then take the force as a axial deformation, change in the length of the rod due to deformation. To get equilibrium the rod will create an internal tensile force N. Therefore the tension in the rod is only normal to area, the x-direction.

$$\sigma_x = \frac{N}{A} \tag{3.5.15}$$

The change in the length can be denoted as ΔL. For a homogeneous, prismatic rod, the extension will be linear. The total displacement as a function of x on the rod is in equation 3.5.16.

$$u = \frac{x}{L}\Delta L \tag{3.5.16}$$

The definition of engineer strain is the total displacement per length, see equation 3.5.17.

$$\epsilon_x = \frac{du}{dx} = \frac{\Delta L}{L} \tag{3.5.17}$$

Hookes law connects the strain to the tension, the law is valid if the material is homogenous, istropic and linear elastic, equation 3.5.19.

$$\sigma_x = E_x \epsilon_x => \epsilon_x = \frac{\sigma_x}{E} = \frac{N}{EA} \tag{3.5.18}$$

By combining equations 3.5.16 and 3.5.19 , the differential equation for a truss can be established. The differential equation can then be solved by integrating with regard to displacement and introducing boundary conditions.

$$\frac{du}{dx} = \frac{N}{EA} \tag{3.5.19}$$

This gives an equation for axial force dependent on the horizontal displacement at the ends of the truss. Due to the integration, integration constant C is introduced, which depends on the physical system's boundary condition.

$$u = \frac{N}{EA}x + C \tag{3.5.20}$$

For position 0 and L its known that end 1 will determine the horizontal position.

$$u(0) = v_{x1} = C, u(L) = v_{x2} \tag{3.5.21}$$

The axial force is therefore dependent on the x deformation between end 1 and 2. Since the system is rigid in bending direction only two coordinates are needed to solve the system.

$$N = \frac{EA}{L}(v_{x2} - v_{x1}) \tag{3.5.22}$$

Using Newton's 3. law, the forces have to be in equilibrium. Therefore the reaction forces are opposite to each other.

$$S_{x1} = -N, S_{x2} = N \tag{3.5.23}$$

The stiffness matrix relates the displacement and forces. Therefore the reaction forces in the truss are known.

$$\begin{bmatrix} S_{x1} \\ S_{x2} \end{bmatrix} = \frac{EA}{L} \begin{bmatrix} 1 & -1 \\ -1 & 1 \end{bmatrix} \begin{bmatrix} v_{x1} \\ v_{x2} \end{bmatrix} \tag{3.5.24}$$

The equation can be expressed by matrix notation.

$$\boldsymbol{S} = \boldsymbol{kv} \tag{3.5.25}$$

The same can be done for a beam where moments and forces are calculated for given rotations and displacement using the stiffness matrix for beams. The following assumptions can calculate elementary beam theory, 1) small displacements, 2) linear elastic and homogenous material, 3) deformations according to the Navier hypothesis, 4) prismatic beam meaning all material constants are constant through the entire beam, 5) normal tension across the beam is neglected. Then vertical and bending stiffness are connected with the truss stiffness matrix. This gives a stiffness matrix for x,y, and rotations neglecting stresses in the volume and in the z-direction. In reality, axial forces will influence beam stiffness by geometrical effects. This second-order effect can be neglected for small axial forces or medium, slender beams. This buckling effect will only lower the capacity if the axial tension is highly utilized and the force is in compression. In RIFLEX SIMA, mooring system trusses, or beams are used. This approximation should give little changes in the solution for a slender and flexible element such as mooring, which takes only primary forces in the axial direction. For many elements, the axial force represents the bending stiffness due to the angular change. Truss elements are not conservative since slender systems are much stronger in the axial direction than for bending and can therefore carry more load than beams. [29]

Bar elements in SIMA used total Lagrangian formulation and linear displacement functions. Therefore green strain and second-order Piola-Kirchoff stress is simplified to engineering stress and engineering strain. Since the total lagrangian formulation is used the incremental rotation of a bar element is done globally, therefore, a rotation matrix is not necessary since the relative change in geometry is directly expressed by the global system. [23]

3.5.7 Anchor system

An anchor‘s principal function is to secure the mooring line to the sea bottom at the predetermined position. Anchor choice will be determined based on water depth, soil, load condition, demanded anchor position accuracy and price of installation. [27] [30]

Different anchor types will demand different marine operations based on weight and size. The soil will be crucial for anchor choice since different soil will give different stiffness and friction. Water depth will have a large influence on the precision necessary, larger water depths, the precision of the anchor, will decrease drastically. Changes in anchor position will influence the pretension and length of the mooring. This will change the inline and outline stiffness of the system, thereby changing the natural frequency of the system.

There are several types of anchors; this is only a selection.
1) Drag embedment anchor: Traditional anchor type has become popular due to its simplicity. The anchor is designed to utilize drag force by penetration of the soil partly or fully, thereby creating a drag force from the friction and mass to the soil. Since the anchor has to penetrate the soil and create enough friction, this demands the correct soil type. Drag anchors are designed primarily to take horizontal loads. Therefore the mooring system should be designed for high horizontal loads and small vertical loads. Its high capacity horizontal capacity is the reason for its strong popularity.

2) Pile anchor: Creates lateral and horizontal resistance due to friction. A pile anchor is a hollow pipe hammered or vibrated into the soil. For safety reasons, pile anchors are hammered deep into the soil to ensure high enough friction.

3) Suction anchor: The suction anchor generates a vacuum from the pump system by pumping out water from the chamber, which creates a pressure difference between the outside and the pipe's interior, forcing the anchor downwards against the sea bottom. After installation, the pump is removed since the vacuum is created. The anchor is a caisson foundation meaning it is a big water-tight chamber open at the bottom. The vacuum creates excellent resistance both in lift and drag. The aspect ratio to the suction anchor varies depending on soil composition, all from 2:1 to 7:1 from stiff to soft clay. Suction anchors need fine particles, and an even sea bottom to create a stable vacuum, making it fit for the North Sea. The vacuum suction anchors are efficient compared to their weight. Experimental testing shows a linear correlation between water flow rate through the anchor and resistance to pullout force. Therefore the fines of the particles and the flow condition, which are also correlated to the grain size, determine the suction anchor's efficiency. [27] [31]

4) Deadweight anchor: Can be used on cohesionless soil since the resistance from the anchor is generated through its weight and not friction to the soil. Another name is gravity anchor.

5) Torpedo anchor: Shaped as a torpedo and suitable for soft clay. Popular when the water depth is high, and therefore an anchor with high precision is necessary.

Figure 3.5.4 shows how anchor choice is determined by geological properties, the seabed slope, loading direction, and the lateral load from the mooring system. [27] [30]

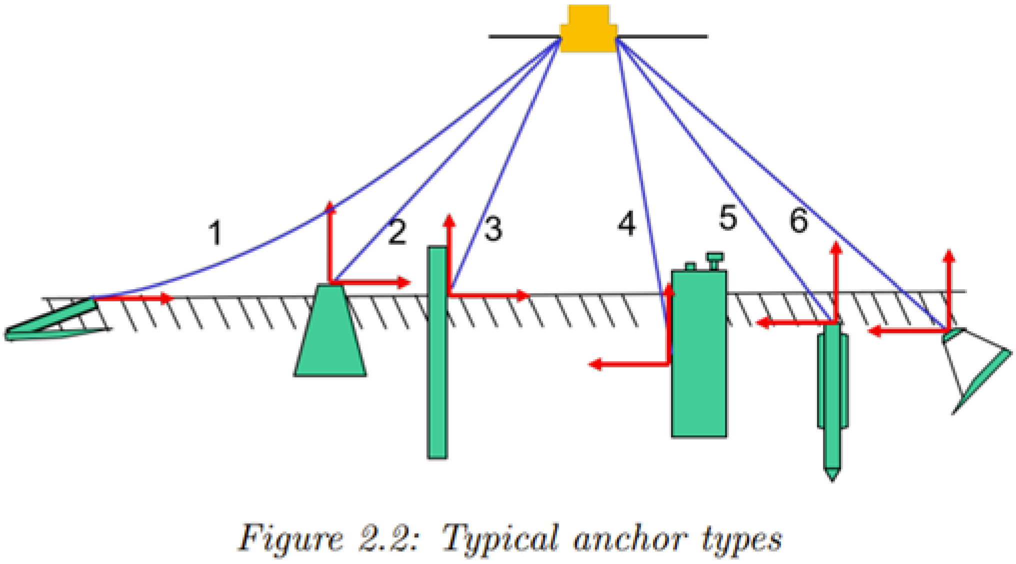

Figure 3.5.3: "Drag embedment anchor (DEA) (No.1), dead weight anchor (No.2), pile anchor (No.3), suction anchor (No.4), torpedo anchor (No.5) and vertical load anchor (No.6). The red arrows indicate in which direction the anchor can take the force" [27]

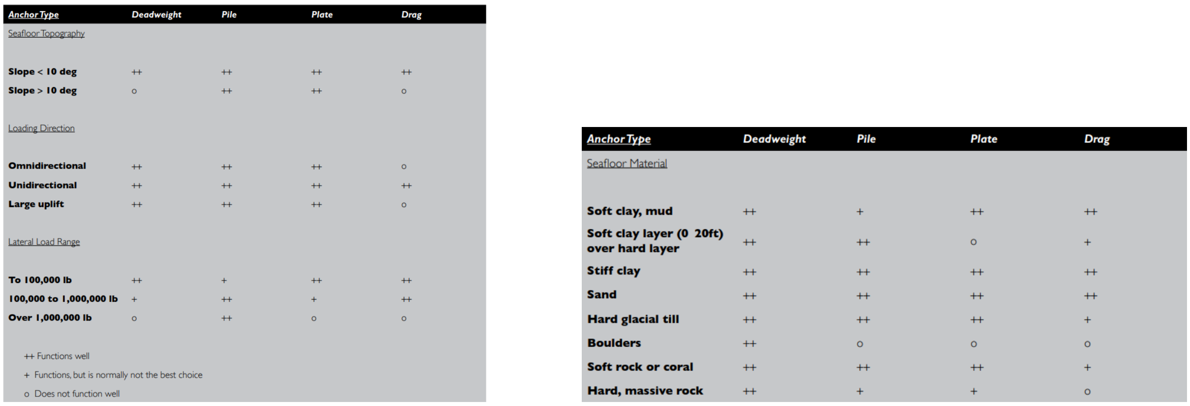

Anchor Type	***Deadweight***	***Pile***	***Plate***	***Drag***
Seafloor Topography				
Slope < 10 deg	++	++	++	++
Slope > 10 deg	o	++	++	o
Loading Direction				
Omnidirectional	++	++	++	o
Unidirectional	++	++	++	++
Large uplift	++	++	++	o
Lateral Load Range				
To 100,000 lb	++	+	++	++
100,000 to 1,000,000 lb	+	++	+	++
Over 1,000,000 lb	o	++	o	o

++ Functions well
+ Functions, but is normally not the best choice
o Does not function well

Anchor Type	***Deadweight***	***Pile***	***Plate***	***Drag***
Seafloor Material				
Soft clay, mud	++	+	++	++
Soft clay layer (0 20ft) over hard layer	++	++	o	+
Stiff clay	++	++	++	++
Sand	++	++	++	++
Hard glacial till	++	++	++	+
Boulders	++	o	o	o
Soft rock or coral	++	++	++	+
Hard, massive rock	++	+	+	o

Figure 3.5.4: Anchor behavioral criteria for seafloor topography, loading direction and lateral load range [30]

Chapter 4

Methodology

4.1 Analysis tools

4.1.1 SIMA

SIMA is a multi-body analysis tool used for coupled dynamic and static simulations. SIMA software is developed by Marintek and distributed by DNV. The software can analyze floating structures with coupled wave, wind, and current effects for structural and mooring analysis. Hydrodynamic coefficients are imported from HydroD, and 3D visualization FEM file from GeniE. HydroD imports 3D model from GeniE where external geometry is specified. HydroD calculates the hydrodynamic coefficients used in SIMA with this information. SIMA was extended to FOWT where modeling of offshore wind turbine blades, wind load models, and wind turbine modeling (with a control system) with flexible blades and tower was added [32]. Therefore an aero-hydro-servo-elastic analysis can be carried out. Also, the newest research version SIMA 4.5 multiple external control system, can be used in the analysis, enabling aero-hydro-servo-elastic analysis for shared mooring systems. In the next public SIMA version 4.6 this is going to be included. The flow chart in SIMA is shown in Figure 4.1.1.

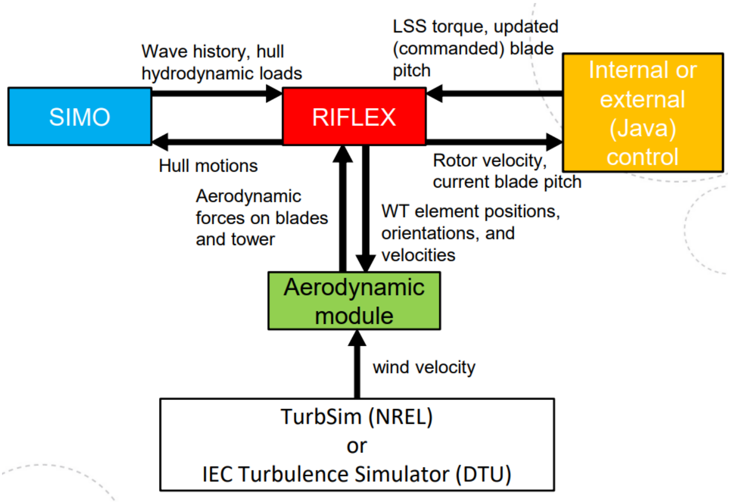

Figure 4.1.1: SIMA modules flow chart [19]

SIMO and RIFLEX were developed separately for different uses. RIFLEX - riser analysis software was developed for dynamic RISER analysis using nonlinear FEM. SIMO, on the other hand, was developed for complex multi-body calculations in marine operations using rigid body assumption. SIMA where developed as a tool utilizing both SIMO and RIFLEX. Figure4.1.1 illustrates how the hydrodynamic data is exported to RIFLEX where forces in elements are calculated, and the equilibrium is calculated for FEM mooring line. After that, the hull motions are exported to SIMO, which dynamically calculates the next time step. SIMA was extended to an aero-hydro-servo-elastic analysis, as a control system and aerodynamic module were added to carry out BEM analysis. The aerodynamic module calculates the aerodynamic forces on the blades and the tower, which is exported to RIFLEX where the internal moments and forces are calculated. Wind turbine element positions are then calculated and exported back to the aerodynamic module with the element's velocities. The rotor velocity and blade pitch are exported to the control system, which updates the blade pitch and torque. Turbulent wind velocity has to be imported into SIMA by a synthetic wind generator. Both Turbsim and Mann turbulence generator has been used in this Master's thesis work. How SIMA administrates the files are shown in Figure 4.1.2.

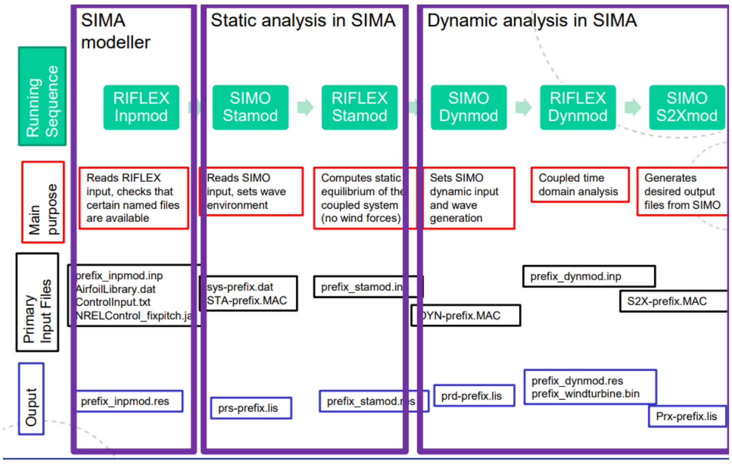

Figure 4.1.2: SIMA file handling [19]

Figure4.1.2 shows how the flow of data is between RIFLEX and SIMO packages.

4.1.2 Synthetic wind generation - Turbsim

Turbsim is a stochastic turbulence program that creates 3D time series of coherent turbulence structures. Turbsim was developed as IEC Normal Turbulence models did not properly model the coherent turbulence structure in the spatiotemporal turbulent velocity field. The program uses a fast Fourier transformation of a power spectral density function. SIMA is compatible with Turbsim file format, which makes the turbulent wind files easy to use. [23] [33]

4.1.3 Synthetic wind generation - Mann turbulence generator

Mann turbulence generator is used in HAWC2 - Horizontal Axis Wind turbine simulation code 2^{nd} generation, which is an aeroelastic code, made for running responses in the time domain. The program is distributed by DTU wind and wasp engineering. The atmospheric turbulence is modeled by an isotropic spectral tensor, also known as Mann uniform shear turbulence model [22]. The model uses neutral-stability turbulence with rapid-distortion theory. [23]

4.2 VolturnUS-S

VolturnUS-S is a 15 MW semi-submersible wind turbine designed by NREL with the IEA wind 15 MW offshore reference wind turbine. The tower was originally designed for a monopile wind turbine but was modified to the semi-submersible since inertial and gravity loads are increased due to floater motions [34]. The tower has a 47% greater mass to increase the stiffness of the VolturnUS-s tower. Also, minor adaption was also done by NREL on the control system for adaptions to the floater motions.Figures 4.2.1 , and 4.2.2 illustrates the model VolturnUS-s. The dimensions of VolturnUS-s are given in Figures 4.2.2, and 4.2.3. More details are available in the NREL reports. [34]

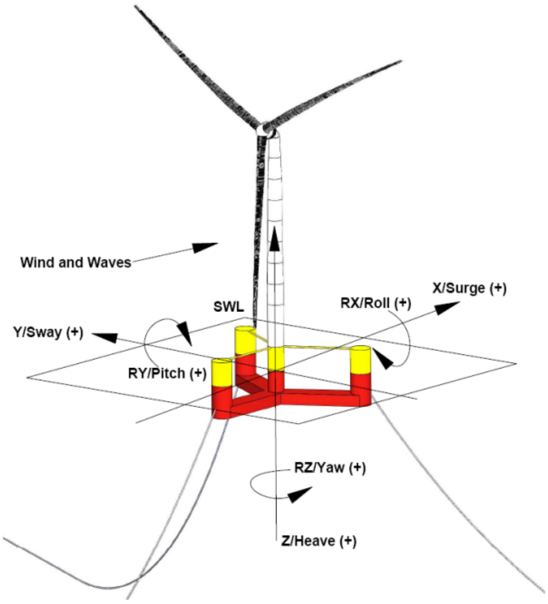

Figure 4.2.1: Modell of VolturnUS-s [34]

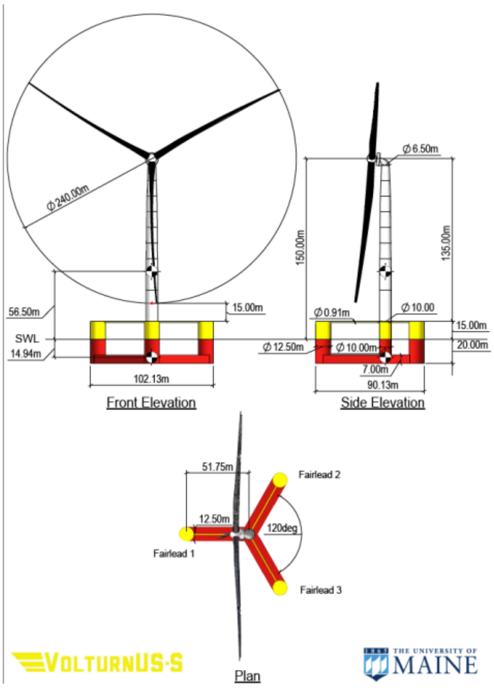

Figure 4.2.2: Dimensions of VolturnUS-s [34]

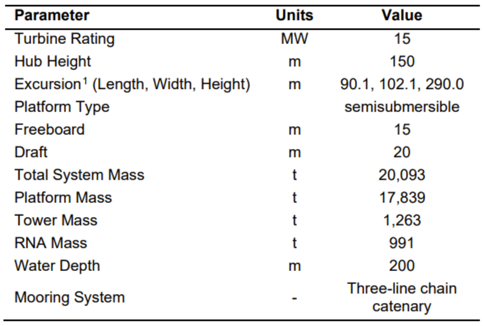

Parameter	Units	Value
Turbine Rating	MW	15
Hub Height	m	150
Excursion[1] (Length, Width, Height)	m	90.1, 102.1, 290.0
Platform Type		semisubmersible
Freeboard	m	15
Draft	m	20
Total System Mass	t	20,093
Platform Mass	t	17,839
Tower Mass	t	1,263
RNA Mass	t	991
Water Depth	m	200
Mooring System	-	Three-line chain catenary

Figure 4.2.3: General system properties of VolturnUS-s [34]

VolturnUS-s wind turbine has a hub height of 150 m which is used further for the generation of turbulent wind, and the total system mass is used to calculate the moment of inertia to verify that all the masses were accounted for. RNA is short for ”rotor nacelle assembly” in Figure 4.2.2. Water depth is changed to 600 m as cost saving potential for the shared mooring system is for the deep water system and to agree with Wilson and Hall mooring system, as the shared mooring systems is based on their article [9]. In Figure 4.2.5, anchor depth of 200 m is used in the VolturnUS-s model.Since Wilson and Hall used a 10 MW wind turbine, the rotor diameter is 178 m compared to 240 m for VolturnUS-s. Furthermore, pontoon and column geometry is used for Morison calculation. The original model before modifications is in Figure 4.2.4.

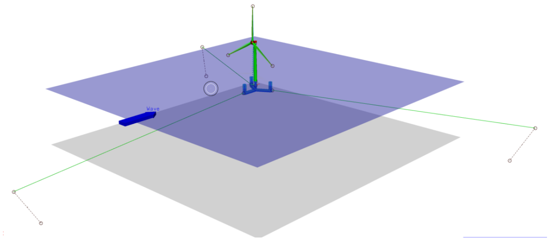

Figure 4.2.4: Modell of Volturn-US in SIMA with original mooring system

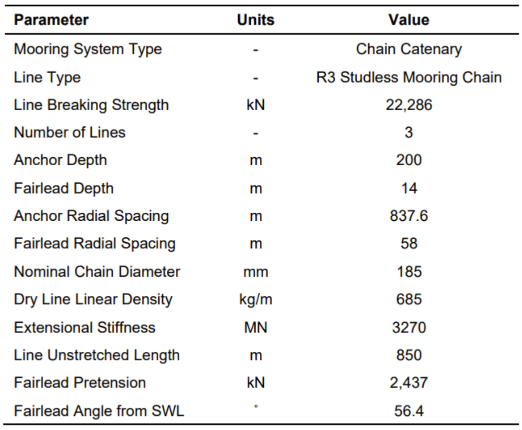

Parameter	Units	Value
Mooring System Type	-	Chain Catenary
Line Type	-	R3 Studless Mooring Chain
Line Breaking Strength	kN	22,286
Number of Lines	-	3
Anchor Depth	m	200
Fairlead Depth	m	14
Anchor Radial Spacing	m	837.6
Fairlead Radial Spacing	m	58
Nominal Chain Diameter	mm	185
Dry Line Linear Density	kg/m	685
Extensional Stiffness	MN	3270
Line Unstretched Length	m	850
Fairlead Pretension	kN	2,437
Fairlead Angle from SWL	°	56.4

Figure 4.2.5: Mooring system properties for the original mooring system,[34]

Volturnus-US has three 850 m long chain catenary lines connected at a 14 m depth to each outer column with equal spacing of 120° degrees. Anchor points are 837.6 m from the center line. The chain diameter was chosen to keep the system radial motion, also known as a watch circle, under 25 m with maximum peak thrust. The chain chosen was the largest currently available in the market. Natural frequencies for VolturUS-s are in Figure 4.2.6.

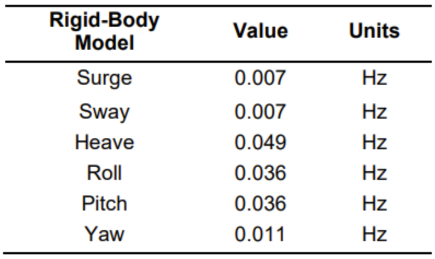

Rigid-Body Model	Value	Units
Surge	0.007	Hz
Sway	0.007	Hz
Heave	0.049	Hz
Roll	0.036	Hz
Pitch	0.036	Hz
Yaw	0.011	Hz

Figure 4.2.6: Rigid-body natural frequency with original mooring system,[34]

NREL conducted decay tests, but the mooring system to VolturnUS-s was not used, meaning that the natural frequencies are not representative. Since the dimension of the mooring line is much larger and the water depth is shallow, it is expected that the mooring stiffness is higher than the mooring systems used in this thesis. Therefore the natural periods in surge-sway are expected to be longer for the new mooring system.

The floating tower dimensions, control system, RAO, hydrostatic stiffness, additional mass, second-order quadratic transfer function, viscous damping from OpenFOAM, and tower bending modes may all be found in the NREL report for the VolturnUS-s system [34].

4.3 Modeling of shared mooring topologies to VolturnUS-s

Four mooring systems are selected from Wilson and Hall's study "Linearized modeling and optimization of shared mooring systems" [9]. It was also necessary to change the original VolturnUS-s mooring system to Wilson and Hall single turbine layout - baseline for a fair comparison between single-body and multi-body systems. Since the original system has a mooring weight of 658 kg/m versus the optimized system of 116 kg/m, the system's stiffness would have been entirely different. Also, the mooring systems are designed for different mooring depths in Wilson and Hall's study and VolturnUS-s (600 m vs. 200 m) [9].

Three shared mooring systems and a reference system were chosen from the models of Wilson and Hall [9]. The simplest optimized systems were chosen, as the numerical simulation increases per floater. Most of the models have two anchored mooring lines per floater since it gives an even distributed stiffness with a linear mooring system. A shared mooring system with one anchored mooring line per floater is selected, to compare how the dynamic behavior is affected few anchored mooring lines. Also, SIMA can only analyze simply shared mooring systems as the turbulent wind file was originally only meant for a single wind turbine. Therefore the wind turbines must be in line, meaning that only two wind turbines can be analyzed in SIMA with coupled analysis. Otherwise, an extensive, computationally demanding wind file must be generated since a wind file width of around 1200 m is necessary (this is dependent on shared mooring topology and rotor diameter). Usually, the width of the wind file depends on the rotor's diameter. Therefore a wind file with a width around five times larger than usual is necessary. Two and one anchored three floater systems were chosen to compare how the floater dynamics are influenced by anchored compared to a shared mooring line.

Axial stiffness for each mooring line has been calculated using a buoyancy force of 15%, and a Youngs E-modulus of 210 GPa, typical for structure steel. For a RIFLEX mooring system, the mooring line's area must be specified to calculate the buoyancy force. Therefore, the area has to be calculated to match the water weight. As the mooring area seems small, the hydrodynamic is assumed constant as 0.33 m for simplicity. The buoyancy force is added to the water weight for the SIMO quasi-static mooring system, and only the mooring hydrodynamics depend on the specified diameter. Axial stiffness was so high that elasticity effects were not observed, as several simulations with 100 times higher axial stiffness were run to test the elasticity. The necessary area of the mooring system can be calculated considering the buoyancy in the system, see equation 4.3.1. The four chosen mooring topologies are illustrated in Figure 4.3.1, where the weight of each mooring line is shown in Table 4.3.1. The letter A stands for anchored mooring weight, and S for shared mooring weight.

$$F_B = 0.1172wL = \nabla\rho g => A = \frac{0.1172w}{\rho g} \tag{4.3.1}$$

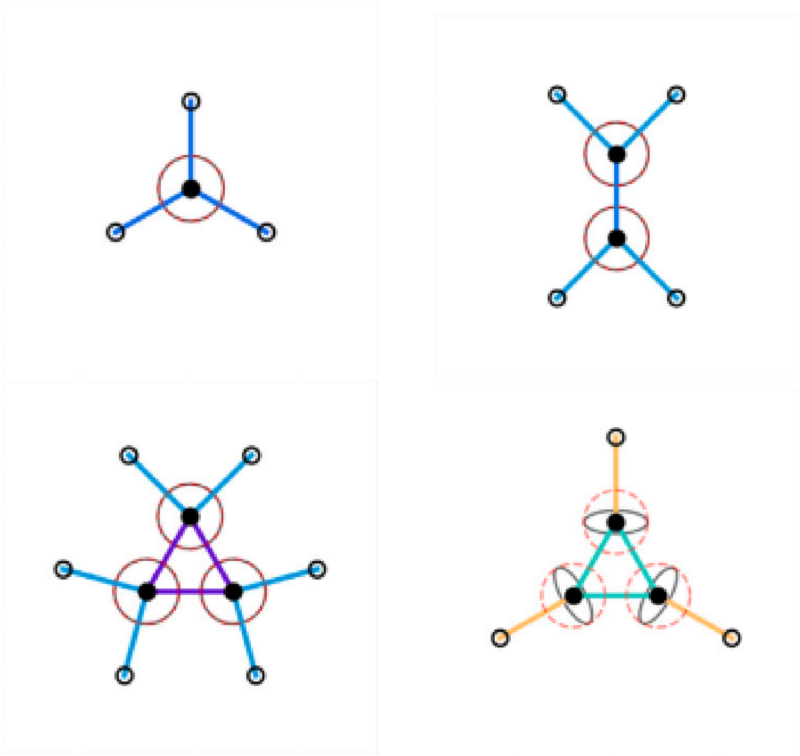

Figure 4.3.1: Mooring systems selected from Wilson and Hall optimization for shared mooring[9]

Table 4.3.1: Mooring line dry weight [9]

System	A/S line [kg/m]	Pre-tension [kN]	k_l - anchor/shared [N/m]
Baseline	116/-	929/-	10575/-
a) - shared mooring	175/176	1393/1970	15863/11467
b) - 9 mooring lines	175/101	1393/1137	15863/6620
c) - 6 mooring lines	875/359	4034/6987	7084/79556

The shared mooring cases are based on models from Hall and Wilson [9], but in those cases, the floaters are only modeled as a point mass and therefore have no fairleads. Figures 4.3.3, 4.3.5, 4.3.7 and 4.3.9 show how the fairleads and rotations have to be taken into account in the SIMA modeling. Nevertheless, static equilibrium in z-translation must be corrected as the total mooring weight differs. Therefore the buoyancy force of the floaters has to be corrected. The catenary equation can calculate the mooring line laying at the seabed, and the total mooring mass can be estimated. Instead, static calculations are carried out, and the needed buoyancy force is calculated using C_{33}, the hydrostatic stiffness in z-translation. Also, the extra mass must be considered when calculating the linearised system's natural period.

Shared mooring cannot be modeled as a regular mooring system in SIMA, as both supernodes have to be connected to the fairlead supernode. Therefore, the nodes are a slave to the floater supernode. Thus, the RIFLEX line has to be stretched and cannot have the "extra" length that creates the catenary mooring shape. There are two possible model solutions to this problem; the latest one is the simplest. Firstly the floaters can be modeled in a reference system where the stretched shared mooring line position has to be used. Therefore, the problem with the supernodes is avoided. After that, the floaters must be freed and return to equilibrium. An example of this is the shared mooring system a) the floaters are 1716 m away from each other,

taking into account the fairleads that are 116 m wide. The shared mooring is 1708 m long, and the distance between the fairleads is 1600 m. Therefore, the reference system to floater 2 has to be moved from 1716 m to 1824 m. This was done initially for floater system a), but a better approach was used later.
Secondly, a shared mooring system can be modeled using a supernode in the middle of the floaters, specifying a z-position that gives a taut mooring system (also here, the z-translation to the fairleads has to be considered), forming a triangle. The shared mooring lines must be separated into two lines connected to the supernode in the middle with one fairlead at its end. When the weight is applied to the analysis, the mooring line will converge to a catenary shape.

As the floaters are rotated, it is crucial not to rotate the systems more than 90° degrees, as SIMA cannot transform the hydrodynamic coefficient for larger rotations. The manual does not specify a maximum rotation of 90° degrees, but it is experienced as the simulations become numerically unstable. Since VolturnUS-s is symmetric, large rotation is not a necessity. Since the models are rotated, the QTF to VolturnUS-s does not generate any second-order loads, as only 0° degrees QTF was calculated in the original VolturnUS-s. Drift force is relevant for mooring systems when the wave height is significant, but for systems with multiple wind turbines with turbulent wind, the thrust force is large compared to the drift force.

The systems are modeled with FEM RIFLEX mooring and SIMO quasi-static mooring lines, which follows the catenary equation. The main difference between RIFLEX truss/beams and SIMO quasi-static mooring is that SIMO mooring is quasi-static, meaning it is not fully dynamic as the stiffness is pre-generated. The tension in the mooring line will therefore be dependent on the extrusion. The SIMO quasi-static mooring calculates the tension for N numbers of horizontal points, which is why the mooring model is computationally fast. Bending stiffness is also neglected, as for trusses. This could be a good approximation for a more complicated analysis to save time if not the mooring line fatigue is of interest and the maximum tension. Figure 4.3.2 shows how the baseline system is adapted to VolturnUS-s in SIMA with RIFLEX mooring elements. Figure 4.3.3, shows how the mooring lines are connected to the floater in the baseline system.

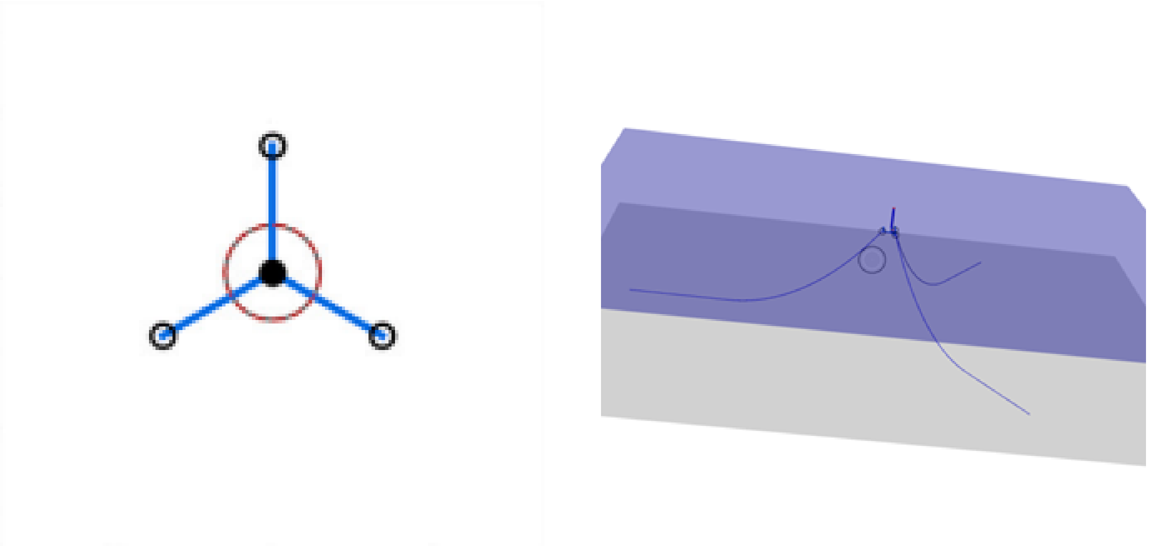

Figure 4.3.2: The baseline mooring system from Wilson and Hall modeled in SIMA[9]

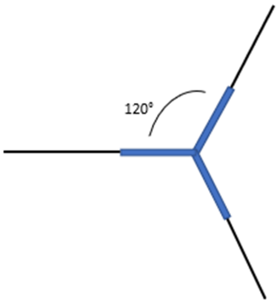

Figure 4.3.3: Mooring configuration to model baseline

Both mooring and fairleads have the same direction for the baseline system, with a 120° degree line spread. This is the same as for the VolturnUS-s model.Figure 6.4.2 shows how system a) is adapted to VolturnUS-s in SIMA with RIFLEX mooring elements. Figure 4.3.5, shows how the mooring lines are connected to the floater in the baseline system. The illustration shows how the mooring connection is not in line with the pontoon.

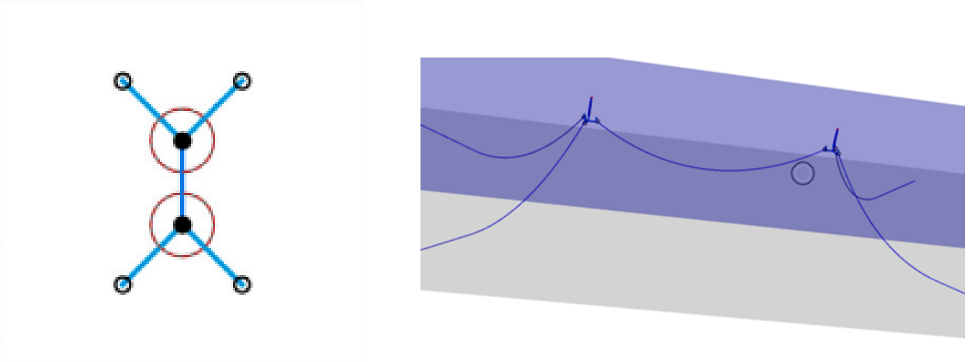

Figure 4.3.4: The shared mooring system a) from Wilson and Hall modeled in SIMA[9]

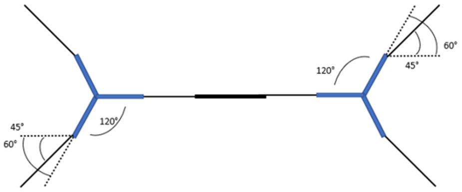

Figure 4.3.5: Mooring configuration to model a)

For the shared mooring system, a) there is a line spread of 90 degrees for the upwind and downwind mooring lines; see Figure 4.3.5. Optimization study to Wilson and Hall, a 90° degree spread is the most efficient for a linear mooring system as the response is symmetric, giving a circular watch circle. As the fairleads have a spread of 120° degrees, the mooring line force is not aligned with the center of gravity, causing a yaw moment. The attack point is 12 m away from the central of gravity. Figure 6.4.3 shows how system b) is adapted to VolturnUS-s in SIMA with RIFLEX mooring elements. Figure 4.3.7, shows how the mooring lines are connected to the floater in the baseline system.

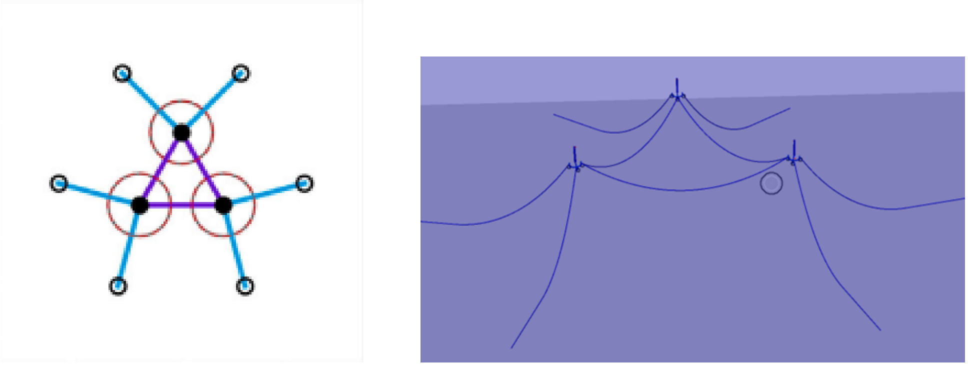

Figure 4.3.6: The shared mooring system b) from Wilson and Hall modeled in SIMA[9]

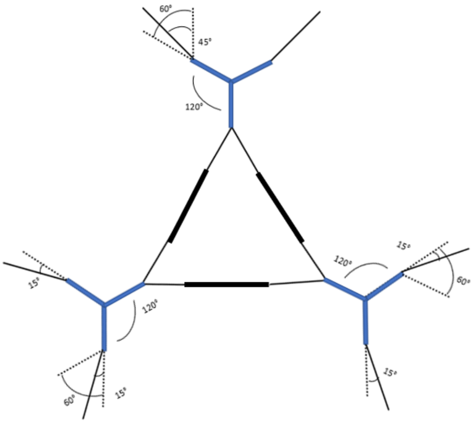

Figure 4.3.7: Mooring configuration to model b)

Model b) from Wilson has three wind turbines connected with one shared mooring and two anchor points per floater. The shared mooring system connects the floaters as an equilateral triangle. The shared mooring lines have a spread of 60° degrees between each other. Each floater has an anchor mooring system with a spread of 90° degrees. Floaters are defined as for Figure 5.2.5, counting from 0° degrees with the clock, beginning with the floater in the right corner. The same is for the mooring system, beginning with the first mooring to floater 1. Floaters one and two are symmetric with 15° and $-75°$ degrees direction from the x-axis, respectively, in floater three, the lines have a direction of 45°,$-45°$ degrees from the y-axis. Respectively, The model is y-symmetric, as shown in Figure 4.3.6. The spread is 90° degrees between the anchored mooring line per floater, giving a circular watch circle for a linearized mooring system. Figure 6.4.4 shows how system c) is adapted to VolturnUS-s in SIMA with RIFLEX mooring elements. Figure 4.3.9, shows how the mooring lines are connected to the floater in system c).

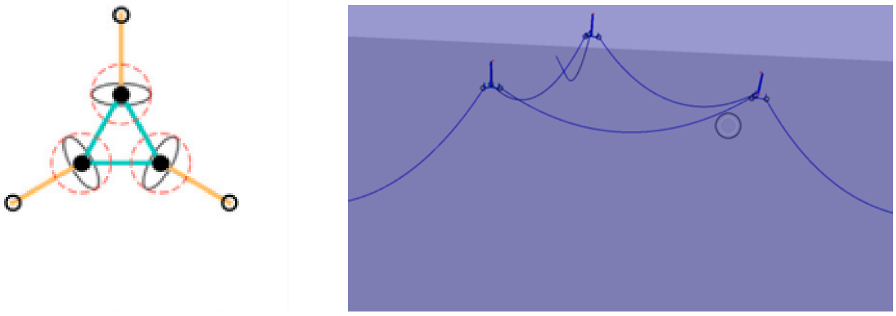

Figure 4.3.8: The shared mooring system c) from Wilson and Hall modeled in SIMA [9]

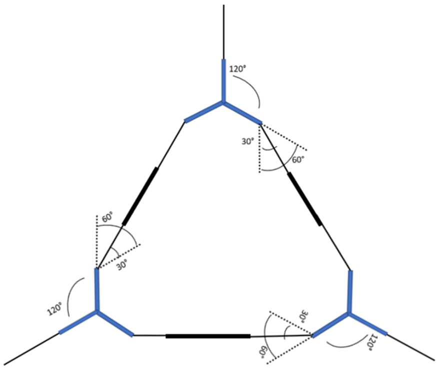

Figure 4.3.9: Mooring configuration to model c)

Model c) has three floaters with a shared mooring system as model b) but only one anchored mooring per floater in −30°, −150°, and 90° degrees for floaters 1, 2, and 3. Meaning the system is symmetric. Since the system only has one anchor per wind turbine, each mooring line has to contribute more to the restoring force than for systems a) and b). Therefore, this system's dry weight is much higher, so the mooring stiffness is sufficient. The shared mooring weight is much higher than for systems a) and b). This is connected to the fact that each anchored mooring has to carry almost all the load for given directions. Mooring one has to carry loads in -x direction, mooring two for loads in the x direction, mooring three for -y direction, and mooring one and two for y loads. If the shared mooring is not stiff enough, the anchored mooring lines stiffness will not be fully shared, causing the system to be soft. Therefore a one-anchored system must have a sufficiently stiff shared mooring so that the loads can be distributed through the system. If the shared stiffness is sufficient, the system will carry the loads together, behaving as a semi-rigid system. Because the system has only one anchor per floater, the system will not have a round watch circle, according to Wilson and Hall [9], but an elliptic one. Each floater has the least stiffness normal to the mooring line direction: 60°, −60°, and 0° degrees. The largest stiffness is in the tangential direction with the mooring line.

4.4 Element convergence study

An element convergence study has been carried out for turbulent wind and irregular waves. The study has been conducted for baseline and a) - shared mooring system. Condition 2 was used, which has the highest thrust force, resulting in more significant surge motions. The upwind mooring line was evaluated since the standard deviation and maximum tension converged more slowly for this line.

An element convergence study is necessary when using RIFLEX elements, as the method's accuracy depends on the elements' refinement and where the refinement is. Due to simplicity, the discretization of mooring lines is even for all. The computational efficiency could be improved by gradually improving the refinement in the touchdown point and where the curvature is the largest. Proper refinement in the touchdown point is necessary as mooring on the seabed increases the friction and proper distribution of the weight in the line. As the weight dominates the tension, an improper distribution of mooring weight would estimate a wrong geometrical stiffness. Since the elements are straight, the mooring line's curvature must be modeled by enough elements. When the floater's extrusion is large, the mooring line becomes more taut, and the curvature is lesser.

In advance, an element size of 10 m was recommended by both supervisors to be sufficient. Therefore it should be sufficient with 180 and 170 elements for anchored and shared mooring lines. How many elements were necessary for shared lines was unknown as no literature mentions this, as quasi-static mooring is often used. Since the shared mooring line goes between two FOWT is expected that the curvature is small and the line has no touchdown point. Therefore, it is expected that it is not needed with 170 elements for shared mooring. However, it is expected that the anchored mooring line needs more elements since the seabed is in deep water (600 m). The curvature would then be considerable at the touchdown point.

It was experienced that surge motion converged more rapidly than the tension, first the mean value, after that standard deviation for surge motion, and then the mean tension. Therefore, the convergence study is only presented for the mooring line's standard deviation and maximum tension.

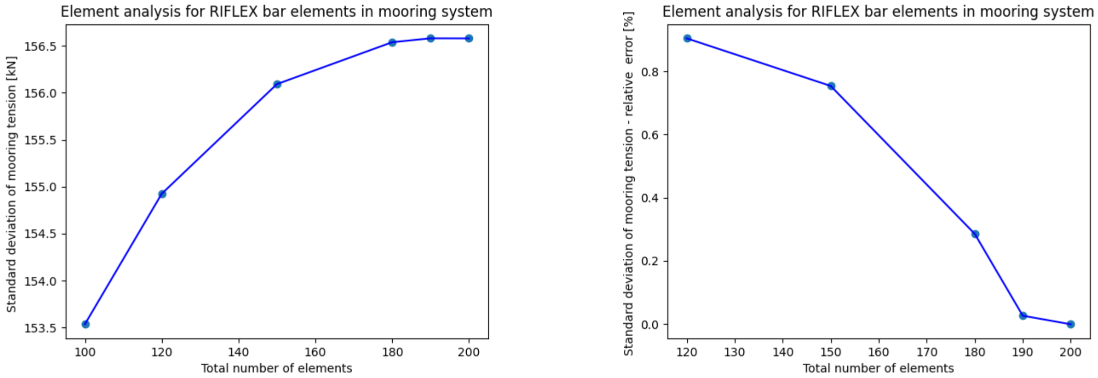

Figure 4.4.1: Element convergence study for wind speed w = 10 [m/s] upstream mooring - baseline - standard deviation [kN] and relative error [%]

There is minimal difference between all the elements for the standard deviation as the relative error is less than one percent. With over 180 elements, the standard deviation converges.

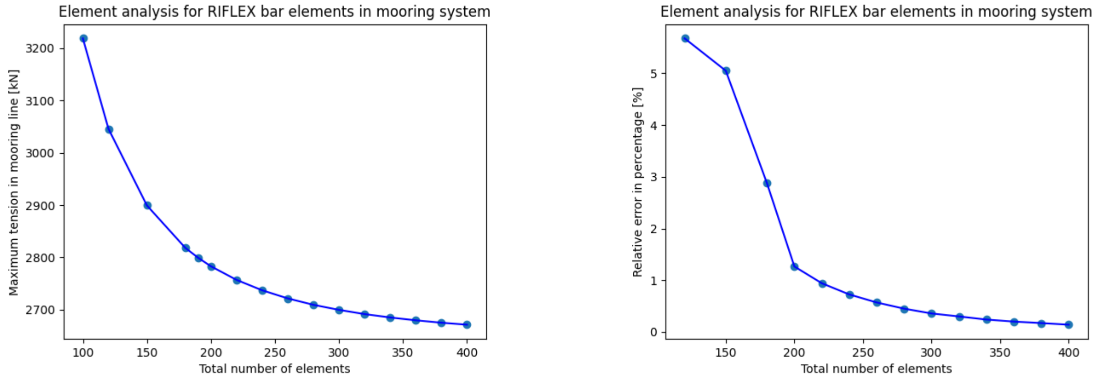

Figure 4.4.2: Element convergence study for wind speed w = 10 [m/s] upstream mooring - baseline - maximum tension [kN] and relative error [%]

The maximum tension is more sensitive to the total number of mooring as it is the maximum of 36000 timesteps. The relative error is less than three percent for 180 and is therefore sufficient, but by choosing 200 elements in the mooring line, the relative error is substantially lesser. The benefit of more elements is deemed unnecessary. Therefore 200 elements are used in further analysis.

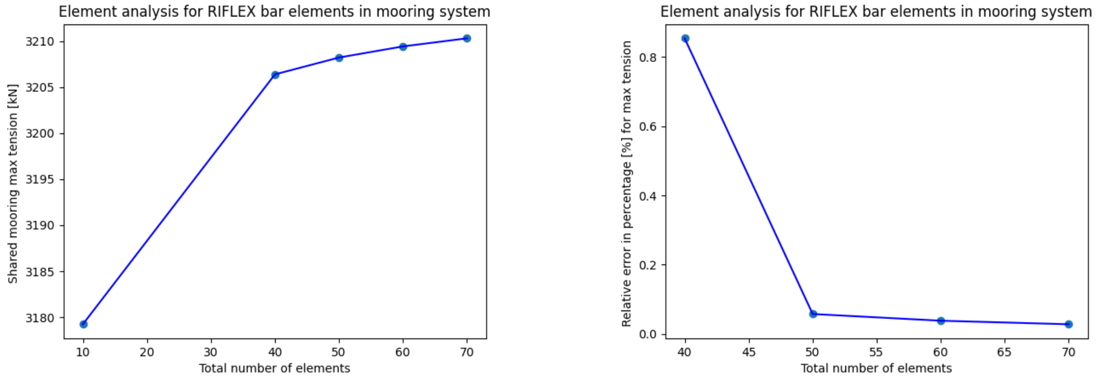

Figure 4.4.3: Element convergence study for wind speed w = 10 [m/s] shared mooring - maximum tension [kN] and relative error [%]

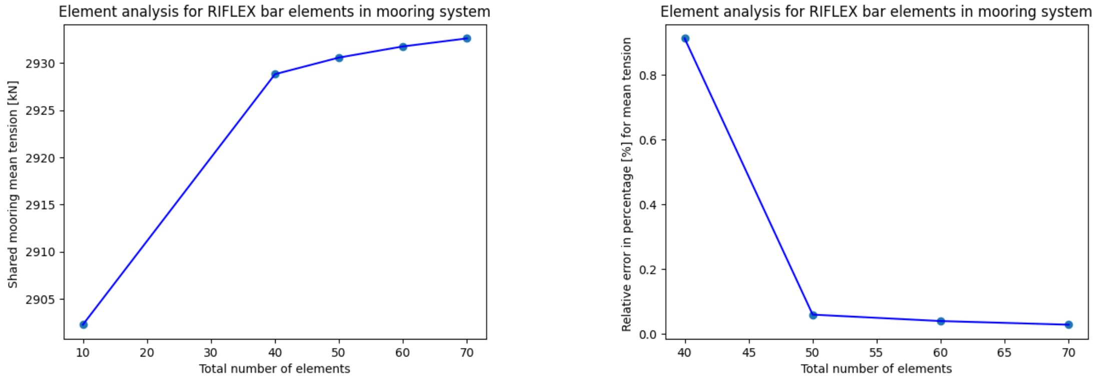

Figure 4.4.4: Element convergence study for wind speed w = 10 [m/s] shared mooring - mean tension [kN] and relative error [%]

As the curvature is small for the shared mooring, and the tension depends on the relative excursion between the FOWT, few elements are necessary. Since the tension depends on the relative excursion, the tension is more stable in the system resulting in only a slight difference in the convergence study between mean and maximum tension. The total number of elements is only for half of the mooring line, as the shared mooring has to be modeled as two separate mooring lines. Therefore 30, 40, 50, 60, and 70 elements are 60, 80, 100, 120, and 140 elements for the shared mooring line. The relative error is less than one percent for all the mooring systems. Thus, 30 elements are used in further analysis. Shared mooring topologies can therefore reduce the total necessary mooring elements in the analysis per floater, both by fewer mooring lines and fewer elements in the shared mooring lines.

Sensitivity analysis was also carried out shared mooring system a) and baseline with 100, 200, and 400 horizontal points, and 100, 200, and 400 elements with turbulent wind condition 1. Since no current exists in the analysis, the mooring lines were not sensitive to the total number of elements since the system follows a catenary shape. Therefore 100 elements are used in further analysis. For horizontal points, only minor differences were in the floater position. A more significant difference was in the mooring line tension. As the differences were so minor, the study is not presented. Since the analysis was not sensitive to horizontal points, 100 points were used in the further analysis. Later on, analyses for systems b) and c) were conducted. As the answers did not match with RIFLEX mooring, 400 points were used for a better comparison.

4.5 Static analysis

Table 4.5 shows how system c) converges statically when external and internal loads are calculated. First values are shown in the global reference frame. Later on, the local reference frame is used.

Position/ relative position	x-surge	y-sway	r_x-pitch	r_z -yaw
Floater 1 initial	0	0	0	30
Floater 2 initial	-850.23	1470.7	0	30
Floater 3 initial	-1700.5	0	0	30
Floater 1 static 100	-2.46	1.65	5.41	0.08
Floater 2 static 100	0.28	-4.4	-6.44	-0.11
Floater 3 static 100	3.7	1.68	-0.2	-0.08
Floater 1 static 600	-0.66	0.32	5.81	0.08
Floater 2 static 600	0.2	-1.6	-5.82	-0.12
Floater 3 static 600	1.4	0.36	-0.2	-0.07

Table 4.5.1: Model C initial and static positions of floaters

Static equilibrium is essential for calculating static floater motions and mooring tension when an external force is applied. Since the system is multibody with shared mooring, the system converges slowly, meaning that the total number of iterations necessary is high.In table 4.5, an example of static iterations has been carried out for system c, which is the most unstable system. Static 100 is run with 100 iterations in body forces, whereas static 600 is run with 600 iterations. Eight hundred iterations are also run with zero difference to 600 iterations; therefore, static equilibrium is achieved. Due to the slow convergence in the static condition, dynamic analyses were fixed in the static condition so that the mooring pretension was calculated at the initial position. After that, the floater was freed in the dynamic calculation. Since the translation phase of the dynamics is removed when calculating the mean, standard deviation and maximum static calculations for free floater are unnecessary, and it is possible to save computational time. The tension in the mooring line must be correct for eigenvalue analysis and static calculations. Therefore, the static condition must converge to estimate correct natural periods, as the tension in the mooring lines determines the stiffness matrix's stiffness for surge and sway. The system converges with a large-pitch angle since the pretension calculated in SIMA does not match with Wilson and Halls's model [9].

Hydrodynamic forces are neglected for eigenvalue calculations, even though the frequencies are so high that the added mass can be approximated as A(0), meaning an infinite long wave. By looking at the frequency-dependent added mass data to Volturnus, periods over 60 s, the added mass has little variation. See Figure 5.2.1. Added mass was neglected both due to simplicity and uncertainties regarding the eigenvalue analysis of SIMA.

4.6 Wind modelling

The wind files were generated using Turbsim and Mann turbulence generators. One-hour simulations were needed as three-hour simulations are only used for hydrodynamic analysis due to the stationarity assumption. Usually, 20 minutes is used for aerodynamic analysis. From a hydrodynamic perspective, 20 minutes is minimal as the system has to start from equilibrium with no environmental force. Therefore the transient phase will be long compared to the duration of the simulation, which cannot be used. Therefore one-hour simulations are often used in aero-hydro analysis as a compromise. For shared mooring, the wind has to propagate from the upwind to the downwind wind turbine. It is, therefore, important to have a long time series so that all the wind turbines experience the turbulent wind at the end of the simulation. Also, since the wind has to propagate and the mooring system is soft, the transient phase is long for all the simulations. Thus, 4000 s were not enough, and 5000 s were generated.

For generating the wind field, it is necessary to specify the grid size, hub height, time step, grid points, which turbulence model shall be used, etc. Kaimal turbulence model is chosen, with a B turbulence characteristic, with normal turbulence, NTM. As the rotor diameter is 240 m, it is necessary with a larger grid width and height. Therefore 250 m were chosen. Forty-eight grid points in vertical and horizontal were used with a time step of 0.05 s, as supervisor Erin Bachynski-Polić used this in her Turbsim files. The mesh size and the number of points give a temporospatial mesh discretization of $\Delta y = \Delta_z = 5.21m$ and $\Delta t = 0.05s$. A coherency, turbulence scale, power law exponent, and mean shear for the disk were chosen by default: 340.2 m, 42 m, 0.14, and 0.007 $[\frac{(m/s)}{m}]$.

Mann turbulence wind fields were generated for LES conditions. Mann was chosen with the exact mesh discretization as Turbsim. As the simulation with shared mooring was tedious, and fatigue was not a part of the thesis scope, a time step of 0.2 s was chosen. Also, the total number of grid points was reduced to 32 points to match the Mann turbulence generator. Only numbers with two as the base can be used when generating Mann turbulence files. Therefore 48 grid points cannot be generated in the Mann turbulence generator. As the analysis was tedious, 32 grid points were chosen, reducing the mesh size to $\Delta y = \Delta z = 7.14m$. In Mann turbulence generator time step cannot be chosen. Therefore, the total number of points in x and Δx must match the necessary time step and length by equations 4.6.1, and 4.6.2. The TI can be chosen by the Mann parameter $\alpha\epsilon^{\frac{2}{3}}$, equation 4.6.3 . The wind fields are independent of the mean velocity. Therefore the mean velocity has to be specified in SIMA. Figure 4.6.1 shows how the wind field propagates through the space with the specified width, velocity and the size of the loaded wind field, N_{slice}.

$$\Delta t = \frac{U_{mean}}{\Delta x} \tag{4.6.1}$$

$$T = \frac{N_x \Delta x}{U_{mean}} \tag{4.6.2}$$

$$\alpha\epsilon^{\frac{2}{3}} = \frac{55}{18} 0.4754 \sigma_{iso}^2 l^{-\frac{2}{3}} \tag{4.6.3}$$

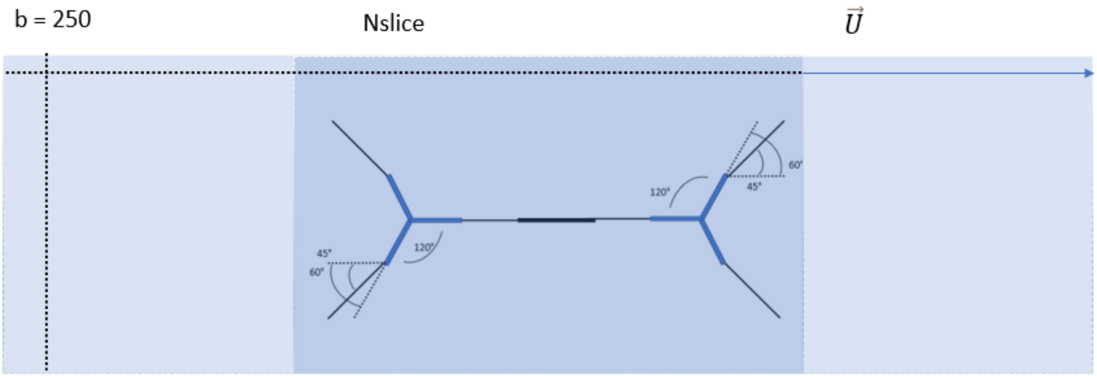

Figure 4.6.1: Wind field propagating through space

When modeling several wind turbines in SIMA it is important to include enough slices so that the temporary wind field is large enough for both of the wind turbines, Figure 4.6.1. If the temporary wind field is not large enough SIMA will struggle with the wind calculations. The total distance between mooring fairleads is 1600 m. From turbine to turbine, the distance is 1716 m. The total number of slices is dependent on the time step and the mean wind speed, see equation 4.6.4. There should also be added a sufficient number of extra slices so that SIMA does not have to make a new temporary wind field for each time step. Also, some extra slices are necessary for the width of the wind file. The wind field will propagate with the mean wind speed, and will therefore use the frozen turbulence hypothesis. That the wind turbulence does not change spatial-temporal.

$$n_{slice} = \frac{u\Delta t}{u_{mean}} \tag{4.6.4}$$

4.6.1 Large eddy simulation

The effects of changing turbulence are captured by looking into differences in upwind and downwind LES simulation in SIMA. LES files are converted into six seeds with upwind and downwind data. The turbulent wind is then transformed into Turbsim format, which is possible to run in SIMA. The six seeds are processed from one LES files by discretise the spatial grid into six long strips. As the turbulent air are moving with the average wind speed, data is found for positions x1 and x2, which are the distance between the two wind turbines.

For each file the statistics remains the same, and will therefore work as a frozen turbulent. The second wind turbine will experience the same turbulent air as the first one. In this analysis wake effects from the wind turbines are neglected. For a large enough distance between the wind turbines compared to the diameter of the rotor, wake effects can be neglected.

Turbsim and Mann turbulence generator files are generated with the same turbulence intensity factor as LES files. Turbulence intensity factor in the transversal and vertical directions are assumed to follow the standard, and are therefore, a fixed ratio to the longitudinal turbulence intensity factor.

By looking into the difference in response for the floaters for the upwind and downwind LES simulations, it is possible to determine if the frozen turbulence assumption is good enough for this particular LES file. Also, spatiotemporal difference in turbulence can effect the dynamic performance to shared mooring. If frozen turbulence assumption is not valid, the system will experience less time lag effects, meaning a overall change in the dynamics of shared mooring systems.

Also, the LES data can look into the overall agreement between CFD data and engineering tools to determine if there is an overall change in performance. This could lead to differences in fatigue, mooring tension and dynamic motions.

Previous research shows when TIMESR and Kaimal model is fitted against meteorological data, the responses are more correct than Mann. Both surge and pith are higher, but yaw is lesser. Mann shows the opposite. The overall agreement is better when fitted against LES data, but the result is the same as for the meteorological data. [12]

4.6.2 Thrust force study

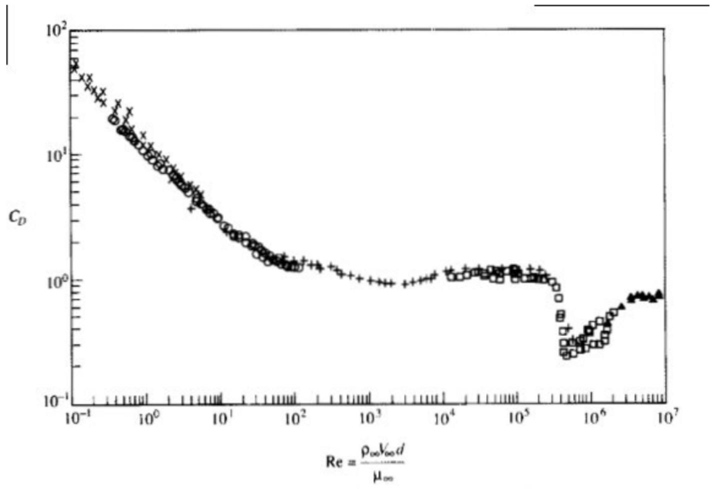

Figure 4.6.2: Experimental data as compiled in Panton, Ronald, Incompressible Flow, Wiley-Interscience, New York, 1984 [18]

The drag coefficient is dependent on the Reynolds number, in equation 4.6.5, which is calculated by the characteristic length D, wind velocity u, and the kinematic viscosity ν (by default, $1.51610^{-5}[\frac{m^2}{s}]$ in SIMA).

$$Re = \frac{uD}{\nu} \tag{4.6.5}$$

Reynolds number is an essential nondimensional coefficient for viscous flows. The Reynolds number is a parameter of flow regimes. The flow transitions from laminar to turbulent for higher Reynolds numbers, and the drag coefficient changes. Panton conducted experiments in 1984 by comparing the drag coefficient with the Reynolds number for cylinders. By calculating the Reynolds number for the lowest diameter in the tower, the Reynolds number is around $3 \cdot 10^6$ for u = 6 [m/s]. In Figure 4.6.2, the drag coefficient is stable at 0.7 for flows over 6 m/s with a Reynolds number of $3 \cdot 10^6$. Therefore, the SIMA calculations overestimated the drag force, as seen in Figure4.6.3. Therefore, it is unrealistic that extreme wind conditions have the most wind force. Drag force is calculated by considering the change in the cross-section of the tower and segment length, equation 7.2.1.

Also, the calculations are conservative in Figure 4.6.3, cause, in reality, the wind velocity would follow the power law. Therefore equation 7.2.1 can be updated. The power coefficient would have an effect on the drag force as the largest cross-sections are at the bottom, where the wind is corrected.

$$Fd = \sum_{i}^{N} \frac{\rho}{2} CdD_i u^2 \Delta L_i \tag{4.6.6}$$

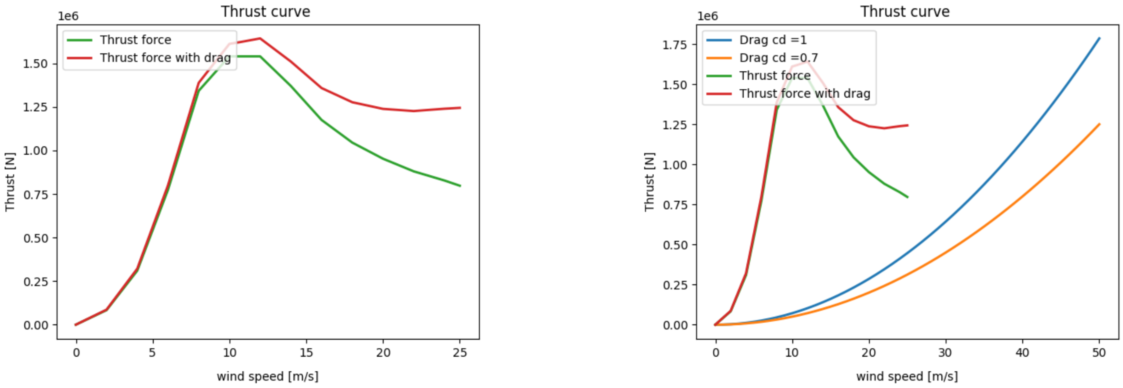

Figure 4.6.3: Thrust curve generated for 15 MW reference wind turbine VolturnusUS with peak shaving

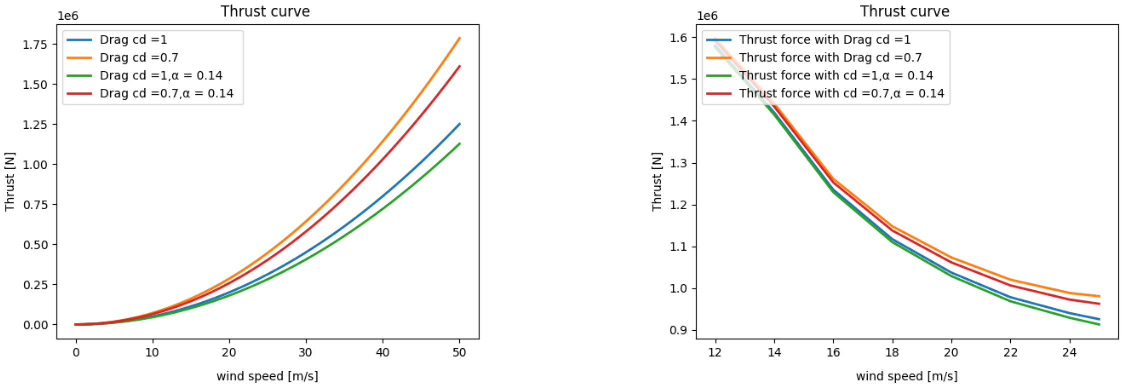

Figure 4.6.4: Thrust curve generated for 15MW reference wind turbine VolturnusUS with drag force correction

$$Fd_\alpha = \sum_{i}^{N} \frac{rho}{2} CdD_i u^2 \Delta L_i \Big(\frac{zi}{z_{hub}}\Big)^\alpha \tag{4.6.7}$$

The power coefficient will be negligible for drag calculations under the cut-out wind speed.

4.7 Simplified wind thrust for floating offshore wind turbine

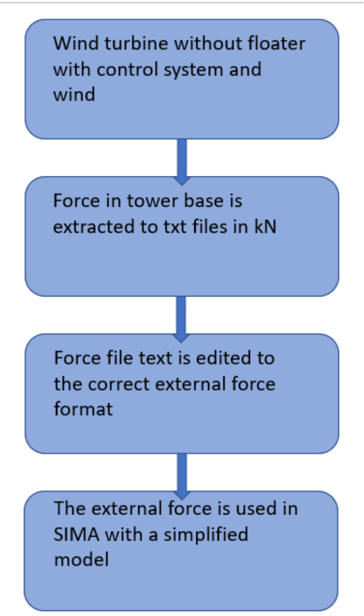

Figure 4.7.1: Flow chart over creating external wind force files

To simplify the process of designing shared mooring, it is necessary to simplify the model, to quickly evaluate different shared mooring concepts influence on the dynamics. Wind turbine simulations in SIMA are tedious since the wind files have to be read and BEM momentum theory has to be used to find the wind forces on the blades. Also, the time step is dominated by BEM theory. The wind field has to have a high refinement, and the dynamic time step has to be much smaller than the wind time step to avoid numerical instabilities.

SIMA uses linear interpolation when it does not have sufficient time steps in the load. This means that rapid changes are smeared to avoid numerical instabilities correcting RPM, thrust, and pitching of blades gradually. In all simulations carried out, the dynamic time step was 10 times as refined as the environmental time step.

High frequencies are filtered out by the sampling rate of the simplified force. Since mooring tension is the primary focus, the sampling rate is only 0.1 s. By the definition of Nyquist frequency, frequencies above 5 Hz are filtered out. Effective a sinusoidal wave needs more than two points, meaning the real boundary is even lower. It is possible to use an even coarser environmental time step, as aerodynamic forces have a long period, and surge and sway natural periods are large. If fatigue is off interest, the selected time step could be chosen even lower. A low dynamic (0.01 s) and environmental (0.1 s) time step is chosen to ensure a good comparison, as the analysis with the wind has a dynamic time step of 0.005 s and an environmental time step of 0.05 s. Figure 4.7.2 shows the model that was used in the calculation of the simplified force files.

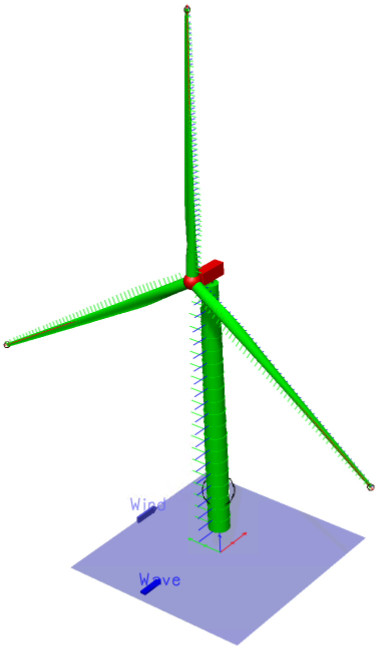

Figure 4.7.2: Model of windturbine with tower, used in ”generation” of simplified force files

By simplifying the wind loads, it is possible to run the simulation with a much coarser time step, and the dynamic time step could be the same as the load time step.

The wind turbine is simplified by removing the floater and fixing the tower at the bottom. Thereafter the stiffness of the tower was increased by 1000 to avoid second order moment from tower deflection. By increasing the stiffness the tower's natural period will be drastically lowered, and it is possible that the high-frequency loads are causing resonance. This was not observed in the time series. Drag from the wind was calculated by assigning tower elements drag coefficient. The coefficient was chosen to be one so that the method is as general as possible. Drag loads were necessary to capture in the simplified model since extreme wind loads for shared mooring are necessary to evaluate, and drag loads on the tower will dominate for a shut downed wind turbine. Since drag loads were necessary for the model, it was not possible to only look at blades, rotor, hub, and nacelle, but also tower had to be included in the model. Therefore wind loads could not be read by wind turbine loads in SIMA, and the loads were read from the lowest node in the tower. Since the loads were read from a RIFLEX element, moments were internal and not external. Also, mass from the tower was subtracted from the z-component of the force. The forces were then read into a text file with the correct format necessary for SIMA external force. In dynamic analysis, it is important that the force is applied in the correct time step. In SIMA, body forces are calculated in the body point, which is floater for wave loads, and wind turbine for wind loads. Downwind floaters will have a phase shift in the force loads, and therefore the loads in the force text file have to be phase shifted so that the forces are applied in the correct time step. If not, the dynamic system will not behave in the same matter. For Wilson and Halls's simplified system, the distance between wind turbines is assumed to be the same as the mooring, 1600 m [9]. Since all the models are rotated so that the distance between the fairleads is 1600 m and symmetrical, the body points are not 1600 m and 800 m phase shifted. Every system has to be phase shifted individually to correct the distance between the floaters. A new force file has to be generated for each wind speed and changes in time step between the models.

$$i = int\left(\frac{x}{u\Delta t}\right) \tag{4.7.1}$$

Since the wind turbine is removed, aerodynamic damping is missing. Aerodynamic damping in surge and pitch is necessary to know since the mooring tension is dependent on them. Aerodynamic damping can be estimated by neglecting the control system and using a first-order Taylor expansion on the thrust, equation 4.7.2. The thrust force can be written in the equation of motion 4.7.3. The damping effect can be estimated by taking the derivative of the thrust [35], see equations 4.7.5, and 4.7.2. The method could be further extended by estimating the damping in yaw, equation 4.7.6. The approach is not frequency dependent and will neglect the inertia effect from the wind. The damping coefficient has to be estimated for each wind speed. This method should be sufficient when the turbine oscillations frequency range does not interfere with the controller bandwidth. Low-frequency interaction effects will be neglected. This method will overestimate the damping for low frequency.

$$T = T_0 + \frac{dT}{dv}\Delta v \tag{4.7.2}$$

$$m\ddot{x} + c\dot{x} + kx = T \tag{4.7.3}$$

$$m\ddot{x} + (c + \frac{dT}{dv})\dot{x} + kx = T_0 \tag{4.7.4}$$

$$b_{er} = \frac{dT}{dv} \tag{4.7.5}$$

$$b_{yaw} = b_{er} z_{hub}^2 \tag{4.7.6}$$

4.8 Linearization of mooring

The mooring system can be approximated using the two-dimensional linear model of Wilson and Hall [9].Most of the mooring stiffness is from the mooring elasticity and the horizontal stiffness. Vertical stiffness can be neglected due to high vertical stiffness for the floater η_3, and the mooring system is often designed to have little contribution in the vertical direction. The approach can be used to model shared mooring systems for offshore wind by using linear springs and point masses as an approximation. Yaw motion is neglected to keep the system as straightforward as possible, but it is possible to extend the model. Hydrodynamics effects such as drift force and radiation are neglected but could be added to the model.

A linear spring is modeled in equation 4.8.1.

$$\tau = \tau_0 + k_l \Delta l \tag{4.8.1}$$

The horizontal tension in the system τ depends on the initial horizontal tension τ_0 and linear horizontal stiffness k_l. The tension is created from strain in the mooring system.l is the projection from three-dimensional to two-dimensional space, the horizontal distance between fairlead to fairlead or fairlead to anchor. The tension in the mooring line will, therefore, strictly increase until equilibrium is found between shared and anchor moorings and the external force.

.

In order to calculate the linear stiffness τ_0 and k_l have to be estimated from a quasi-static mooring model or by using FEM mooring with RIFLEX. This can be done by either evaluating displacement versus force and linearizing the stiffness to the mooring system or calculating the geometric contribution using the catenary equation.

.

A restoring force is generated in the opposite direction of the displacement in the mooring lines heading, the equation 4.8.2.

$$\Delta f_{\tilde{x}} = -k_l \Delta \tilde{x} \tag{4.8.2}$$

Even though mooring systems only have stiffness directly in their heading, a perpendicular force is created due to line tension and change in heading from the displaced system. The restoring force from the mooring line is, therefore, a function of the change in the line heading from displacement and the change in tension. The change in force can therefore be written in vector form by the displaced distance Δy in equation 4.8.3.

$$\boldsymbol{\Delta f} = \boldsymbol{f_2} - \boldsymbol{f_1} = (\tau_0 + \frac{\partial \tau}{\partial y}\Delta y) \begin{Bmatrix} -cos\theta(\Delta y) \\ -sin\theta(\Delta y) \end{Bmatrix} - \tau_0 \begin{Bmatrix} -1 \\ 0 \end{Bmatrix} \tag{4.8.3}$$

Figure4.8.1 shows how the force from the stiffness changes due to heading and pretension. If the new heading has a small offset $\Delta y << l$, the angle can be approximated with a small angle assumption and tension magnitude. Meaning transverse stiffness can be approximated as tension divided by mooring length. $k_t = \frac{\tau_0}{l}$

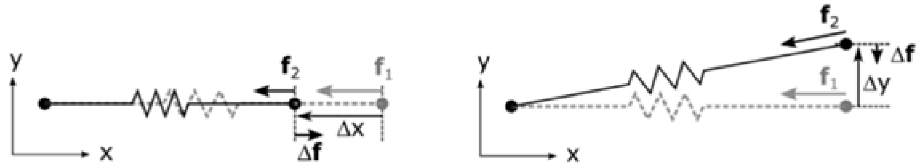

Figure 4.8.1: Effective mooring stiffness [9]

$$\Delta f_y = -\frac{T_0}{l}\Delta y = -k_t \Delta y \tag{4.8.4}$$

The force change depends on the stiffness of the line and the position to end A and B in the x and y direction.

$$\boldsymbol{\Delta f} = \boldsymbol{K_{line}\xi} \begin{bmatrix} k_{11} & k_{12} & k_{13} & k_{14} \\ k_{21} & k_{22} & k_{23} & k_{24} \\ k_{31} & k_{32} & k_{33} & k_{34} \\ k_{41} & k_{42} & k_{43} & k_{44} \end{bmatrix} \begin{Bmatrix} \xi_{xA} \\ \xi_{yA} \\ \xi_{xB} \\ \xi_{yB} \end{Bmatrix} = \begin{Bmatrix} f_{xA} \\ f_{yA} \\ f_{xB} \\ f_{yB} \end{Bmatrix} \tag{4.8.5}$$

The system stiffness can be calculated by adding all the line stiffnesses together. Each line stiffness has a heading that will affect the line's contribution to system stiffness. The rotation matrix, which is based on trigonometry, considers the heading.

$$\boldsymbol{R} = \begin{bmatrix} cos(\theta) & sin(\theta) & 0 & 0 \\ -sin(\theta) & cos(\theta) & 0 & 0 \\ 0 & 0 & cos(\theta) & sin(\theta) \\ 0 & 0 & -sin(\theta) & cos(\theta) \end{bmatrix} \tag{4.8.6}$$

$$\boldsymbol{K_{line}} = \boldsymbol{R} \begin{bmatrix} k_l & 0 & -k_l & 0 \\ 0 & k_t & 0 & -k_t \\ -k_l & 0 & k_t & 0 \\ 0 & k_t & 0 & k_t \end{bmatrix} \boldsymbol{R^T} \tag{4.8.7}$$

After each local line stiffness is transformed into a global stiffness reference system, each line stiffness component has to be placed correctly into the system stiffness matrix based on connectivity. A system matrix with three wind turbines in 2 DOF gives a six times six matrix, but the line stiffness matrix is only a four-by-four matrix. The stiffness matrix can be separated into four components, each containing two by two matrix. This is done for simplicity when showing how the connectivity algorithm works in the equations 4.8.8, and 4.8.9.

$$\boldsymbol{K_{line}} = \boldsymbol{R} \begin{bmatrix} \begin{bmatrix} k_l & 0 \\ 0 & k_t \end{bmatrix} & \begin{bmatrix} -k_l & 0 \\ 0 & -k_t \end{bmatrix} \\ \begin{bmatrix} -k_l & 0 \\ 0 & -k_t \end{bmatrix} & \begin{bmatrix} k_l & 0 \\ 0 & k_t \end{bmatrix} \end{bmatrix} \boldsymbol{R^T} \tag{4.8.8}$$

$$\boldsymbol{K_{line}} = \boldsymbol{R} \begin{bmatrix} \boldsymbol{k^L_{11}} & \boldsymbol{k^L_{12}} \\ \boldsymbol{k^L_{21}} & \boldsymbol{k^L_{22}} \end{bmatrix} \boldsymbol{R^T} \tag{4.8.9}$$

Example from Wilson and Hall [9]:

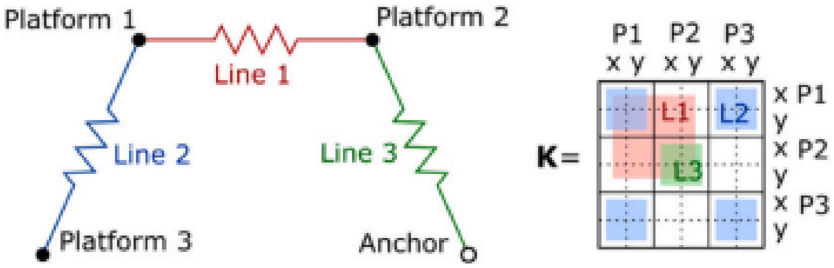

Figure 4.8.2: Hypothetical array showing how connectivity relations are established [9]

In the example from Wilson and Hall in Figure 4.8.10, line 2 is connected to platforms 1 and 3. Line 1 is connected to platforms 1 and 2, and line 3 to platform 2 and anchor. Each platform will contribute to 2 DOF off stiffness. Therefore, the system is a six-by-six matrix containing information about stiffness in each platform's x and y direction. Every stiffness term is bold in equation 4.8.10 since every term is a two-by-two matrix.

Line 2 will contribute to the stiffness of platforms 1 and 3, taking position 11, 13, 31, and 33 in the matrix in equation 4.8.10. Line 1 is connected to platforms 1 and 2 and will therefore take place 11, 12, 21, and 22 in the stiffness matrix. Since platform 2 only have stiffness contribution from line 3, coupling terms are zero. All the values that are not diagonal in the stiffness matrix couple the stiffness, connecting the displacement between the systems.[9]

$$\boldsymbol{K} = \begin{bmatrix} \boldsymbol{k}_{11}^{L1} + \boldsymbol{k}_{11}^{L2} & \boldsymbol{k}_{12}^{L1} & \boldsymbol{k}_{12}^{L2} \\ \boldsymbol{k}_{21}^{L1} & \boldsymbol{k}_{22}^{L1} + \boldsymbol{k}_{11}^{L3} & \boldsymbol{0} \\ \boldsymbol{k}_{21}^{L2} & \boldsymbol{0} & \boldsymbol{k}_{22}^{L2} \end{bmatrix} \tag{4.8.10}$$

Example baseline system:
Since the baseline system only has one platform, it has no shared mooring lines, and the stiffness matrix can not be coupled, see equation 4.8.11. All stiffness is only connected with platform 1. Even though there is no coupling between platforms coupling in the y and x-direction will happen due to the transformation matrix.

$$\boldsymbol{K} = \begin{bmatrix} \boldsymbol{k}_{11}^{L1} + \boldsymbol{k}_{11}^{L2} + \boldsymbol{k}_{11}^{L3} \end{bmatrix} \tag{4.8.11}$$

Example system a):

Lines 1 and 2 are connected to platform one and anchor. Lines 3 and 4 are connected to platforms two and anchor in equation 4.8.12. S stands for shared mooring line connecting platforms one and two motions together. The connection will create coupled terms meaning the displacement in platform one will influence platform two.

$$\boldsymbol{K} = \begin{bmatrix} \boldsymbol{k}_{11}^{S1} + \boldsymbol{k}_{11}^{L1} + \boldsymbol{k}_{11}^{L2} & \boldsymbol{k}_{12}^{S1} \\ \boldsymbol{k}_{21}^{S1} & \boldsymbol{k}_{22}^{S1} + \boldsymbol{k}_{11}^{L3} + \boldsymbol{k}_{11}^{L4} \end{bmatrix} \tag{4.8.12}$$

Example system b).

Lines 1 and 2 are connected to platform 1, line 3 and 4 to platform 2, and line 5 and 6 to platform 3. All of the lines are connected to anchors on the other end of the mooring line, and are, therefore, only contributing to diagonal stiffness. Shared mooring 1 is connected between platform 1 and 2, shared mooring 2 is connected between platform 2 and 3, and shared mooring 3 is connected between platforms 1 and 3. Shared mooring 1 is, therefore, in global matrix position 11, 21, 22, 12. Shared mooring 2, 22, 32, 33, 32, and shared mooring 3, 11, 13, 33, 31 in equation 4.8.13.

$$\boldsymbol{K} = \begin{bmatrix} \boldsymbol{k_{11}^{S1}} + \boldsymbol{k_{11}^{S3}} + \boldsymbol{k_{11}^{L1}} + \boldsymbol{k_{11}^{L2}} & \boldsymbol{k_{12}^{S1}} & \boldsymbol{k_{12}^{S3}} \\ \boldsymbol{k_{21}^{S1}} & \boldsymbol{k_{22}^{S1}} + \boldsymbol{k_{11}^{S2}} + \boldsymbol{k_{11}^{L3}} + \boldsymbol{k_{11}^{L4}} & \boldsymbol{k_{12}^{S2}} \\ \boldsymbol{k_{21}^{S3}} & \boldsymbol{k_{21}^{S2}} & \boldsymbol{k_{22}^{S2}} + \boldsymbol{k_{22}^{S3}} + \boldsymbol{k_{11}^{L5}} + \boldsymbol{k_{11}^{L6}} \end{bmatrix} \tag{4.8.13}$$

Example system c).

System c) is connected in the same manner as system b) with the exception of one line less for each platform. Hence one less diagonal term for the whole diagonal in equation 4.8.14. Also, the transformation matrix will differ, as not shown, due to different angles in the mooring lines. Meaning x and y stiffness will differ for each mooring line in the global stiffness matrix. y.

$$\boldsymbol{K} = \begin{bmatrix} \boldsymbol{k_{11}^{S1}} + \boldsymbol{k_{11}^{S3}} + \boldsymbol{k_{11}^{L1}} & \boldsymbol{k_{12}^{S1}} & \boldsymbol{k_{12}^{S3}} \\ \boldsymbol{k_{21}^{S1}} & \boldsymbol{k_{22}^{S1}} + \boldsymbol{k_{11}^{S2}} + \boldsymbol{k_{11}^{L2}} & \boldsymbol{k_{12}^{L2}} \\ \boldsymbol{k_{21}^{S3}} & \boldsymbol{k_{21}^{S2}} & \boldsymbol{k_{22}^{S2}} + \boldsymbol{k_{22}^{S3}} + \boldsymbol{k_{11}^{L3}} \end{bmatrix} \tag{4.8.14}$$

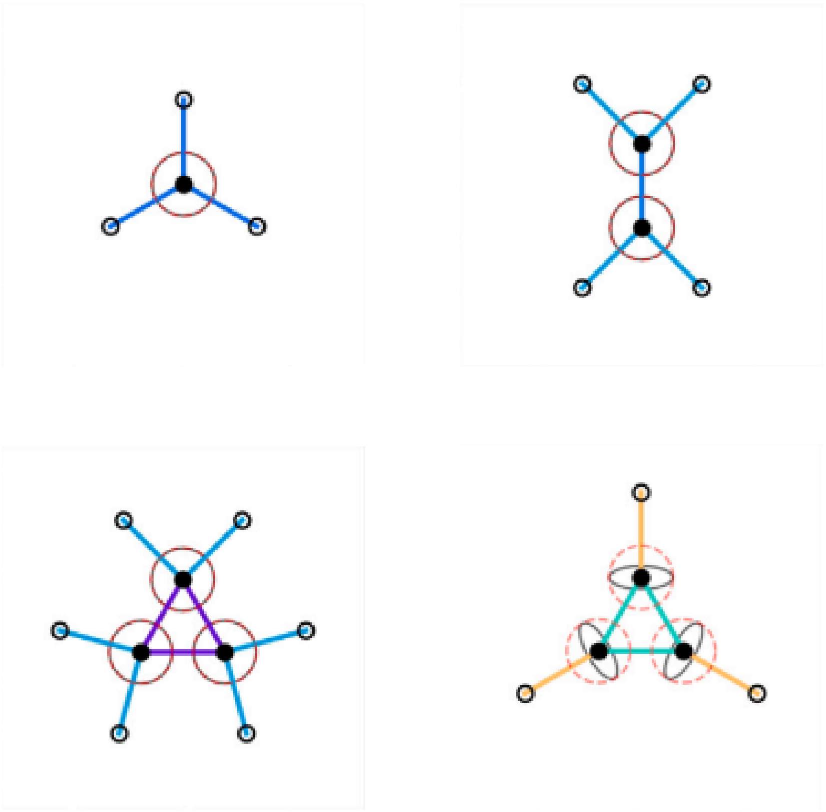

Figure 4.8.3: Wilson and Hall's linearized systems - baseline, a), b) and c) [9]

4.8.1 Validation of linear model

SIMO linear model was used to verify statically the linearized system in Python . SIMO linear body was just a mass with linear springs and is therefore modeled in the same matter as Hall and Wilson, see Figure 4.8.4. The linear springs are modeled with fixed elongation couplings. The linear springs are then connected to the correct body point for the body floater. The coupling is defined as a linear elastic spring with pretension for the system according to [9] for 1600 m mooring line. The linear stiffness is then added as the force generated for 1 m displacement in the table for fixed elongation coupling, and the stiffness is then calculated for the system. It was not observed differences between the models.

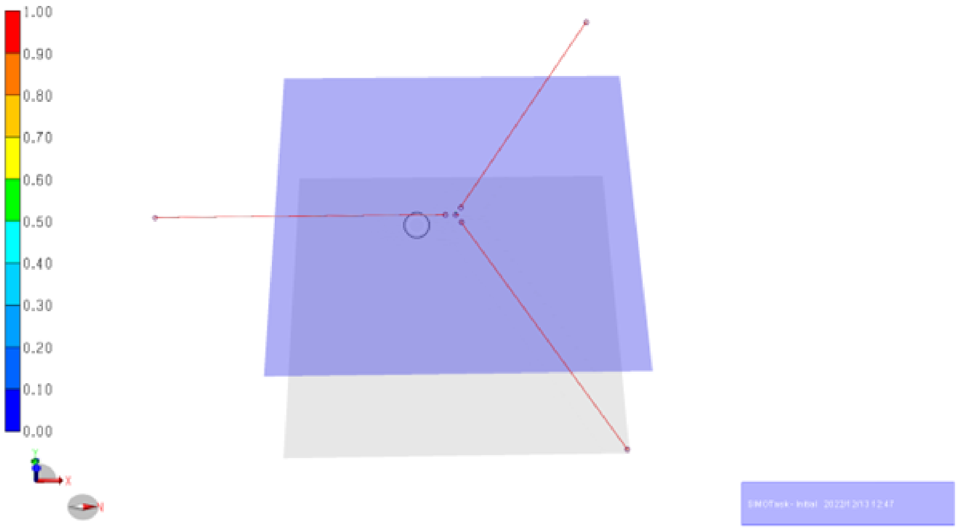

Figure 4.8.4: Linear validation model in SIMO for system

4.9 Dynamic extension of linearized mooring

To further evaluate the linearized mooring, Wilson and Hall [9] linearized static model has been extended from static to dynamic analysis. The dynamic model utilizes the stiffness matrix calculated for static analysis. Mass is modeled as in a point for each floater, with the zero frequency added mass $A(0)$. For damping only linear viscous damping is used, and quadratic viscous damping is neglected. For low frequencies, the quadratic damping is approximately zero. Aerodynamic linear damping is added to the damping matrix. Aerodynamic force is calculated as a time series in x and y for a fixed wind turbine, assuming no hydrodynamic coupling effect. Hydrodynamics is estimated using a Morison model approximating Volturnus-S with strip theory for pontoons and columns. Pontoons are then assumed cylindrical, with the side used as characteristic diameter. The hydrodynamics for the pontoons and columns will then be completely different due to the strips being directed vertically and horizontally, but also, the pontoons are not normal to the flow. To get the normal component of the velocity, it has to be decomposed into the normal velocity. The force direction is, therefore, in the local reference system. The force has to be decomposed back to the global reference system. Since the force is working normal on the pontoon, the forces have to be integrated along the length of the pontoon, see Figure 4.9.1.

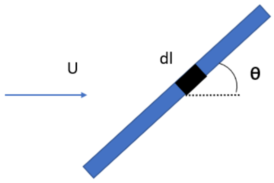

Figure 4.9.1: Rotated pontoon relative to wave velocity

$$u_N = sin(\theta)u \tag{4.9.1}$$

$$dF_l(t) = \rho\frac{\pi D^2}{4}C_a\dot{u}_{Nw}(t)dl + \frac{1}{2}\rho DC_D u_{Nw}(t) \mid u_w(t) \mid dl \tag{4.9.2}$$

$$dF_l(t) = \rho\frac{\pi D^2}{4}C_a\dot{u}_w(t)sin(\theta)dl + \frac{1}{2}\rho DC_D u_w(t)\sin(\theta) \mid u_w(t) \mid dl \tag{4.9.3}$$

$$dF_g(t) = dF_l(t)sin(\theta) \tag{4.9.4}$$

$$dF_g(t) = \rho\frac{\pi D^2}{4}C_a\dot{u}_w(t)sin(\theta)^2dl + \frac{1}{2}\rho DC_D u_w(t)\sin(\theta)^2 \mid u_w(t) \mid dl \tag{4.9.5}$$

Since the strip theory is horizontal, z will be constant for all the strips, although the depth of the pontoon is 7 m. A new x-coordinate has to be used for each strip since the wave force is dependent on the phase of the wave. It is therefore important with a sufficient number of strips, if not, the force could be over or underestimated. The floater force is then approximated by calculating the force for 3 pontoons and 4 columns. A phase shift between floaters and rotation is added to the script, so that the hydrodynamics of several floaters can be calculated.

To validate the Morison model, regular waves were run in Python and SIMA using the Morison strip theory without drag force. In SIMA it is possible to have a strip over the entire segment or use interpolation between the ends. SIMA was closer to the potential theory, especially for the interpolation function. SIMA was difficult to compare to the Python code since SIMA does not give precisely the chosen wave amplitude and wave period. It is only the closest pregenerated data. Also, SIMA uses the actual velocity and acceleration for the wave and not deep water approximation as the Python code. Calculations using Morison equation are dotted, and the solid line is the transfer function from the potential solver in Figure 4.9.2.

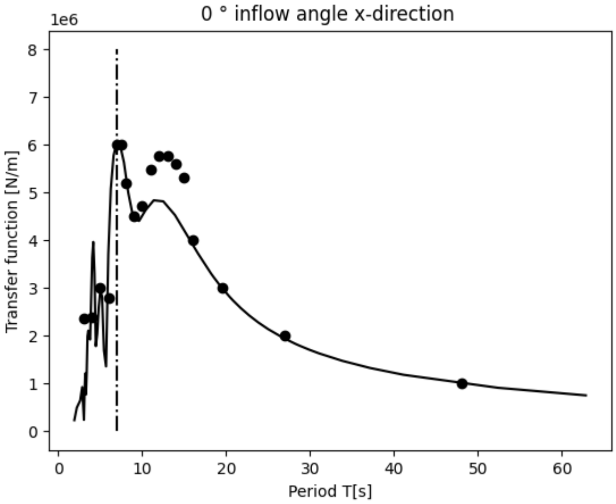

Figure 4.9.2: Potential theory versus Morison strip theory

The dotted line in Figure 4.9.2 and Figure .1.1 is the definition for a small volume structure $\frac{\lambda}{D} > 5$, and is where the Morison equation is expected valid for a bottom fixed cylinder. Morison equation using strip theory is a very good approximation for even for small periods as 3 s for VolturnUS-s floater, even though the added mass coefficient was $C_a = 1$. The largest difference in the answers is when the added mass changes much between 10 s and 20 s. Analysis has been carried out for 0°, 30°, 45°, 60°, and 90°, which can be found in the Appendix. For all inflow angles, Morison equation with strip theory seems to calculate the force with good accuracy. For each segment, 100 points have been used to capture the cancellation effects, and the floater has been fixed by applying an extremely large horizontal stiffness.

A hypothesis why Morison works so well for Volturnus is that both pontoons and columns are very slender and far from each other, causing less hydrodynamic interaction. A problem with using the Morison equation for a floater is that the damping force is not estimated. It is necessary to have some data from potential theory to choose damping, otherwise, resonance will cause too large dynamic loads. It is also possible to import transfer function and radiation data to the simplified dynamic tool.

In the dynamic calculation, an iterative scheme is added to correct the body velocity for the nonlinear drag term. To get the correct drag force in each time step, it is necessary to recalculate the drag and iterate it until an acceptable error. In each iteration, the relative velocity is updated, which changes the drag force. Thereafter CAA calculates a new velocity and compares it with the previous one.

Wilson and Hall do not calculate the tension in the mooring line as the pre-tension is specified for the system [9]. Therefore the tension in the mooring line is calculated by the system matrix from static calculations by taking the inverse of the system matrix. The system matrix is not $n * n$ and therefore, the inverse cannot be found since the determinate is not zero. The system matrix cannot be $n{\cdot}n$ since one floater has several mooring lines and only two degrees of freedom. A solution to this problem is by using Moore-Penrose inverse $S^{\dagger}$, which is often used in cyber physical testing to assign winches the correct tensions. It should be noted that Moore-penrose assumptions are not tested, since it is common to use on system matrices, but it could assign wrong tensions. Also, S^* is the conjugate transpose which is a transpose of the matrix for real numbers, which is the case for the system matrix. The tension in the mooring lines would therefore be calculated based on the force history and mooring line configuration. Pretension is thereafter assigned to each mooring line.

$$S\tau = f \tag{4.9.6}$$

$$S^\dagger = (S^*S)^{-1}S^* \tag{4.9.7}$$

$$\tau = S^\dagger f = (S^*S)^{-1}S^*f = (S^TS)^{-1}S^Tf \tag{4.9.8}$$

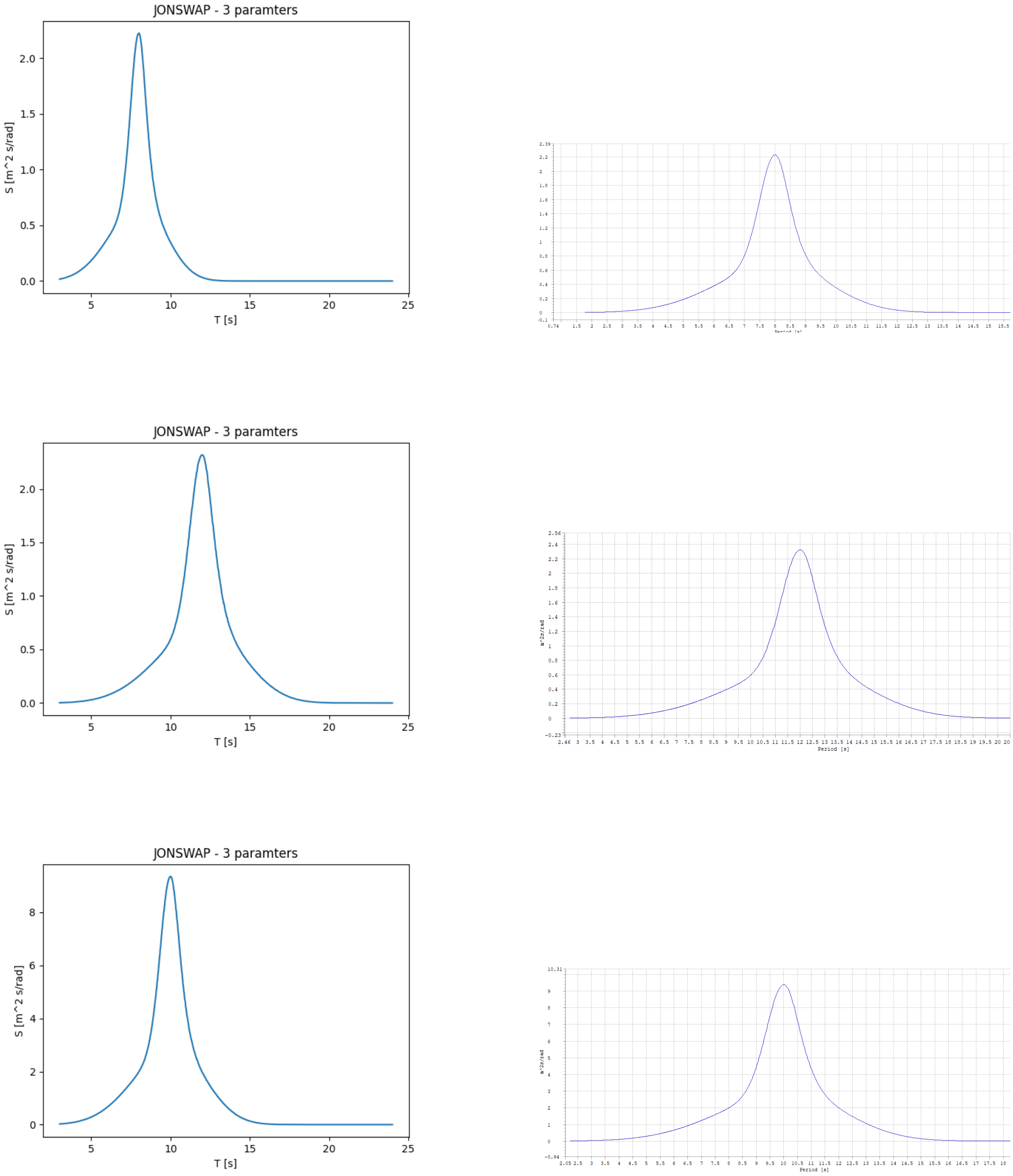

Figure 4.9.3: Comparison between SIMA and script Jonswap spectrum for wave conditions 1,2 and 3

The program was further expanded to include irregular waves. Jonswap spectrum was therefore calculated in Python as described in equation 3.4.14 and compared to JONSWAP in SIMA. Several values were compared for conditions 1, 2, and 3, but no differences existed.
Spectrum is necessary to calculate if irregular waves are needed. A sea condition is defined for a given Hs and Tp, significant wave height and peak period. The spectrum shows the energy distribution for several wave periods for a sea condition. A sea condition is only valid for short-term statistics. The wave process is assumed to be ergodic (one realization is representative), stationary (variance and mean value do not change in time), and normally distributed with zero mean.

Wave surface was then generated by a resolution of $N = 1000$, waves. 1000 waves are deemed sufficient by Faltisen [16] if a random frequency is chosen in each frequency interval from the JONSWAP spectrum. Each regular wave is assigned a random phase, and the amplitude is calculated from the JONSWAP spectrum with the corresponding frequency 4.9.4.
In each interval, the frequency could be anything between $(wj - \Delta\frac{w}{2}), (wj + \Delta\frac{w}{2})$, and are uniformly randomly chosen.

ω_{min} and ω_{max} were chosen as 0.26 and 2.09 $\frac{rad}{s}$ for condition 1, and were chosen where the spectrum had little energy.

A time step of $\Delta t = 0.1s$ is chosen for each wave since this environmental loading time step was used in SIMA.

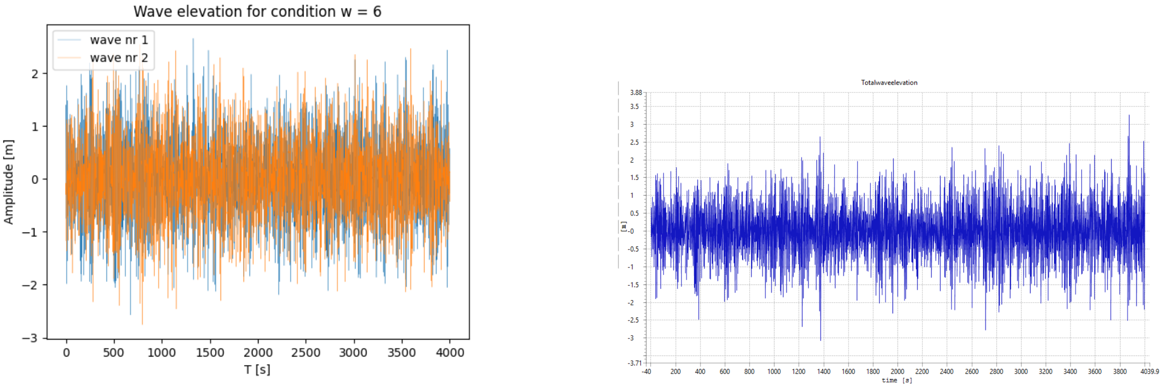

Figure 4.9.4: Comparison between SIMA and script, random wave surface for wave condition 1

Since waves propagate at different speeds depending on the frequency and wave number, phase shifts between the floaters and different x-coordinates are not possible between strips and floaters. Therefore, the script has to calculate the velocity and acceleration for each strip for each floater, both for the columns and pontoons. Columns also need to be stored, since the exponential term in velocity and acceleration is dependent on the wave number. Irregular waves contain a total number of wave numbers corresponding to the total number of regular waves in the time series.

Figure4.9.5 shows the relation between the different scripts that make up CAA regular and irregular wave calculator.

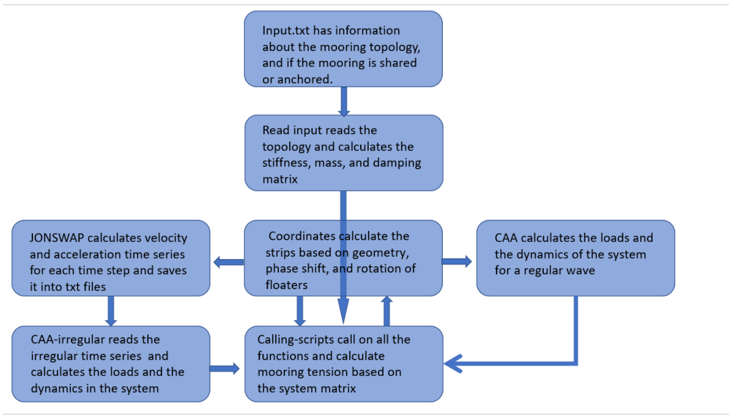

Figure 4.9.5: Flow chart showing CAA regular and irregular wave script

Input reads the information as a text file containing the total number of floaters, mooring lines, and topology. Read input reads all the information and calculates the stiffness, mass, and damping matrix. Mass, added mass, static force, mooring stiffness, and linear damping are specified in this script. Therefore read input works as a static calculator and facilitator for the dynamic calculation. The coordinates function reads the geometry specifications for the floater, the total number of strips, the rotation of the floater, and the global coordinates of all the floaters specified. In CAA regular, the wind files, period and amplitude, time series length, and time step are imported from main script - calling. The dynamic analysis is then carried out with the use of Numba fasthmath to speed up the calculations. Numba fasthmath transfers the Python code into machine code, and works fast for numerical calculations. Therefore, the CAA script for regular and irregular waves is adapted to the necessary Numba format. Numba fasthmath is not necessary, but the total number of strips and drag correction is costly numerically. Another approach is to develop a solver by using a transfer function and not correcting the drag force or not generating waves, as the wind is the dominating force. The dynamic calculations are then returned to the calling script, which saves the time series and calculates the tension in the mooring lines using the system matrix. This process is the same for regular and irregular waves. JONSWAP calculator calculates the JONSWAP spectrum for given H_s , T_p, and the acceleration and velocity for each strip using Numba fasthmath. The data is then saved in a file for each pontoon and column. CAA irregular wave script calculates the dynamic similarly to regular waves, except acceleration and velocity are pre generated and not calculated in the CAA script. Then the dynamic time series is returned to the main script.

4.10 Dynamic cases

In Table 4.10.1, all the dynamic simulations are summarized based on mooring topology, wind solver, and environmental conditions, see Table 4.10.2. In total, 274 one-hours realizations have been simulated in SIMA.

(seeds)	baseline	model a)	model b)	model c)
Turbsim wind (6)	w = 6,10,20,49	w = 6,10,20,49	x	x
Turbsim comparison (1)	w = 6,10,20,49	w = 6,10,20,49	x	x
Simplified wind (6)	w = 6,10,20,49	w = 6,10,20,49	w = 6,10,20,49	w = 6,10,20,49
SW quasi-static mooring (2)	w = 6,10,20,49	w = 6,10,20,49	w = 6,10,20,49	w = 6,10,20,49
LES (6)	x	w = 7.5,12,16	x	x
Mann turbulence LES (6)	x	w = 7.5,12,16	x	x
Turbsim LES (6)	x	w = 7.5,12,16	x	x
Frozen turbulence (6)	x	w = 7.5,12,16	x	x
Real turbulence (6)	x	w = 7.5,12,16	x	x

Table 4.10.1: Dynamic simulations conducted

	Wind mean speed [m/s]	TI	Hs [m]	Tp [s]
Condition 1	6	0.14	3	8
Condition 2	10	0.14	2.5	12
Condition 3	20	0.14	5.5	10
Condition 4	49	0.14	5.5	10

Table 4.10.2: Dynamic conditions

Four conditions have been run dynamically to evaluate the performance of the four mooring systems. They were selected from pregnerated conditions by supervisor Erin Bachynski-Polić in Integrated dynamic analysis of wind turbines. The extreme condition was selected separately based on data from the North Sea. As the wind was calculated for 10 m height, power law was used to estimate the wind speed at hub height. Sea states for the maximum condition could not be used as the mooring system did slack since the displacement was extremely large. Therefore a rough sea state would give negative tension in the downwind mooring system.

A wind turbine has four different working areas. Cut-inn, rated wind speed, and cut-out wind speed where the wind turbine behaves dynamically differently. Therefore, conditions 1,3 and 4 were selected. Condition two was chosen because the maximum thrust is close to the rated wind speed. A condition close to and not the rated wind speed was intentionally chosen, as the servo system would have a significant influence. .

Chapter 5

Static comparison study

5.1 Static analysis of different shared mooring concepts

The rose plot is generated for 1.5 MN, which is close to the maximum thrust force, and 0.375 MN a fourth of the maximum thrust. Watch circle is generated from the script, which is based on a linearized mooring system. As Wilson and Hall commented in their research, systems with a high degree of symmetry will have a circular watch circle [9]. If the system is less symmetric the watch circle is then not circular, but elliptic. These systems are beneficial if the elliptic watch circle is aligned the same way for all the floaters. Such a system can be used if the statistical data in a rose plot is larger for one direction. An example of such a system is given by Wilson and Hall in Figure5.1.1. They did run an optimization study for three different layouts for a two-floater system with different mooring topology. The watch circle is defined by Wilson and Hall as the response radius for different inflow angles. A linear response is highly beneficial as the mooring stiffness does not change with different waves and wind inflow angles. Nevertheless, natural periods will then be less dependent on the force direction. Since added mass can vary on the direction of the force due to non-symmetry, the mass term in calculating natural periods changes, causing different natural periods.

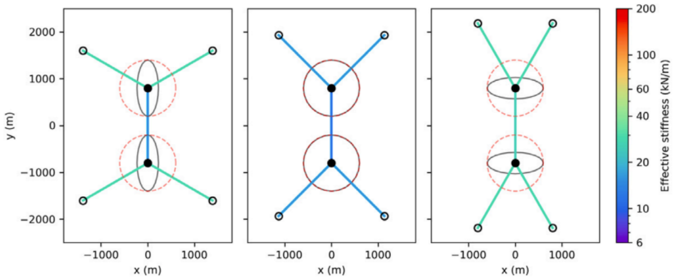

(a) 120° (1.19 kt/turbine) (b) 90° (0.70 kt/turbine) (c) 60° (1.32 kt/turbine)

Figure 5.1.1: Watch circles for different lay out for a two floater system [9]

Linearity in the mooring system is also discussed by Gozcu et.al shown by progressive and degressive stiffness curves in Figure 5.1.2. A linear mooring system reduces the steady loads excursion and reduces peak loads from slowly varying and wave frequency mooring loads.

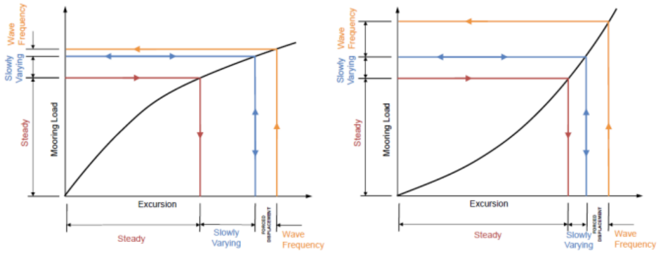

Figure 5.1.2: Exemplary mooring stiffness curve with different gradient. [10]

Static analysis has been carried out for 0° to −120°. For the baseline system, the mooring system is 120° separated from each other. This causes symmetry, meaning there are no differences in the response for 0°, −120°, −240°. In this cases, the force will be in line with 1 upwind mooring and 2 downwind mooring, which is 60° rotated relative to the force vector. For incoming wind angles of around −60°, it can be observed that the linear model predicts the floater excursion. The deviation between linear and nonlinear mooring increases until 0° and −120°. This means that the mooring system behaves linearly when two mooring lines are upwind and the nonlinearity in the stiffness is maximum when only one mooring line is upwind, therefore not share the floater loads. For 0.375 MN, the difference the nonlinear mooring stiffness is circular and closer to the linear stiffness.

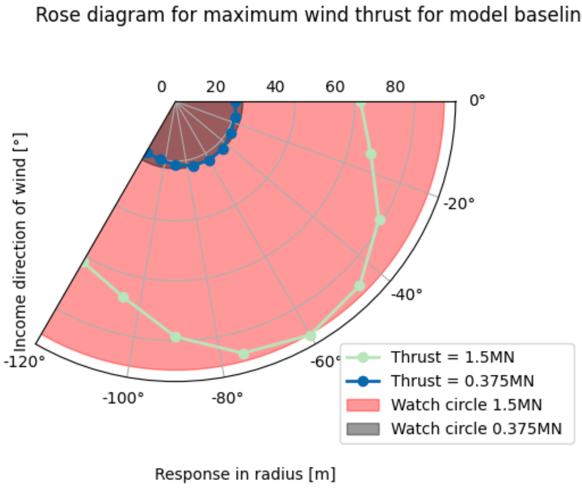

Figure 5.1.3: Rose plot for baseline system, comparison linear and nonlinear mooring

This means that the watch circle is circular for some linear symmetric mooring configurations and becomes more elliptic for larger nonlinear effects. In Figure5.1.4 mooring one is upwind and mooring two is downwind mooring. Force on the floater from the mooring system is calculated for the local reference systems, see equations 5.1.1, and 5.1.2. Some nonlinearities can be seen for upwind mooring −60°, but it is very small. Also, the extra force from the nonlinearity is cancelled out since downwind loses some stiffness. As seen in the figure, force on the floater behaves linearly. For 0° the force is only linear under 20 m extrusion before the systems behave highly nonlinear. Also, the downwind mooring loses its stiffness more linearly, causing less cancellation effects.

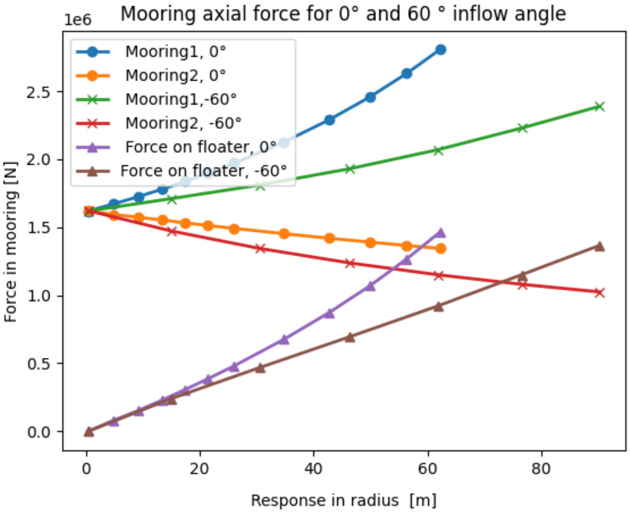

Figure 5.1.4: Mooring force for different income angles of wind

$$F1_{0^\circ} = f_{up} - 2f_d cos(60^\circ) = f_{up} - f_d \tag{5.1.1}$$

$$F1_{60^\circ} = (f_3 + f_2)cos(60^\circ) - f_1 = f_3 - f_1 \tag{5.1.2}$$

For mooring system, a) shared mooring is introduced. Since the mooring system is linear and the mooring system is symmetric around x-axis and y-axis both floaters behave statically the same, meaning both floaters has the same watch circle. This is not the case for a real mooring system. A linear mooring system will behave as a spring model, and will not differentiate if the mooring system is upwind or downwind. Floater 1 will mostly get its stiffness from the shared mooring. For large extrusion, the downwind anchored mooring will lose more and more of its stiffness, meaning the displacement between floaters 1 and 2 has to increase to mobilize a higher force in the shared mooring. It is not necessary to examine more than 90° incoming wind angle due to the symmetry in the floating system.

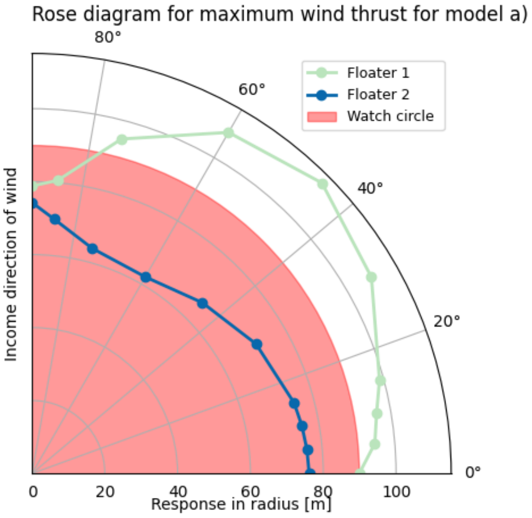

Figure 5.1.5: Rose plot for system a), comparison linear and nonlinear mooring.

For 90° income angle of wind, both floaters will get stiffness from an upwind anchored mooring due to its symmetry. Meaning the forces are low in the shared mooring as seen in Figure 5.1.3. Shared mooring force increases since the upwind mooring are pulling the floaters apart with a much higher force than the downwind mooring is pressing the floaters together.
Combination force is a difference force between mooring upwind and downwind, illustrating that the response is linear see equation 5.1.3. This is also illustrated in Figure 5.1.9.

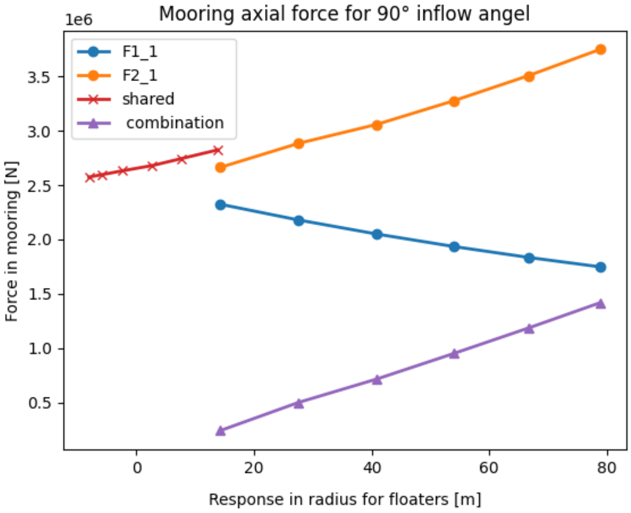

Figure 5.1.6: Mooring force for 90° inflow angle

$$F1_{90^\circ} = (f_{up} - f_{do}) sin(45^\circ) \tag{5.1.3}$$

For 0° income angle response radius is different for upwind and downwind mooring lines since upwind mooring belongs to floater 2 and downwind mooring belongs to floater 1. This causes a softening effect for floater 1, see F1 forces in Figure 5.1.7. F1 forces are the difference between forces in downwind and shared mooring, see equation 5.1.4, and upwind and shared mooring for floater 2. Since floater 2 has both the upwind mooring lines and the shared mooring force increases very little in tension, the stiffness will increase nonlinear. This can also be seen in Figure 5.1.9.

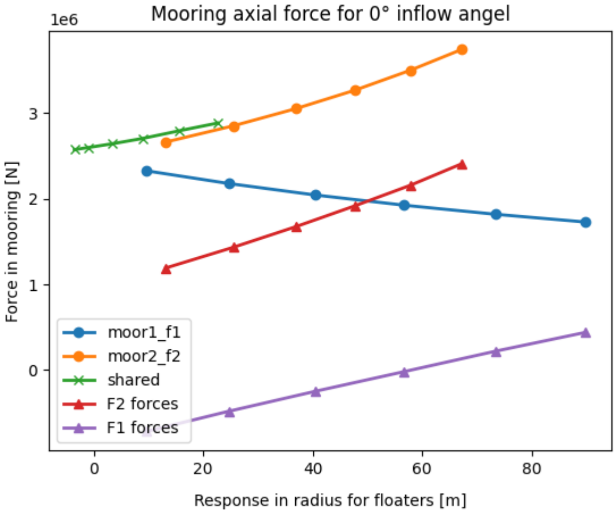

Figure 5.1.7: Mooring force for 0° inflow angle.

$$F1_{0^\circ} = 2f_{up}sin(45^\circ) - f_s \tag{5.1.4}$$

$$F1_{0^\circ} = -2f_{do}sin(45^\circ) + f_s \tag{5.1.5}$$

The inflow angle off 60° explains why there is such a large difference in extrusion for floater 1 and 2. Floater 2 will have the only mooring line that is upwind. When the extrusion is larger, the downwind mooring will contribute less and the shared mooring behaves very linear, meaning floater 1 stiffness will experience a softening effect much larger than previous. This can be observed in Figure 5.1.9, where 60° response F1 has a large degressive curve.

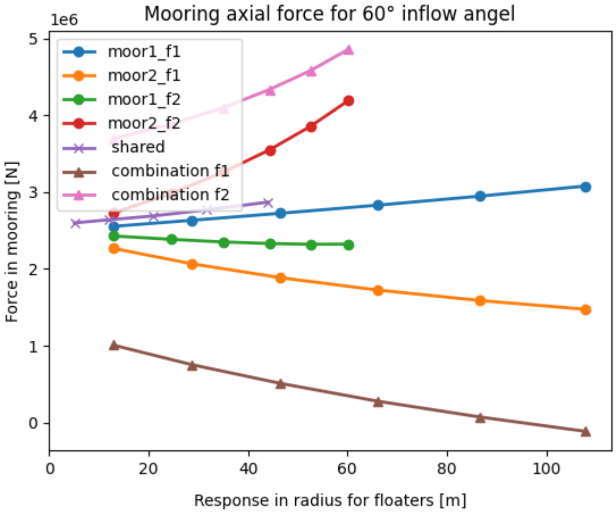

Figure 5.1.8: Mooring force for 60° inflow angle.

$$F1_{60^\circ} = f_{up}cos(15^\circ) - f_{do}cos(15^\circ) + f_s cos(60^\circ) \tag{5.1.6}$$

$$F1_{60^\circ} = f_s cos(60^\circ) + f_{f1}cos(15^\circ) + f_{f2}cos(15^\circ) \tag{5.1.7}$$

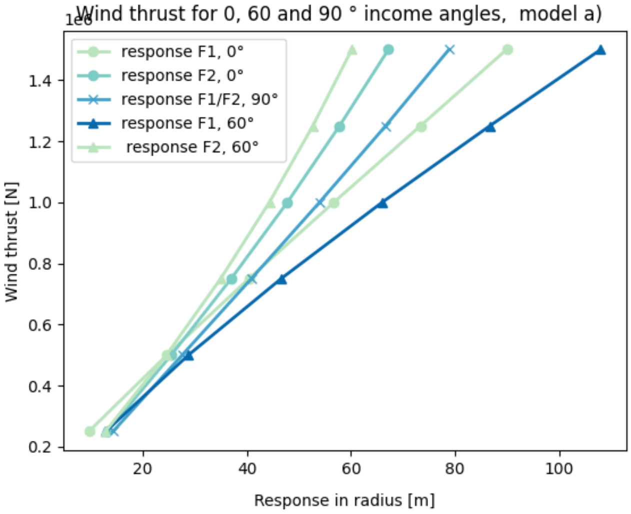

Figure 5.1.9: External force plotted against response in radius for system a).

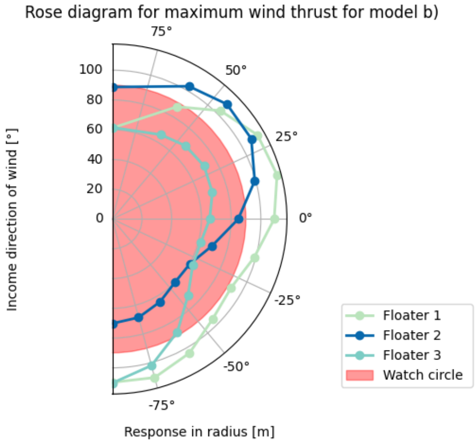

Figure 5.1.10: Rose plot for system b) , comparison linear and nonlinear mooring.

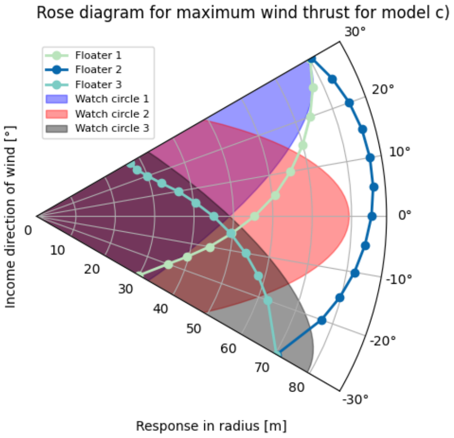

Figure 5.1.11: Rose plot for system c), comparison linear and nonlinear mooring.

Floater system b) and c) are fundamentally different both for nonlinear and linear mooring. Since floater system b) - two anchors per wind turbine has such a large amount of mooring lines, only y-symmetry exists, meaning 0° to 180° inflow angle has been examined. The system has two anchor mooring lines that are normal on each other. This causes cancellation effects for the linear mooring system, causing all three floaters to have the same stiffness. Therefore all three watch circles are the same for system b). System c) behaves very differently, because it only has one anchored mooring line per floater. Therefore there are no cancellation effects. Each floater will have the largest stiffness in line with its anchored mooring. This causes elliptical watch circles. Floater system c) is symmetric for each integer of 60°. For 30°, 150°, $-270°$ mooring 3, 2, and 1 is upwind and the two other mooring lines are downwind.

Floater 2 motions deviate the most from the linear system since it is dependent on the stiffness from a shared mooring. Only for large displacements, the anchored mooring for floater 2 can decompose the force and contribute to the stiffness. For 30° inflow angle, floater 1 gets its stiffness from shared mooring, this will increase the force on floater 2 and 3. Since floater 3 moves closer to floater 2, the shared mooring between them contributes less to the stiffness. Floater 2 gets, therefore, an additional softening effect for angles as 30° and $-30°$ since the other floaters contribute to lower stiffness.

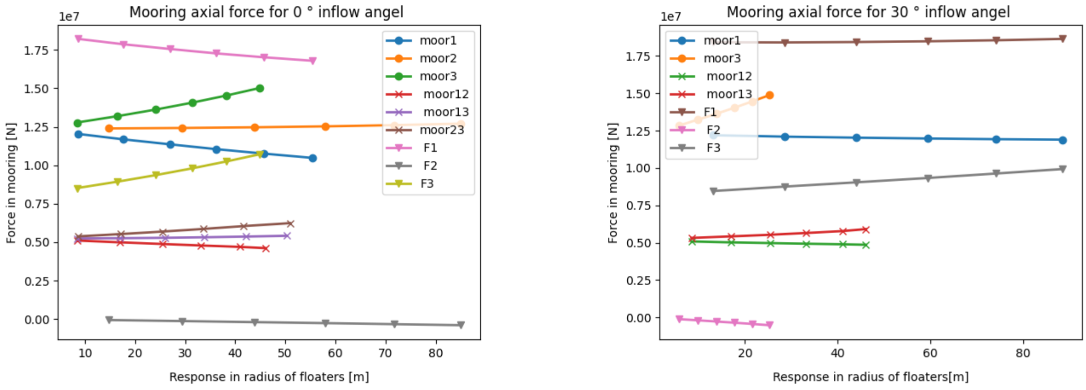

Figure 5.1.12: Mooring force for 0° and 30° inflow angle.

5.2 Eigenvalue study

Natural periods are essential for a dynamic system as the motions of a system can be dominated by resonance. It is essential to identify the natural periods in surge, sway, and yaw and design the mooring system to have natural periods away from environmental loading, especially wave loads. Also, second-order hydrodynamic loads could be of significant order if a natural period is excited. As VolturnUS-s QTF was not calculated for the floater rotations needed, second-order loads are neglected. Figure 5.2.2 shows the frequency spectrum from wind loads on a 10 MW wind turbine divided by the standard deviation of wind in x. As the Figure illustrates, the most energy is concentrated between 100 s and 1000 s. Therefore it is challenging to avoid resonance for turbulent wind. Thus, it is important with enough aerodynamic damping and a few natural periods that could be excited by the turbulent wind.

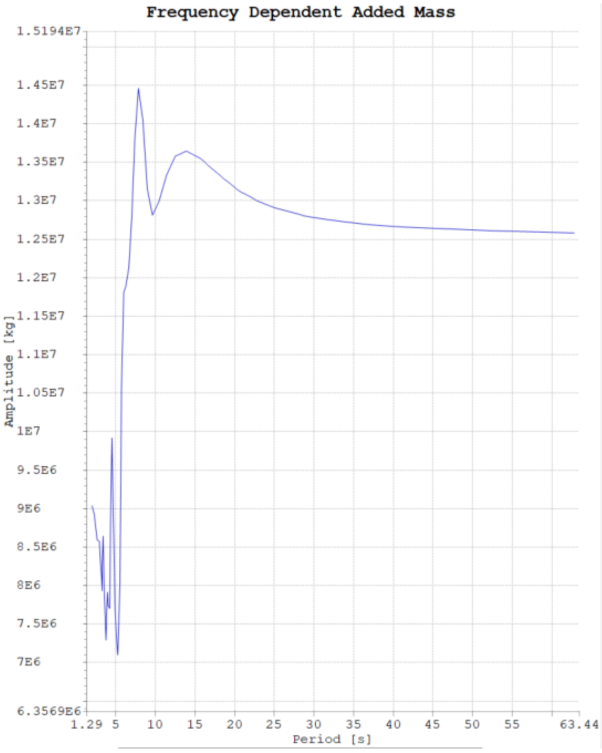

Figure 5.2.1: Added mass in surge-surge direction for Volturnus

Compared to the linearized system, the natural periods are for a system without added mass, as the eigenvalue calculations in SIMA use the added mass A(T= 0), which underestimates the system's mass. Using A($T = \infty$) would be correct as the added mass is asymptotic and converges for periods higher than 30 s, see Figure 5.2.1. Eigenvalue in SIMA can estimate the natural periods using A($T = \infty$), but only in the frequency domain, which can only be used for SIMO. This is not an option since both RIFLEX and SIMO are used in SIMA. Therefore, the system has to be modeled as a point mass, which has not been done. It is also possible to conduct a decay test in dynamic analysis using a constant force and then count the oscillations in the system, which has been done for Section 6.1. This method is relevant for natural periods when the added mass varies with the frequency. As the simulation is done dynamically, the correct added mass would be assigned.

Analysis has been carried out for initial and displaced positions for maximum thrust as the stiffness in the system is not linear, meaning the system becomes stiffer for large displacements, and the natural periods will change.

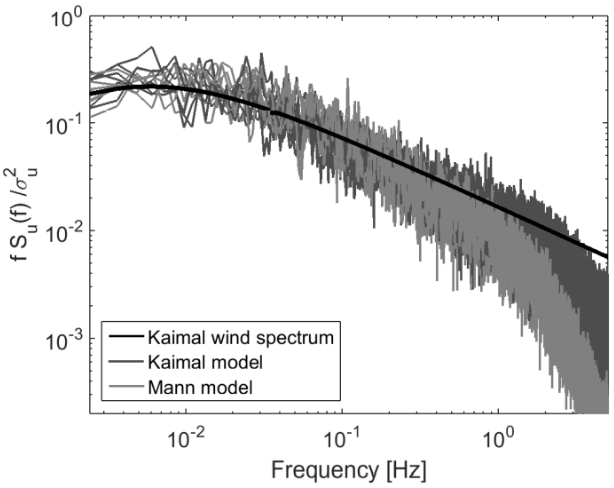

Figure 5.2.2: Wind spectrum from loads on a 10 MW wind turbine for different turbulence models [13]

Mooring weight	Pretension-lin [kN]	Pretension SIMA	Error %
116	961	961	3.22 %
176	1956	2130	6.64 %
175	1397	1504	7.55 %
101	1137	1212	5.83 %
175	1393	1449	3.72 %
359	4034	4363	7.02 %
875	6987	7476	6.14 %

Table 5.2.1: Pretension in mooring lines versus linearized pretension to Hall and Wilson [9]

Decay test	SIMA Natural period [s]	Linearized system [s]	Error %
216.68	216.11	221.66	2.6 %
-	215.77	221.66	2.8 %

Table 5.2.2: Natural periods without added mass - base system

Eigenvalues in linearized Python script are calculated by transforming the stiffness and mass matrix into A matrix and then finding the eigenvalue to matrix A, according to dynamic Theory 3.1.35. Then the eigenfrequency is calculated by taking the square root of the eigenvalue. A decay test has been run to validate the eigenvalue analysis in SIMA, which gives the same value. Since total numbers of oscillations and amplitude are read from SIMA, small differences would occur compared to SIMA eigenvalues. The relevant theory is in the Section 3.1.1. Natural periods are very similar to the linear system compared to nonlinear system. Eigenvectors are calculated by using the eigenvalues of the stiffness and mass matrices. The eigenvectors show how the resonance mode behaves. All the eigenmodes can be seen in Appendix .2.1, .2.2, and .2.3, .2.4. As the linearized model has two degrees of freedom per floater, surge, and sway, only two natural periods and eigenmodes can be calculated for the system. Often several natural periods are close by the ones for surge and sway since coupling with other degrees of freedom and FEM elements influences the natural periods.

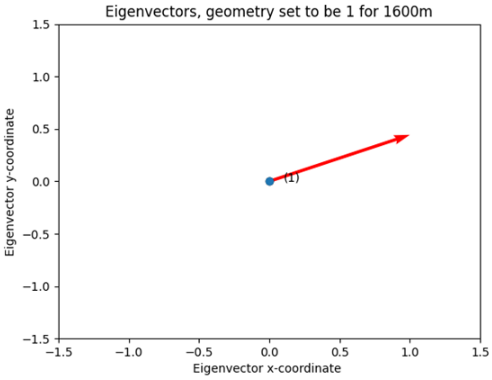

Figure 5.2.3: Eigenvalue mode 1 from the linearized model - baseline

Mode SIMA	Natural period [T] SIMA	Modes code	Natural period [T] code	Relative [%]
6	138.99	3	150.30	7.92
5	160.54	1	172.58	7.50
3	219.66	2/4	221.91	1.02

Table 5.2.3: Natural periods - 2 anchors per floater, 2 bodies model a)

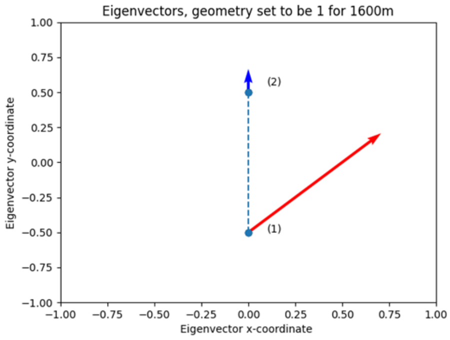

Figure 5.2.4: Eigenmode 1 linearized system for model a)

The natural periods are underestimated and overestimated for system a) compared with the SIMA natural periods. The mooring system in SIMA and Wilson and Halls should be the same, but it is observed that the pretension differs some between the models. Differences between the software could cause it, as Wilson and Hall use MoorPy, which uses the quasi-static equation. In

SIMA, there are no differences between RIFLEX and quasi-static mooring, but the quasi-static mooring is discretized into several elements. Therefore the shape of the mooring line shall be the same. In Moorpy, it could be only one element, causing a difference in the pretension and, therefore, differences in the natural periods.

Mode SIMA	Natural period [T] SIMA	Modes code	Natural period [T] code	Relative [%]
5	214.87	2	207.08	3.76
4	216.22	5/6	221.79	2.58
6	166.24	3/4	172.49	3.74
7	147.894	1	150.22	1.58

Table 5.2.4: Natural periods - 2 anchors per floater, model b)

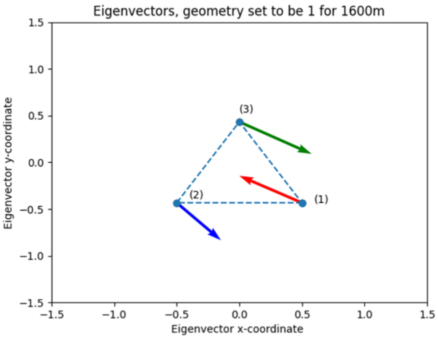

Figure 5.2.5: Eigenmode 1 linearized system for model b)

The linear and nonlinear systems agree with each other for system b) as the relative error is negligible. Even if the mooring stiffness is linear for small displacement, only two degrees of freedom is modeled, meaning that coupled motions with yaw and pitch can influence the calculated natural periods in SIMA. The good agreement between the linearized model and SIMA may be because the system is less sensitive on the difference in pretension as it gets its stiffness from multiple mooring lines. Also, as seen in Figure 5.2 model B) agrees well with the linear pretension for the anchored mooring. As Wilson and Hall nondimensionalized the horizontal tension on weight, this assumption may be insufficient for some systems when calculating the natural periods.

Mode SIMA	Natural period [s] SIMA	Modes code	Natural period [s] code	Relative [%]
9	75.84	1	76.06	0.29
3	313.50	2	269.66	16.26
7	85.18	3	91.41	7.31
8	84.79	4	91.41	7.81
4	189.11	5/6	213.07	12.67

Table 5.2.5: Natural periods - 1 anchors per floater, model c)

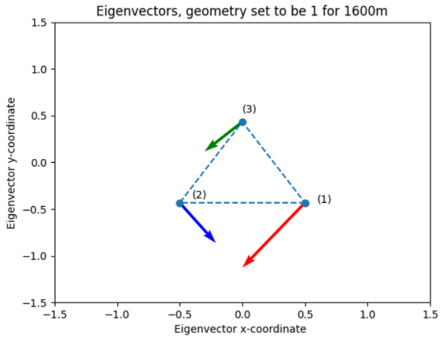

Figure 5.2.6: Eigenmode 1 linearized system for model c)

Table 5.2.6: Eigenmodes - 1 anchor per floater, model c)

The natural periods are the worst for system c). As the absolute error of pretension is the largest for system c), it is expected that the natural periods are not calculated well. Also, the mooring weight is substantial as the mooring weight is 1.97 kt/turbine [9]. It is expected that the mooring weight will influence the natural periods. For a good analysis, adding the mass to the floater is necessary for the linearized model.

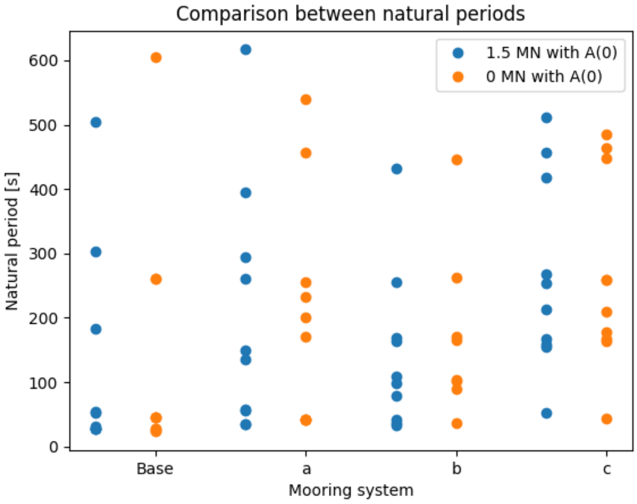

Figure 5.2.7: Natural periods for system baseline, a, b, and c with A(T=0) at zero and maximum thrust

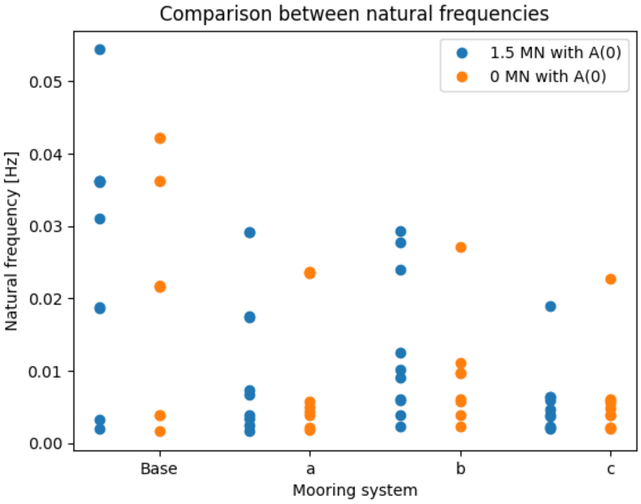

Figure 5.2.8: Natural frequencies for system baseline, a, b, and c with A(T=0) at zero and maximum thrust

Figures 5.2.7 and 5.2.8 show how the natural periods and thereby, frequencies change due to the nonlinearity and mooring topology. The highest natural periods for system b are not shown as the periods are around 1000 s. As the stiffness increases for the upwind floaters, the downwind mooring lines lose their tension. The downwind floaters would get their stiffness from the shared mooring lines, and the floaters get more coupled. Therefore the natural periods are changed entirely as the stiffness is unevenly distributed. Therefore, the natural periods are more clustered for zero thrust force. Also, many of the natural periods seem almost unaffected by the thrust force. In section 5.1, the floater's stiffness was discussed. The downwind floaters have a relative linear stiffness compared to upwind floaters for maximum thrust. Therefore, some natural periods are expected not to change much as the stiffness properties have not changed.

It is observed that the three-floater system's natural periods change less than for two and one-floater systems when maximum thrust is applied. A possible explanation is that the resonance motions are highly coupled between the systems, thus less sensitive to stiffness changes. As system c) upwind mooring becomes highly nonlinear for large displacements, it was expected that the natural periods should change much. Also, the system mass may be very high compared to the changes in stiffness when three floaters are coupled together. Therefore the natural periods are less affected.

By looking at Tables 5.2.7, 5.2.8, 5.2.9, and 5.2.10, it is clear that several natural periods are the same for all the systems, as the systems were optimized to have the same linear stiffness. Primarily four groups are identified at around 460 (457, 464, 467), 260 (261, 256, 260, 262), 200 (209, 201), and 170 (172, 178, 171) s. The base system has only a natural period of around 260 s. The natural period at 200 s is only for systems a) and b). Both systems have in common that they only have two anchored mooring lines per floater. System c) has a unique natural period group of around 100 s, which is half of the unique period of systems a) and b). Therefore, this resonance mode is likely connected to the one-anchored mooring system.

5.2.1 Summary of natural periods

,

Modes	SIMA eigenvalue [Hz]	SIMA eigenvalue [T]
1	0.00167	597.87
2/3	0.00383	261.01
4/5/6	0.02163	46.24
7/8	0.03619	27.63
9/10	0.04226	23.67

Table 5.2.7: Natural frequency for base system with added mass A(T=0)

Modes	SIMA eigenvalue [Hz]	SIMA eigenvalue [T]
1	0.00185	539.73
2	0.00219	457.47
3	0.00391	256.05
4	0.03619	233.00
5	0.00499	200.52
6	0.00583	171.44
7/8/9/10	0.02353	42.50
11/12/13	0.02892	34.58
14/15	0.03618	27.59
16/17/18/19/20	0.046	21.74.59

Table 5.2.8: Natural frequency for system a) with added mass A(T=0)

Modes	SIMA eigenvalue [Hz]	SIMA eigenvalue [T]
1	0.00206	484.86
2	0.00215	464.21
3	0.00223	448.76
4/5	0.00385	259.93
6	0.00477	209.59
7	0.00562	177.92
8	0.00600	166.74
9	0.00612	163.5
10-15	0.02269	44.06-42.92
16/17/18	0.02600	38.46-36.98
19/20	0.03416	29.27

Table 5.2.9: Natural frequency for system b) with added mass A(T=0)

Modes	SIMA eigenvalue [Hz]	SIMA eigenvalue [T]
3	0.00224	446.74591
4	0.00381	262.34077
5	0.00585	171.07707
6	0.00604	165.60091
7/8	0.00970	103.07355
9	0.01104	90.56287
10/11/12	0.02720	36.76050
13-21	0.03121	32.04536-31.52
22-30	0.04954	20.18602-17.56

Table 5.2.10: Natural frequency for system c) with added mass A(T=0)

Chapter 6

Verification of simplified wind, mooring, and degrees of freedom study

6.1 Dynamic verification study

To verify if the models behave dynamically the same, a decay test has been carried to get an insight in eigenperiods and damping ratio.

Both hub and blades has been removed from the modified model for simplify the analysis and thereby save computational effort.

Total mass has been estimated by looking at point mass in hub and summation of RIFLEX element for blades, thereafter the mass has been redistributed to the SIMO body floater.

If the systems should behave dynamically the same the central of gravity should be equivalent for both the models. Therefore floater central of gravity has been changed to compensate in the change. Central of gravity can be estimated by first order of inertia.

$$X_G^j = \frac{\sum_{i=1}^n m_i x_i^j}{\sum_{i=1}^n m_i}, j = 1, 2, 3 \tag{6.1.1}$$

The blades local moment of inertia are estimated with the distance from the hub.

$$I_{44} = \int_B y^2 + z^2 \, dm \tag{6.1.2}$$

$$I_{55} = \int_B x^2 + z^2 \, dm \tag{6.1.3}$$

The cross product moment of inertia was initially calculated, but when conducting decay tests their influence was not noticed and therefore not included in further analysis.

$$I_{46} = \int_B xz \, dm \tag{6.1.4}$$

After calculating local moment of inertia, the parallel axis theorem was used to move the inertia axis system to the floater central of gravity.

T [s]	η_1	η_2	η_3	η_4	η_5	η_6
VolturnUS-S	296.95	298.4	21.28	31.98	32.1	145.55
Baseline	297.35	298.1	21.28	31.58	31.62	145.1
n	2	2	31	31	11	5

Table 6.1.1: Decay results in all degrees of freedom for rigid body

	m [kg]	Ixx$[Nm^2]$	Ixy	Ixz	Iyy	Iyz	Izz	X$_G[m^2]$	Z$_G[m^2]$
VolturnUS	1.79e7	1.65e10	0	0	1.65e10	0	2.37e10	0	-14.94
Baseline	1.8239e7	2.7273e10	0	0	2.7275e10	0	2.3716e10	-0.23	-12.03

Table 6.1.2: Floater properties before and after modifications

The eigenperiods are very close to each other. Possible difference between them could is caused by error in calculation. Moment of inertia was calculated before floater central of gravity was changed, therefore moment of inertia is too big.

The natural period in surge and sway can be compared to those in eigenvalue analysis. 297 s is very close to the 303.6 s, the eigenvalue with force. As the added mass is larger for the decay test, the decay period is expected to be longer than for the eigenvalue analysis. However, the decay analysis oscillates between 90 m and -10 m for the surge motion. Therefore the stiffness will vary, and the system becomes softer than with constant thrust. The extra added mass and loss of stiffness effects cancel each other out.

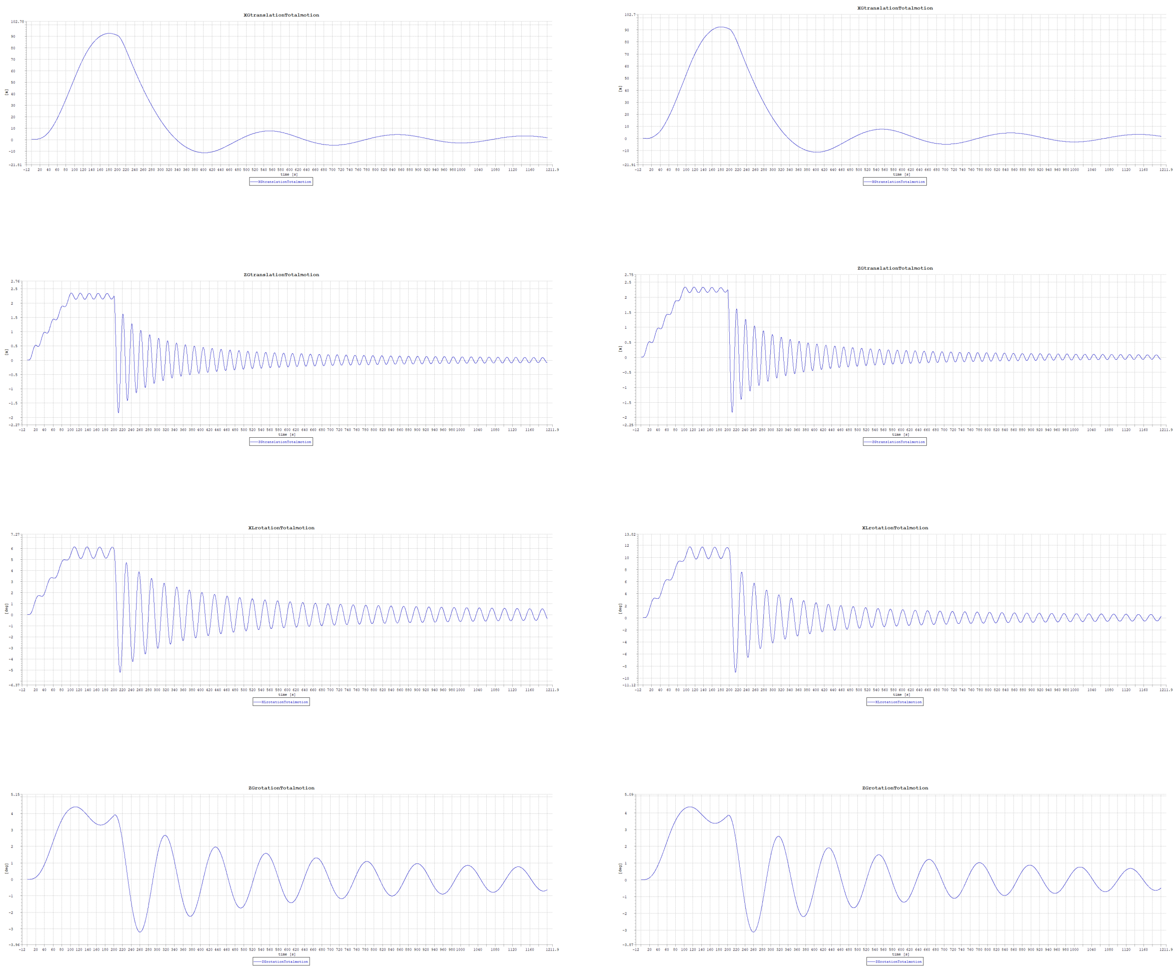

Figure 6.1.1: Decay test from VolturnUS-S reference platform with modified mooring system and equivalent model without hub and blades.

6.2 Dynamic analysis of shared mooring fidelity

It is important to simplify the wind force as it is the most numerical demanding in a coupled analysis. Few softwares can analyze multiple FOWT with aero-servo-hydro-elastic coupling. The new SIMA version is limited to inline FOWT with turbulent wind, as the turbulent wind field has to be enormous to analyze shared mooring system, which is not inline. With mean wind speed and irregular waves, the dynamic of a shared mooring system cannot be evaluated. Therefore, It is important to develop an analysis methodology that can evaluate shared mooring systems effectively.

The methodology for generating simplified force files is discussed in Section 4.7. A simplified force vector in a global coordinate system instead of a fully coupled wind analysis has several benefits. The system's dynamics are not changed (except for the elasticity effects from blades), and it is possible to simulate turbulent wind for complex shared mooring systems. The compromise with using a force vector in a global reference system is that the forces are not coupled with the floater motions and velocity and themselves since the forces are pre-calculated. As the floater velocity is not considered, the relative wind field and the blades pitching are affected. The forces calculated could be slightly off if the servo system is sensitive to wind velocity.

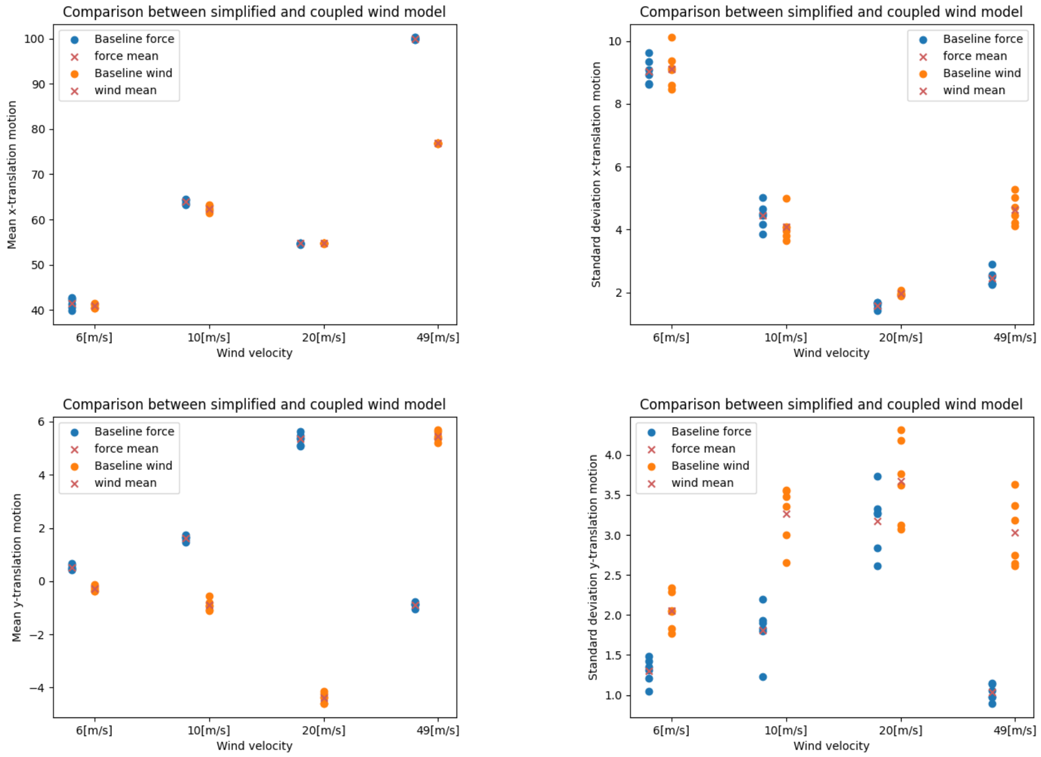

Figure 6.2.1: Comparison study of mean and standard deviation of wind turbine motion x and y

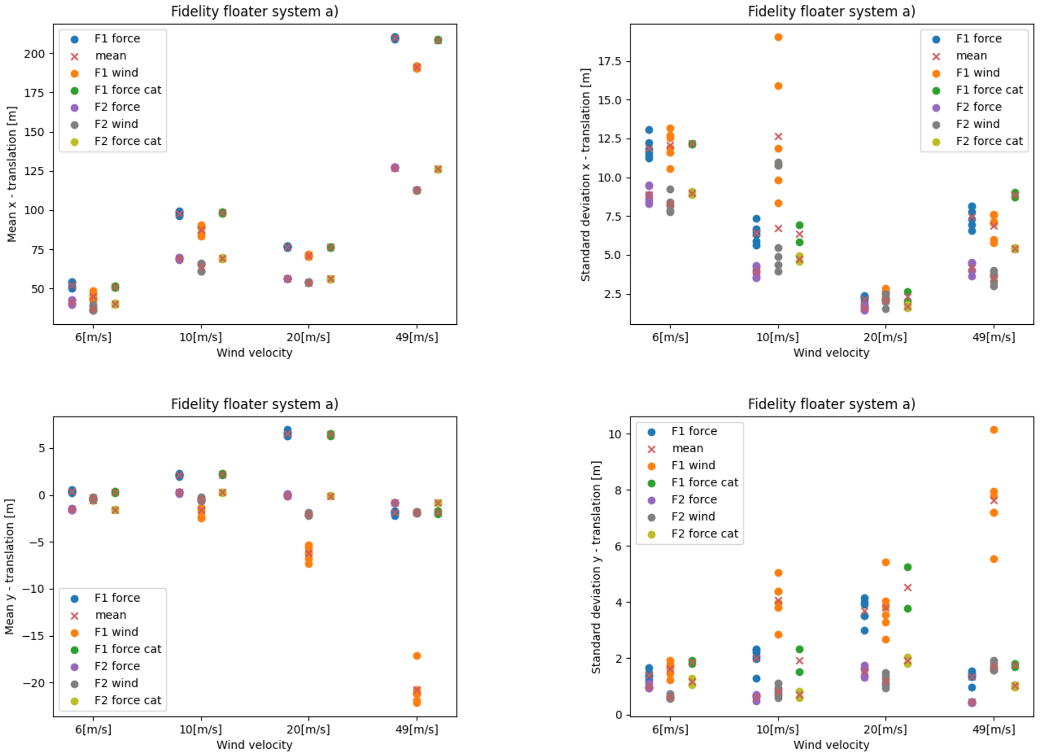

Figure 6.2.2: Comparison study of mean and standard deviation of wind turbine motion x and y for shared mooring

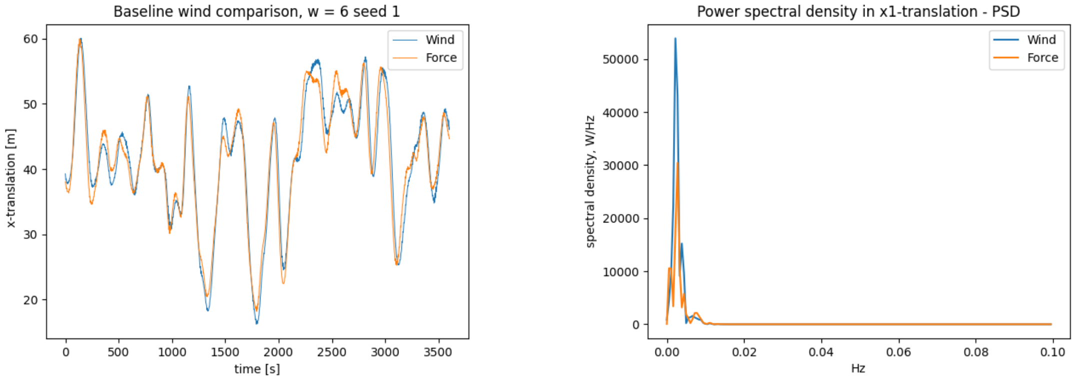

Figure 6.2.3: Time realization and spectral analysis for w = 6 [m/s], baseline fidelity, peak frequencies = (x1: 0.00222, 0.00388) [Hz]

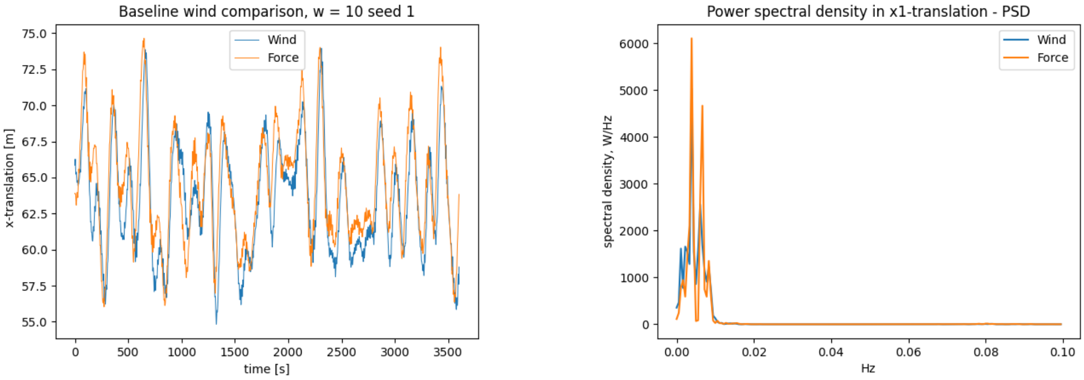

Figure 6.2.4: Time realization and spectral analysis for w = 10 [m/s], baseline fidelity, peak frequencies = (x1: 0.00111, 0.00388, 0.0061, 0.00833) [Hz]

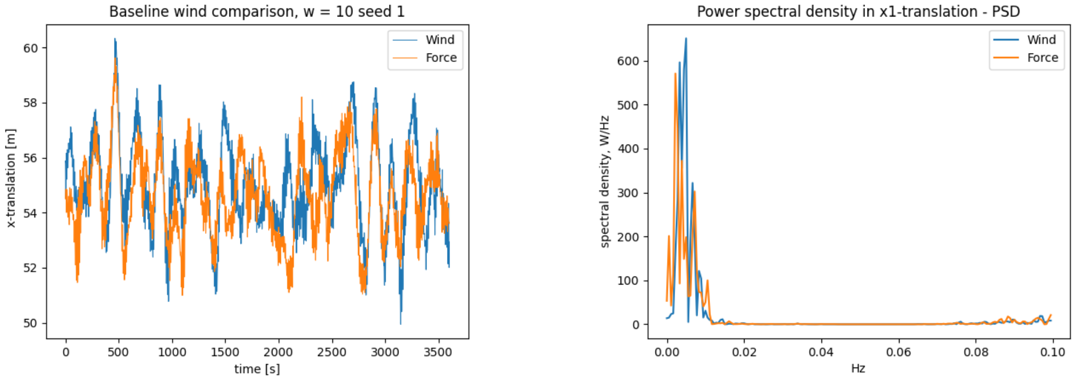

Figure 6.2.5: Time realization and spectral analysis for w = 20 [m/s], baseline fidelity, peak frequencies = (x1: 0.00333, 0.00498, 0.0066. 0.0083) [Hz]

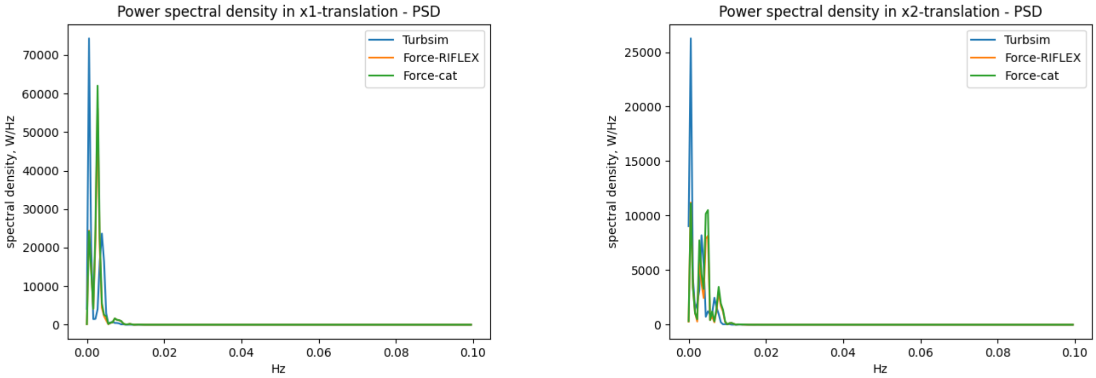

Figure 6.2.6: Time realization and spectral analysis for w = 6 [m/s], model a fidelity, peak frequencies = (x1: 0.000555, 0.00385, 0.0072), and (x2: 0.000555, 0.00333, 0.005, 0.00698)[Hz]

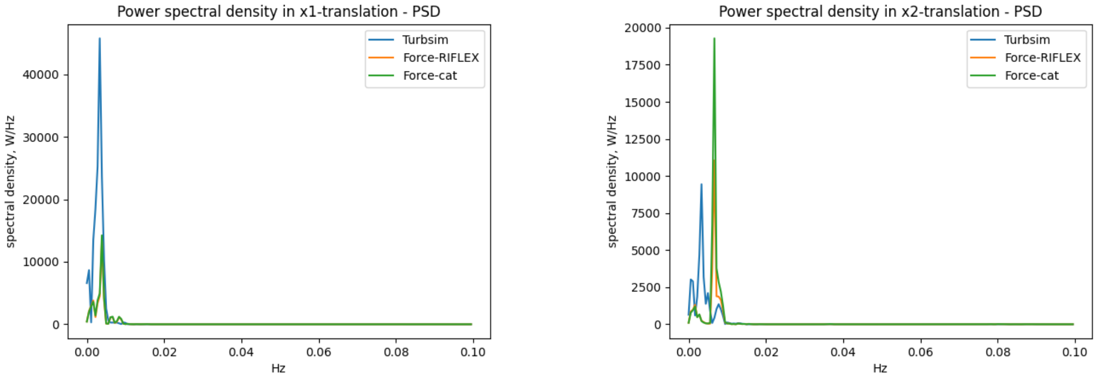

Figure 6.2.7: Time realization and spectral analysis for w = 10 [m/s], model a fidelity, peak frequencies = (x1: 0.000333), and (x2: 0.000333, 0.06667)[Hz]

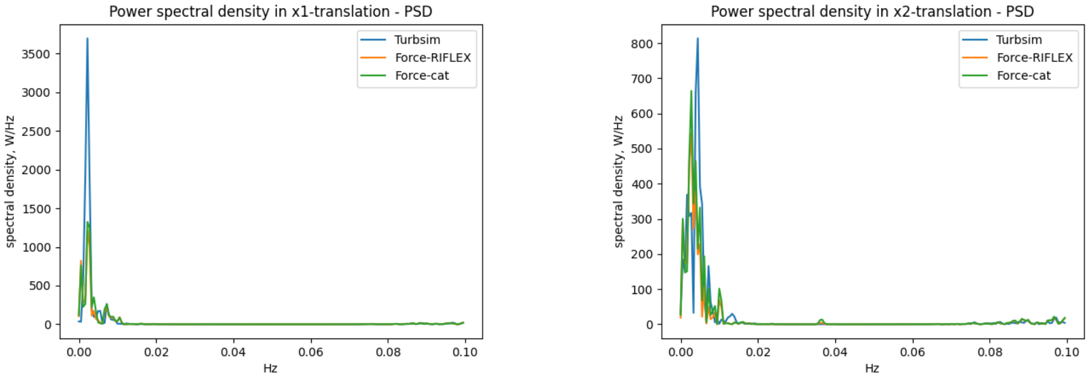

Figure 6.2.8: Time realization and spectral analysis for w = 20 [m/s], model a fidelity, peak frequencies = (x1: 0.00222, 0.00722), and (x2: 0.00055, 0.0049, 0.00722,0.0133)[Hz]

The simplified force model is accurate in surge motion for the mean and standard deviation for the baseline and the shared mooring system, with a few exceptions.

The standard deviation is quite large for high wind speed w = 49 m/s, both for the mean and standard deviation for the baseline and shared mooring system. As the mean value is quite different between the force and wind model, it is expected that the standard deviation cannot be the same, as the stiffness is entirely different. Strangely, the extreme wind condition has a substantial surge motion compared to condition 2. In section 4.6.2, the wind force shall not differ much between the maximum wind thrust and the drag force from the extreme wind. By further investigation, the blade was not pitched when the force file was generated, even though the variable for pitching of the blades had an input of 90° degrees in the condition set. Therefore it seems that the variable dependency was destroyed when the force file was generated. Since the blade was not pitched, not only the tower generated drag but also the blades. Thus, overestimating the drag force.

As the time series for wind fields are not the same, it is not expected that all the standard deviations calculated shall be the same for the models. Originally it was thought to compare the same realization for the wind field, but a more course wind file where needed when simulating turbulent wind on a shared mooring system. For the time realizations in Figures 6.2.3, 6.2.4, and 6.2.5, the same wind fields are simulated for comparison between the time series, and spectral analysis is carried out to compare the resonance in the systems. As the aerodynamic damping is simplified as linear and independent on the servo, it is expected that the force model is not suitable for resonance. It is known from previous studies that linearized damping overestimates the damping in the system. Therefore, if the system is excited by resonance, the standard deviation of the time series would be lesser for the force model. For spectral analysis w = 6 m/s for baseline, the spectral has a very high peak that is larger for the wind model. The peak is located at 257.7 s. A resonance mode of 256 s is calculated in eigenvalue analysis, meaning the system is resonant.

The force model differs for condition 2 for the shared mooring system. The standard deviation for the downwind floater has a large spread compared to the upwind floater and the force model. By looking at several spectral analyses for condition 2, the amplitude in the spectral analysis changes much. Therefore, condition two seems to be struggling with resonance at 150 s, which agrees with 149.2 s from the eigenvalue analysis. The cut-out wind speed is 11.6 m/s, and the distance between the wind turbines is 1716 m. This gives a time lag of 147.93 s, which is close to the natural period in surge for system a). This could also explain why the simplified model cannot predict this resonance phenomenon as the wind control system is removed. The standard deviation is 1.83 m/s wind speeds likely reach the rated wind speed several times.

It is highly likely that the other wind conditions also have resonance, as the spectral analysis contains much energy at the resonance modes. The time lag between the turbines for condition 1 is 286 s. Therefore wind speeds at 6.7 m/s will excite the resonance mode. According to NTM, used in the turbsim file, the standard deviation is 1.4 m/s. Therefore it is highly likely that the resonance mode is excited. Condition 3 has little energy for the resonance modes, as the phase lag is 85.8 s, far from the natural periods.

Forces from the wind turbine were read from tower segment one. This was done to include the drag force. A problem with this technique is that the forces and moments follow the local reference system. For both of the moments, the sign was switched as the moments are internal. Therefore shear moment sign should have been switched. This was not discovered since the tests were carried out for small wind speeds; therefore, the difference was negligible.

The standard deviation in sway is very close between the models, especially for the shared mooring system. The shared mooring system's large sway motions will cause a rotation of the shared mooring line, which increases the mooring stiffness in sway. This stabilizes the system, causing less sway motions for the same wind speeds. The standard deviation is lesser for the baseline system has a higher stiffness.

If the sign were correct, the simplified force would have been quite good. This alone is not expected to influence the standard deviation in sway, since the system is symmetric, and the stiffness should therefore be the same. Nevertheless, sway motions will affect the mooring system's direction and yaw motions.

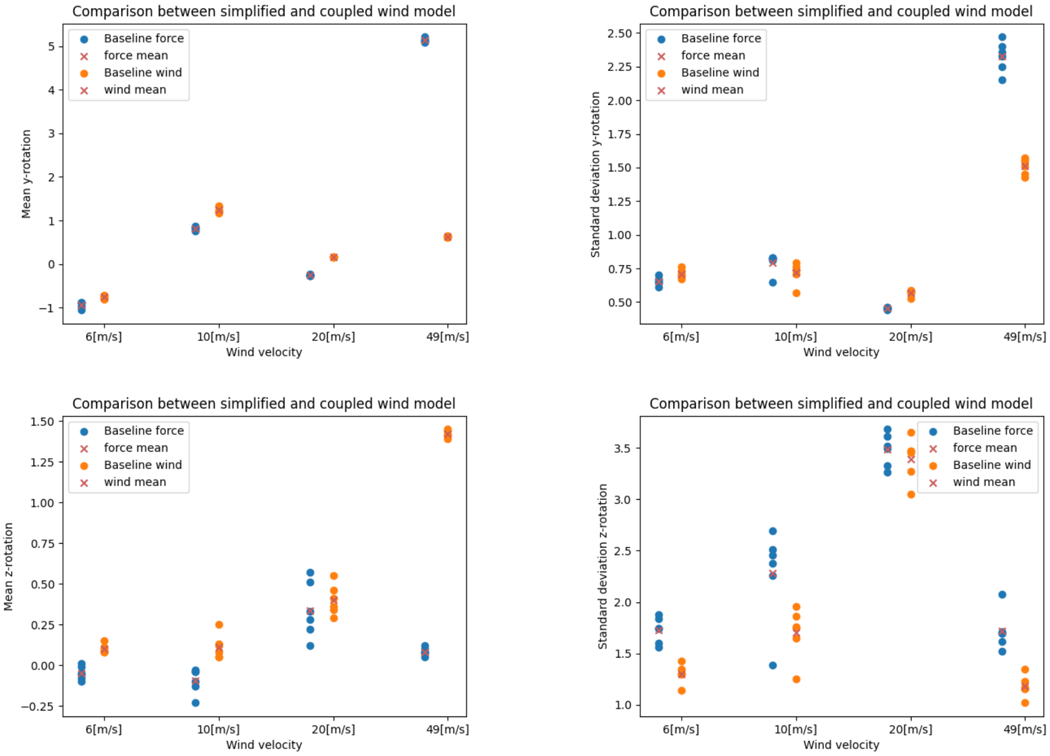

Figure 6.2.9: Comparison study of mean and standard deviation of wind turbine pitch and yaw motions for baseline system

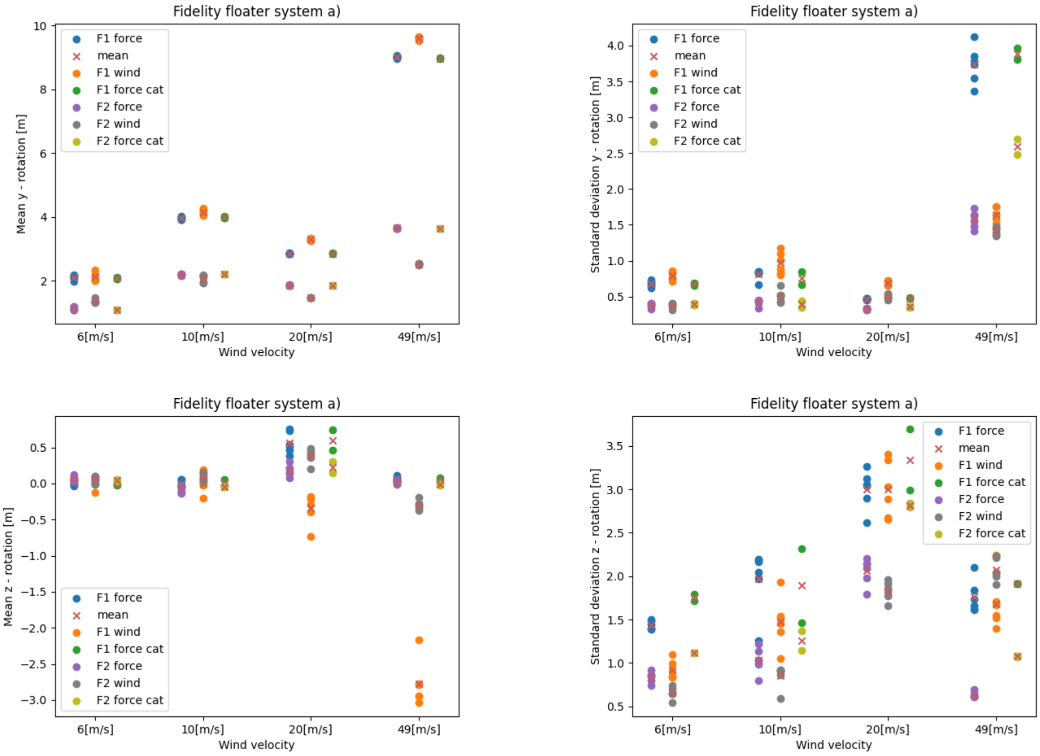

Figure 6.2.10: Comparison study of mean and standard deviation of wind turbine pitch and yaw motions for system a)

Pitch motions are very close to each other for the standard deviation and mean value with and without shared mooring. The mean value is larger for the downwind floater for wind conditions and the standard deviation. For the upwind floater, the force model is the largest. It is, therefore, less difference between the force model.
This could be explained by the feed-forward induced motions from the control system. This is an aero-servo effect induced by the control system to regulate the thrust force. The blades pitch to regulate the thrust force, causing a sudden change. The relative velocity changes as the force changes, and the control system regulates the thrust force. This causes oscillations in the system and will affect the standard deviation in pitch.
This effect would be the largest when the thrust force is close to the cut-out wind speed. The difference between the simplified force and wind model is the largest for w = 10 in pitch and smallest for w = 20 for standard deviation and mean value.

The standard deviation and mean yaw motion have the worst agreement with the force model. The mean yaw motions are quite good for the shared mooring system, as there is almost zero yaw due to the shared mooring line. The force model overestimates the standard deviation and underestimates the mean yaw motion. The yaw moment is precalculated on a fixed wind turbine, and its generated from the coherence in the wind. In reality, when the system rotates in yaw, the thrust force will be decomposed, and the inflow area will increase. Therefore a decomposed force is generated in sway. As the inflow area increases, the yaw moment would increase. Thus, the force model underpredicts the yaw moment. A larger standard deviation is expected as no linear damping in the force model is not estimated. Therefore, the agreement in yaw would have been better with damping, as resonance motions would not dominate the standard deviation.

The force model has several assumptions that would affect the results. The relative velocity is the same as the velocity of the waves/wind. In reality, the relative velocity, the difference between the incoming velocity and the floaters' motion, is the velocity the system experience when calculating thrust and drag. When the system moves with the wind/wave, forces will become larger and lesser when the system moves against the wind/ wave. This changes the mean value and the standard deviation. The assumption will be most valid for systems with less dynamic motions, as the velocity is lower. The relative velocity effect is especially interesting in pitch, surge, and sway.

The pitch would be especially affected since the force is uncoupled. Normally when the tower pitches, the thrust is decomposed. This contributes to a larger pitch moment. When comparing the wind and force model, the wind has a larger pitch motion, which sounds reasonable as the force is not decomposed in the force model.

Also, when the tower pitches, all the tower elements are not normal to the wind, and the force has to be decomposed for the thrust force. The model would therefore be more precise for less pitch rotation, as the composition contribution is lesser. It is important to point out that mean values are off dynamic motions, and static calculations have been subtracted. The system has a rotation in pitch from static calculations, which would affect the performance of the simplified model.

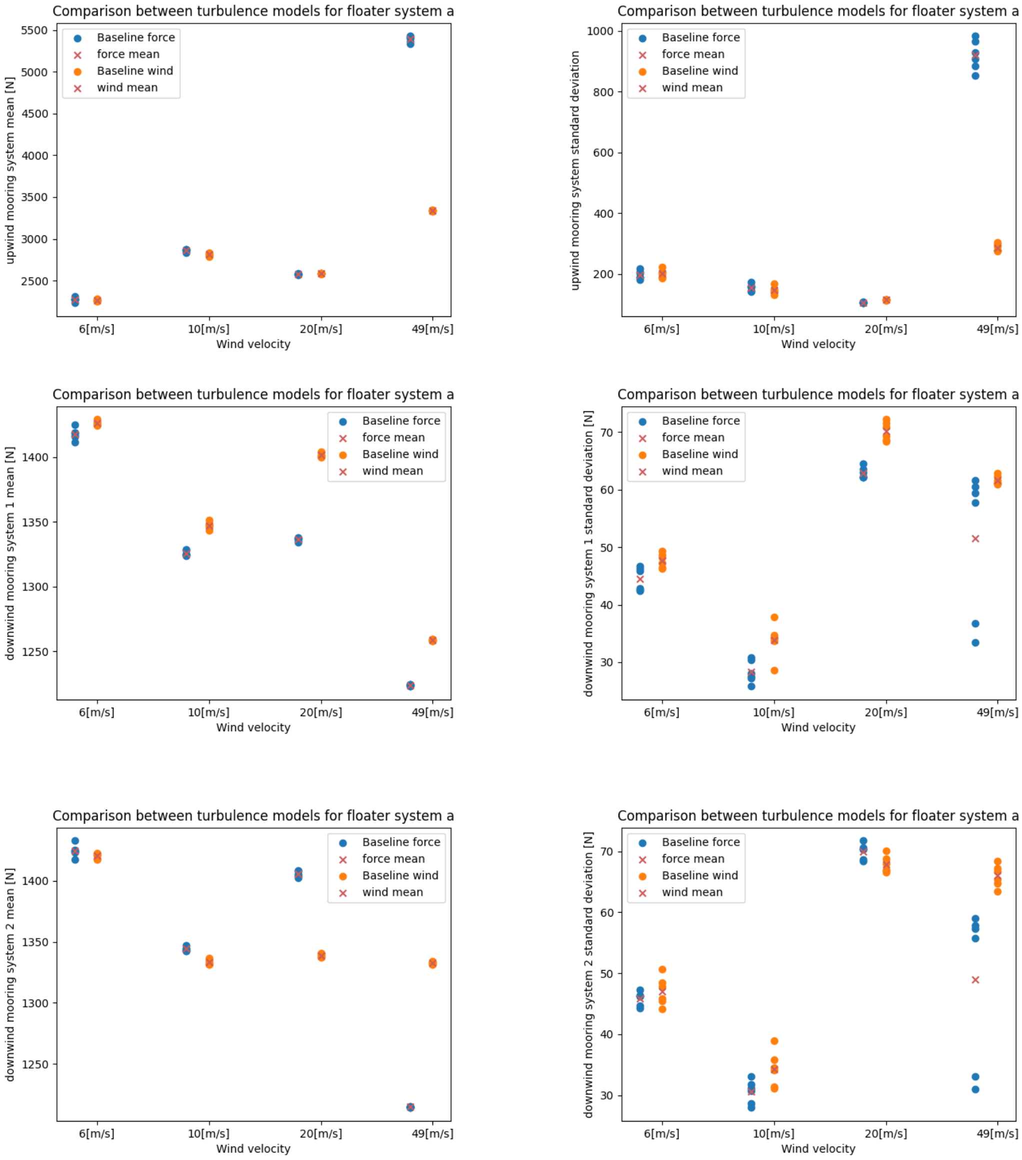

Figure 6.2.11: Comparison study of mean and standard deviation of mooring tension in baseline system

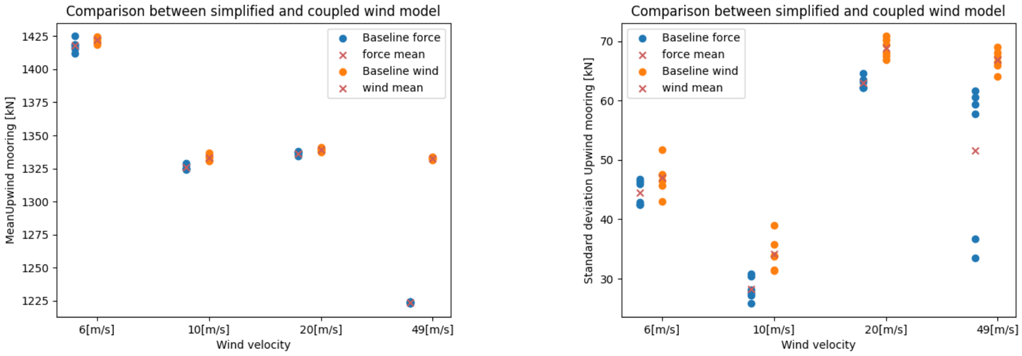

Figure 6.2.12: Comparison study of mean and standard deviation of mooring tension downwind - flipped mooring line

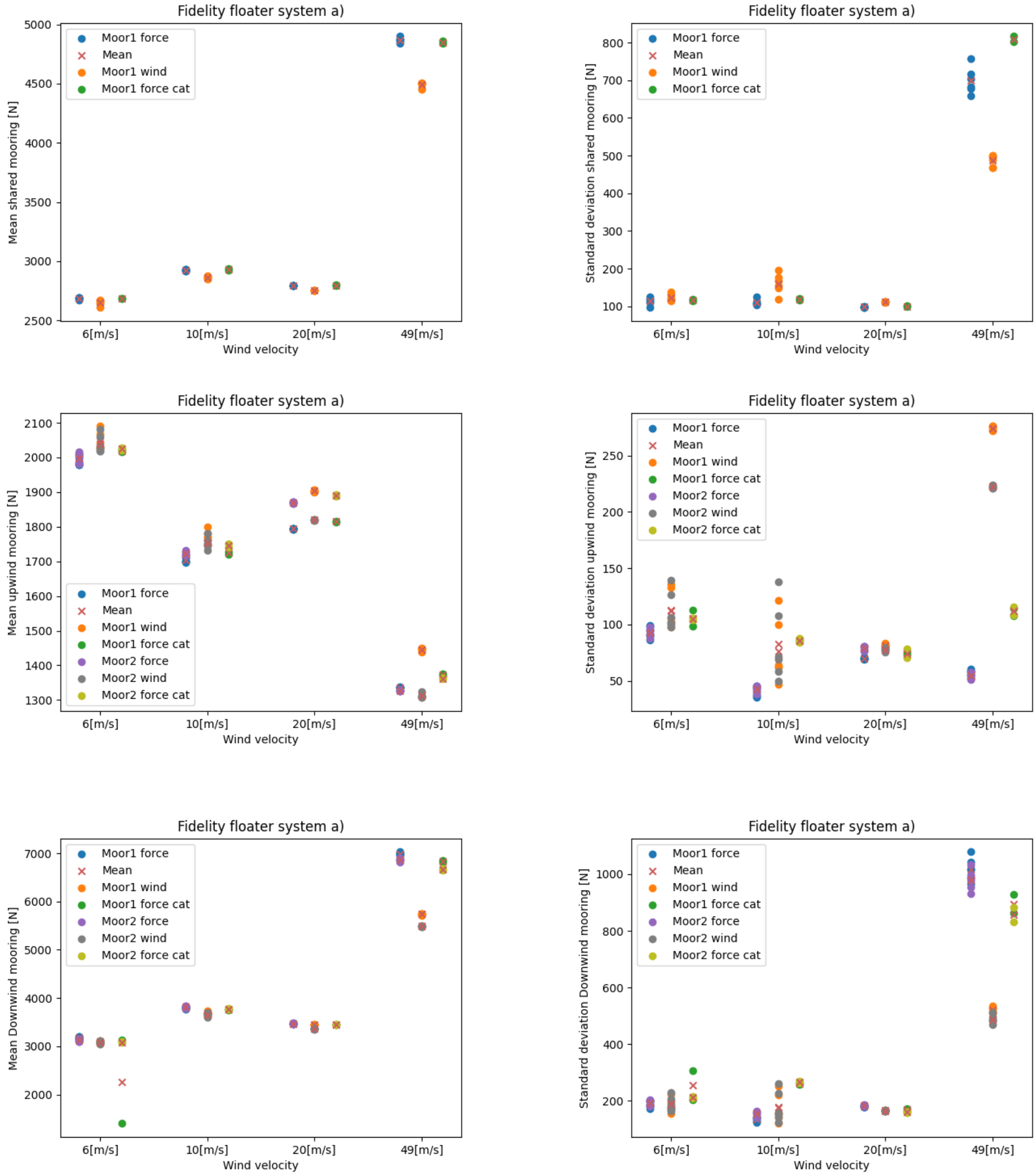

Figure 6.2.13: Comparison study of mean and standard deviation of mooring tension in system a) for shared , upwind and downwind mooring

Surge, sway, and pitch in the floater are a mooring system's most important degrees of freedom. As explained earlier, extreme wind conditions can be disregarded as the surge motion is incorrect due to errors in the pre-generated wind file.

Downwind mooring means and standard deviation tension are very close to each other for both of the systems. The downwind tensions seem very wrong as the sway motions are in the wrong direction for the force model. When the mooring lines are flipped so that the correct sway motion is considered, the difference is negligible for mean tension in Figures 6.2.11, and 6.2.13. As the mean tension is larger for the wind model, the standard deviation is larger as the mooring line is more responsive.

For large sway motions, the floater will come closer to the anchor point, and the pretension in the system will drop. As the wind model has a negative sway motion, the floater is closer to anchor 1, and the tension in the mooring line is lesser for downwind one than two.

The upwind mooring line has a very accurate mean and standard deviation for both systems. As the shared mooring system experience resonance for condition 2, the standard deviation for mooring tension is not as good as for the other conditions.

Shared mooring line tension has an excellent agreement between the models. The shared mooring line's tension depends on the floaters' relative displacement. Therefore, the shared mooring line was expected to have a significant standard deviation, as it depends on the dynamics of the two floaters. The mean tension and standard deviation are stable for the shared mooring line, and it is lesser than the upwind mooring line even though the mooring line dimension is, in practice, the same.

6.3 Quasi-static mooring study

Quasi-static mooring is an efficient way to calculate position and mooring tension in dynamic analysis. Since the tension is calculated for n points where the tension and stiffness are pregenerated for a mooring line with a catenary shape, the dynamic calculation is much faster than RIFLEX mooring. The algorithm uses linear interpolation between the closest points to the position for each time step. A drawback of this method is that the maximum tension in the mooring line cannot be calculated. Nevertheless, SIMA needs one fixed supernode to use a quasi-static mooring. Therefore, the method cannot be used for the shared mooring lines in SIMA, and only the anchored mooring lines can be modeled using quasi-static mooring.

The simplified force model was analyzed with both quasti-static mooring for anchored mooring lines and FEM mooring to see if lower fidelity affects the system's dynamic. Baseline system as not been presented as there were no visible differences between the quasi-static and FEM mooring. This was expected as it is well known that quasi-static mooring is in good agreement with the FEM mooring system.

Quasi-static mooring for system a) is previously presented with the wind and force model in Figures 6.2.2, 6.2.10, 6.2.13.

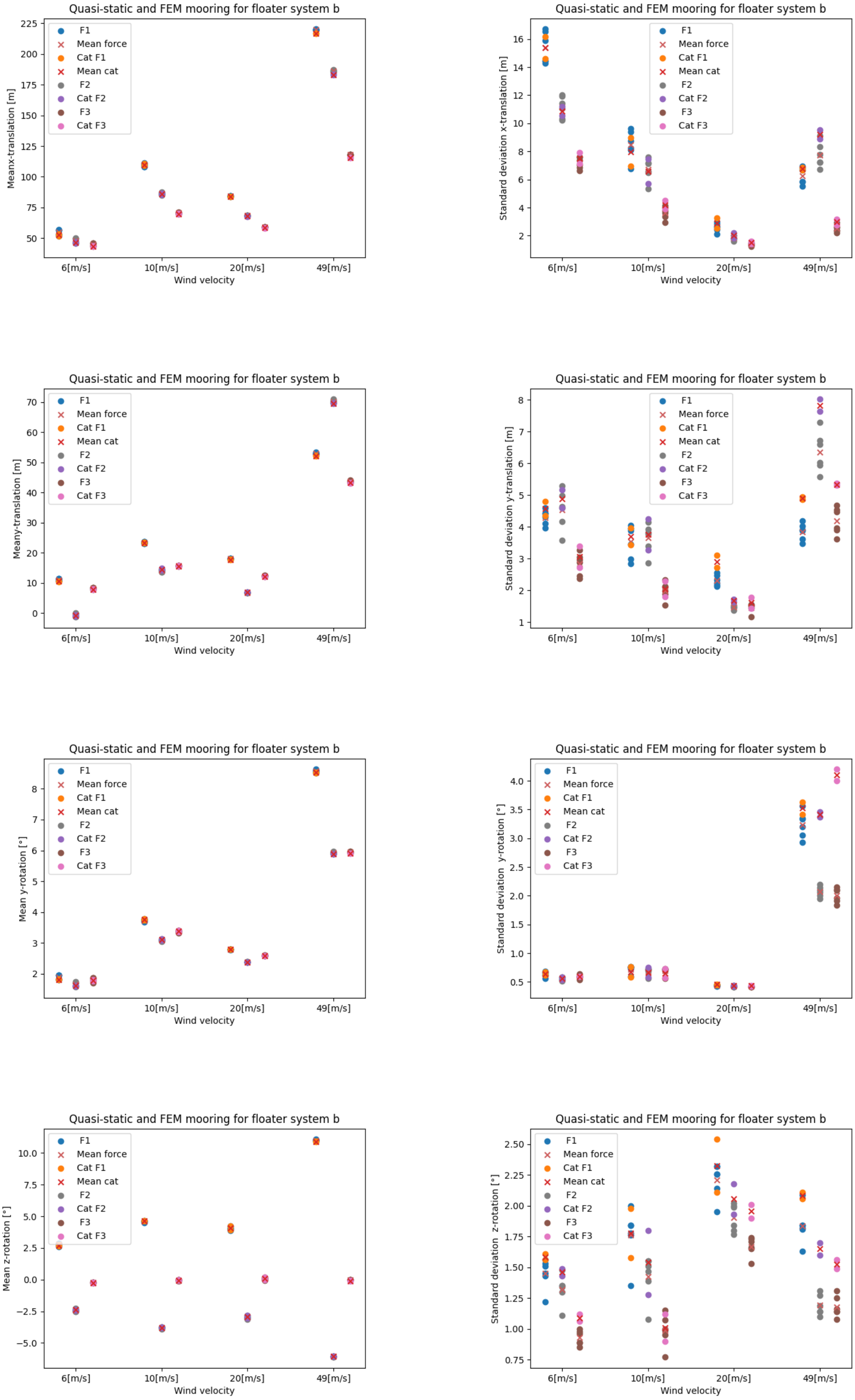

Figure 6.3.1: Comparison between RIFLEX and quasi-static mooring for system b - translation.

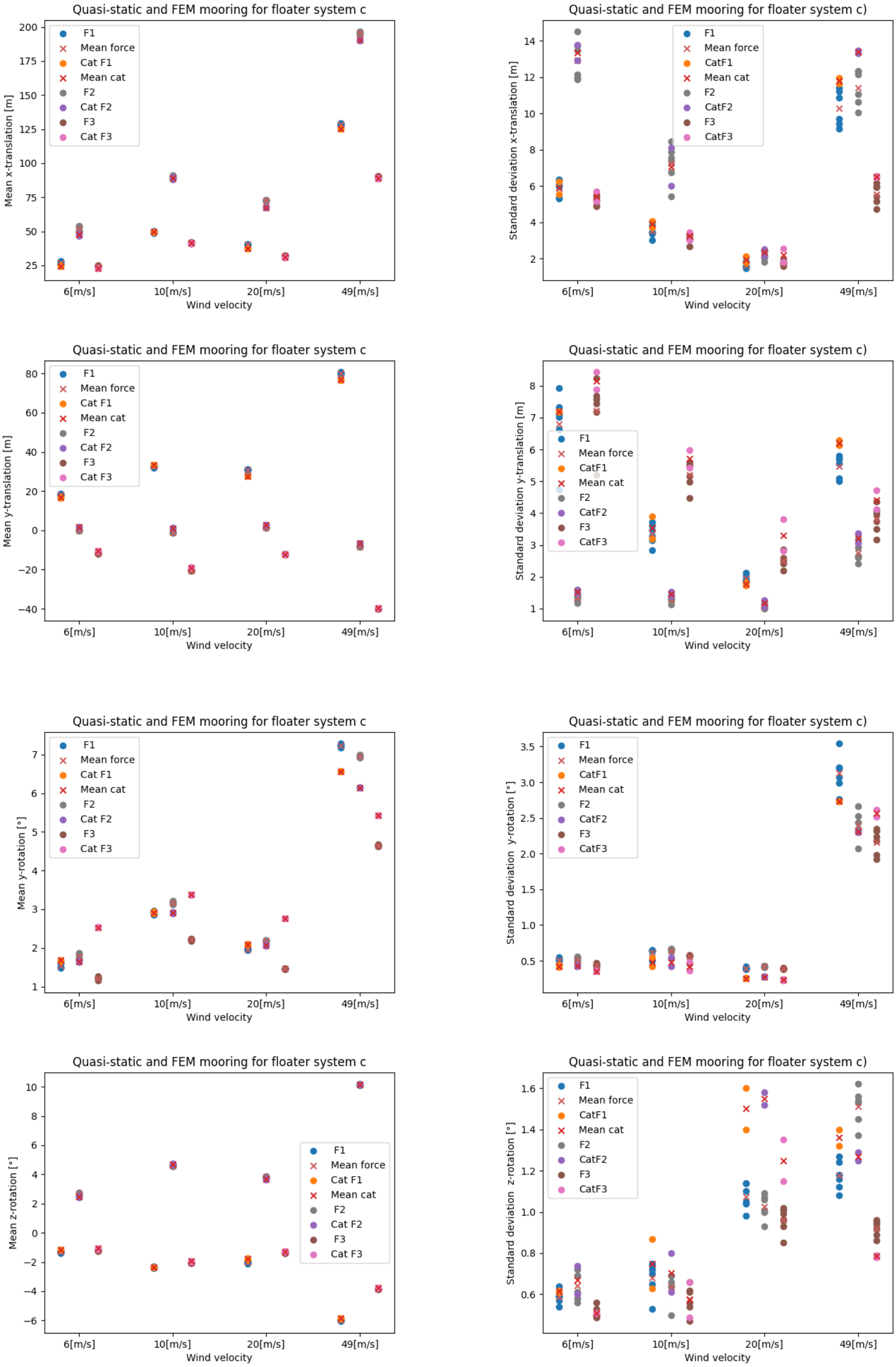

Figure 6.3.2: Comparison study of mean and standard deviation of wind turbine motions in system c).

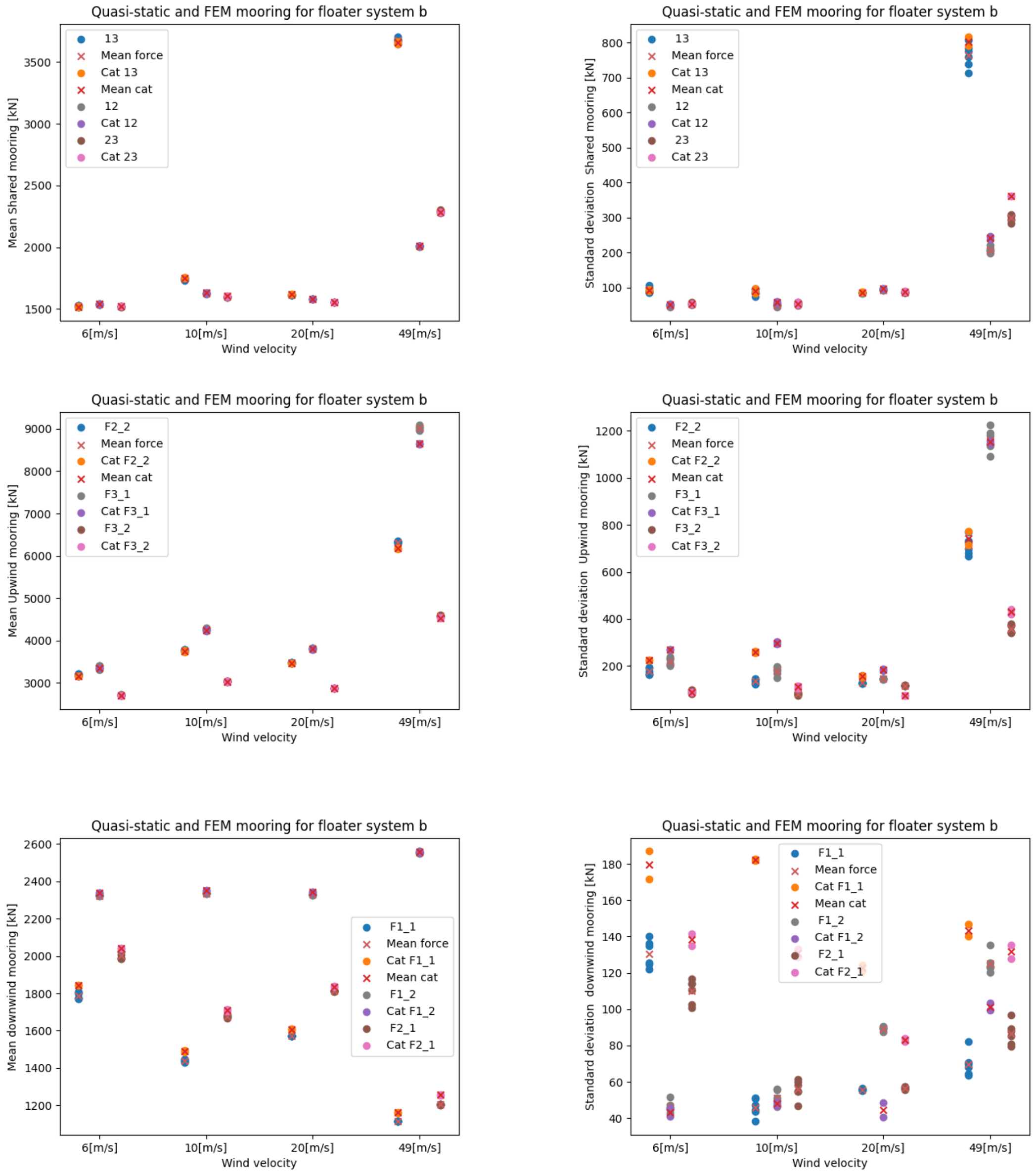

Figure 6.3.3: Comparison study of mean and standard deviation of mooring tension in system b) for shared, upwind, and downwind mooring.

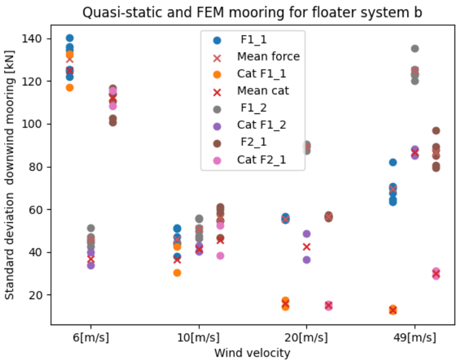

Figure 6.3.4: Standard deviation of downwind mooring tension in system b), corrected transient phase

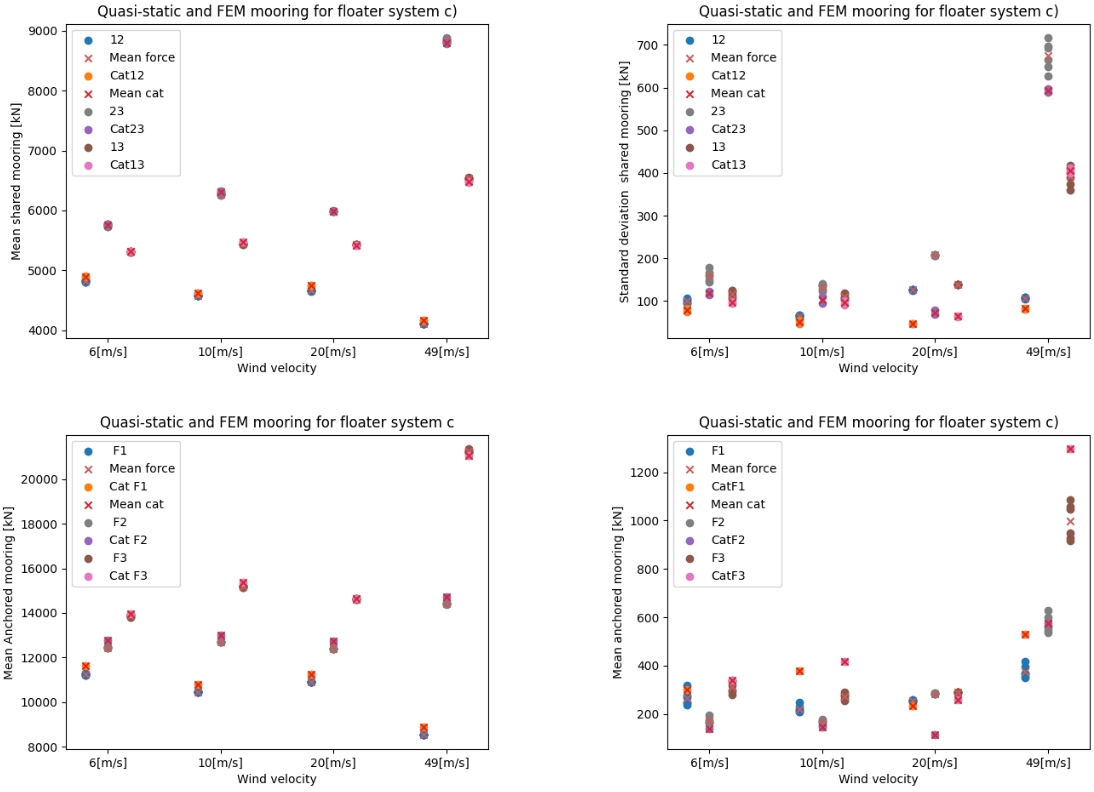

Figure 6.3.5: Comparison study of mean and standard deviation of mooring tension in system c) for shared and anchored mooring

There is little difference between quasi-static and FEM mooring in the mean and standard deviation for translation and rotation, with a few exceptions. The difference is the smallest for system a). As the quasi-static mooring has only two seeds, it is challenging to evaluate the standard deviation. The quasi-static mooring seems to have a larger dynamic difference between the seeds than the FEM mooring, but the difference is small for system a).

There is no difference in the mean for all the degrees of freedom except the mean pitch to floater three in system c). As there is no difference in the other floaters and the standard deviation is correct, this is probably an error in the data reading.

The standard deviation is very close to each other for system b), but the quasi-static mooring system overpredicts the pitch and yaw motion for high wind speeds. System c) the FEM and quasi-static mooring pitch motion agree, but the system overpredicts the yaw motion for large wind speeds, the same as for system b).

In Figure 6.3.3, the nine mooring lines have been plotted as shared, downwind, and upwind dependent on mooring type and wind direction. Floater three will have two upwind mooring lines, floater two, one of each, and floater one, two downwind mooring lines. In Figure 6.3.5 shared mooring is plotted in one figure and the anchored mooring in another, as there are only six mooring lines. The mean tension there is no difference between the models for systems a), b), and c). There are some differences between the quasi-static mooring and RIFLEX mooring for the standard deviation. Observed differences increase with the mooring complexity. Since the quasi-static mooring tension is connected with the visualization file and cannot be stored with SIMO results file (This will be corrected in the newer version, as it is possible to assign variables to SIMO body), it is not possible to read the data with a script. Therefore the mooring tension is saved as text files for each mooring line, which is tedious.

Quasi-static mooring overpredicts the tension in the downwind mooring lines, especially for condition 2, where the maximum thrust is generated and, therefore, the most significant translation. Some of the standard deviations are correct, for instance, for system a), but the deviation is large for system b). The problem with large displacements as this system experiences due to the soft mooring, the tension in the mooring lines has a large spread. Therefore many horizontal points in pre-calculations of the horizontal stiffness are necessary. The accuracy of the pre-calculated tension is then dependent on the maximum and minimum selected tension divided by the total horizontal points. If no minimum tension is selected, SIMO will calculate it based on the environmental condition. For small tensions, the accuracy is very sensitive to the chosen minimum tension. Few horizontal points are available if the tension is close to the minimum and the calculated tension is coarse. The agreement between quasi-static and FE mooring is dependent on the downwind mooring line rotation. The downwind mooring lines with lower mean tension also have a worse agreement for the standard deviation.

The upwind mooring there is a good agreement between the mooring models. The standard deviation is overpredicted for environmental condition 2 for systems b) and c). The system nonlinearity may affect the quas-static mooring tension, since the SIMO mooring linear interpolates between horizontal points, the stiffness must not change too much. If so, the stiffness is overpredicted, and the mooring tension is higher. By selecting a too-large Tmax the predicted stiffness could be correct for small displacements, but when the displacement is significant, the nonlinearity dominates the system. Thus, the stiffness calculation is too coarse.

The difference is minimal for shared mooring except for environmental condition three for system c). There are several reasons why shared mooring has a better comparison than upwind and downwind mooring. Firstly, the dynamic position is estimated well with quasi-static mooring. The mooring tension is only dependent on the relative displacement between the floaters. Secondly, FEM mooring is used for the shared mooring lines, as it is not possible to use SIMO mooring.

The quasi-static mooring line downstream has a longer transient phase than 150 s, therefore, 400 s are taken off the time series in Figure 6.3.4. By correcting the transient phase, the standard deviation is very good for conditions one and two but not condition 3. Condition 3 is less dynamic, and the tension will vary less. The system is, therefore, more sensitive to the total number of horizontal points, thereby under-predicting the dynamic tension.

In overall, shared mooring tension can be predicted with high accuracy if the floaters motions are predicted well by quasi-static mooring. Since RIFLEX elements model the shared mooring, the tension is only dependent on the floaters motions, something quasi-static mooring predicts very well. Quasi-static mooring can be used to calculate the tension in the anchored mooring, but the standard deviation could be wrong if the discretization is too coarse (too few horizontal points versus the difference between maximum and minimum tension).

SIMO selects the minimum tension for the entire system. Thus, whether this estimate is good for all the mooring lines is questionable. Shared mooring system has mooring lines in many different directions, causing the mooring lines to have a different mean tension. It is, therefore, essential to select a good minimum tension if the tension is off interest for a complex shared mooring system with quasi-static mooring lines.

Maximum tension was selected as 5e7 N for system c) and 1e7 N for the other system. 5e7 was chosen as 1e7 N, and 2e7 N crashed in the previous analysis due to the maximum wind speed condition. The maximum wind speed condition should have been run separately to increase the accuracy of the quasi-static mooring. Also, a good estimate of minimum tension should have been used instead of the default value. The systems were run with RIFLEX mooring, a good estimate of minimum and maximum tension where available but not used as 400 horizontal points were thought to have a good accuracy even if the maximum tension was set as high. According to SIMO manual THMIN, will be set as a ≪tension as low as possible for the algorithm≫ [23]. It is, therefore, plausible that the minimum horizontal tension is set to low, further decreasing the accuracy.

6.4 Dynamic analysis of shared mooring with linearized mooring system

As shared mooring analysis are tedious, simplified analysis is necessary to evaluate the dynamic performance of different shared mooring topologies. In the simplified analysis, the numerical method, constant average acceleration method were used to calculate the dynamic behavior of the systems. The floaters are analyzed as rigid bodies with two degrees of freedom(sway and surge), point mass, and linear stiffness. The wind forces are estimated using the force model from the previous analysis. Wave forces are calculated with Morison using regular and irregular waves with nonlinear Morison drag.

From previous static analysis, it can be observed that the linear stiffness matrix has some limitations, as the systems are highly nonlinear. Since the stiffness matrix is linear, the stiffness matrix is symmetric, giving the same response for all the floaters in the same system. Since, the stiffness is linear, the tension in the mooring lines will vary less. Also, the natural periods are not calculated correctly as the pretension in SIMA does not match Hall and Wilsons data. The analysis could therefore be further improved by using precise pretension and stiffness from quasi-static analysis. See Sections 4.7, 4.8, and 4.9 for further details.

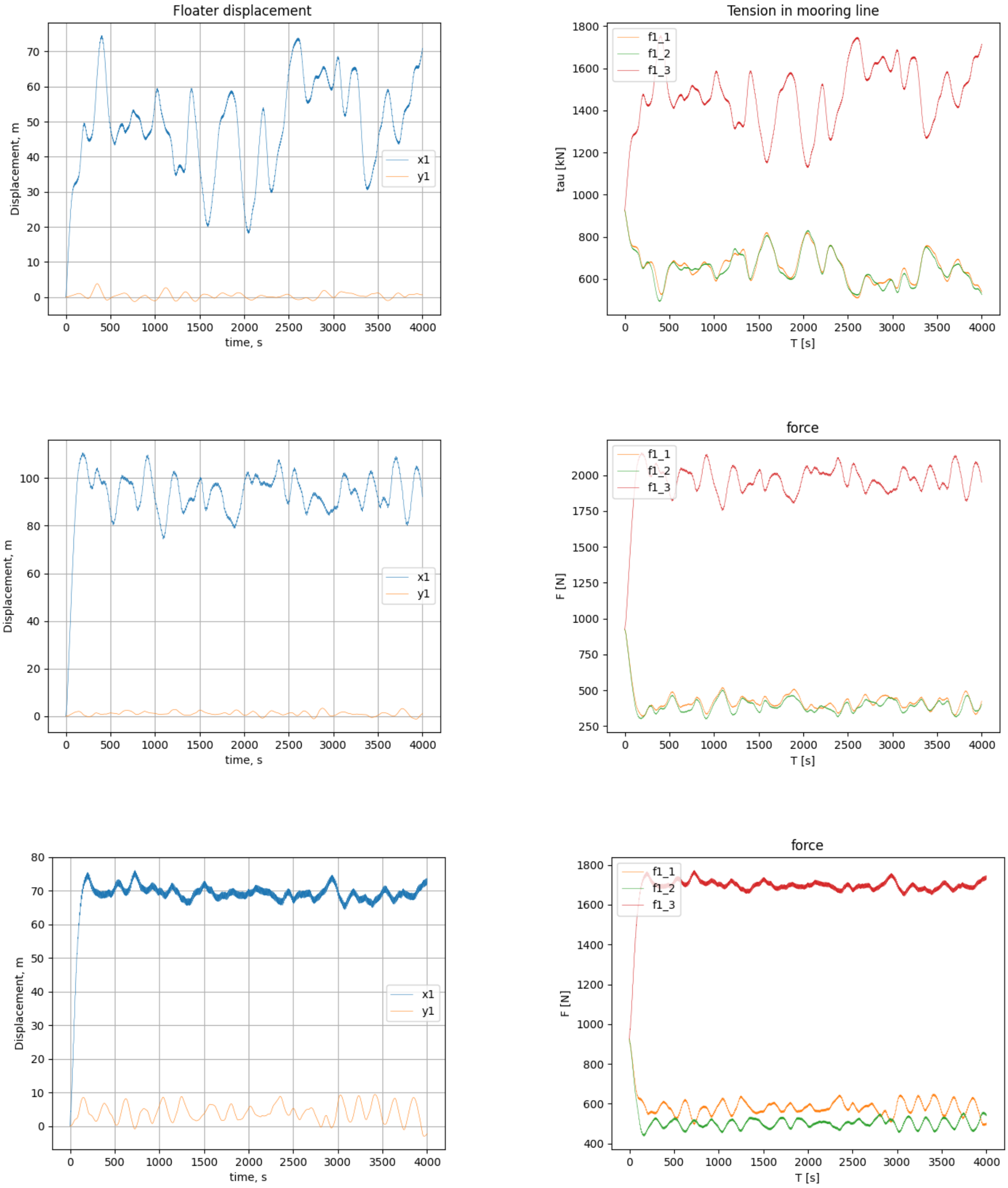

Figure 6.4.1: Simplified dynamic analysis with regular waves - baseline.

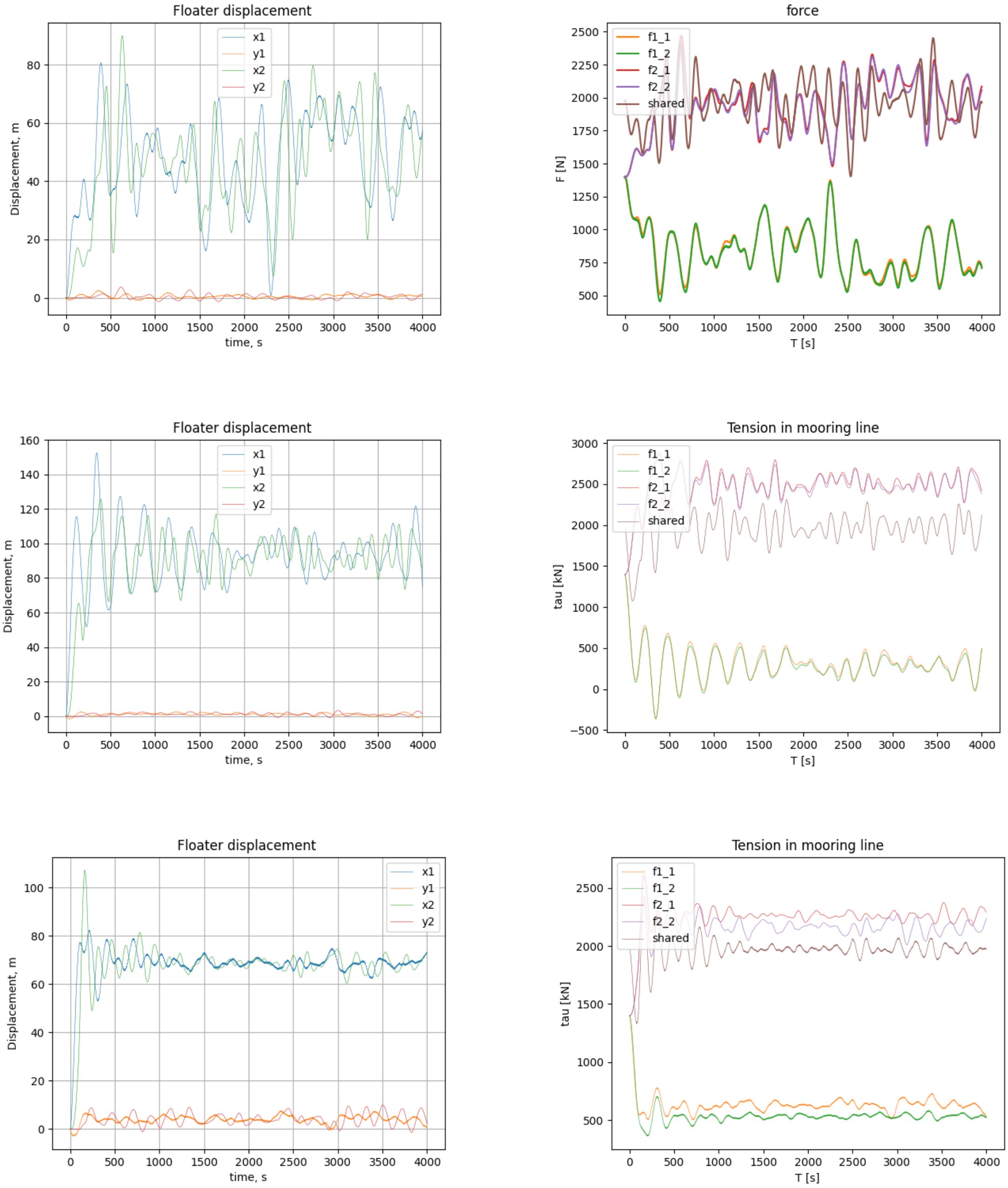

Figure 6.4.2: Simplified dynamic analysis with regular waves - model a).

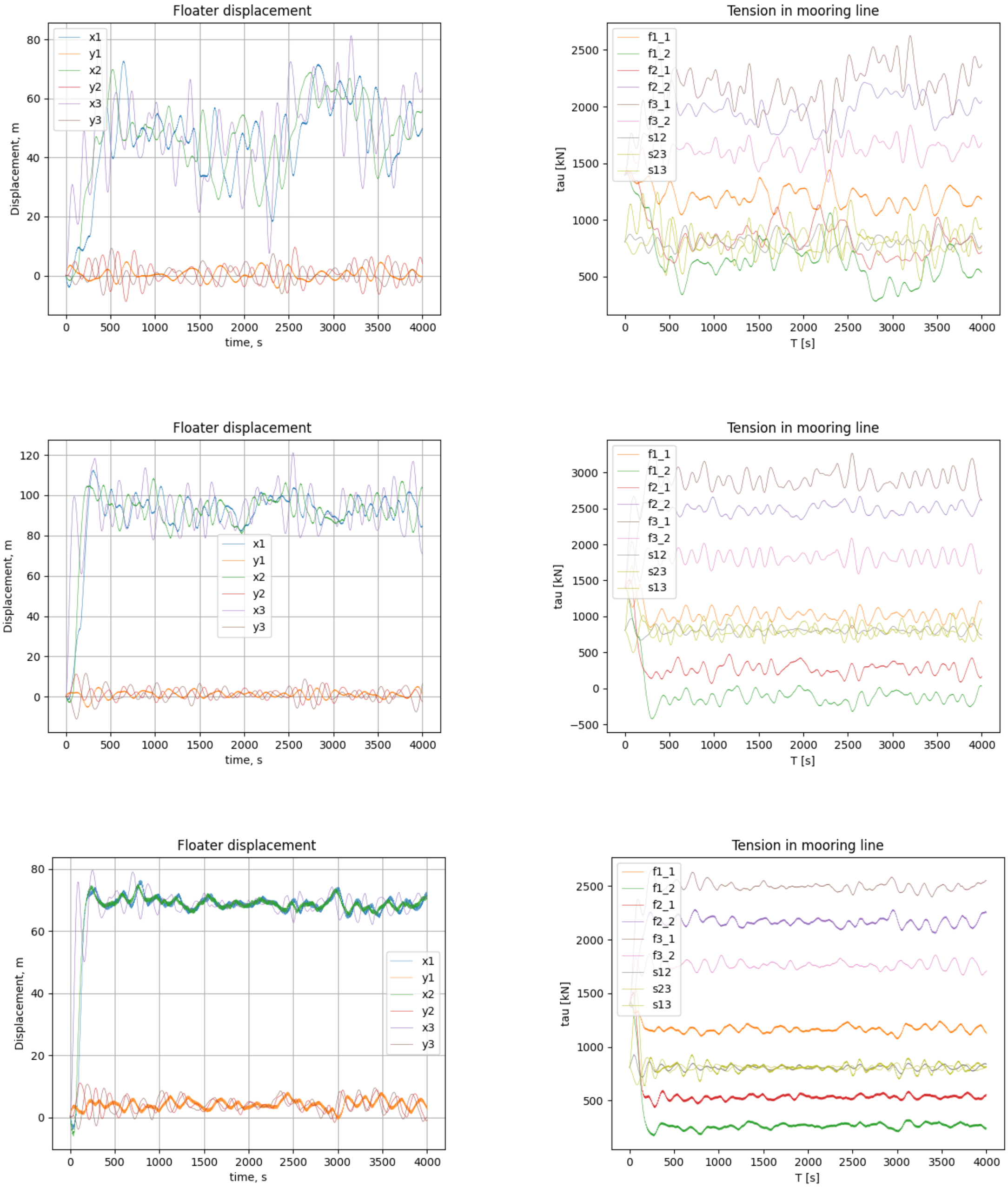

Figure 6.4.3: Simplified dynamic analysis with regular waves - model b).

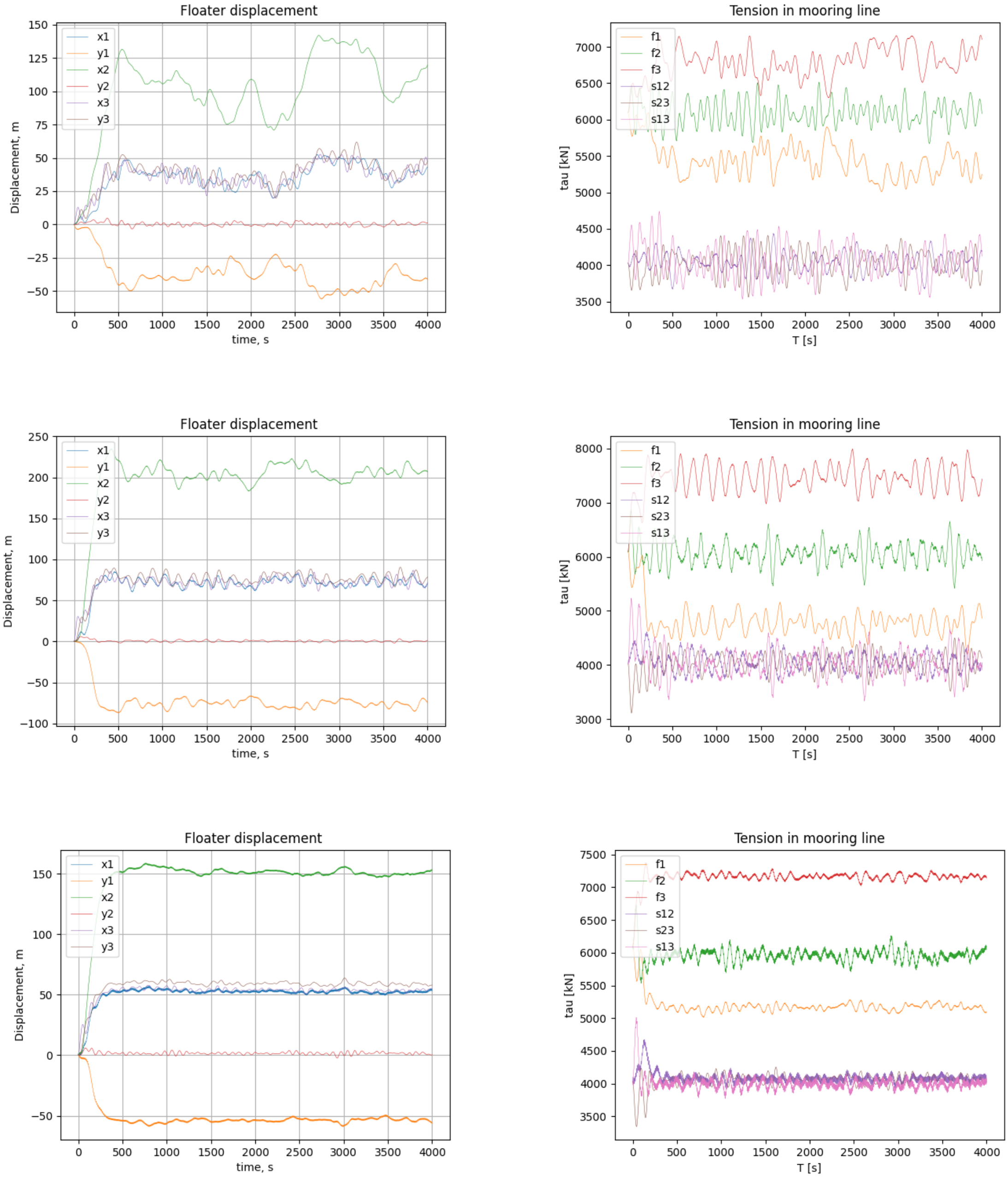

Figure 6.4.4: Simplified dynamic analysis with regular waves - model c).

The mean response is the same for system baseline, a) and b) as expected, as the systems have the same static response and turbulent wind time series. As the stiffness is linear, there is minimal difference between the floaters in the same system for both mean and standard deviation. The system behaves, therefore, more ideal as all the floaters dynamic performance is similar to each other. The standard deviation is larger for the linearized model then SIMA. For baseline system 12.5 m , 7 m and 2 m versus 9 m , 5 m and 2 m and 6 m , 11 m , 5 , versus 12.5 m , 7.5 m and 2.5 m for system a). The standard deviation is closer to each other for the baseline system than shared mooring. Since, the stiffness is not evenly distributed, upwind floater stabilizes the motions with its large tension in the anchored mooring line for large displacements. This is a positive effect with the nonlinear mooring system, but the consequence is that the upwind mooring line has a large tension in it.

Sway motions seem to be predicted realistically, as the mean and standard deviation are not far from SIMA calculations. The trends are the same for the linear system as SIMA. Standard deviation and mean value in sway increase with wind speed, and the upwind floater is more sensitive to sway motions as the downwind floater affects it.

The tension in the upwind and downwind mooring lines is underpredicted. The upwind mooring line tension is much closer to the tension in SIMA than downwind. As the motion is overpredicted for the baseline system, the tension in the downwind mooring is unrealistic low. Also, the shared mooring is underpredicted as it is around 2000 kN, and varies little with the environmental conditions.

The simplified dynamic analysis has a large standard deviation because the dynamics and environmental loads are calculated for the same time step. In SIMA the dynamic time step is chosen ten times larger than the environmental time step for turbulent wind to ensure a smooth dynamic analysis. Between the environmental time steps, SIMA linear interpolates between the external loads, causing a stable dynamic analysis.

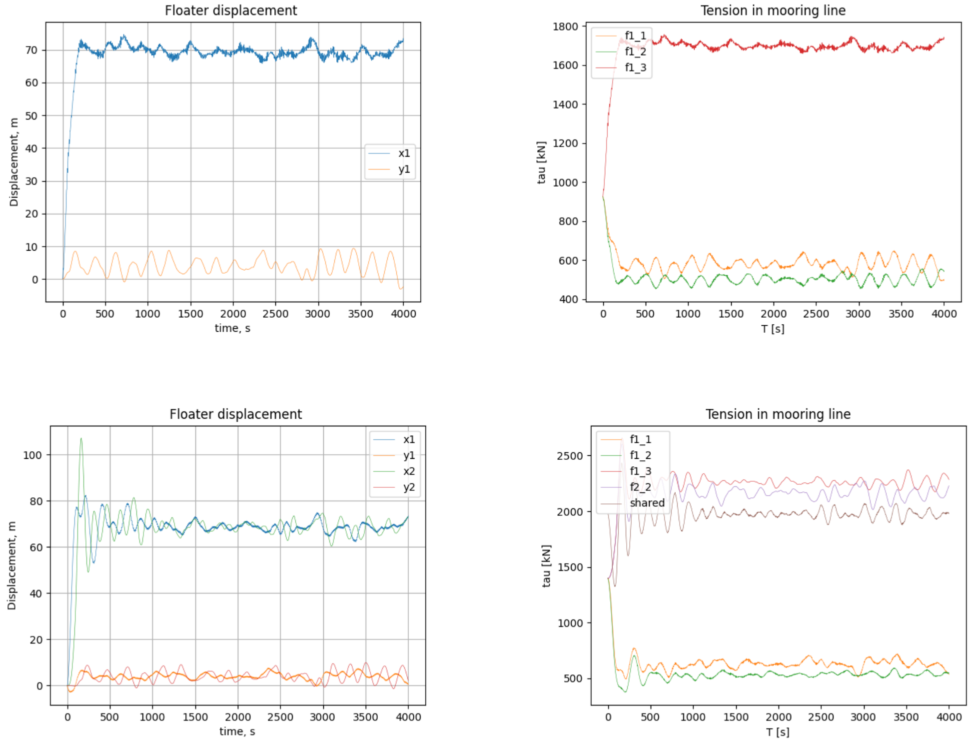

Figure 6.4.5: Simplified dynamic analysis - comparison of regular and irregular waves - model baseline and a)

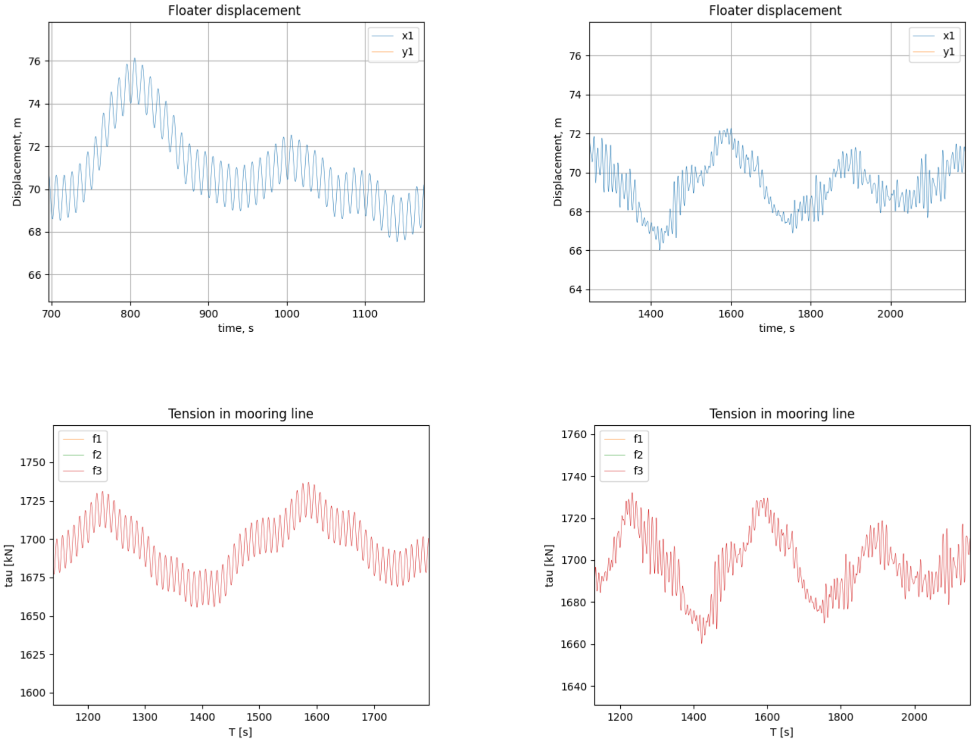

Figure 6.4.6: Simplified dynamic analysis - comparison of regular and irregular waves - model baseline - enlarged

Waves have little influence on a wind turbine's dynamics, but it has been observed in SIMA that the wave affects the maximum tension in the mooring line. As quasi-static mooring pregenerates the mooring tension and, thereby, shape, the mooring line is not dynamic as RIFLEX mooring. As the FEM mooring is calculated dynamically, mooring weight distribution and, thus, stiffness changes dynamically. As the linearized mooring line is only dependent on the floater motions, the effect of waves on the tension is little, as seen in Figure 6.4.6.

Therefore, using waves on a linearized mooring system is unnecessary, as the wind force will dominate the system dynamically if not wave resonance is a problem. Adding second-order drift force would have a larger effect on the system. A positive effect of using irregular waves is that the standard deviation is less in the surge motion.

Chapter 7

Comparison of shared mooring topologies influence on dynamic response study

7.1 Dynamic analysis of shared mooring topology

A comparison study of shared mooring topologies has been conducted to see how shared mooring affects floater dynamics as the global stiffness and mass matrix are changed. As previously shown, shared mooring introduces several new natural periods in the wind frequency, which can excite resonance modes. In Section 5.2, several of the natural periods are common for several of the systems, as the systems have been optimized with the same objective. Therefore, the same resonance modes are expected to be excited for several systems. Previous studies have indicated that thrust accumulation is a problem for shared mooring, but the studies were limited as all the floaters were inlined, and several of the floaters did not have anchored mooring lines. Wilson and Hall have shown, from their studies, that a softening effect is to be expected when the floater has no anchored mooring line. This is not a problem for the chosen topologies since all floaters have anchored mooring lines, but thrust accumulation could still be a problem in the dynamic analysis of shared mooring.

The fully aero-servo-hydro-elastic analysis could not be conducted as SIMA is not yet designed to handle complex shared mooring systems. The simulations would have been very computationally demanding as the wind files have to be seven times larger. SIMA has to run BEM analysis for three wind turbines, which is demanding. Therefore, the simplified force model has been used, as the results in Section 6.2 have been satisfactory.

The simplified model had, as previously mentioned, wrong sign in sway, but it is expected that this effect is negligible as the response in sway is large for system b) and c) in sway from the thrust force in x, and therefore y force is just a secondary force. If the mooring system had been linear, the response is positive and negative sway would be the same, as the stiffness would not have been affected. As the mooring topology is complex, the stiffness is not the same in positive and negative sway for large displacements, but previous results show that the y force is small. Nevertheless, yaw coupling with the thrust force is expected to influence systems b) and c), as the response is large in sway for linear response analysis. It is therefore expected that the thrust force decomposed in a sway contribution. As the stiffness is larger in sway for systems b) and c), the simplified force model would be conservative in the response, both for the mean and standard deviation.

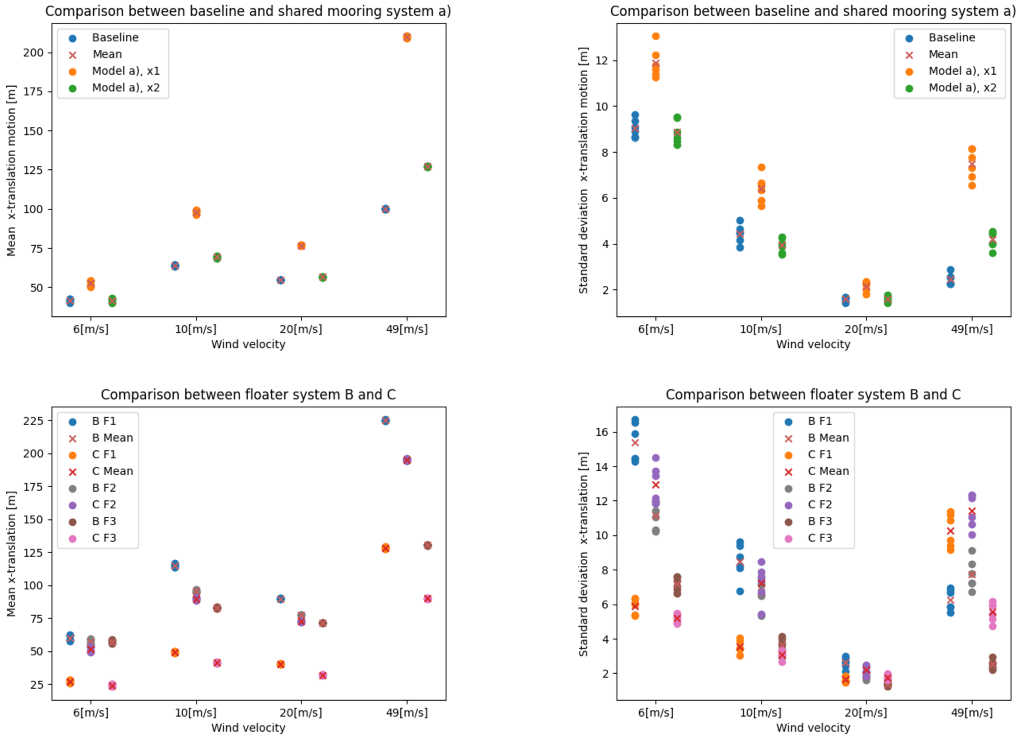

Figure 7.1.1: Comparison between shared mooring topology for - surge motion

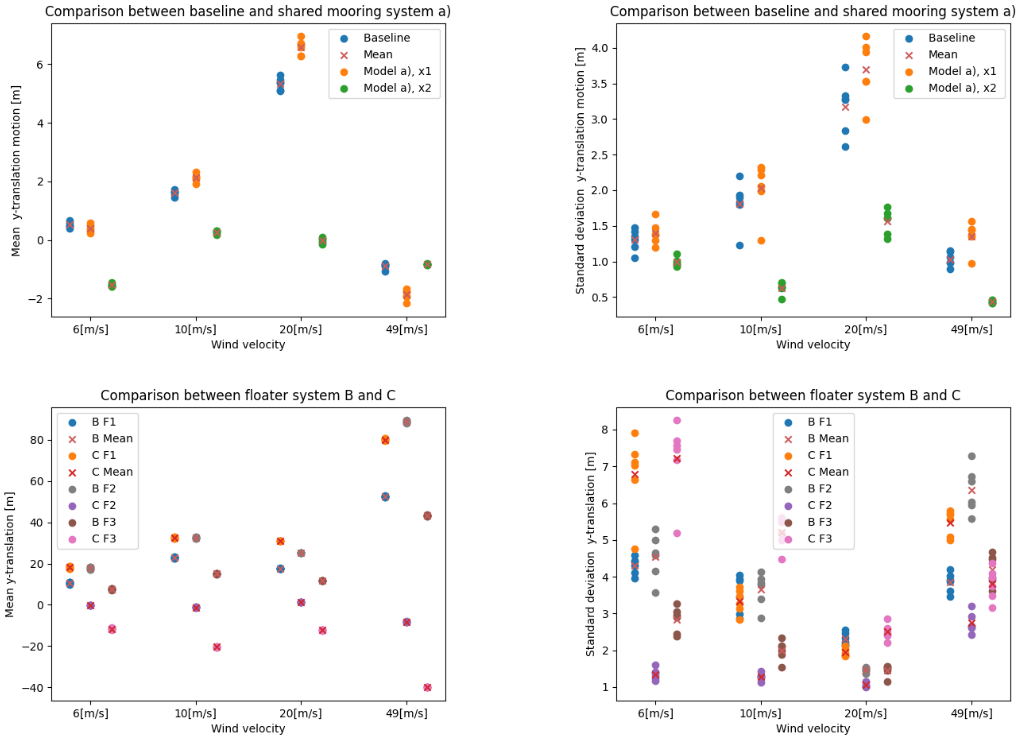

Figure 7.1.2: Comparison between shared mooring topology for - sway motion

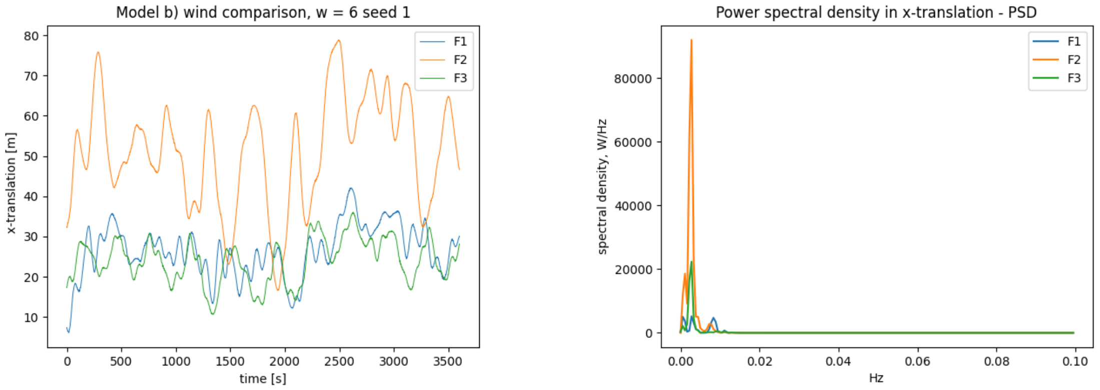

Figure 7.1.3: Time realization and spectral analysis for w = 6 [m/s], model b, peak frequencies = (x: 0.0011, 0.002775, 0.00833) [Hz]

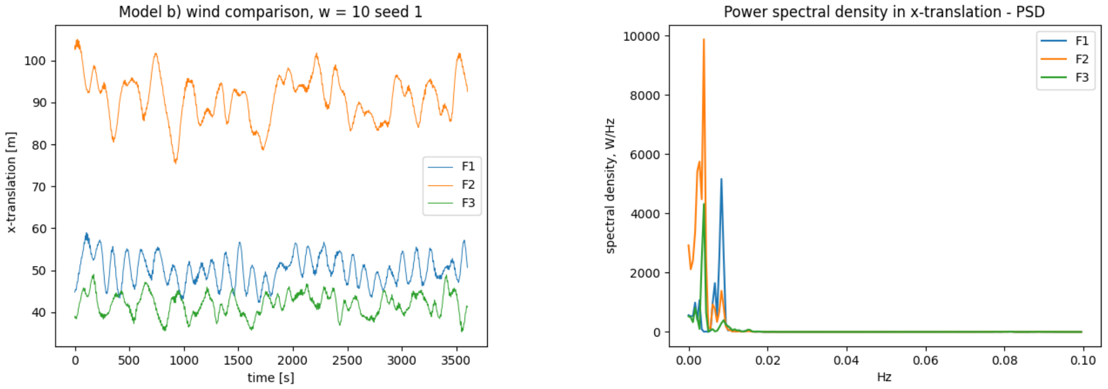

Figure 7.1.4: Time realization and spectral analysis for w = 10 [m/s], model b, peak frequencies = (x: 0.00388, 0.006667, 0.0083) [Hz]

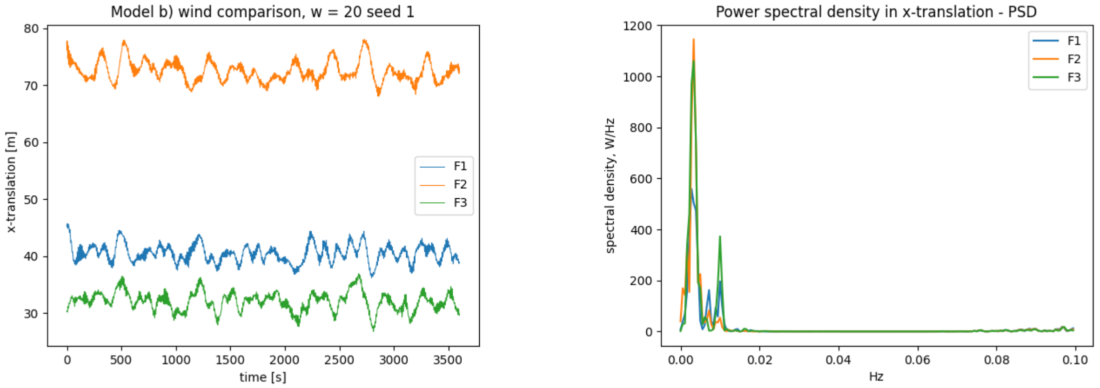

Figure 7.1.5: Time realization and spectral analysis for w = 20 [m/s], model b, peak frequencies = (x: 0.0033, 0.0072, 0.01) [Hz]

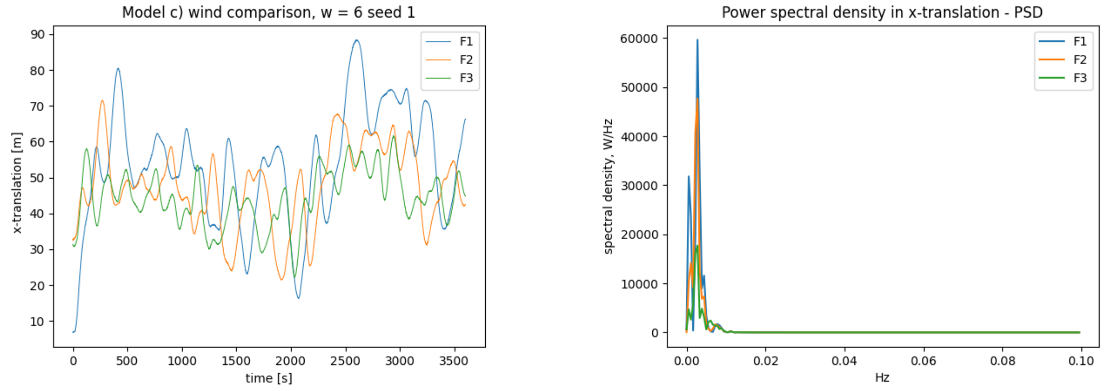

Figure 7.1.6: Time realization and spectral analysis for w = 6 [m/s], model c, peak frequencies = (x: 0.0055, 0.002778, 0.00444) [Hz]

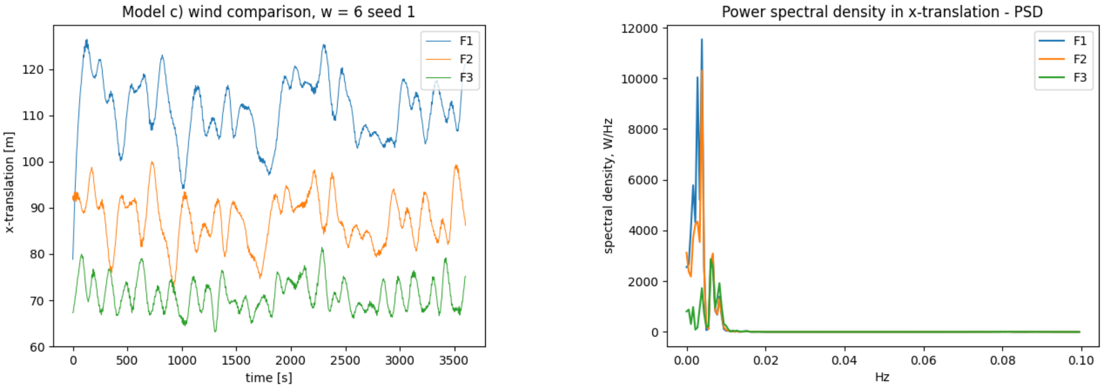

Figure 7.1.7: Time realization and spectral analysis for w = 10 [m/s], model c, peak frequencies = (x: 0.00166, 0.00388, 0.00667, 0.0083) [Hz]

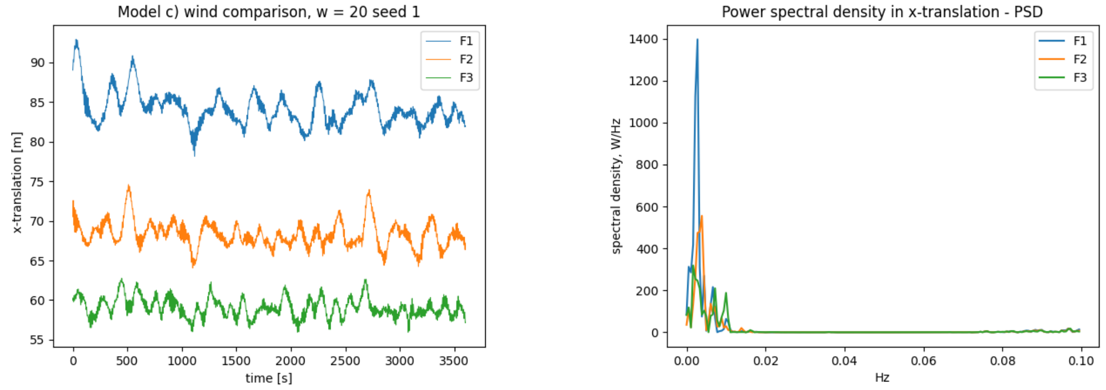

Figure 7.1.8: Time realization and spectral analysis for w = 20 [m/s], model c, peak frequencies = (x: 0.00667, 0.01) [Hz]

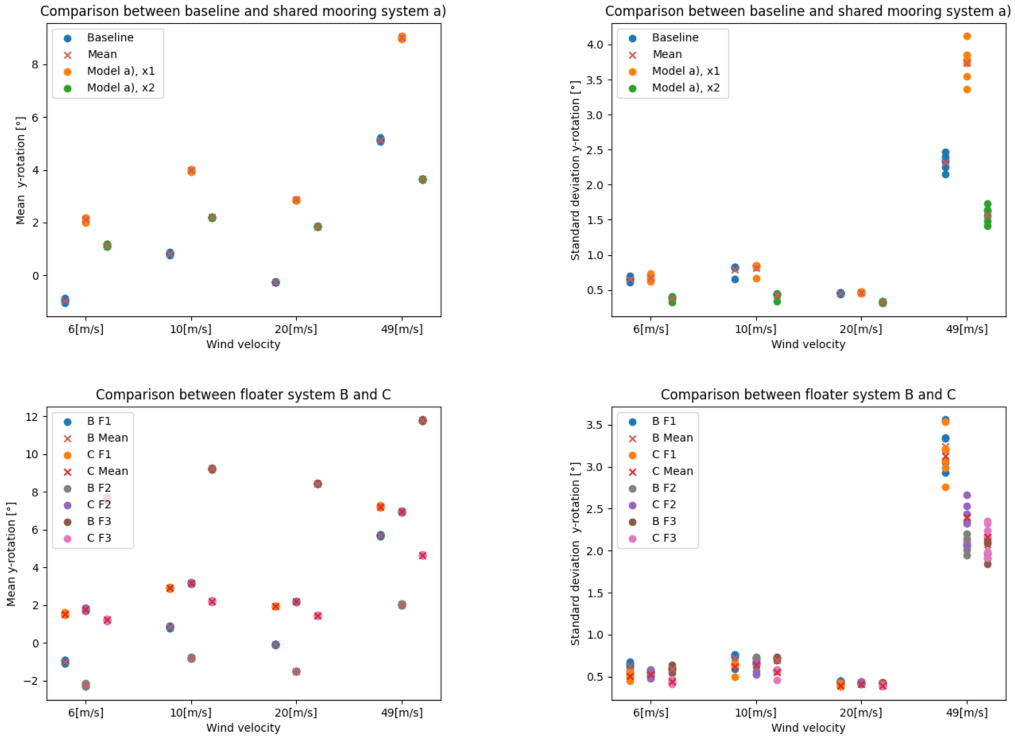

Figure 7.1.9: Comparison between shared mooring topology for - pitch motion.

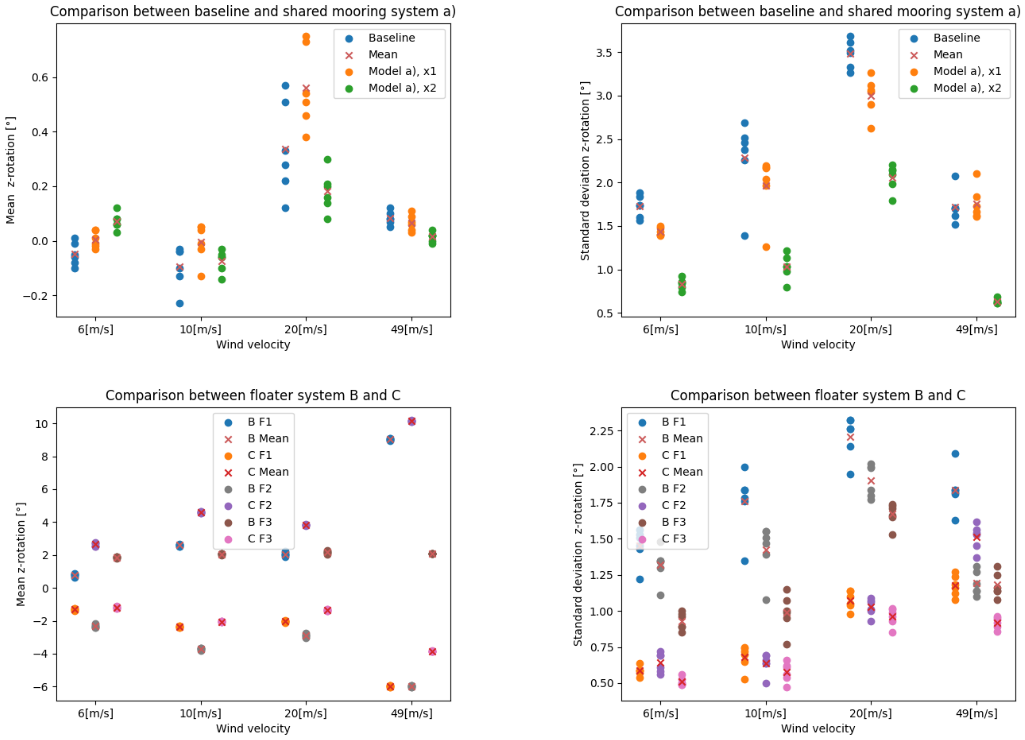

Figure 7.1.10: Comparison between shared mooring topology for - yaw motion.

In Figure 7.1.1 and 7.1.2, the standard deviation and mean translation in surge are compared for different mooring systems, where system baseline and a) - two floaters and b) and c) are shown together.
System a) has a larger response and standard deviation in floater one than the baseline system for all wind conditions. The response and standard deviation are expected larger for system a) floater one, as there is a large difference in the stiffness between the systems. Floater two response is unexpected as the stiffness between floaters one and two are almost equal. Therefore, the response is expected to be lesser for the baseline system, but the difference is negligible. Also, the standard deviation is lesser for under-rated wind speed. As the response is lesser than the static calculations for floater two, there are cancellation effects in the oscillation from floater one, and the dynamic load factor is less than one.

The systems behave very differently in the extreme wind condition. Even though the condition gives an unrealistic high response since the blades are not pitched and the drag coefficient is too large, it highlights a major difference between the anchored and shared mooring system. Since the wind turbine is shut down, the system has little dynamics since the wind force is only dependent on drag. This can be observed in Figure 7.1.1, where the standard deviation is almost the same for the extreme and almost rated wind speed.

The stable drag force seems to create a "thrust" accumulation effect in the shared mooring system. This is plausible as the standard deviation is larger for floater 2 in wind condition three than the baseline floater even though the stiffness difference should have been smaller, since the displacement is smaller for this condition. The same effect can be seen in systems b) and c).

Since both of the floaters are inline with each other, the forces from wind turbine one is transferred to the shared mooring system into the anchored mooring line. The shared mooring system is taut as the drag force is very large, making the floaters move together. Normally not all the thrust force from the floaters would be transferred into the anchored system due to dynamic cancellation effects.

The shared mooring configuration for system b) and c) are the same, except for the anchored mooring system. Due to the high symmetry configuration b) has little difference in the stiffness for zero degree inflow angle. This the opposite for configuration c), where floater 1 and 3 has a much higher stiffness than floater 2, where the wind direction is normal on its anchored mooring line. Therefore, floater two depends on floater one and three motions.

Floater two behaves dynamically quite similarly to each other for all conditions. The standard deviation is, as expected, lower for system b) as floater 2 has an upwind anchored mooring line for zero degree inflow angle, even though this difference is small.

Mean and the standard deviation is less for floater 1 and 3, as the stiffness is much higher for floater system c) as the upwind mooring line takes the most loading. Therefore, floater 1 gets a high stiffness due to the non-linearity in the mooring. Since floaters 1 and 3 are in line with the shared, the systems are highly coupled.

System b, two anchored mooring per floater, mean motions are very similar in the system, but the standard deviation for floater 3 is much lower than for the two other floaters. Since floater 3 is upwind, it is not dependent on the shared mooring stiffness and has two upwind anchored mooring lines. This makes the system much more stable. For wind condition 1, the mean response in the same for all the floaters. As the displacement is small enough, the system behaves linearly in surge.

System b) and c) behaves very differently in sway than baseline and system a), since the shared mooring lines are not in line with the thrust force. This effect can be observed in the linearized mooring model. The system behaves similarly to sway as in surge, but the response is less symmetric.

Several peak frequencies are the same for system baseline, a), b) and c), where some are close to the natural periods. Other frequencies could naturally come from the energy in the wind. 260 s has a large peak for both of the systems for several wind conditions. The period in response matches the natural period for both of the systems. As the periods in the spectrum are very long, and the time realization is short, the spectrum would be sensitive to small changes in periods.

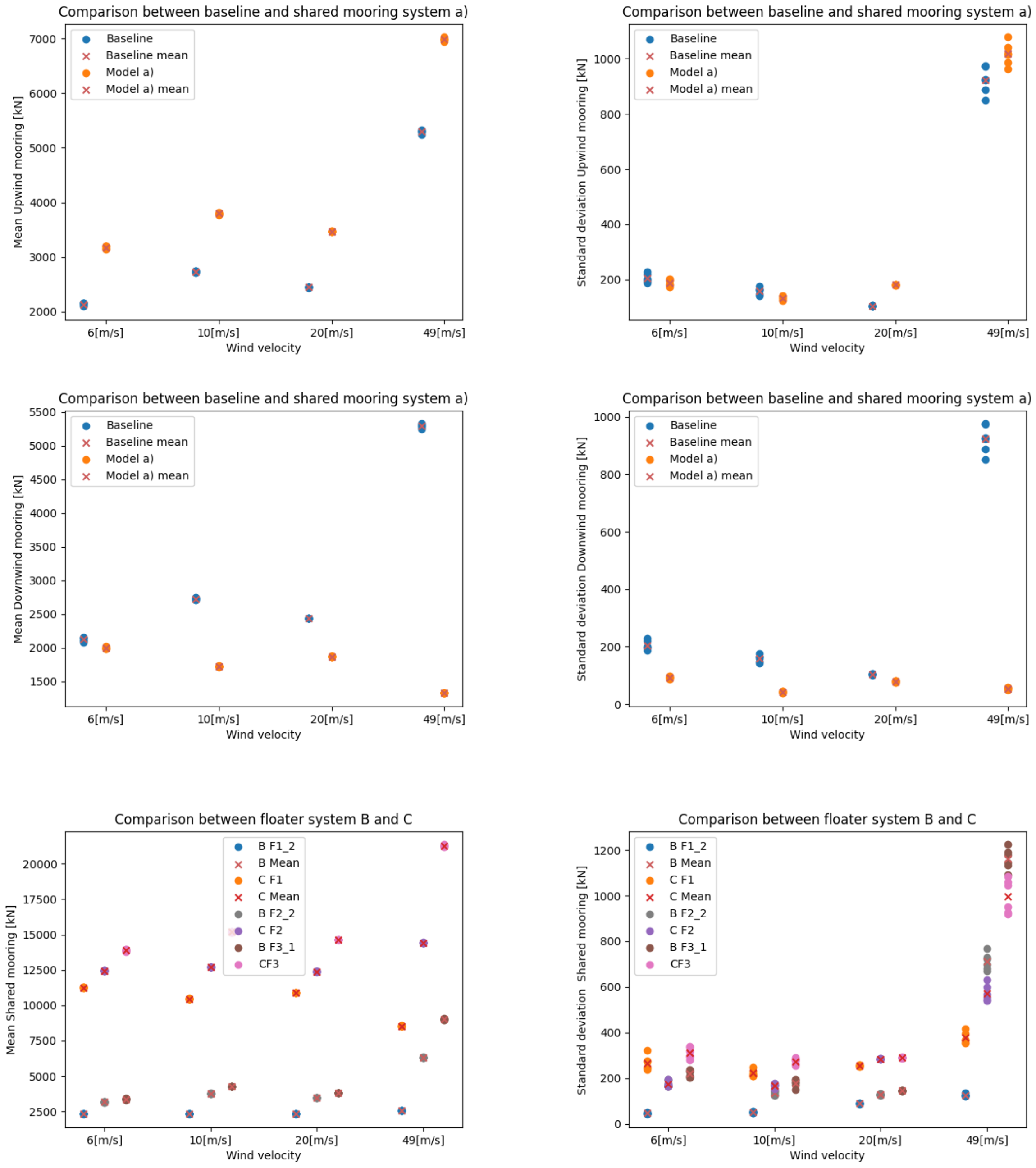

Figure 7.1.11: Comparison between shared mooring topology for - upwind and downwind mooring

The upwind mooring tension is larger for the system a) since the upwind mooring lines) have to carry the thrust load for both of the floaters. The tension in the mooring line will be dependent on the mooring line stiffness and the excursion of the systems. The mean tension difference between the system does not seem to change for different wind conditions, with the exception of extreme wind conditions. Since the shared mooring system has to carry twice the drag force as the drag force behaves less dynamically, the system will be more non-linear due to the large excursions, and the mooring line is heavier, creating more geometric stiffness. This gives a high standard deviation in the mooring tension even if the surge standard deviation is less than in other wind conditions.
The upwind mooring tension is lesser than the baseline for under-rated wind due to the mass cancellation effect, but not for over-rated wind speeds where the shared mooring line is tauter, and the systems move together, causing thrust accumulation.

Also, since the thrust force is larger and closer to the rated speed, the mooring line is more tensioned, making the floater more stable dynamically, and the standard deviation in the wind is relatively lesser for higher wind speeds. Therefore the system is more dynamic for lower wind speeds, as observed for the baseline system. This is not the case for the shared mooring line, where the standard deviation increases after the rated wind speed, even though the standard deviation for the surge is lesser. There could be several plausible explanations for this. This could be caused by the sway motions increasing the tension in the upwind mooring. The standard deviation is larger for shared mooring in sway than for the baseline due to the shared mooring. Also, when the system behaves less dynamically, the shared mooring line is tauter, making floater 1 and 2 more coupled together, making the mooring line more responsive for thrust in floater 1. The same effect can be observed for topology b) and c) and for extreme wind conditions.
The tension in upwind mooring in system b) is in large contrast to the anchored mooring in system c), where the pretension dominates the tension due to the large weight in the mooring lines. Therefore it is a small difference in tension between the upwind and downwind mooring. System b) has a more evenly distributed tension since the thrust load is distributed onto three mooring lines. Even though all three mooring lines have different orientations, the mean tension and standard deviation are close to evenly distributed due to the load transfer from the shared mooring. This is also observed in surge and sway, where the motions are almost the same.

The standard deviation for tension is high in system c), but the differences between the maximum standard deviation in system b) and c) are small. The difference gets larger for over-rated wind speeds. The dynamic tension is, therefore, relatively much lesser for system c). For wind condition 3, there is almost no difference in the dynamic tension between the upwind mooring lines for system b) and c).

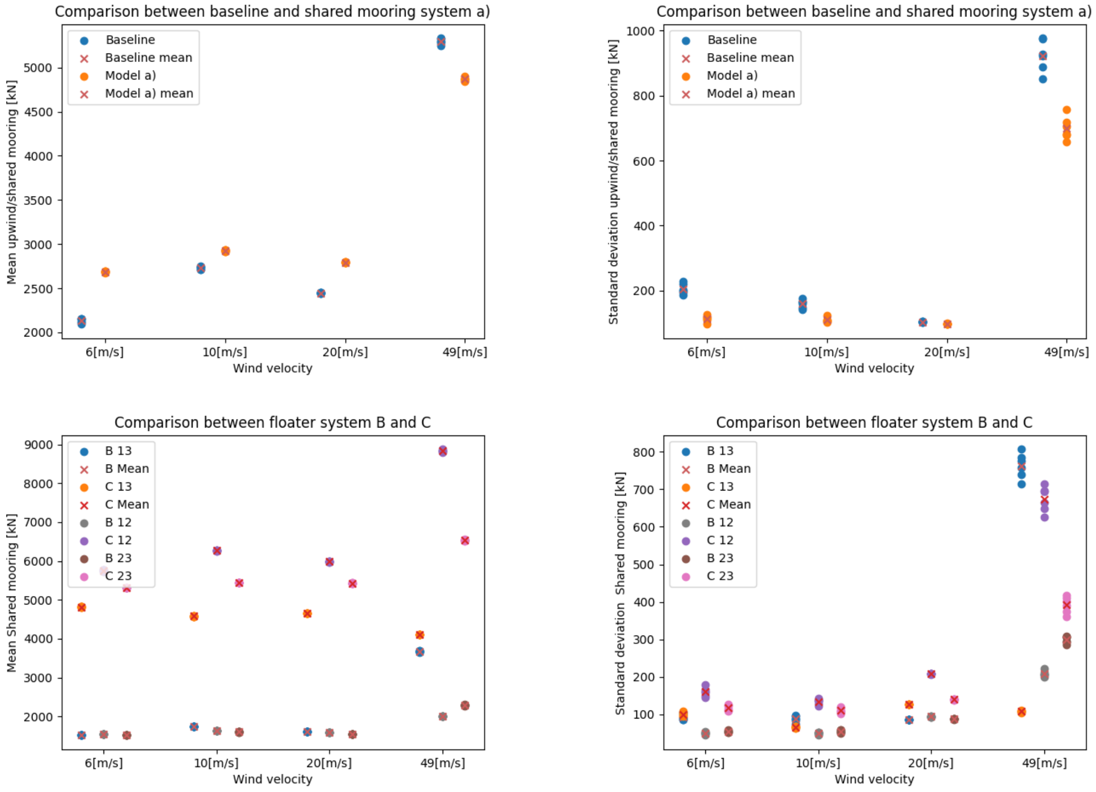

Figure 7.1.12: Comparison between shared mooring topology for - shared mooring

In Figure 7.1.12, shared mooring is compared to the upwind mooring line for the baseline system. The upwind mooring line is much lighter, with 116 kg/m compared to the shared mooring, with 176 kg/m. The systems have a large difference in the pretension. For under-rated wind speed, the standard deviation is smaller for the shared mooring since the pretension is larger making the mooring line more stiff. Also, the shared mooring has a more linear stiffness since the difference in extrusion is smaller, and the line has less nonlinearity since the shape is less catenary. The standard deviation for over-rated wind speed is almost the same for the systems.

The standard deviation in the shared mooring lines is very similar for the different wind conditions. The two-anchored mooring system has a more even-distributed stiffness; therefore, the response is more similar between the floaters. Therefore, there is little variation in the shared mooring tension. The largest mean shared mooring tension and the standard deviation is between floater 2 and 3. It is also here the extrusion is the largest.
The simplified force is imported as an external force in a global reference system, uncoupling the thrust force and the floater motion. The local reference system is possible to use in SIMA, but was not chosen since pitch and yaw could have been overestimated. A possible approach to evaluate the simplified model is by adding artificial yaw stiffness in the wind model and seeing if sway motions are the same for both models.

To correct the simplified model it could be an idea to separate the forces and moments into two different external file where moments are in the global reference system and the forces are local. Then thrust will be decomposed by yaw motions and correct the sway motion. Pitch moment can be neglected at the moment external force file since the thrust force will generate all the moment. The thrust force has to be placed in the hub height.

A problem with this is that drag force cannot be calculated with the thrust force since the drag force has a distribution over the entire tower. Drag force is only necessary to calculate for high wind speeds. If it is necessary, it is possible to only simulate the influence of drag force by either using constant wind or by using turbulent wind without wind turbine. Since the wind turbine is not in the model BEM calculations are not necessary, and would still save computational time. If constant wind are used, drag force can be pre calculated by hand or python, and its not necessary to use any wind field in SIMA. A problem with estimate the drag force on the tower in the simplified estimation and not add it to the external force is that reflex elements are necessary.

If tension in shared mooring is of interest, shared mooring would be modeled as Riflex elements. Therefore it is not a problem if the tower is also using reflex elements. If a SIMO model is wanted, quasi static mooring is highly efficient and accurate in shared mooring. Since it is not possible to model quasi-static mooring between floaters in SIMA, linear spring can be used. This will be a simplification which is conservative since the shared mooring is non-linear. It is observed in static calculations that shared mooring is not as non-linear as anchored mooring. This is probably something to expect as the shared mooring has a less catenary shape. Also, the relative extrusion is less. For this reason, the shared mooring line will behave more linear, meaning a linear spring could be a good approximation.

Therefore is it possible to simulate shared mooring system in SIMO if the simplified force model is used. SIMO is very fast in comparison to SIMA, and could be a natural first step in evaluating different topologies in shared mooring.

7.2 Cost study

Hall introduces a cost model for drag embedment anchors and mooring lines. The total cost will be wrong since the material cost has changed drastically the latest years, but it can be a good tool to evaluate if the shared mooring is economical due to the thrust accumulation effect. Also, all the systems are evaluated for wind and waves coming from the same inflow angle. Previous studies have shown that this assumption is not conservative for floating wind turbines. Nevertheless, the stiffness is very nonlinear due to the large extrusion causing large stiffness differences between the models. The baseline system will have the highest stiffness for 0° degrees inflow angle. For this system, the largest mooring tension would then be evaluated for waves and wind in the same direction. This is in large contrast with systems b) and c), where the largest extrusion is for 0 degrees inflow and, therefore, the lowest mooring tension. System a) will have the lowest extrusion for 0° degrees inflow angle.

$$A_{drag} = 100 N_a F_{a,max} + 5000 N_a [\$] \tag{7.2.1}$$

$$A_{vertical} = 120 N_a F_{a,max} + 8000 N_a [\$] \tag{7.2.2}$$

$$A_{suction} = 150 N_a F_{a,max} + 11000 N_a [\$] \tag{7.2.3}$$

$$M_{line} = 0.42 \sum_i T_{i,max} N_i L_i \tag{7.2.4}$$

Hall proposes three cost models based on the anchor type [36]. The necessary anchor type would depend on the soil, loading direction, and maximum load. As shared mooring reduces the total number of anchors, it is important that the relative cost between the material in the mooring line and the anchor is correct. Shared mooring would therefore be more economical when complex anchors are needed.

N_a is the total number of anchors, and N_i is mooring line number i, L_i length of mooring line i and $T_{i,max}$ is the maximum tension experienced for the mooring, and $F_{a,max}$ is the maximum anchor force. The cost is in 2013 [USD \$] dollar. [9] [36]

Mooring no	Seed no	Maximum tension [kN]	Mean tension [kN]
1	14	1874.37	1404
2	17	1685.95	1334
3	8	3549.23	2862
Max tension	8	3549.23	2862

Table 7.2.1: Maximum mooring tension for system baseline

Mooring no	Seed no	ULS standard [kN]
1	14	2350
2	17	2648
3	8	4923
Max tension	8	4923

Table 7.2.2: The maximum ULS loading in mooring lines for system baseline

Mooring no	Seed no	Maximum tension [kN]	Mean tension [kN]
shared	9	3381.22	2115
$F1_1$	2	2338.56	2006
$F1_2$	16	2373.98	1866
$F2_1$	8	4377.27	3793
$F2_2$	8	4671.3	3817
Max shared	9	3381.22	2115
Max anchor	8	4671.3	3817

Table 7.2.3: Maximum mooring tension for system a)

Mooring no	Seed no	ULS standard
shared - class 1	9	4605
shared - class 2	9	5398
$F1_1$	2	3190
$F1_2$	16	3315
$F2_1$	8	5953
$F2_2$	8	6457
This		
Max shared	s13	3190
Max anchor	$F2_2$	6457

Table 7.2.4: The maximum ULS loading in mooring lines for system a)

Mooring no	seed no	Maximum tension [kN]
s13	8	2200.01
s12	18	2135.01
s23	13	2070.52
$F1_1$	17	2949.62
$F1_2$	4	2419.04
$F2_1$	8	2000.01
$F2_2$	1	2325.11
$F3_1$	12	4949.71
$F3_2$	16	3402.79
Max shared	s13	2200.01
Max anchor	$F3_1$	4949.71

Table 7.2.5: Maximum mooring tension for system b)

Mooring no	seed no	Maximum tension [kN]
s13	8	3619
s12	14	3592
s23	13	3467
$F1_1$	4	3435
$F1_2$	17	4113
$F2_1$	1	3182
$F2_2$	8	5786
$F3_1$	12	7886.7
$F3_2$	16	5469
Max shared	s13	3619
Max anchor	$F3_1$	7886.7

Table 7.2.6: The maximum ULS loading in mooring lines for system b)

Mooring no	seed no	Maximum tension [kN]
s13	3	5193.71
s12	17	6850.27
s23	18	5983.72
F1	2	12248.82
F2	15	13506.04
F3	11	16166.65
Max shared	s12	6850.27
Max anchor	F3	16166.65

Table 7.2.7: Maximum mooring tension for system c)

Mooring no	seed no	Maximum tension [kN]
s13	3	8121
s12	18	10884
s23	17	9361
F1	2	19043
F2	15	21039
F3	11	24962
Max shared	s12	10884
Max anchor	F3	24962

Table 7.2.8: The maximum ULS loading in mooring lines for system c)

Maximum tension and ULS condition have been found in tables 7.2.2, 7.2.3, 7.2.5, 7.2.7, 7.2.4, and 7.2.6, and 7.2.8 for all the realizations for the respective system except for the extreme wind (since the blades are not pitched, the loads would have been overestimated). ULS has been calculated with safety factors from section 3.5.2. Most systems have several anchored mooring lines if one of the mooring lines breaks. Therefore safety class 1 has been used for most anchor mooring lines. Since the shared mooring lines are critical for the system stiffness, safety class 2 has been used, including the anchored mooring lines for system c).

The time realization with the maximum dynamic load will often be dimensioning for the system, but not always as seen in Tables 7.2.6 ,7.2.8 and 7.2.4 for shared mooring. For baseline, the maximum tension is dimensioning.

The dimensioning mooring lines: maximum anchored and shared mooring lines for all systems are dimensioned by the maximum mooring tension realization as it dominates the ULS.

It is important to check which condition has the largest ULS and not choose the condition with the maximum tension, as a combination of high mean and maximum load could be dimensioning for shared mooring systems.

The maximum tension in upwind mooring lines is found for wind condition two for all systems, but shared mooring is more complex as for system c) wind condition three is worse. For system b), the nondimensioning shared mooring lines also have the maximum in wind condition three. Wind condition 1 is the condition of least interest, but it creates the maximum tension for shared mooring line between floater one and three in system c).

	Baseline	a)	b)	c)
Anchored mooring lines [-]	3	4	6	3
shared mooring lines [-]	0	1	3	3
Floaters [-]	1	2	3	3
Shared mooring cost [M$]	0	2.43	4.73	14.74
Anchored mooring cost [M$]	8.09	14.19	22.55	36.82
Drag embedment [M$]	1.08	1.77	3.00	4.86
VLA [M$]	1.30	2.13	3.61	5.84
Suction pile [M$]	1.63	2.13	2.67	7.31
Cost pr floater - Drag [M$]	9.17	9.19	10.10	18.81
Cost pr floater - VLA[M$]	9.39	9.37	10.30	19.14
Cost pr floater - Suction [M$]	9.72	9.64	10.60	19.62

Table 7.2.9: System cost estimated by 2013 $ currency

system	w_t [kg/m]	w_p [kg/m]	D_p [mm]	Class	Proof load	ULS load
Baseline	116	114	70	R5	4723/ 4107	4923
System a)						
Anchor	175	175	87	R5	7037/ 6150	6457
Shared	176	175	87	R3	4734/ 3803	3190
System b)						
Anchor	175	175	87	R5	7037/ 6150	7886.7
Shared	101	100	66	R5	4223/ 3672	3619
System c)						
Anchor	875	873	194	R5	19294/ 16777	24962
shared	354	345	122	R5	9173/ 7977	10884

Table 7.2.10: Real mooring system

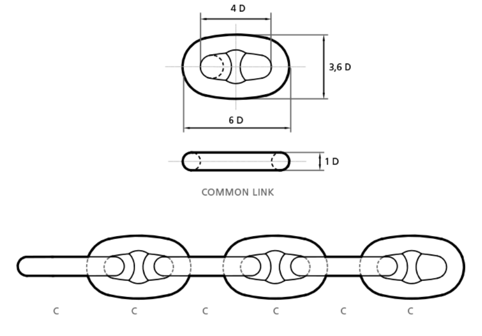

Figure 7.2.1: Stud link chain illustration from Sotra anchor and chain [37]

In Table 7.2.9, system cost has been calculated for three different anchor types. The maximum dynamic load for all realizations (except 50-year wind) has been used in anchor and mooring line cost calculations. Based on Connolly and Wilson's cost calculations for 600 m water depth, the cost per FOWT is expected to be between nine to ten million dollars, but their calculations are based on a 5 MW wind turbine with a maximum displacement of 20 m, quasi-static mooring, and steady load from the wind turbines rated thrust force. Even if the analysis is of different nature, the cost analysis is close to each other, see Table 7.2.2.
There are little differences in the cost for the system's baseline, a) and b). Since the mean loads are large for system c) both the mooring and anchor cost is higher. Nevertheless, the mooring systems need to be adequately optimized, as Wilson and Hall did not consider the nonlinearity. This assumption is suitable for a small response radius. It is important to optimize the shared mooring systems so that loads are more evenly distributed in the mooring lines. Thus, the maximum mooring tension would be smaller, and the shared mooring systems would be more economical, see Table 7.2.2.

Mooring dimensions were selected based on the mooring weight. As the mooring system is optimized to reduce the weight, and did not consider the static and dynamic loads, the dimension of the system is under-dimensioned as R5 chain is not enough. Normally wind turbines use offshore class R3 steel since R4 and R5 steel could struggle with fatigue as the MBL - mean breaking load is increased but not the fatigue lifetime. Table 7.2.1 provides both the proof load with and without material factor. As the normal operation of the FOWT is not a ULS condition, having a sufficient safety factor is important.

A mooring system with a weight larger than 610 kg/m was not specified in the tables to Sotra anchor and mooring [37]. Therefore weight was estimated for 875 kg/m mooring system. The area was estimated using an elliptic shape of the external and internal areas based on illustrations from Sotra anchor and chain approximating the internal height as the diameter as shown in Figure 7.2.1.

7.3 Marine operation

Simplified marine operations and reduction in material and anchor cost is the huge benefits with shared mooring. As shown by Wilson and Hall shared mooring reduces the weight of the total mooring system when the mooring system behaves linear and the total number of anchors is reduced. Some consequences that are not discussed is that in shared mooring, upwind mooring lines has to take up the global forces in the system. There are cancellation effects due to dynamics, meaning that the mean force are lesser then the static force. Therefore it is not a complete thrust accumulation for the upwind floater, but the mooring forces are larger.

When the loads are distributed on fewer anchors, each anchor has to carry more forces. Shared mooring will save operational cost in the installation of anchors, but if the anchor size has to increase since the forces are larger in the mooring system. Larger installation vessels and more material could be necessary. This would increase the cost per anchor. It is therefore an optimization problem if shared mooring could reduce the anchor cost.

A problem with shared mooring is the installation of the mooring lines. Fewer mooring lines and shared mooring lines that are installed near the water surface reduces the operation complexity, but since each floaters stiffness are dependent on each other, it is necessary to install the entire system as a whole. Even though the entire installation time is lesser, several floaters has to be installed at the same time, increasing the installation time per system. When the installation time increases there would be fewer available time slots where it is possible to install the system due to Hs and Tp restrictions on a system that is not completely installed.

This could be solved by using several installation vessels at the same time working together on a shared mooring system, but this could increase the cost for the project. If its not possible to install the entire shared mooring system in one period, anchored moorings could be installed and the shared mooring could be lowered to the seabed with a polyester rope in the end connected to a buoyancy element at the sea surface. The steel weight from the shared mooring on the seabed will have a catenary shape, giving the system geometric stiffness. Since the system does not have any anchors the end of the mooring will have zero pretension. In the next operation slot the next floater is installed and the shared mooring line is lifted up by the polyester line connected to the buoyancy element at the sea surface. Thereafter the polyester line is removed from from the line and the shared mooring is connected to the other floater.

Shared mooring line would probably be a combination between chain and rope / polyester with chain - rope - chain for shared mooring and anchored mooring. Chain is necessary at the start of the mooring line to submerge the line and get catenary shape and weight to the system, and chain is needed at the seabed to avoid wear on the rope and stopping the mooring line to be taut. Polyester or nylon is beneficial to use in mooring lines to save mooring line materials.

Chapter 8

Wind modelling study

8.1 Turbulence modelling

The wind is the most critical environmental load for a wind turbine since the thrust force introduces fatigue and the largest response in the mooring lines. Nevertheless, surge and sway resonance modes can be excited as the wind has longer periods than waves. Only second-order wave forces such as drift and difference-wave frequency can have periods larger than 100 s. Since the force is a second-order effect, the loads are smaller than the wind loads.

Few studies have been carried out where the synthetic turbulent wind has been compared to real wind data since wind is often measured at 10 or 15 m, whereas hub height for wind turbines is above 100 m. Both Kaimal and Mann uniform shear model has been compared/ fitted to real wind, but only for a restricted area. Therefore, it is important to investigate the difference between the turbulence models as it can affect the dynamic behavior of the FOWT.

Mann turbulence generator, Mann corrected, Turbsim (Kaimal), and LES (Large eddy-simulation) have been compared to each other for system a) - shared mooring system. To see how turbulence modeling affects the dynamic behavior of shared mooring systems. The main difference between FOWT and coupled FOWT (shared mooring) is that the wind will propagate from the upwind floater to the downwind. The wind turbines could therefore influence each other and the wind loading.

The turbulence models are compared to LES, which Adam Wise has generated, and it is the next to compare the data with as wind experiments are not available. It is therefore expected that the turbulence models shall fit the LES data. The wind files generated are adapted to LES statistic data for a good comparison. Mann turbulence generator is corrected as it often gives different statistical data than ordered.

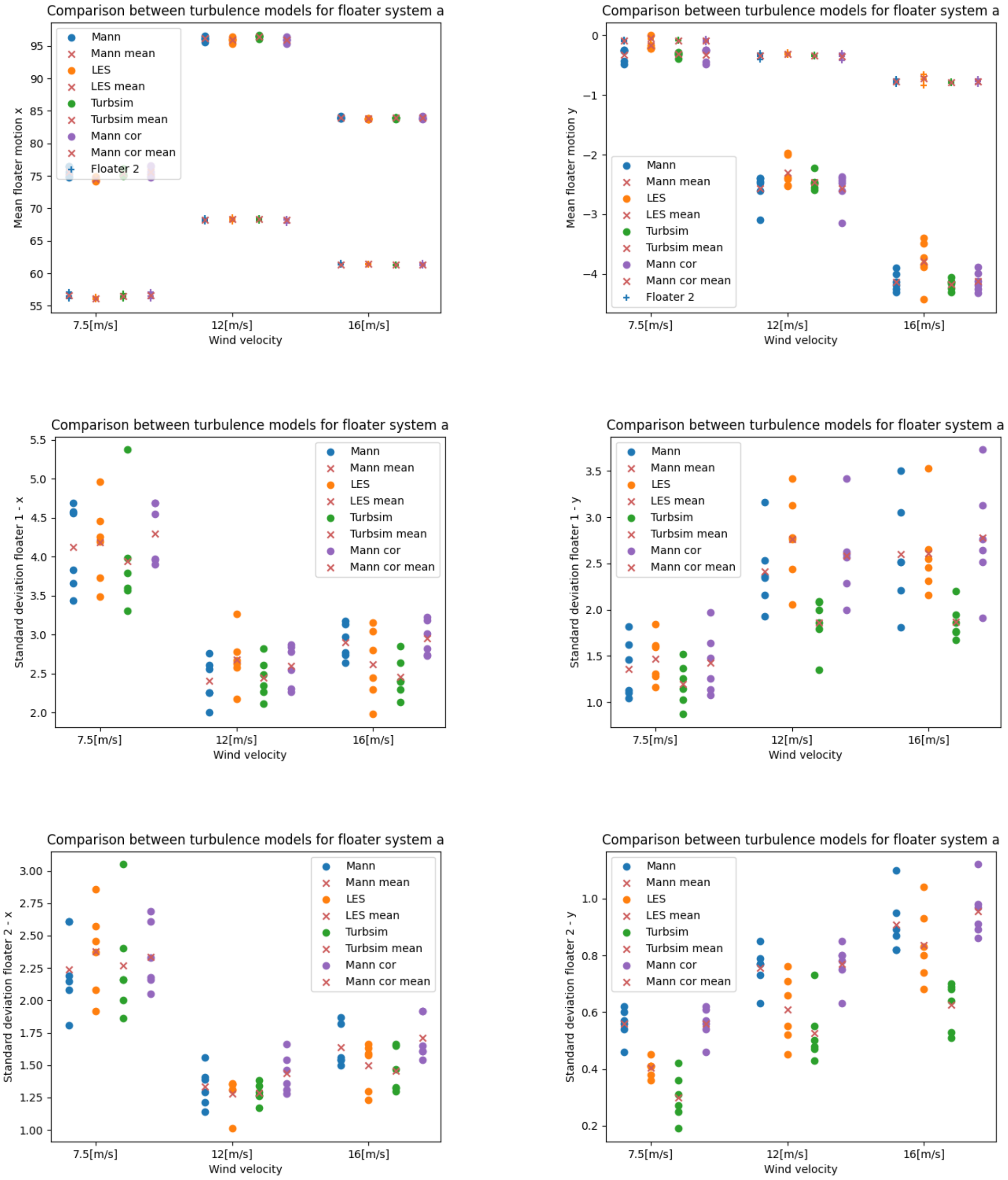

Figure 8.1.1: Comparison between turbulence models - translation

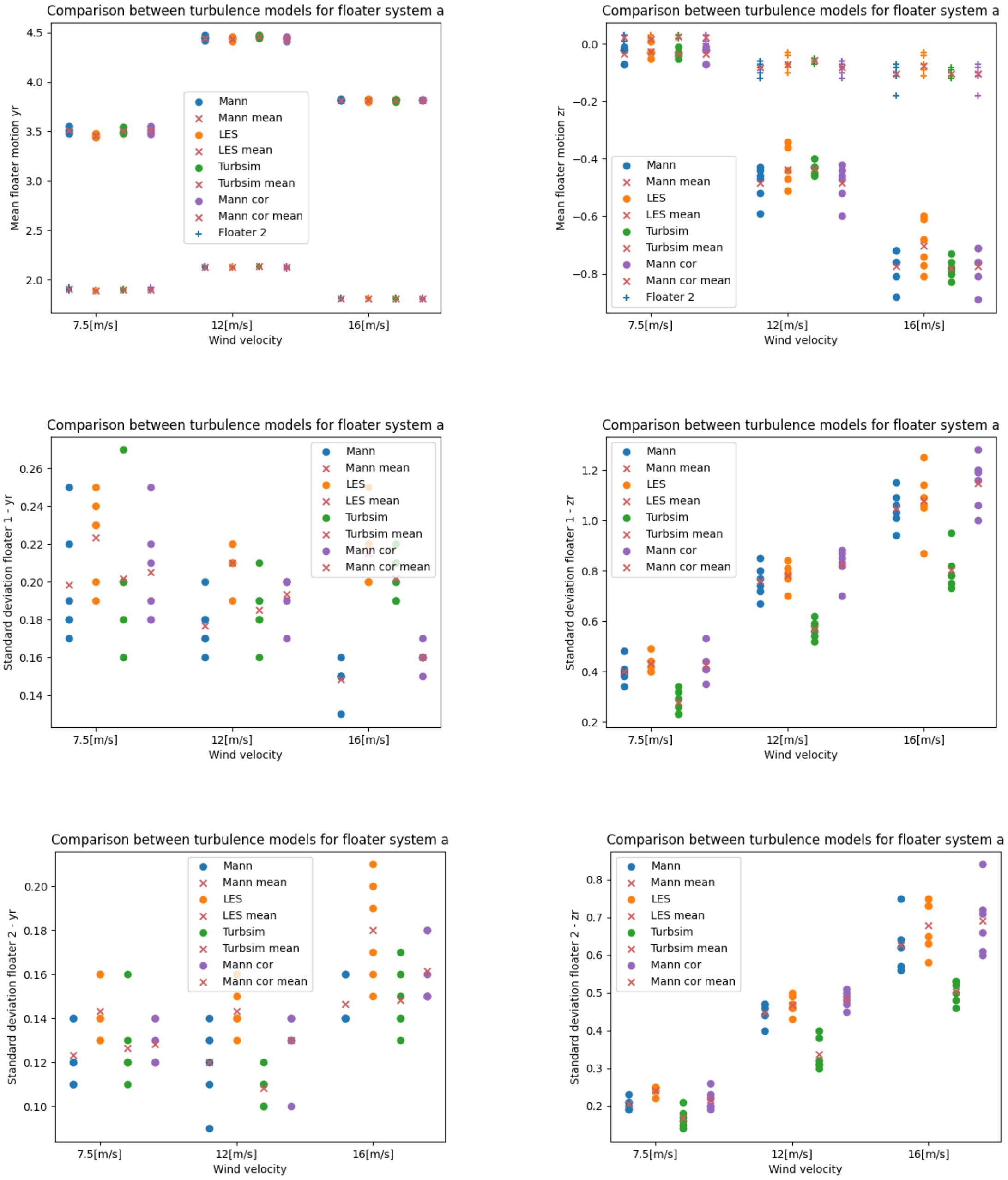

Figure 8.1.2: Comparison between turbulence models - rotation

	7.5 [m/s] s1	7.5 [m/s] s2	12 [m/s] s1	12 [m/s] s2	16 [m/s] s1	16 [m/s] s2
Mann-cor:						
Mean	7.4503	7.4951	11.982	11.832	15.844	15.851
Std	0.3027	0.28748	0.49169	0.53332	0.68797	0.66607
Mann:						
Mean	7.4466	7.4936	11.975	11.843	15.86	15.853
Std	0.26424	0.27443	0.42676	0.46359	0.59311	0.62654
Turbsim:						
Mean	7.4316	7.4699	11.939	11.935	15.976	15.913
Std	0.24651	0.25307	0.43069	0.4952	0.60659	0.56888
LES:						
Mean	7.384	7.443	11.924	11.894	15.888	15.797
Std-x	0.31623	0.29265	0.45473	0.54461	0.74589	0.72847
Std-y	0.29983	0.25206	0.47845	0.43681	0.70277	0.64295
Std-z	0.226916	0.21568	0.34626	0.33911	0.48418	0.45786

Table 8.1.1: Mean wind speed and standard deviation for seed 1 and 2 for different turbulence models

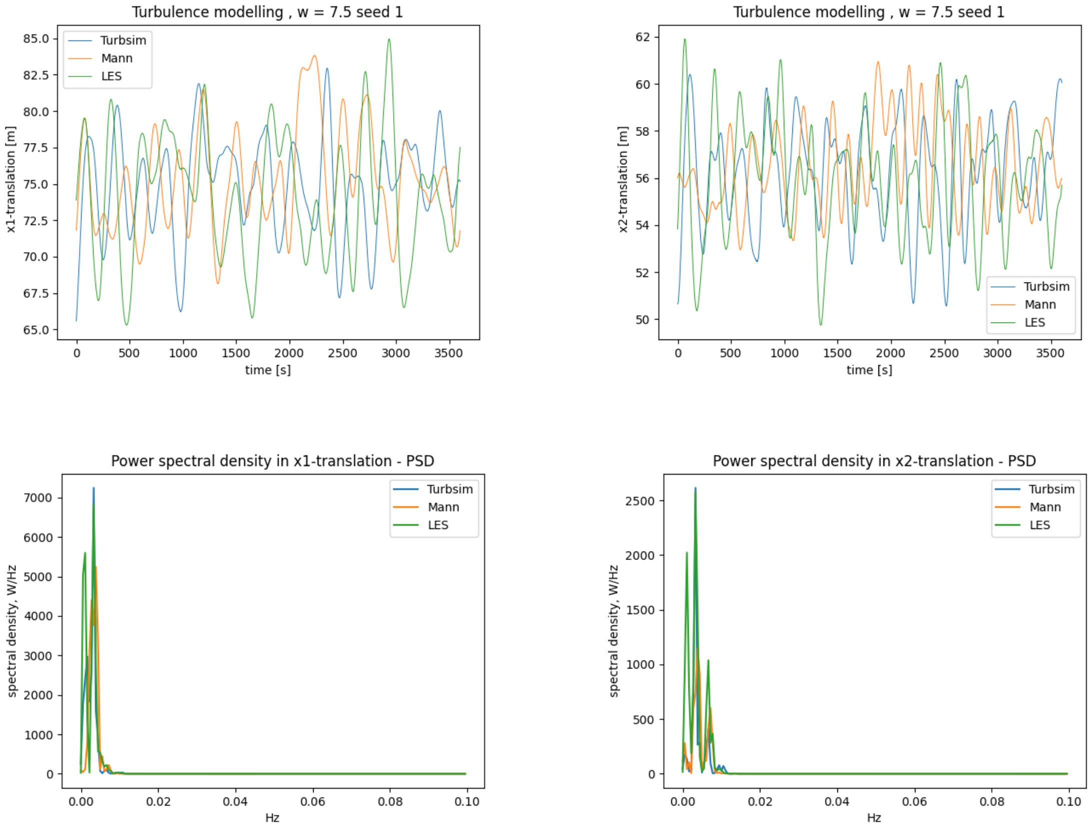

Figure 8.1.3: Time realization and spectral analysis for w = 7.5 [m/s] Turbulence modeling, peak frequencies = (x1: 0.0011, 0.00333) and (x2: 0.0011, 0.00333, 0.00666-0.0072) [Hz]

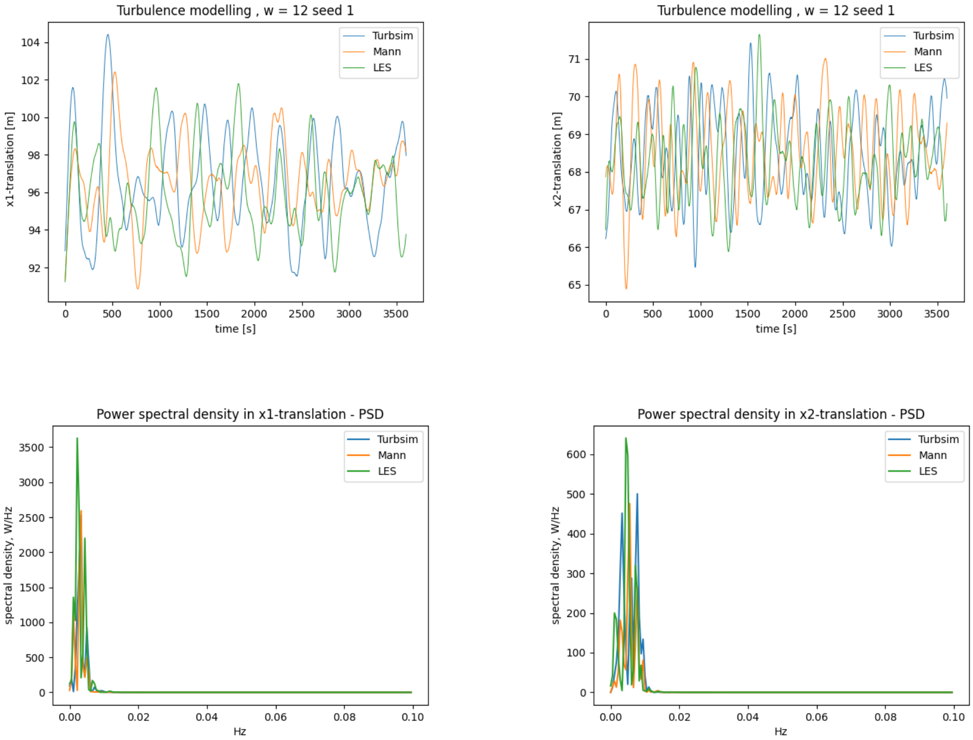

Figure 8.1.4: Time realization and spectral analysis for w = 12 [m/s] Turbulence modeling, peak frequencies = (x1: 0.0011, 0.00222, 0.00445) and (x2: 0.0011, 0.0049, 0.0078, 0.00945) [Hz]

the

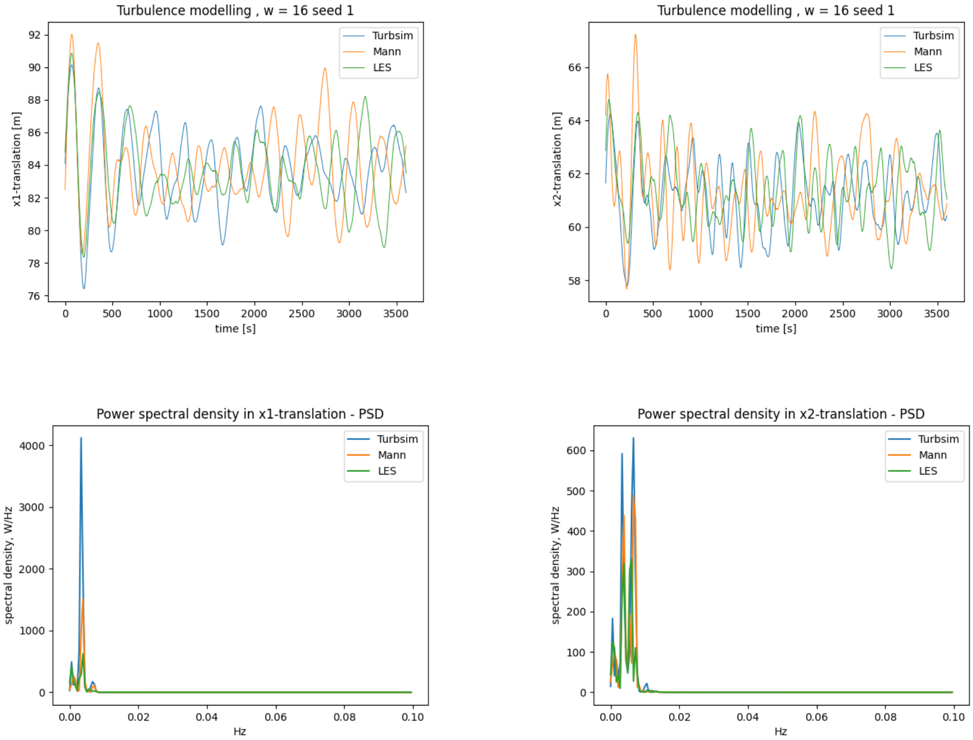

Figure 8.1.5: Time realization and spectral analysis for w = 16 [m/s] Turbulence modeling, peak frequencies = (x1/x2: 0.0005, 0.00333, 0.00667) [Hz]

Seeds one and two are shown in Table 8.1.1, with standard deviation and mean wind speed in x-direction/ surge. The statistical data should be the same for the corrected Mann turbulence generator and Turbsim as they are corrected to LES. As observed, corrected Mann underpredicts wind conditions 1 and 2 seed 2. Wind conditions 2 (seed 1) and 3, the standard deviation is far from LES. Mann not corrected standard deviation is consequently lower then LES, as expected. Therefore, some errors have happened in the corrected Mann simulation.Most probably a mix-up in the scaling in SIMA. It is expected that Turbsim should have the same turbulence intensity as ordered, but it is consequently lesser.

A possible explanation is that Turbsim chooses a lesser standard deviation close to the ordered turbulence. The deviation between the standard deviations would be negligible for larger turbulence intensities. If the turbulence intensity had followed the Normal turbulence model, the standard deviation would have been five times larger. Another assumption is that ordered turbulence intensity is not compatible with the settings in Turbsim. An underpredicted standard deviation will affect the standard deviation in the surge as the dynamics in thrust are underpredicted.

Mann and Kaimal turbulence model has the peaks located in the same place as LES, which is expected since they are resonance modes that are general for the system. There are large differences for some conditions in the peak amplitude, thereby, the energy in the resonance mode. In wind condtion 1, turbsim and LES is close to each other for the highest peak. Mann turbulence generator underpredicts the energy at this frequency. The lowest frequency is not observed for Turbsim and Mann. Since, the period is 909 s which is not close to any natural periods, it is likely only a long wind component in the wind. As the time series is short, much of the energy gets concentrated at this frequency. The period is very long, meaning it is unrealistic that it gets statistically generated in Turbsim and Mann.

The peaks are also underestimated for wind condition two for the largest peaks. Wind condition three stands out as both Turbsim and Mann overpredict the peaks for both seeds at periods 150 s, 300 s, and 2000 s.

The standard deviation in the surge is about twice as large for floater 1 compared to floater 2 as observed from previous analysis. There are few differences between the standard deviation for LES, Kaimal and Mann turbulence generator. Kaimal model seems to underestimate the dynamics in the system, since the standard deviation is always lesser than LES. This is correct as the gotten standard deviation is lesser for Turbsim than LES. For w = 7.5 Kaimal has one seed that is an outliner, increasing the average. This could indicate that Turbsim triggers resonance or that the wind standard deviation matches better LES for this condition.

Mann turbulence generator is conservative for wind conditions 1, 2 and 3, with and without correction. It is observed in Table 8.1.1 that the corrected standard deviation is too large for seed 1 for condition 2. Since, the standard deviation is lesser in the wind speed for not corrected Mann, and the standard deviation is larger in the response, the main difference must be the coherence in the wind.

Bachynski-Polić and Eliassen found that the Kaimal model estimates higher responses for low wind frequencies and lower responses for high frequencies in surge compared to the Mann turbulence model. Meaning Turbsim shall be larger than Mann when comparing surge motions.

There could be several reasons why the results were different. Bachynski-Polić and Eliassen use wind speeds off 8, 14 and 20 [m/s] and are using reference B for turbulence intensity factor, $I_{ref} = 0.14$ compared to 0.04 in the LES files. The IEC standard then calculates the standard deviation in the wind field. $\sigma = I_{ref}(0.75U_{hub} + b)$ where b is 5.6 [m/s]. This gives that the standard deviation in σ_u is 1.624, 2.254 and 2.884 compared to LES data which is 0.3, 0.48 and 0.64, assuming the TI is constant 0.04.

The turbulence in the wind field is, therefore, fundamentally different. The second and most likely argument is that Turbsim is underpredicted as the standard deviation in the wind is also underpredicted. Therefore, it is difficult to know if the system would have followed the same trend as observed for Bachynski-Polić and Eliassen.

Sway has the same overall trend as surge, where the Kaimal specter underestimates sway motions, and Mann turbulence generator can both under-predict and over-predict the answers. Both Kaimal and Mann follow the standards for turbulence intensity. See equation 3.3.4 and 3.3.5. For LES the wind is as turbulent in u and v, and therefore does not follow the standard.

Sway follows a global trend where the standard deviation in sway increases for higher wind speed. Since the turbulence intensity is approximately the same for all the wind conditions, the standard deviation in v is larger for higher wind speeds.

The mean sway translation gets more negative for floater 1 for increased wind speed. The difference is quite drastic between wind conditions 7.5 and 12 [m/s] where the sway is about zero to -2.5. In rated speed, the blades are very pitched to decrease the lift force, causing less thrust and aerodynamic loads. This causes a larger drag force which is normal to lift. Since lift force contributes to a thrust force in x-direction, drag force will generate a sway force.

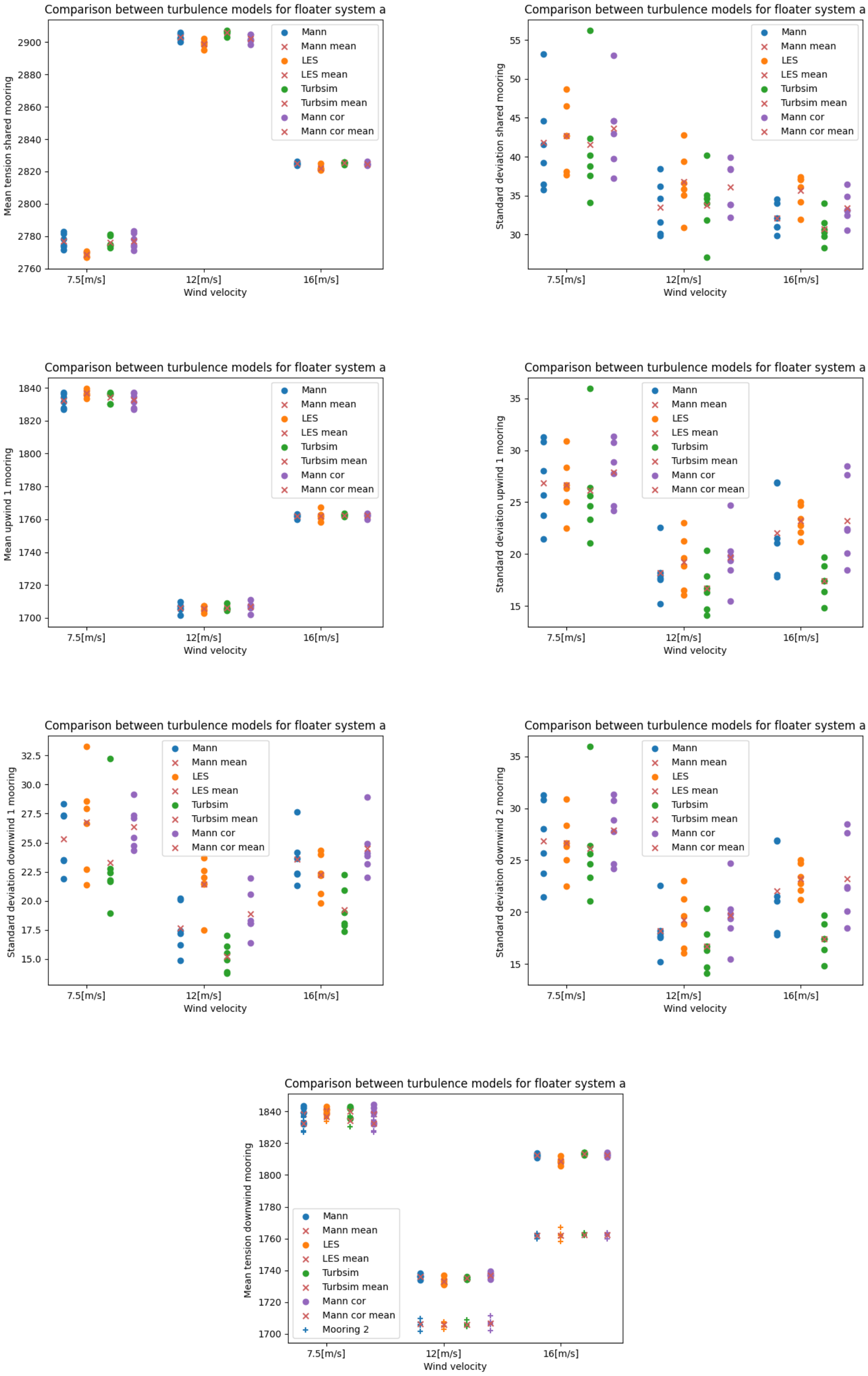

Figure 8.1.6: Comparison between turbulence models - mooring

8.2 Frozen turbulence assumption

Frozen turbulence assumption importance has been tested by approximating the wind thrust as a simplified force. The LES files have been discretized into 6 seeds by dividing the space in the y-axis. Time series are then generated by extracting wind data from hub height from the position of the two wind turbines. The wind fields were generated in Turbsim format, and therefore possible to read in SIMA. Wind with frozen turbulence is possible to run in SIMA, but for comparison, it's important that both frozen and real turbulence is run in the same way, avoiding differences by the simplified model. The real turbulence cannot be run as it is only possible to run one turbulence field at a time. The simplified model is used with linearised damping in surge and pitch. For wind speeds with missing linearized damping, such as $w = 7.5$, linear interpolation approximates the damping. Linear damping has been used to get as close to real turbine dynamics as possible. Without aerodynamic damping, resonance responses would have dominated the system, as the hydrodynamic damping is zero for long periods, causing a large fictive difference between frozen and real turbulence.

A problem with using linear damping is that the controller is not included in the analysis, which is important for damping. Linear damping is overestimated for low frequencies (0.05 Hz) and the opposite for high frequencies. Since surge and sway motions are of relevance in a mooring system, the resonances of interest are underpredicted. Other resonance modes, such as tower bending, would be overestimated.

The frozen turbulence assumption is evaluated in the downwind floater, as the turbulent wind is the same for the upwind floater. Also, the floater one's stiffness is softer and behaves more linearly compared to the upstream floater.

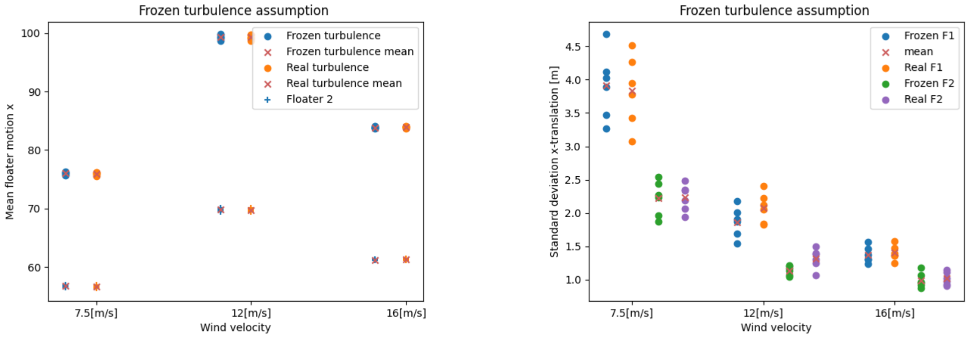

Figure 8.2.1: Comparison between real and frozen turbulence in x-translation

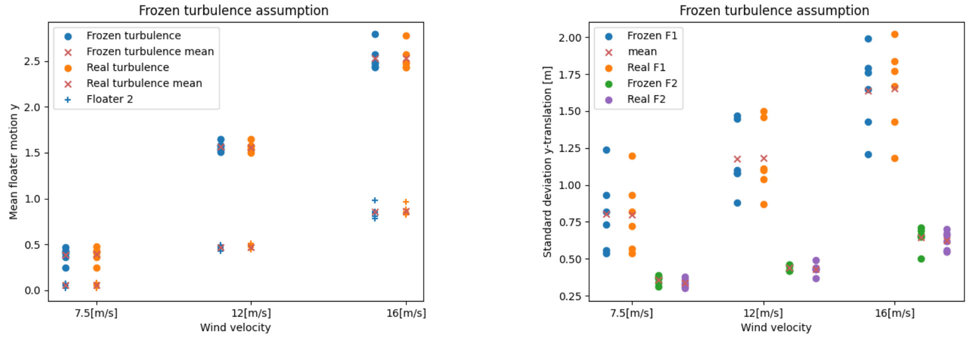

Figure 8.2.2: Comparison between real and frozen turbulence in y-translation

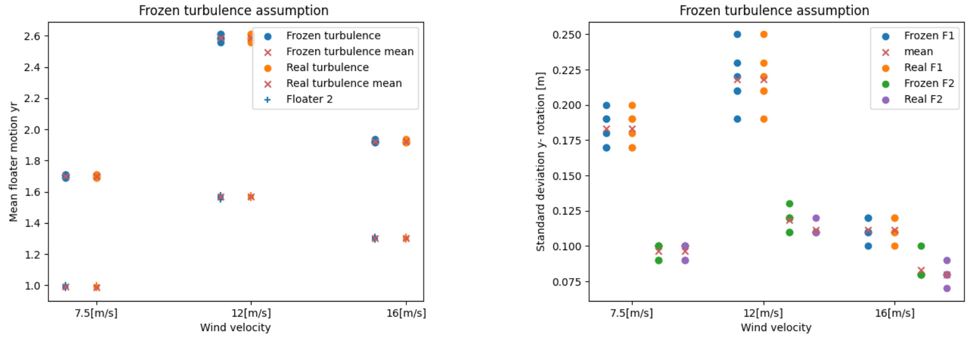

Figure 8.2.3: Comparison between real and frozen turbulence in y-rotation

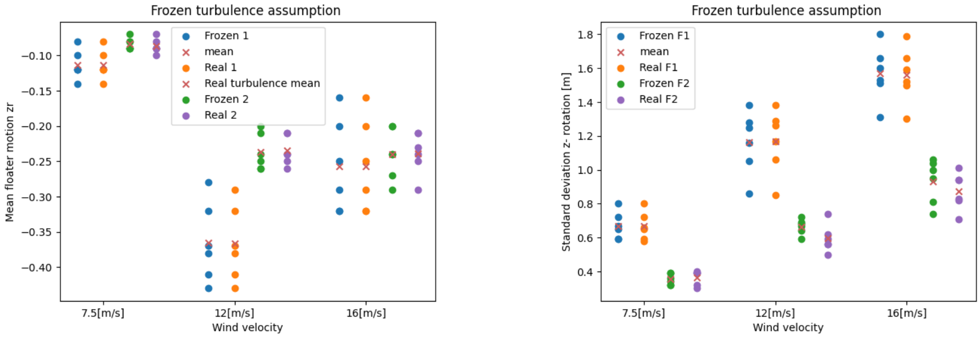

Figure 8.2.4: Comparison between real and frozen turbulence in z-rotation

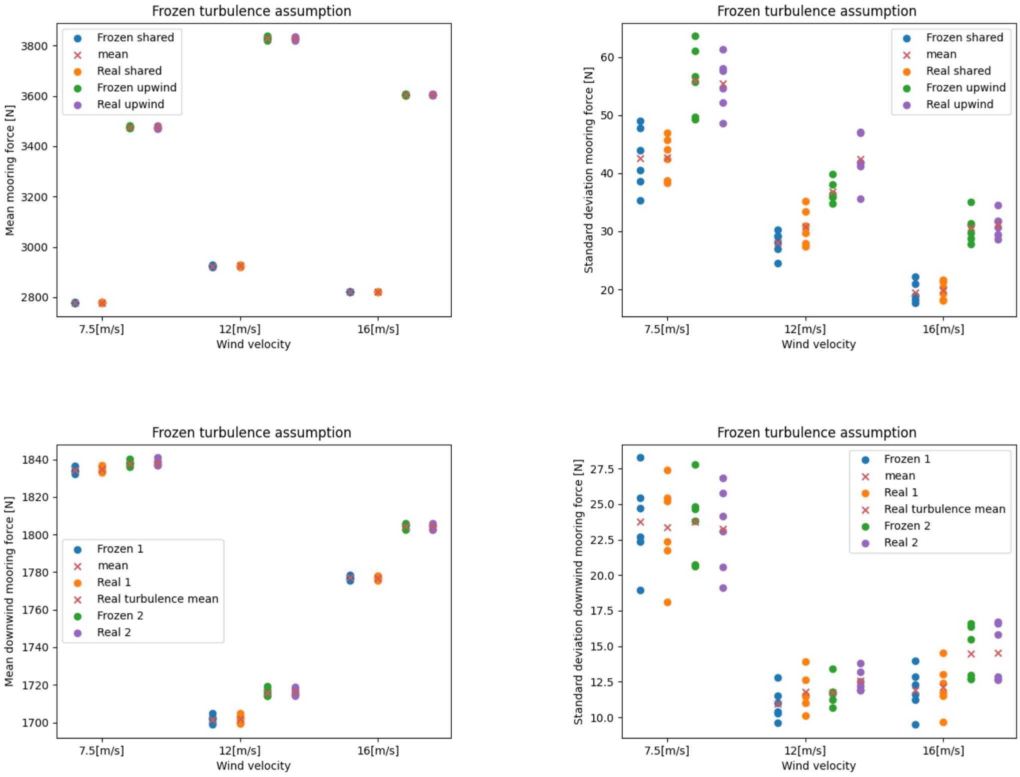

Figure 8.2.5: Comparison between frozen turbulence assumption and real turbulence - mooring.

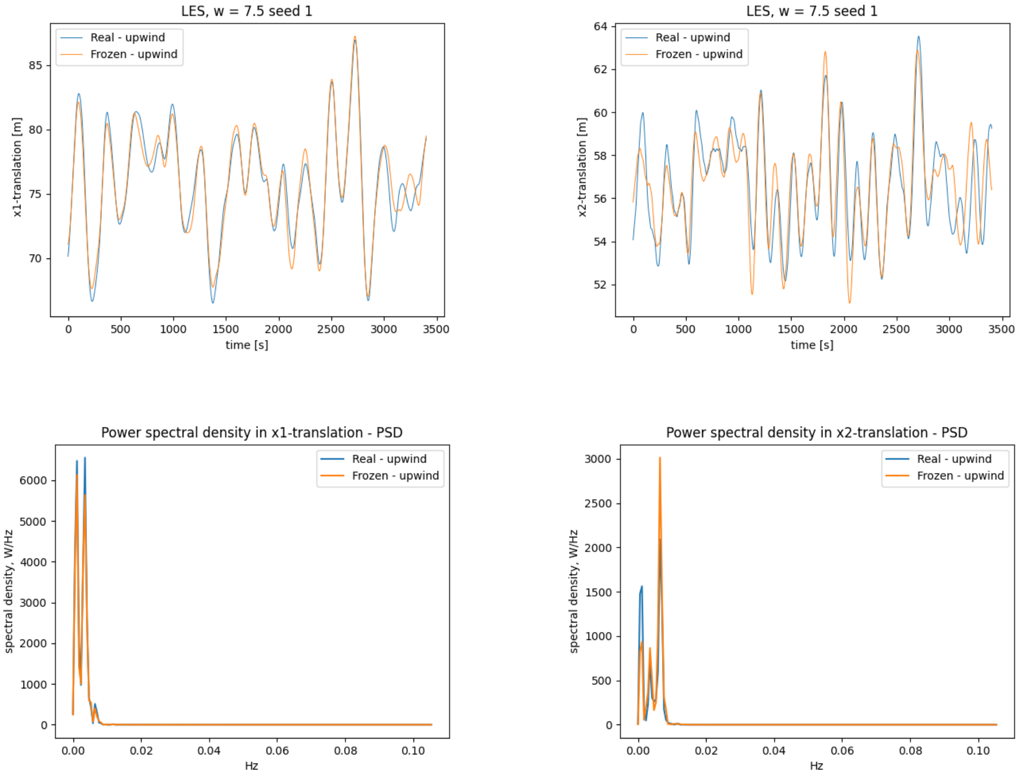

Figure 8.2.6: Time realization and spectral analysis for w = 7.5 [m/s] LES, peak frequencies = (0.001176, 0.003529, 0.0065) [Hz]

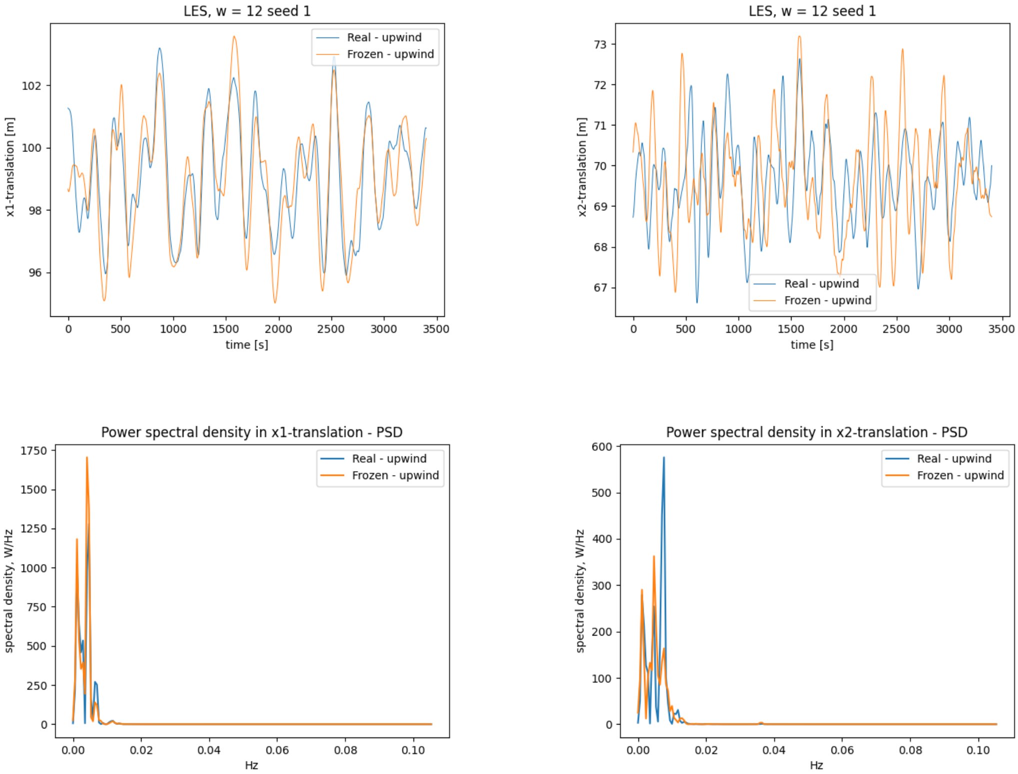

Figure 8.2.7: Time realization and spectral analysis for w = 12 [m/s] LES, peak frequencies = (x1: 0.00115, 0.004118, 0.00645) and (x2: 0.00117, 0.0047, 0.00765) [Hz]

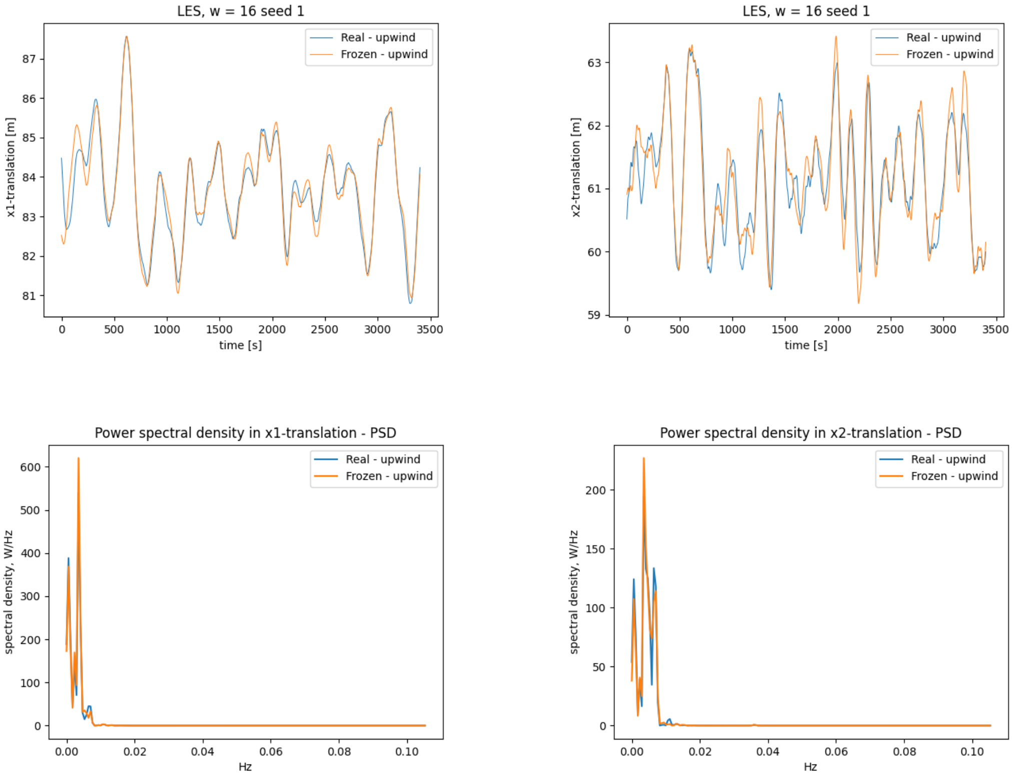

Figure 8.2.8: Time realization and spectral analysis for w = 16 [m/s] LES, peak frequencies = (x1: 0.00058853, 0.00353, 0.00645) [Hz]

The standard deviation in x-translation is more clustered for the frozen turbulence assumption, whereas the real turbulence is more evenly spread out for wind condition one. The difference is small for floater two since the turbulent wind is the same in both analyses. The small difference is only caused by the motions in floater one. Also, for floater two, the standard deviation is more evenly spread out, whereas the frozen turbulence is clustered in three groups. For floater one, the standard deviation is lesser for five out of six seeds for the frozen Turbulence 8.2.1. As the frozen turbulence is more clustered together, the real turbulence may excite more resonance. Spectral analysis for seed 1 shows that the peaks are larger for the real turbulence. This is true for all realizations for wind condition 1. Seed nr 5 is the outliner, and the peak is four times larger than the other conditions. The large difference is, therefore must, likely cause by the difference in resonance, as the peak period at 283 s is close to resonance at 294 s.

The mean value of standard deviation is larger for real turbulence, meaning that frozen turbulence underestimates the dynamics in x-translation in the system. This is consequently for all the measurements, with the exception of floater 1 for wind speed w = 7.5 m/s. One realization in frozen turbulence increases the average drastically for this wind speed. By neglecting this realization, the mean value of real turbulence would always be larger.

For wind condition two, the spread in standard deviation is larger for the frozen turbulence in floater 1. In this case, for all realizations, the standard deviation is much larger for real turbulence, causing a larger mean value, around 0.2 m. Also, for floater 2 the spread is very small for frozen compared to real turbulence. In Figures for spectral analysis .4.1, .4.2, and .4.3 frozen turbulence has larger peaks than real turbulence. Therefore the difference is not caused by resonance.

For wind condition three and probably for other wind speeds higher than the rated wind speed, the difference in standard deviation is negligible. The difference is in the second decimal place.

In sway, there are some differences in the mean value, even though they are very small. For the mean and standard deviation, frozen turbulence overestimates the sway motion for wind condition one, but the spread is larger in wind conditions two and three for real turbulence. The values are also more clustered for frozen turbulence, the same as in surge.
The pitch motion seems very little affected by the difference in real and frozen turbulence. The bending moment induced by the wind loads will be mostly dependent on the thrust from the wind turbine due to the large moment arm. Only one seed from w = 12 and w = 16 (m/s) for floater 2 seems to be a outliner. If disregarding those seeds, the frozen turbulence assumption is slightly conservative. Since the standard deviation is larger in surge for real turbulence, the pitch motion is expected to be larger. A theory is that the coherence in yz has changed slightly when the wind has propagated. This is possible as the yaw is also conservative for frozen turbulence assumption, even if the difference is small.

The main drawback for the comparison study between frozen and real turbulence is that the turbulence intensity parameter is very small compared to the standard. This means that the standard deviation is very small for the wind speed. Since the wind speed is so stable, energy distribution will take a longer time, meaning that turbulence changes in time will be slow for this LES data compared to turbulence intensity parameters used in the standards. Therefore the frozen wind hypothesis will be more valid for low turbulence intensity factors. For shared mooring setups with larger distances between the floaters, the turbulent wind would have a longer propagation span, giving the flow more time to exchange energy. For higher mean wind speeds, the wind will propagate faster to the next floater, giving the flow less time to exchange energy. Therefore the frozen wind hypothesis will be stronger for higher wind speeds. Also, larger wind speeds will often have a more stable wind field, according to the standard, as the relative standard deviation is lesser for the same turbulence intensity.

Another drawback in the comparison study is that all the seeds are obtained from the same time series, assuming the coherence is spatial zero when in reality, the realization is dependent on each other.

Chapter 9

Conclusion and further work

,

9.1 Conclusion

Three shared mooring topologies were compared to anchored FOWT in time domain analysis and static, considering four different environmental conditions, under-rated, rated, and cut-out wind speeds. Four different fidelity levels were used in the analysis: fully coupled analysis, simplified wind, simplified wind with quasi-static mooring, and simplified dynamic analysis. The different analysis methods were compared, and the simplified force model was used in further studies investigating the dynamic performance of shared mooring systems.

The main findings are summarized in the same order as the thesis:

- Shared mooring lines are less sensitive to element size than anchored mooring lines. As a rule of thumb, the shared mooring line elements could be three times larger than for anchored mooring lines. The static performance depends on topologies and nonlinearities in the mooring stiffness. Therefore, optimizing the shared mooring system concerning static performance is essential. The linearized mooring predicts the static motions well and will give a uniform stiffness distribution if the mooring system is symmetric.
- It is observed that the total number of natural periods increases with shared mooring topologies, and the periods are approximately the same for the systems. The linearized model predicts the natural periods well and is expected to be a good solution if calibrated properly.
- Simplification of the wind gives adequate results when compared to rigid body motions, and the modeling technique could be further improved by local reference modeling of force and controller-dependent damping. Also, the comparison would have been better with three-hour simulations. Quasi-static mooring gives accurate results for rigid body motions and tension for less complex mooring systems. Tension is the most sensitive parameter, and the quasi-static mooring has to be carefully modeled if the parameter is of interest. Since the shared mooring is modeled with FEM and the tension depends on motions, the quasi-static method accurately predicts the shared mooring tension.

- The linearized system dynamic performance is limited by the stiffness matrix and the refinement of the dynamic time step. The model overpredicts upwind floaters' mean motions and underpredicts downwind floater motions. Since the mooring stiffness is linearized, the tension is underpredicted. The model is only adequate for the first estimate or if the mooring stiffness is close to linear.

- Mann turbulence generator is conservative in surge and yaw standard deviation compared to the specific large-eddy simulation. Turbsim underpredicts all motions since the standard deviation in the wind is smaller.

- There is little difference between frozen and real turbulence, especially for large wind speeds, where the time lag is less between the floaters. The frozen turbulence assumption is conservative in yaw, and the pitch motion is no different. Surge and sway are larger for real turbulence. The frozen turbulence hypothesis is conservative for mooring tension in wind conditions one and three.

9.2 Further work

Some possible improvements were identified in the master thesis but not assessed due to limited time. In the thesis, the following work could have been improved:

- Natural periods are important in a shared mooring system since they have several high natural periods, and most likely, resonance is observed in the systems. Even though natural periods are calculated for the systems, decay tests are necessary to know the natural periods precisely. The natural periods calculated with eigenvalue analysis in SIMA give a lower and upper bound for the natural period as the stiffness is minimum and maximum. The difference between $A(T = 0)$ and $A(T = \infty)$ is about 3e5 kg. Compared to the total mass of one floater $m_f = 2.009e6$ kg, the difference is around 15% in mass when not considering the mooring line mass. Even though spectral analysis for response has been carried out, highlighting the natural periods in the system, a confirmation would be necessary.

- There are some differences in the pretension between the linearized model and SIMA. As the pretension is higher in SIMA, some natural periods are lower than for the linearized model. Therefore, both pretension and linear stiffness for each mooring line could be updated.

- A wind width of 250 m was used as VolturnUS-s has a rotor diameter of 240 m. As the floaters move in sway, it is unknown if the wind fields follow the floater, and if it do so, which floater do it follow. If the wind is stable in space, some parts of the blades do not experience turbulent wind. Creating a yaw moment further strengthens the sway motion, creating a negative loop. Therefore, the relative wind on the outermost blade should be investigated.

- Investigate the dynamic performance of complex shared mooring systems with coarse wind and compare the accuracy with the simplified wind model and refined wind. It is then possible to evaluate the performance of the simplified wind model against other methods with the same fidelity.

- In shared mooring systems, it is important to model the resonance correctly, as the system has many long natural periods which can be excited by the turbulent wind. Linear damping has limitations, as the control system is not in the damping calculations, and the aerodynamic added mass is neglected. Therefore linear damping is a good approximation if there is little resonance in the system and the frequency range is distant from the controller bandwidth. As the damping coefficient is dependent on the control system for lower frequencies than the controller bandwidth, it could be necessary to use a thrust linearization, including the controller, or estimate damping and aerodynamic added mass by forced oscillation using FFT.

- It should be investigated if it is possible to improve the simplified force model by separating the force into force files with local and global reference systems, with x force in the local reference frame. When the floater pitches and rotates, the force would then be decomposed. Most likely, the pitch and yaw would then be overestimated, but sway would be calculated more correctly.

- SIMO model of shared mooring could further improve the analysis time in evaluating shared mooring topologies. Since RIFLEX elements cannot be used, nonlinear spring can be used by specifying the force-elongations from shared mooring systems with RIFLEX elements. Also, it shall be further investigated if it is possible to run quasi-static shared mooring in SIMA.

- The linearized model script could be further developed using the first-order transfer function from potential flow theory. Firstly, a transfer function will accurately calculate the hydrodynamic force, including radiation and correct diffraction force. Also, the computational time is reduced as acceleration from waves is not necessary to generate as the inertia force is known.

- The linearized model can be further developed by interpolating the wind and wave force. Currently, the CAA algorithm calculates the dynamics every 0.1 s. However, this is also the same time step as the environmental loading, causing too large motions in the system. By linear interpolation between the time step, loading is applied more evenly in time.

- The current mooring system is optimized to have enough stiffness so the floater does not move more than 90 m, which is the watch circle constraint. The chain mooring line's nonlinear stiffness properties create an uneven distribution between the floaters, causing the watch circle constraint not to be fulfilled. Also, a watch circle constraint of 90 m is considerable, contributing to a sizeable nonlinear effect. Since the mooring system is optimized on mooring weight versus system stiffness, the mooring lines' dimensions need to be considerably larger to handle the significant tension in the mooring lines. Therefore a new mooring system has to be dimensioned with larger dimensions, and a fatigue study is necessary to identify the shared moorings effect on fatigue. The ratio in weight between shared and anchored mooring has to be reconsidered, considering the nonlinearity, as the stiffness is not evenly distributed. If the system is optimized for evenly distributed response, the linear model could be a good fit dynamically. This has to be investigated.

- Suppose the mooring systems have a more even stiffness, and the natural periods are evaluated. In that case, a new cost study is necessary as the economy of the shared mooring system would change.

- When conducting turbulence modeling, the turbulence intensity must match the order. By calibrating the Mann turbulence files against the wind speed at the hub, a small error is introduced as the velocity in the hub height is in the local reference system. The pitch motion is small, so the error shall not be large. Another approach is to calibrate the wind file by taking the standard deviation of the wind file and not using SIMA for this or fixing the floater. Another effect only valid for small velocities is that the wind velocity is calculated as the relative wind speed. Thus, the calibrating mann turbulence generator will overestimate the standard deviation in the wind speed with the approach that has been used. Since Turbsim is underestimating the standard deviation in the wind speed, it is possible to increase the TI until it matches what is ordered, and the comparison would have been fairer.

- Since only one data point is available in SIMA with wind data, it is difficult to evaluate the coherence. Therefore, multiple SIMO bodies could be strategically placed around both of the wind turbines in the yz frame. This would have provided statistical data, enabling calculation of the coherence in u, v, and w. Then it would have been possible to compare how the coherence in v and w affects the BEM calculation and evaluate if the coherence is causing the difference, as the standard deviation in the wind is designed to be the same. Also, by having multiple points in x, the coherence in u is known, and the frozen turbulence assumption could be further evaluated.

Bibliography

[1] Sander Nesse-Hansen. *Dynamics of arrays of floating structures with shared mooring.* NTNU, Department of Marin technology, 2022.

[2] DNV. *Energy transition outlook 2021.* URL: `https://www.dnv.no/Publications/energy-transition-norway-2021-212201`. (accessed: 12.12.2022).

[3] DNV. *Energy transition outlook 2022.* URL: `https://www.dnv.no/Publications/energy-transition-norway-2022-235535`.

[4] NVE. *Kostnader for kraftproduksjon.* URL: `https://www.nve.no/energi/analyser-og-statistikk/kostnader-for-kraftproduksjon/`. (accessed: 12.12.2022).

[5] ORECCA. *offshore Renewable Energy Conversion platforms.* URL: `https://orecca.rse-web.it/map.phtml`. (accessed: 12.12.2022).

[6] Margoyles. "Deep water". In: *The European Wind Energy Association* (2013).

[7] Connolly and Hall. "Comparison of pilot-scale floating offshore wind farms with shared moorings". In: *Ocean Engineering* 171 (2019). DOI: `10.1016/j.oceaneng.2018.08.040`.

[8] Goldschmidt and Musklus. "Coupled mooring systems for floating wind farms". In: *Energy Procedia* 80 (2015), pp. 255–262. DOI: `10.1016/j.egypro.2015.11.429`.

[9] Wilson and Hall. "Linearized modeling and optimization of shared mooring systems". In: *Ocean Engineering* 241 (2021). DOI: `10.1016/j.oceaneng.2021.110009`.

[10] Bailey Borisade Gozcu Kontos. Bredmose. "methods for multiple floaters and dynamic cables at farm level". In: *corewind* (2021).

[11] Liang, Jiang, and Merz. "Mooring Analysis of a Dual-Spar Floating Wind Farm With a Shared Line". In: *Journal of Offshore Mechanics and Artic Engineering* (2021). DOI: `https://doi.org/10.1115/1.4050965`.

[12] Mahe Hermille Fotini K Chow Erin E. Bachynski-Polić Irene Riverra-Arreba Adam S.wise. "Effects of atmospheric stability on the structural response of a 12 MW semisubmersible floating wind turbine". In: *Wind Energy* (2022). DOI: `10.1002/we.2775`.

[13] Eliassen.Lene Bachynski. Erin E. "The Effect of Turbulence Model on the Response of a Large Floating Wind Turbine". In: *ASME 2017 36th International Conference on Ocean, Offshore and Arctic Engineering* (2017/09/25). DOI: `10.1115/OMAE2017-61179`.

[14] Astrid Nybø. "The impact of turbulence modelling on large offshore wind turbine response". en. phd. The University of Bergen, 2022. URL: `https://bora.uib.no/bora-xmlui/handle/11250/3023277` (visited on 04/28/2022).

[15] Carl M.Larse et al. *Marin dynamics.* Akademika forlag, 2014,2019.

[16] O.M.Faltinsen. *Sea loads on ships and offshore structures.* 1st ed. Cambridge university press, 1990.

[17] Langen and Ragnar. *Dynamisk analyse av konstruksjoner.* Tapir, 1979. ISBN: 978-82-519-0362-2.

[18] Jr John D.Anderson. *Fudamentals of Aerodynamics.* McGrawHill Higher Education, 2005. ISBN: 13:978-0-471-49972-5.

[19] Erin Bachynski-Polić. *Lecture note from - Integrated dynamic analysis of wind turbines - TMR03.*

[20] J.G Mcgowan James F Manwell and A.L Rogers. *Wind Energy Explained: Theory, Design and Application.* Wiley, 2009.

[21] DNV. "Floating wind turbine structures,DNVGL-ST-0119". In: (2021).

[22] *IEC-turbulence-simulator.* URL: `https://www.wasp.dk/weng/iec-turbulence-simulator`.

[23] SINTEF. *SIMA Documentation.* URL: `https://sima.sintef.no/doc/4.4.0/sima/index.html`. (accessed: 10.06.2023).

[24] Y.Izumi J.C. Kaimal J.C Wyngaard and O.R Cote. "Spectral characteristics of surface-layer turbulence". In: *Q.J.R. Meteorol. Soc.* (1972).

[25] etc Keith Walker. "An evaluation of the predictive accuracy of wake effects models for offshore wind farms". In: *Wind Energy* (2016). DOI: `10.1002/we.1871`.

[26] Bjørnar Pettersen. *Hydrodynamikk.* Akademika forlag, 2018. ISBN: 9810300035890.

[27] Xu Kun. "Design and comparative analysis of alternative mooring systems for floating wind turbines in shallow water with emphasis on ultimate limit state designs". en. phd. NTNU, 2021. DOI: `10.1016/j.oceaneng.2020.108377`. URL: `https://ntnuopen.ntnu.no/ntnu-xmlui/handle/11250/2989406` (visited on 12/16/2022).

[28] Jørgen Amdahl. *Lecture note from - Design of Ocean Structures - TMR4195.*

[29] Kolbein Bell. *Konstruksjonsmekanikk.* Fagbokforlaget, 2014.

[30] Seibert.Michael G James H VanZwieten. *Anchor selection study for ocean current turbines.* 2014. URL: `https://www.tandfonline.com/doi/abs/10.1080/20464177.2014.11020293`.

[31] Rao Martand Singh. "Experimental and numerical investigation of heat and mass movement in unsaturated clays". en. ISBN: 9781303209499. phd. Cardiff University, 2007. URL: `https://orca.cardiff.ac.uk/54608/` (visited on 04/28/2022).

[32] *Marine operation and mooring analysis.* URL: `https://www.dnv.com/services/marine-operations-and-mooring-analysis-software-sima-2324?&utm_campaign=structure_sesam`.

[33] NREL. *Turbsim.*

[34] Anthony Viselli Habib Dagher Andrew Goupee Evan Gaertner Nikhar Abbas Matthew Hall Allen Christopher and Garrett Barte. "Definition of the UMaine VolturnUS-S Reference Platform Developed for the IEA Wind 15-Megawatt Offshore Reference Wind Turbine. Golden, CO: National Renewable Energy Laboratory". In: *NREL* (2020). DOI: `10.2172/1660012`.

[35] Bachynski.Erin E. Souza.Carlos Eduardo S Hegseth.John Marius. "Frequency-Dependent Aerodynamic Damping and Inertia in Linearized Dynamic Analysis of Floating Wind Turbines". In: *Journal of Physics: Conference Series* 1452 (2020-01). DOI: `10.1088/1742-6596/1452/1/012040`.

[36] Matthew Thomas Jair Hall. *Mooring line modelling and design optimization of floating offshore wind turbines.* 2013.

[37] *Sotra Anchor Chain.* URL: `https://www.sotra.net/?produkter=stud-link-chain`.

Appendices

.1 Morison equation with strip theory

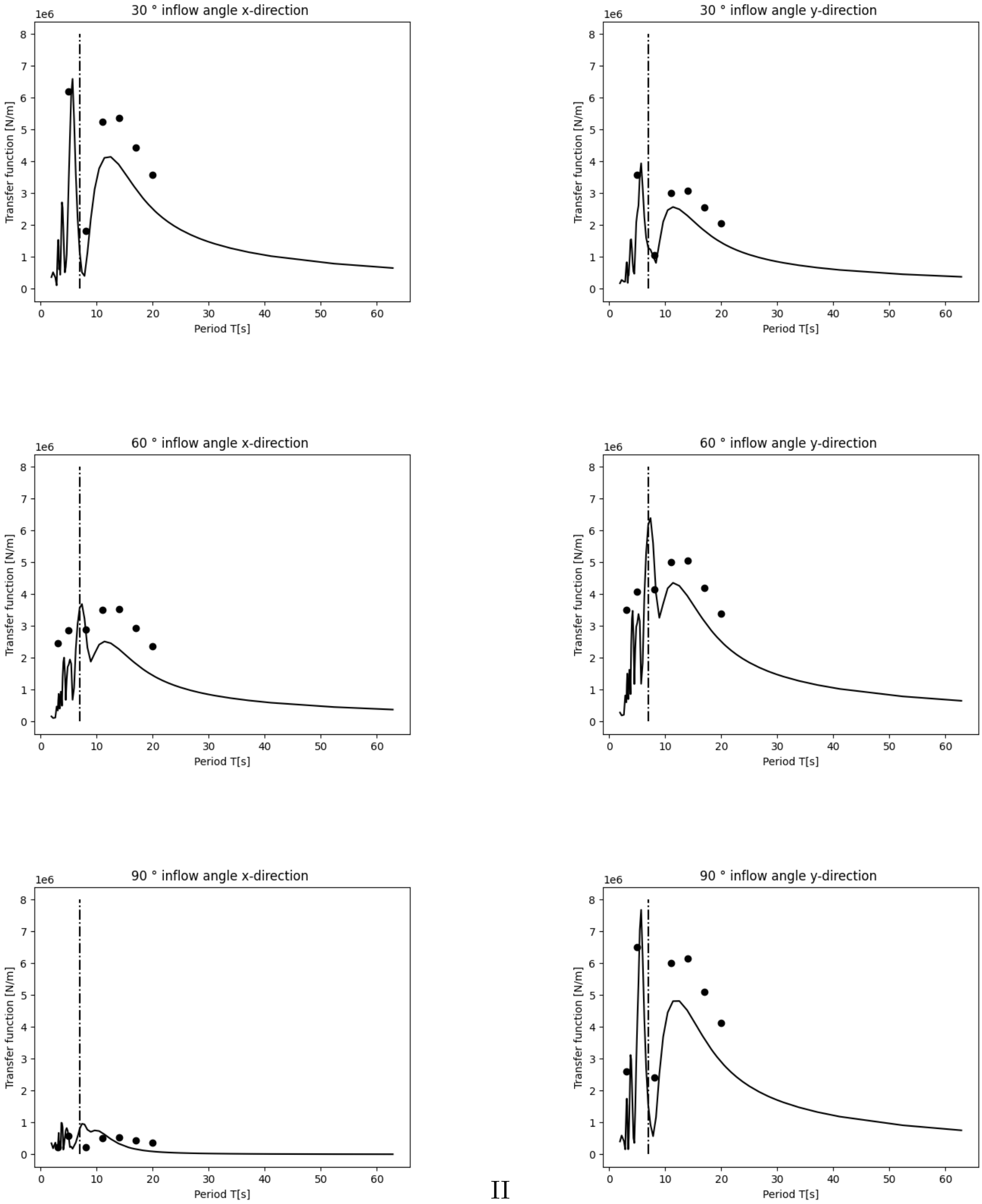

Figure .1.1: Potential theory versus Morison strip theory

.2 Eigenvalue modes

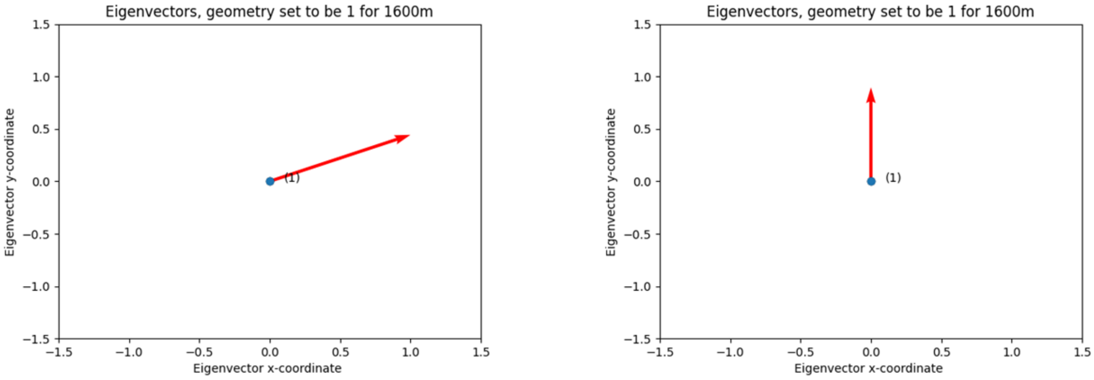

Figure .2.1: Eigenvalue modes from the linearized model - baseline

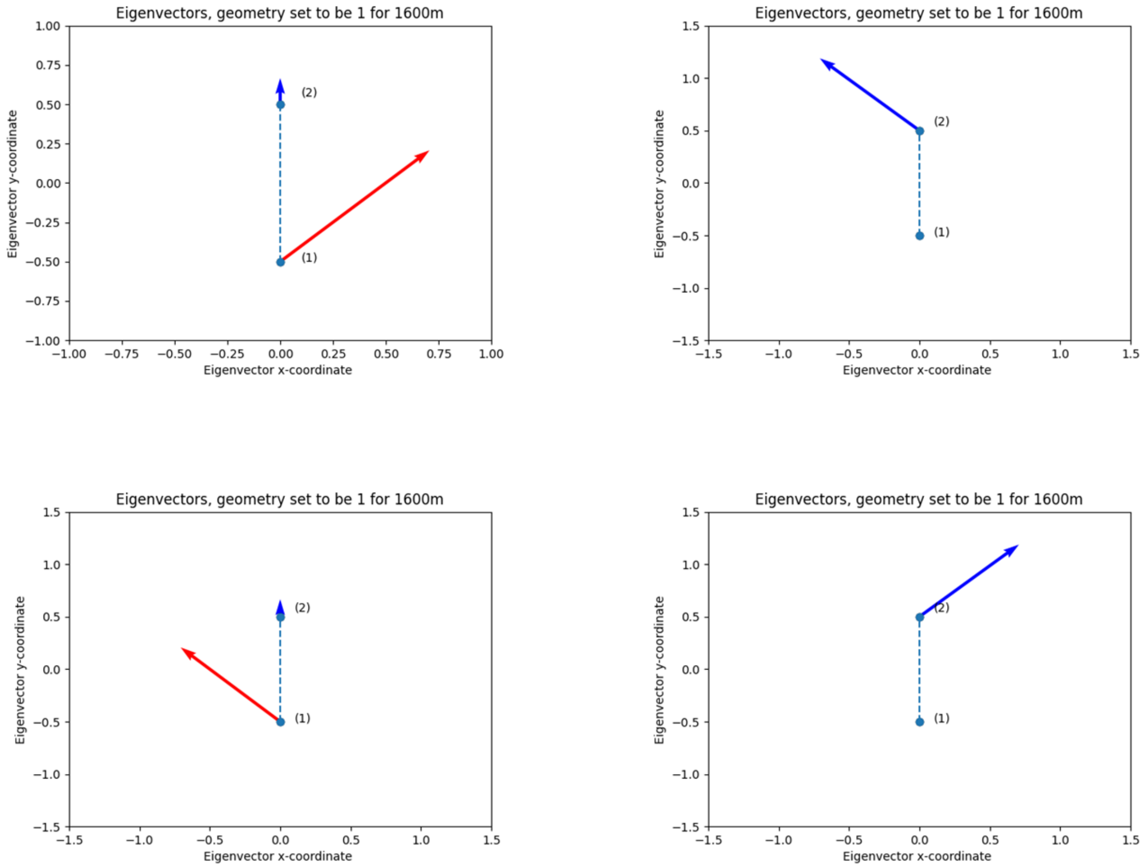

Figure .2.2: Eigenmodes linearized system for model a)

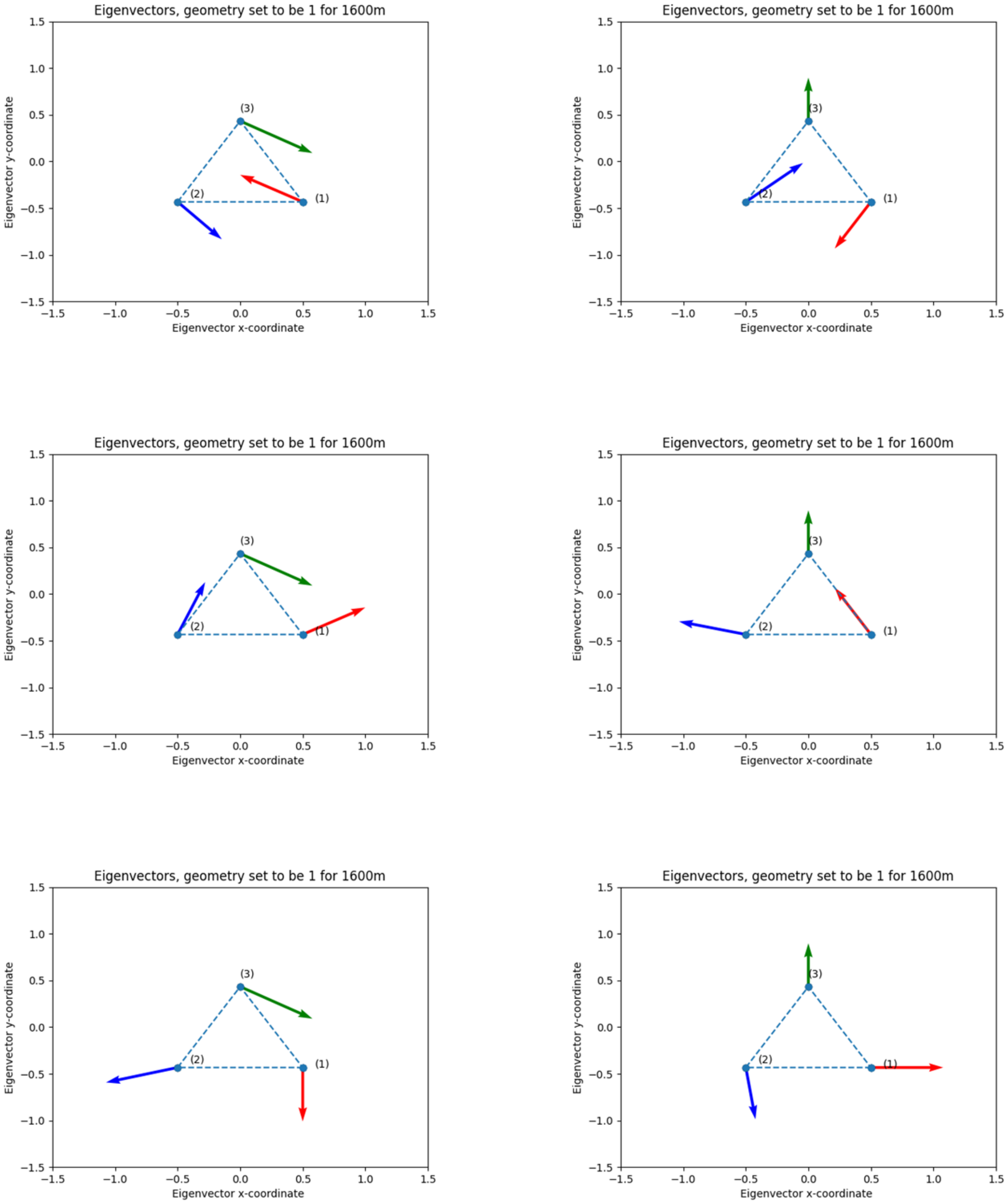

Figure .2.3: Eigenmodes linearized system for model b)

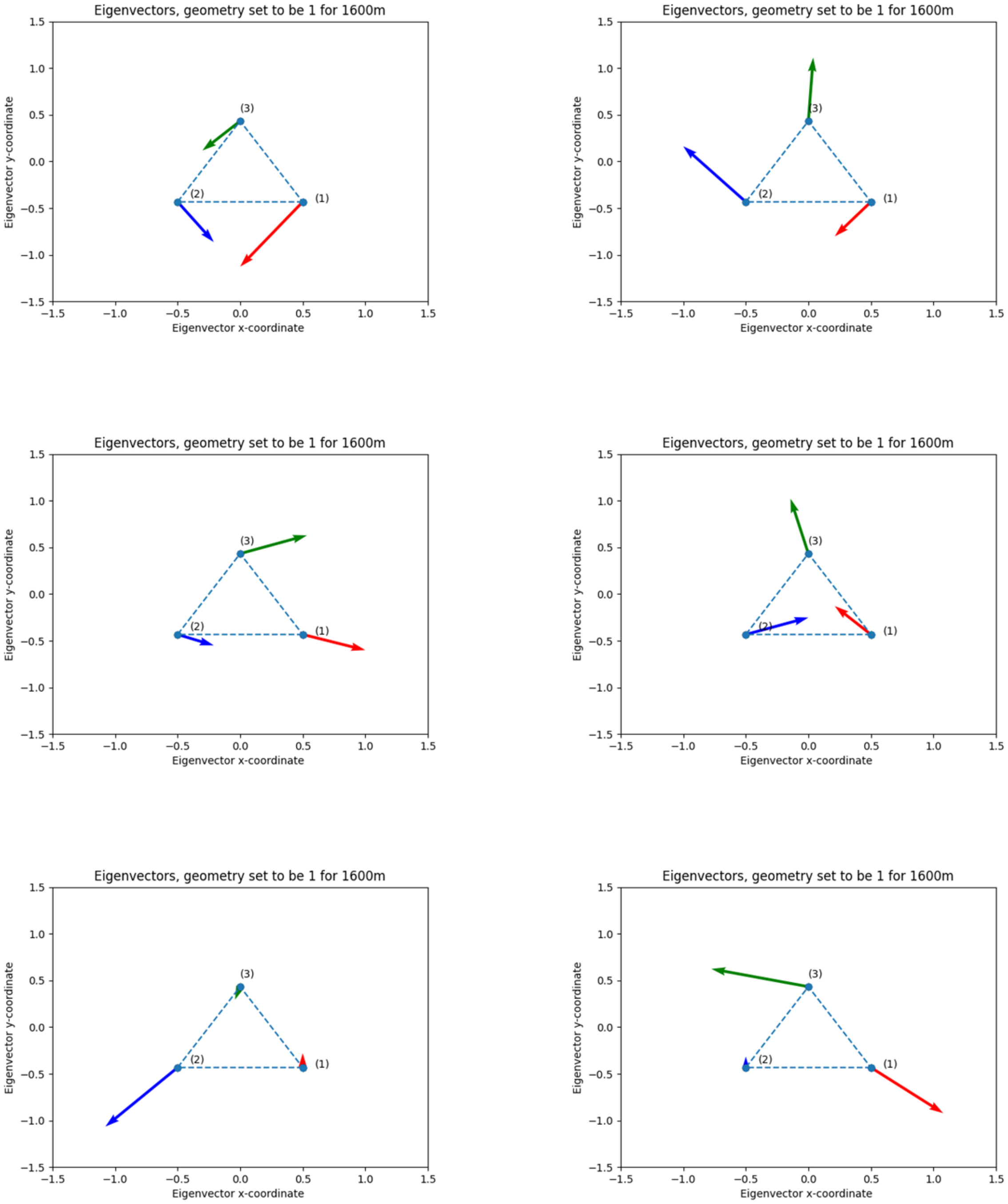

Figure .2.4: Eigenmodes linearized system for model c)

.3 Statistic data from linearized dynamic analysis

	Mean	Standard deviation	Maximum
w = 6 [m/s]			
mooring 1 [kN]	68.94	655.74	655.74
mooring 2 [kN]	70.67	648.49	648.49
mooring 3 [kN]	138.55	1473.77	1473.77
surge [m]	12.46	49.25	49.25
sway [m]	0.9	0.38	0.38
w = 10 [m/s]			
mooring 1[kN]	39.4	415.47	415.47
mooring 2 [kN]	39.25	392.62	392.62
mooring 3 [kN]	77.05	1969.91	1969.91
surge [m]	6.93	93.86	93.86
sway [m]	0.82	1.19	1.19
w = 20 [m/s]			
mooring 1 [kN]	29.66	580.31	580.31
mooring 2 [kN]	20.74	501.35	501.35
mooring 3 [kN]	19.96	1696.34	1696.34
surge [m]	1.79	69.26	69.26
sway [m]	2.45	4.1	4.1
Irregular			
mooring 1 [kN]	28.79	579.72	579.72
mooring 2 [kN]	20.63	500.77	500.77
mooring 3 [kN]	16.95	1697.51	1697.51
surge [m]	1.52	69.37	69.37
sway [m]	2.45	4.1	4.1

Table .3.1: Summary of average, standard deviation and maximum displacement and tension for the simplified system waves

	Mean	Standard deviation	Maximum
$F1_1$[kN]	173.41	835.16	835.16
$F1_2$ [kN]	177.69	825.8	825.8
$F2_1$ [kN]	190.1	1958.84	1958.84
$F2_2$ [kN]	186.71	1949.4	1949.4
shared [kN]	193.3	1961.71	1961.71
surge F1 [m]	15.3	47.85	47.85
sway F1 [m]	0.64	0.39	0.39
surge F2 [m]	16.6	46.85	46.85
sway F2 [m]	0.87	0.4	0.4

Table .3.2: Summary of average, standard deviation and maximum displacement and tension for the simplified system model a) - w = 6 - regular waves

	Mean	Standard deviation	Maximum
$F1_1$[kN]	134.39	304.45	304.45
$F1_2$ [kN]	129.92	276.73	276.73
$F2_1$ [kN]	124.38	2513.89	2513.89
$F2_2$ [kN]	121.3	2486.4	2486.4
shared [kN]	164.01	1970.39	1970.39
surge F1 [m]	11.85	93.29	93.29
sway F1 [m]	0.53	1.17	1.17
surge F2 [m]	10.89	92.94	92.94
sway F2 [m]	0.75	1.16	1.16

Table .3.3: Summary of average, standard deviation and maximum displacement and tension for the simplified system model a) - w = 10 - regular waves

	Mean	Standard deviation	Maximum
$F1_1$[kN]	44.34	627.73	627.73
$F1_2$ [kN]	38.92	529.37	529.37
$F2_1$ [kN]	58.89	2266.43	2266.43
$F2_2$ [kN]	75.31	2167.03	2167.03
shared [kN]	85.05	1976.81	1976.81
surge F1 [m]	3.5	68.97	68.97
sway F1 [m]	1.32	4.15	4.15
surge F2 [m]	5.59	69.1	69.1
sway F2 [m]	2.48	4.19	4.19

Table .3.4: Summary of average, standard deviation and maximum displacement and tension for the simplified system model a) - w = 20 - regular waves

.4 LES

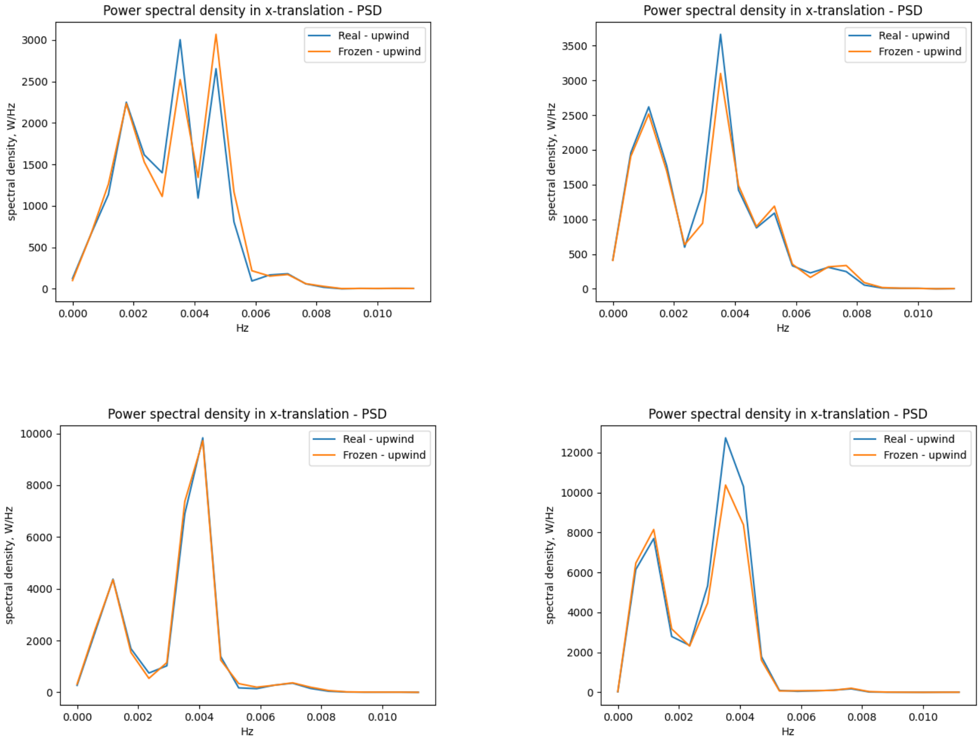

Figure .4.1: Real and frozen turbulent wind - spectral analysis - w = 7.5 [m/s],for seed 2, 3, 4, and 5

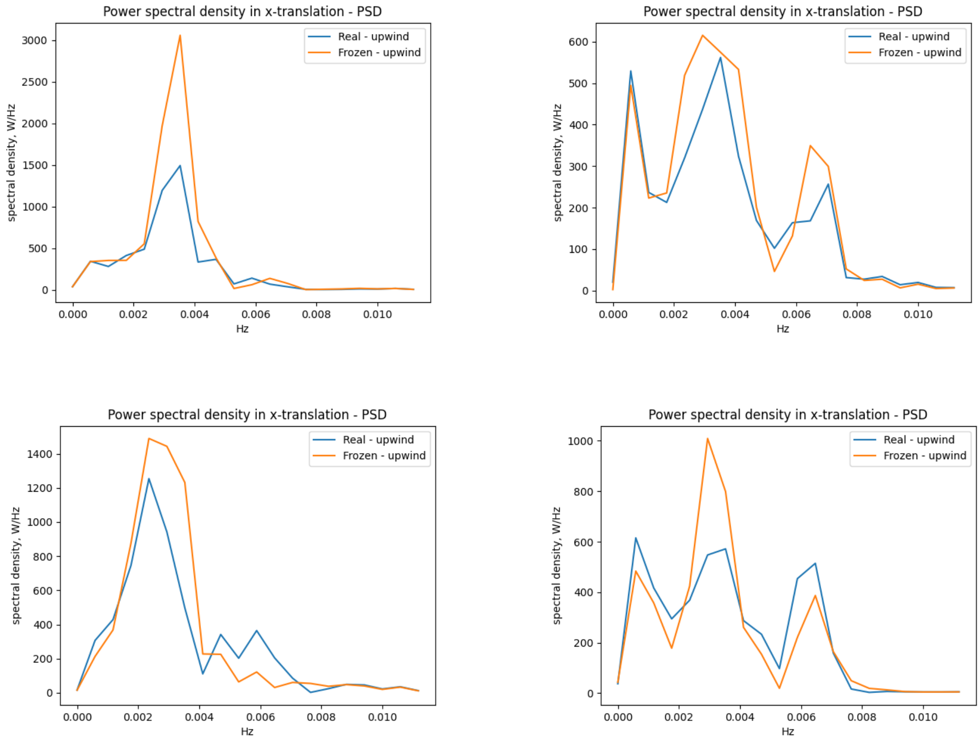

Figure .4.2: Real and frozen turbulent wind - spectral analysis - w = 12 [m/s],for seed 2, 3, 4, and 5

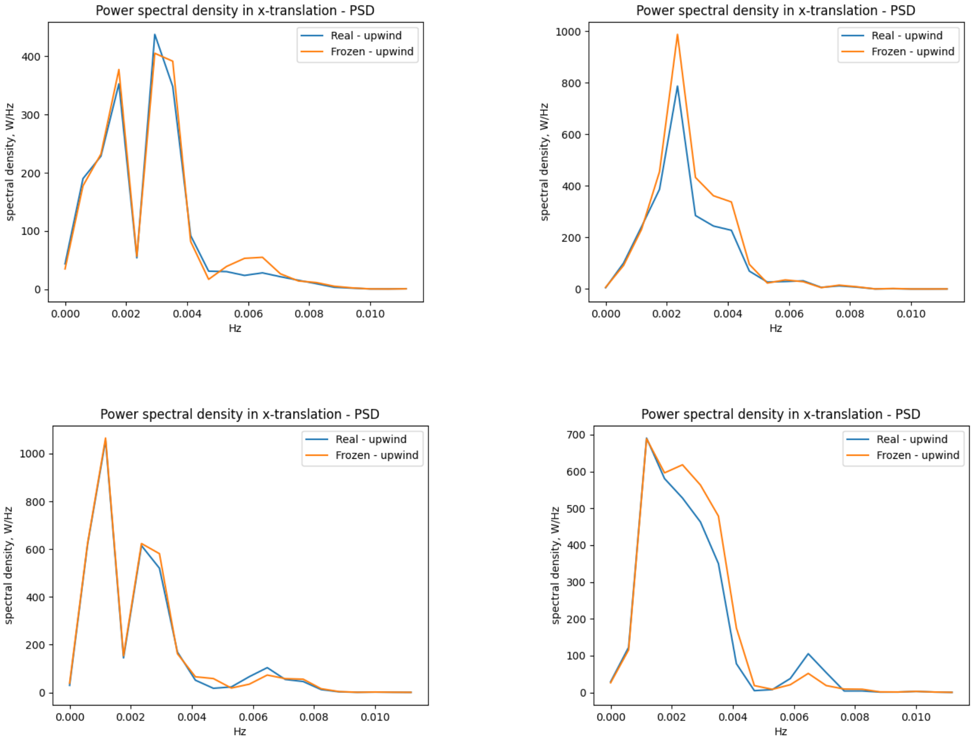

Figure .4.3: Real and frozen turbulent wind - spectral analysis - w = 16 [m/s],for seed 2, 3, 4, and 5

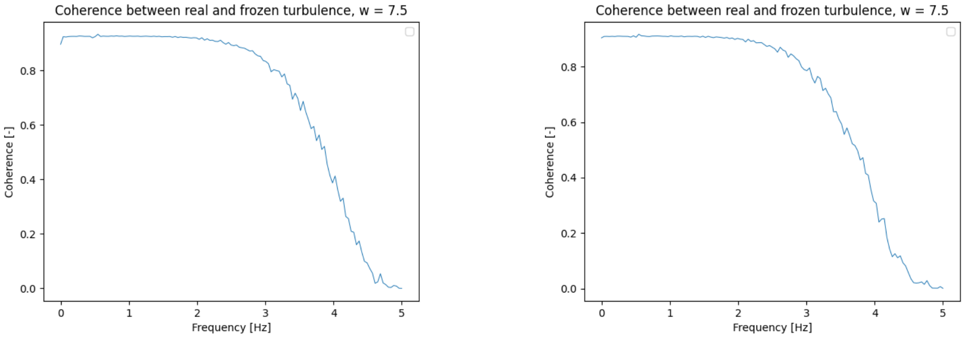

Figure .4.4: Real and frozen turbulent wind - coherence - w = 7.5 [m/s],for seed 1, and 2

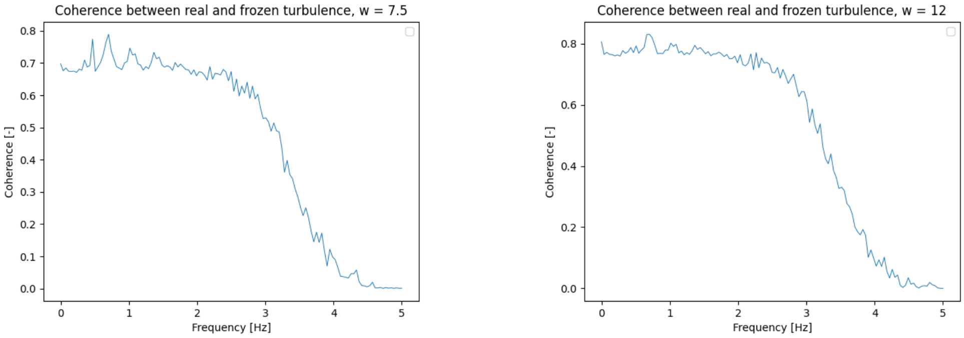

Figure .4.5: Real and frozen turbulent wind - coherence - w = 12 [m/s],for seed 1, and 2

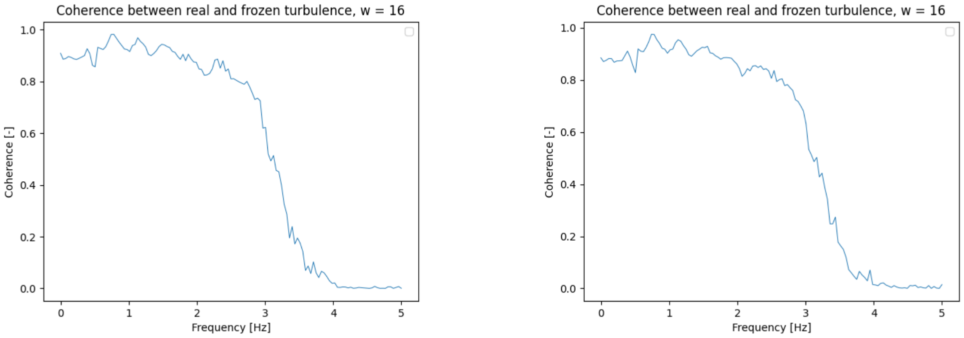

Figure .4.6: Real and frozen turbulent wind - coherence - w = 16 [m/s],for seed 1, and 2

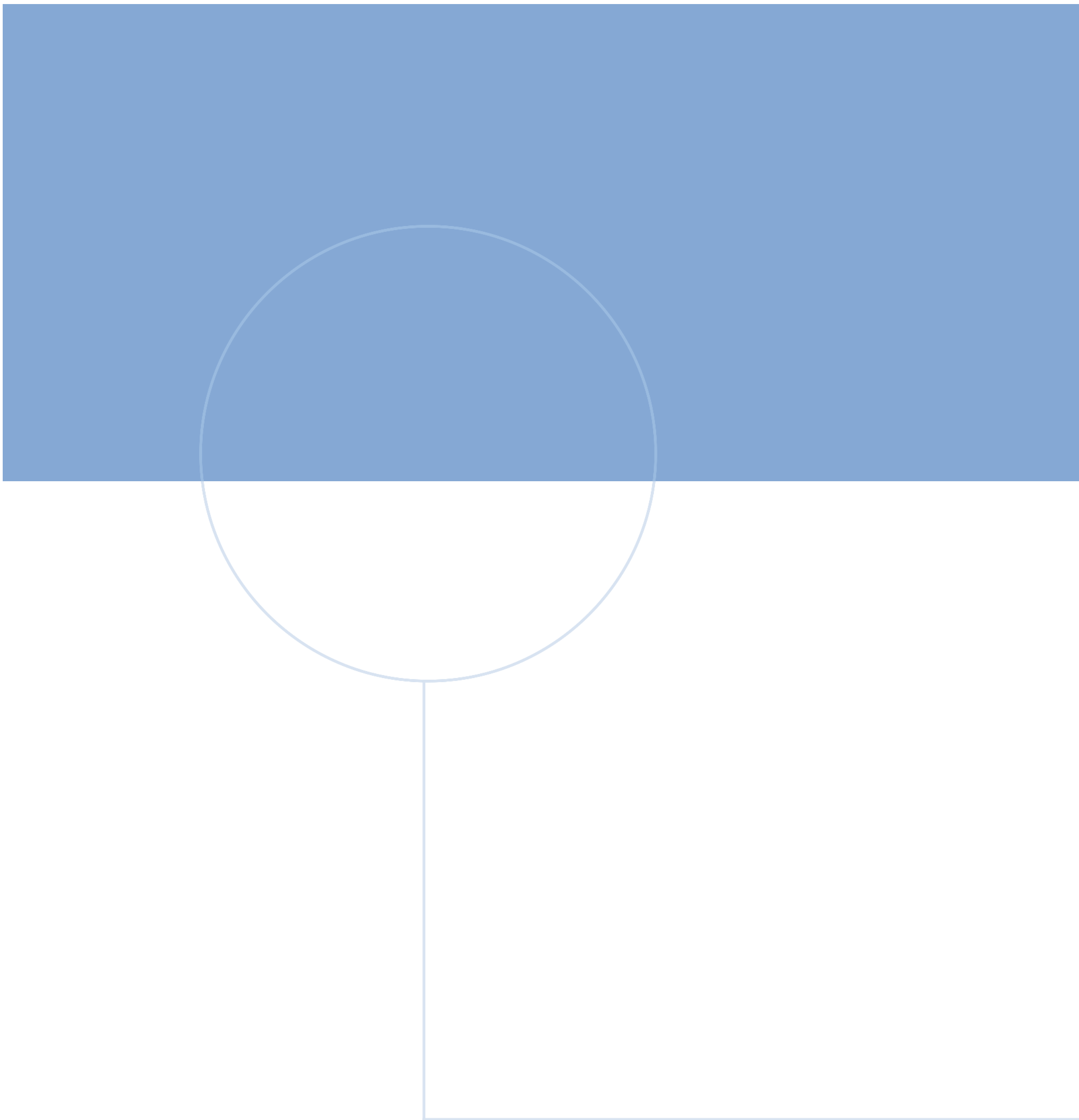

NTNU
Norwegian University of
Science and Technology

AkerSolutions